Forschungszentrum Jülich
IBG 2 – Institute for Bio- and Geosciences

# Analyzing photosynthetic performance in natural fluctuating environment using light-induced fluorescence transient (LIFT) method in high-throughput

Dissertation

genehmigt von der der Landwirtschaftlichen Fakultät
der Rheinischen Friedrich-Wilhelms-Universität Bonn
zur Erlangung des Grades
Doktor der Agrarwissenschaften (Dr. agr.)

Beat Keller

Bonn, Januar 2018

Gutachter: Prof. Dr. Uwe Rascher

Zweiter Gutachter: Prof. Dr. Frank Hochholdinger

Tag der mündlichen Prüfung: 24. September 2018

Erscheinungsjahr der Dissertation: 2018

# Zusammenfassung

In der vorliegenden Arbeit wurde die Wissenslücke bezüglich der Photosynthese Wechselwirkung mit ihrer fluktuierenden Umgebung durch die Erfassung von über einer Million Chlorophyllfluoreszenzmessungen unter Feldähnlichen- und Feldbedingungen bearbeitet. Fünf Nutzpflanzenarten wurden in einer hohen raumzeitlichen Auflösung beobachtet. Dabei wurde die lichtinduzierte Fluoreszenztransienten (LIFT) Methode als ein Hochdurchsatz-System etabliert, das über den Pflanzenbestand scannt. Die LIFT-Methode verwendet eine Reihe von Anregungslichtblitzen, um eine variable Fluoreszenz ($F_v$) zu induzieren. Anschließend wird die Fluoreszenzrelaxation ($F_r$) beobachtet. Der resultierende Fluoreszenztransient spiegelt die gekoppelte Kinetik der Reduktion des primären Chinon-Elektronenakzeptors ($Q_A$) und die anschließende Reoxidation wider. $F_v$ normalisiert mit dem induzierten Fluoreszenzmaximum ergibt die Quanteneffizienz des Photosystems II ($F_v/F_m$ im Dunkeln und $F_q'/F_m'$ im Licht), was die Menge der photosynthetisch transportierten Elektronen pro Photon widerspiegelt.

Das lokale Fluoreszenzmaximum ($F_mQ_A$) und die maximale Fluoreszenz ($F_m$) wurden aus 60 cm Entfernung unter Verwendung von LIFT-Lichtblitzen induziert, die sich in Anregungslänge und Leistung unterschieden. $F_mQ_A$ reduzierte die Elektronentransportkette nicht vollständig, was die Bestimmung der Reoxidationseffizienz 5 ms nach der $Q_A$-Reduktion ($F_{r2}/F_m$ im Dunkeln bzw. $F_{r2}'/F_m'$ im Licht) ermöglichte. Dieser neu etablierte Parameter war abhängig von der Funktionalität der Elektronentransportkette und der Temperatur. Im Gegensatz dazu war $F_q'/F_m'$ hauptsächlich von der Lichtintensität abhängig. Unter kontrollierten Bedingungen korrelierte die Elektronentransportrate (ETR) basierend auf $F_q'/F_m'$ mit der ETR, die aus $CO_2$-Assimilationsmessungen berechnet wurde.

In dieser Studie wurde ein ausreichend großer Datensatz einschließlich Spektralmessungen unter feldähnlichen Bedingungen gesammelt, um Faktoren zu identifizieren, die den Tages- und Jahreszeitengang der Photosynthese bestimmen. Gemäß der Lasso-Regressionsanalyse war $F_q'/F_m'$ abhängig von der photosynthetisch aktiven Photonenflussdichte (PPFD) und den Spektralindizes. Das lineare Modell erklärte fast 50% der Varianz in $F_q'/F_m'$, welche über zwei Vegetationsperioden gemessen wurden. Der zweite Parameter $F_{r2}/F_m$ bzw. $F_{r2}'/F_m'$ wurde stark durch die Temperatur und die Nutzpflanzenart bestimmt, z.B. unterschied sich winterharter Raps und Soja bei niedrigeren Temperaturen deutlich. Nur ein geringer Einfluss auf die gemessenen Parameter wurde für die verschiedenen Jahre, Tageszeiten und damit Saison- oder Pflanzenentwicklungsstadium festgestellt. Im Folgenden wurden genotypische Unterschiede am Parametermittelwert oder der Wechselwirkung der Parameter mit den Umweltfaktoren PPFD und Temperatur analysiert. Zunehmender Trockenstress verringerte die $F_q'/F_m'$ in Mais. Im Gegensatz dazu stieg die $F_{r2}/F_m$ bzw. $F_{r2}'/F_m'$ als Reaktion auf Trockenheit an, was auf einen verstärkten zyklischen Elektronentransport hindeutet. Eine Infektion mit echtem Mehltau wurde durch $F_q'/F_m'$ festgestellt, bevor die Symptome mit dem Auge sichtbar waren. Bei einer Anayse aller gesammelten Felddaten war $F_q'/F_m'$ wieder abhängig von PPFD, korrelierte jedoch stärker mit der Reflexion von Sonnenlicht bei 685 nm auf dem gemessenen Blatt. Die Reaktion von $F_{r2}/F_m$ bzw. $F_{r2}'/F_m'$ auf die Temperatur war auch im Feld zu beobachten und erklärte 79% aller Varianz in Mais. Der LIFT-Screening-Ansatz identifizierte tolerante Genotypen bezüglich der Licht- und Temperaturnutzungseffizienz unter Kontroll- und Stressbedingungen. Die Interaktion der betrachteten Parameter in Bezug auf PPFD und Temperatur ermöglicht die Vorhersage und Optimierung der photosynthetischen Leistung unter verschiedenen Umweltbedingungen.

# Abstract

In the present work, the knowledge gap concerning the interaction of photosynthesis with its fluctuating environment was filled by acquiring over one million chlorophyll fluorescence measurements in semi-field and field conditions. Five crop species were monitored in high spatio-temporal resolution. Hereby, the light-induced fluorescence transient (LIFT) method was established as high-throughput system scanning over the crop canopy. The LIFT method uses a series of excitation flashlets to induce variable fluorescence ($F_v$) and to monitor fluorescence relaxation ($F_r$). The resulting fluorescence transient reflects the coupled kinetics of primary quinone electron acceptor ($Q_A$) reduction and its subsequent reoxidation. $F_v$ normalized with the induced maximum fluorescence level results in the quantum efficiency of the photosystem II ($F_v/F_m$ in the dark and $F_q'/F_m'$ in the light) reflecting the amount of photosynthetically transported electrons per photon.

The local fluorescence maximum ($F_mQ_A$) and maximum fluorescence ($F_m$) were induced from 60 cm distance using LIFT flashes differing in excitation length and power. $F_mQ_A$ did not fully reduce the electron transport chain which enabled the determination of the reoxidation efficiency 5 ms after $Q_A$ reduction ($F_{r2}/F_m$ in the dark respective $F_{r2}'/F_m'$ in the light). This newly established parameter was dependent on the functionality of the electron transport chain and temperature. In contrast, $F_q'/F_m'$ was mainly dependent on light intensity. Under controlled conditions, electron transport rates (ETR) based on $F_q'/F_m'$ correlated to ETR retrieved from $CO_2$ assimilation measurements.

For the first time, a sufficiently large data set including spectral measurements was collected under semi-field conditions to identify factors determining the diurnal and seasonal photosynthesis pattern. According to Lasso regression analysis, $F_q'/F_m'$ was dependent on photosynthetic photon flux density (PPFD) and spectral indices. The designed linear model accounted for almost 50% of the variance in $F_q'/F_m'$ measured over two growing seasons. The second parameter, $F_{r2}/F_m$ respective $F_{r2}'/F_m'$, was highly determined by temperature and crop species, e.g. separating the response of winter hard rapeseed and soybean at lower temperatures. Only minor influence on the measured parameters was detected for different years, daytime, measuring date and hence seasonal or plant development stage. In the following, genotypic differences were detected on the parameter mean or the interaction of the parameters with environmental factors. Especially in soybean, genotypic differences in $F_q'/F_m'$ and $F_{r2}'/F_m'$ were more consistently detected when instead of the mean, the interaction with PPFD and temperature was considered. Analyzing the mean of selected time periods was useful for detection of stress response. Increasing drought stress decreased $F_q'/F_m'$ under controlled and semi-field conditions in maize. In contrast, $F_{r2}/F_m$ respective $F_{r2}'/F_m'$ increased in response to drought probably reflecting enhanced cyclic electron transport. Powdery mildew infection was detected by $F_q'/F_m'$ before symptoms were visible by eye.

Drought response of photosynthesis was also detected in soybean under field conditions. Summarizing all collected field data, $F_q'/F_m'$ was still dependent on PPFD, but even stronger correlated to reflectance of sunlight at 685 nm on the target leaf. The response of $F_{r2}/F_m$ respective $F_{r2}'/F_m'$ to temperature persisted, and explained 79% of all variance in maize. The LIFT screening approach identified tolerant genotypes regarding light and temperature use efficiency under control and stress conditions. Analyzing the response curves of the considered parameters related to PPFD and temperature allows the prediction of photosynthetic performance and optimization of genotypic selection in various environments.

# Table of contents

# 1 Introduction

Global increase in agricultural production reached a plateau in the last decades (Alexandratos and Bruinsma, 2012). At the same time, food production in 2050 needs to increase by 60% compared to 2006 while maintaining its sustainability (FAO, 2016). One step towards this aim is to improve photosynthesis processes in order to increase plant production, e.g. by accelerating recovery from photoprotection or decreasing photorespiration (Long et al., 2006; Murchie et al., 2009; Parry et al., 2011; Ziska et al., 2012; Evans, 2013). A recent field trial with genetic modified regulation of photoprotection showed first success in that direction (Kromdijk et al., 2016). However, the targeted processes and its dynamics in natural field environment are largely unknown (Murchie et al., 2009; Evans, 2013). The underlying problem is the lack of methods providing sufficient temporal and spatial resolution in measuring photosynthetic performance to understand photosynthetic regulation mechanisms and to select genotypes under natural conditions (Rascher and Nedbal, 2006; Furbank and Tester, 2011; Meacham et al., 2017).

## 1.1 Photosynthesis

Photosynthesis is a crucial process for life on earth converting solar energy, water and $CO_2$ into chemical energy and carbohydrates (Croce and van Amerongen, 2014). It drives 90% of carbon and water fluxes in the bio- and atmosphere fixing approximately 120 Gt of $CO_2$ per year (Joiner et al., 2011). Photosynthesis can be separated into four distinctive steps: (1) light absorption by the chlorophyll-based antennae followed by excitation transfer to photosystem II (PSII) reaction centers, (2) charge separation in the PSII reaction centers leading to oxidation of water and reduction of primary quinone electron acceptor ($Q_A$), (3) electron transport chain along $Q_A$ via plastoquinone (PQ) pool and cytochrome $b_6f$ complex to photosystem I (PSI), and (4) secondary light absorption by PSI reaction center completing electron transport via ferredoxin by reduction of $NADP^+$ to NADPH (Croce and van Amerongen, 2014). Water oxidation is catalyzed by the $Mn_4O_5Ca$ oxygen evolving complex (OEC) splitting the electrons from water molecules (Delosme and Joliot, 2002; Pérez-Navarro et al., 2016). The electron transport generates a proton gradient across the thylakoid membrane which drives synthesis of adenosine triphosphate (Croce and van Amerongen, 2014). Finally, adenosine triphosphate, NADPH, and 3-phosphoglycerate drive $CO_2$ assimilation catalyzed by the Rubisco enzyme (Bassham, 2003).

### 1.1.1 Regulation mechanisms

Photosynthesis is a highly controlled process reacting to environmental changes in short and long-term acclimation (Demmig-Adams et al., 2012; Kono and Terashima, 2014). Light harvesting and subsequently photosynthesis is regulated by three competing energy pathways: (1) stable charge separation reducing $Q_A$ and driving electron transport, (2) emission of absorbed light energy as chlorophyll fluorescence, and (3) dissipation of excess energy as heat (Butler, 1978). Plants continuously balance the energy distribution into pathway (1) and (3) aiming for efficient use of harvested light energy while protecting itself from excess energy producing reactive oxygen species (Demmig-Adams et al., 2012).

Over 80 years ago, it has been discovered that a dark-adapted plant exposed to ambient light reacts with a fluorescence induction which relaxes (quenches) after seconds (Kautsky and Hirsch, 1931). This fluorescence quenching process was attributed to photosynthetic process requiring light energy (Kautsky and Hirsch, 1931). Indeed, fluorescence quenching analysis provides information about

photosynthetic energy use, e.g. an isolated thylakoid under *constant* background irradiation dissipates a certain amount of absorbed energy as fluorescence (F') diminished by photochemical and non-photochemical quenching (NPQ). In order to disentangle these quenching processes, 3-(3,4-dichlorophenyl)-1,1-dimethylurea (DCMU) which blocks the reoxidation of $Q_A$ was used in isolated thylkaoids. The light-adapted fluorescence maximum ($F_m'$) was assessed when the photochemical energy pathway was suddenly blocked (set to zero) by DCMU resulting in fully reduced $Q_A$ (Butler, 1978; Lazár, 1999; Baker, 2008). Thus, the differences in fluorescence ($F_q' = F_m' - F'$) before and right after DCMU application is related to photochemical energy use (Butler, 1978; Baker, 2008). Maximum fluorescence ($F_m$) is reached after some minutes when the DCMU treatment leads to NPQ relaxation but keeping $Q_A$ reduced (Butler, 1978; Baker, 2008). Thus, the difference between $F_m$ and $F_m'$ is related to NPQ (Butler, 1978; Baker, 2008). This quenching analysis was greatly facilitated by applying a strong saturating light flash which reduces all $Q_A$ without the use of DCMU (Schreiber et al., 1986a). Using the *same* low measuring excitation energy, the induced fluorescence signal when all $Q_A$ are oxidized (minimal fluorescence, $F_o$) and reduced (maximum fluorescence, $F_m$) results in the variable fluorescence ($F_v = F_m - F_o$) (Schreiber, 2004; Baker, 2008). The saturating flash (SF) is too short (< 1 s) to manipulate NPQ levels which allows the calculation of the maximum quantum efficiency of PSII ($F_v/F_m$) (Butler, 1978). Analogous in the light-adapted state, the PSII operating efficiency ($F_q'/F_m'$) indicates how many electrons per absorbed photon are transported through the electron transport chain (Genty et al., 1989; Baker, 2008).

When a plant is exposed to strong light or fluctuating high-light, the thylakoid lumen gets acidified due to sudden increase in water oxidation and electron transport (Adams III et al., 2006; Croce, 2015). Within seconds, the PsbS protein induces a photoprotection mechanism which increases the dissipation of excess energy as heat in the antennae of PSII (Belgio et al., 2012; Ruban et al., 2012; Rochaix, 2014). In a slower process within minutes, the xanthophyll cycle converts violaxanthin to zeaxanthin correlating with increasing NPQ levels (Adams and Demmig-Adams, 1995; Niyogi et al., 1998). The recovery from NPQ takes several minutes linked to slow deactivation of zeaxanthin (Long et al., 2006; Nilkens et al., 2010). The quenching of the fluorescence signal can be used to study energy partitioning into NPQ ($= F_m/F_m' - 1$) and photochemistry (Bilger and Björkman, 1990; Baker, 2008).

### 1.1.2 Plant photosynthesis in a fluctuating environment

Many photosynthetic acclimation mechanism were identified and studied under controlled conditions (Kalaji et al., 2016). To the author's knowledge, only a few studies report about diurnal or seasonal acclimation in photosynthesis identifying regulation mechanism and influencing factors under natural environment (Adams and Demmig-Adams, 1995; Ribeiro et al., 2004; Pieruschka et al., 2008; Demmig-Adams et al., 2012; Moura dos Santos et al., 2013). Seasonal response of photoinhibition (based on $F_v/F_m$) in a perennial shrub was for example associated with drought periods (Moura dos Santos et al., 2013). NPQ levels persisted over long or short time period depending on the species and the seasonal condition (Demmig-Adams et al., 2012). Understanding interaction of biological processes with the natural environment is critical for selection of genotypes and prediction of phenotypes under field conditions (Millet et al., 2016; Tardieu et al., 2017).

The photosynthetic response to increasing light intensities under controlled conditions with decreased $F_q'/F_m'$ and increasing NPQ is well studied (Niyogi et al., 1998; Von Caemmerer, 2000). Light response curves are accurately modeled with a function consisting of a square root term, a curvature factor and the asymptote indicating light saturation (Von Caemmerer, 2000). However, response from rapid light curves differed from light curves derived under natural sunlight conditions (Rascher et al., 2000;

Meacham et al., 2017). Compared to controlled conditions, plants exposed to natural conditions showed less performance in electron transport rates at high light intensities (Rascher et al., 2000; Ribeiro et al., 2004; Meacham et al., 2017; Vialet-Chabrand et al., 2017). Possible explanations are long lasting NPQ or increased photoinhibition under natural sunlight (Long et al., 2006; Jia et al., 2013). In agreement, diurnal courses of photosynthesis show typically a midday depression (Ribeiro et al., 2004; Moura dos Santos et al., 2013). Additional processes as occurring sunlight flecks by canopy movement further increase the complexity of photosynthetic response to light in the field (Jia et al., 2013; Kono and Terashima, 2014; Townsend et al., 2017).

Plants grow in a wide range of temperature by optimizing their photosynthetic capacity at given growth temperature (Yamori et al., 2014). However, extreme temperature values (above 35°C and below 4°C) disturb protein functioning and membrane fluidity resulting in decreased performance of photosynthesis (Iba, 2002; Mathur et al., 2014). At hot temperature, photosynthesis is the first affected process in plant cells whereas especially PSII is sensitive to high temperature (Sharkey and Schrader, 2006; Mathur et al., 2014). Temperature affects membrane fluidity, therefore the organization of PSII reaction centers, light harvesting complexes and the OEC (Strasser, 1997; Mathur et al., 2014). Also the PQ within the electron transport chain is sensitive to heat stress (Mathur et al., 2014). After electron transport, ribulose-1,5-bisphosphate carboxylase/oxygenase (Rubisco) activity can be a limited factor under heat stress resulting in increased photorespiration (Wise et al., 2004; Kim and Portis, 2005; Yamori et al., 2012; Mathur et al., 2014). Therefore, net photosynthesis as well as $F_v/F_m$ or $F_q'/F_m'$ are decreased at hot temperature (Wise et al., 2004; Kim and Portis, 2005; Marutani et al., 2012; Wang et al., 2012a).

At cold temperature, net photosynthesis, $F_v/F_m$ and $F_q'/F_m'$ decrease gradually with temperature down to 4°C (Van Heerden et al., 2003; Warren and Dreyer, 2006; Al-Shoaibi, 2008; Sui, 2015). The response to cold stress differs when both shoot and roots or only the shoot are subjected to cold (Strauss and van Heerden, 2011; Suzuki et al., 2011). Subjecting the whole plant to cold temperature resulted in photoinhibition of PSII and decreased $O_2$ evolution compared to non-stressed plants (Suzuki et al., 2011; Krüger et al., 2014). When cold temperature was applied only on the shoot, it resulted in a severe loss of thylakoid membrane function decreasing NPQ capacity and reoxidation efficiency of $Q_A^-$ (Suzuki et al., 2011). Plants acclimate to cold temperature by adjusting the amount of trienoic fatty acids in the chloroplast membrane (Iba, 2002). This process is controlled by the activity of fatty acid desaturases maintaining membrane fluidity and therefore the function of proteins which are integrated into the membrane (Upchurch, 2008). In agreement, overexpression of chloroplast omega-3 fatty acid desaturase gene (*Lefad7*) in tomato increased the content of trienoic fatty acids and maintained higher net photosynthesis than the control after 6h exposure to 4°C (Liu et al., 2013).

Vapor-pressure deficit (VPD) drives leaf transpiration during dry periods with hot temperature (Will et al., 2013; Zhang et al., 2017). Therefore, decreasing sensitivity of leaf transpiration in response to VPD potentially can increase water use efficiency (Zhang et al., 2017). VPD correlates negatively with $CO_2$ assimilation but showed only little effect on fluorescence parameters (Peterson, 1990; Lawson et al., 2002). $C_3$ species showed higher transpiration efficiency than $C_4$ at high VPD (Morison and Gifford, 1983). Low VPD resulted in reduced leaf transpiration rate and increased net $CO_2$ assimilation (Morison and Gifford, 1983; Peterson, 1990; Ribeiro et al., 2004; Zhang et al., 2017). In agreement, decreased rates of photosynthesis were observed in a common bean field trial in semi-arid climate when VPD increased (Moura dos Santos et al., 2013).

Drought stress is a major factor threating agricultural productivity (Parry et al., 2005; Passioura, 2007). Drought stress decreases $F_v/F_m$ and net $CO_2$ assimilation showing significant differences between drought sensitive or drought tolerant genotypes (Wang et al., 2012b; Jedmowski et al., 2013). In response to drought, $F_v/F_m$ decreased less compared to net $CO_2$ assimilation (Wang et al., 2012b). One reported explanation is that the fraction of electron flow through PSII used for carbon assimilation decreased whereas cyclic electron flow increased (Zivcak et al., 2013). This was demonstrated in wheat leaves by measuring PSI absorbance changes and PSII fluorescence simultaneously (Zivcak et al., 2013). Consequently, this stress response is difficult to detect using $F_v/F_m$ parameter since it occurs downstream of $Q_A$. In agreement, drought stress was efficiently detected using fast fluorescence induction which resolves processes as light absorption and electron transport beyond $Q_A$ (Zivcak et al., 2008; Jedmowski et al., 2013; Kalaji et al., 2016). In summary, fluorescence parameters detect a wide range of environmental acclimation of photosynthesis to changing light, temperature, VPD and drought.

### 1.1.3 Photosynthesis on leaf and canopy level

Photosynthetic assimilation rates on canopy level are higher than on leaf level since the light is absorbed by multiple leaf layers per area (Evans, 2013). In addition, photosynthesis changes within the canopy due to acclimation to different light regimes (Kaiser et al., 2017). However, most of photosynthesis studies are conducted with handheld instruments, which restrict the measurement to leaf level. In addition, leaves need to be moved prior to measuring, which can already influence the measurement, e.g. changing the leaf to sun angle can increase NPQ levels within seconds (Ruban et al., 2012). One possibility to overcome this limitation are remote sensing methods which estimate gross primary production on large canopy scale (Guanter et al., 2014; Schickling et al., 2016). This methods are further developed to provide information about plant growth conditions in a high spatial resolution (Rascher et al., 2015). A method between leaf level and regional scale, which provides photosynthetic information in high spatio-temporal resolution, is currently missing.

### 1.1.4 Genotypic selection for improved photosynthesis

Through conventional and molecular breeding as well as genetic modification the harvest index of rice and wheat is reaching a maximum (Parry et al., 2011). In contrast, optimizing photosynthesis efficiency was not much addressed and reveals potential for the increase in biomass and yield, e.g. through selection of photosynthesis efficiency and capacity (Zhu et al., 2010; Parry et al., 2011; Evans, 2013). Quantitative trait locus (QTL) studies suggesting quantitative inherited control of photosynthesis performance resulting in many QTL across the genome (Yin et al., 2010; Czyczylo-Mysza et al., 2013). Detected QTL explained between 5-25% of phenotypic variance with heritability of measured fluorescence parameters including $F_v/F_m$ at around 50% (Yin et al., 2010; Czyczylo-Mysza et al., 2013). QTL of fluorescence parameter were also detected under stress treatments, e.g. drought and salt stress (Guo et al., 2008; de Miguel et al., 2014; Foroozanfar et al., 2014). Genetic modified tobacco plants recovering faster from light protected state under field conditions increased their efficiency of energy use for photochemistry and biomass production (Kromdijk et al., 2016). However, in most of these studies is the measured trait based on the condition at the time of measurement neglecting the highly interactive photosynthetic response to environmental changes.

## 1.2 Spectral and fluorescence measurements

Fluorescence based remote or proximate sensing methods are able to provide fast information about photosynthesis in large scale. In contrast, gas exchange methods measuring $CO_2$ assimilation directly are limited in throughput due to the time to reach steady state level (Driever et al., 2014; Haritha et

al., 2017). There are two distinct approaches to get information about photosynthetic apparatus using fluorescence: (1) passively retrieved fluorescence intensity which is always a side product when (sun) light is absorbed from the antennae and (2) actively manipulating the $Q_A$ redox state by a short, strong light flash in order to fully reduce $Q_A$ and to derive $F_v/F_m$. It is critical to understand that both approaches are not directly comparable: In the first method the result is an absolute value of fluorescence intensity (separated from reflected sunlight or excitation light in the fluorescence region) (van der Tol et al., 2014). In the second approach, this fluorescence intensity (as other reflected irradiation in the detector range) is excluded and only relative fluorescence difference between initial and fully reduced $Q_A$ are measured (Schreiber, 2004).

### 1.2.1 Spectral measurements

The full reflectance spectrum from leaves bares information especially used in remote sensing to retrieve information about plant productivity over large areas (Rascher et al., 2015; Schickling et al., 2016). First, reflectance at specific wavelengths is used to calculate vegetation indices as normalized difference vegetation index (NDVI), MERIS Terrestrial Chlorophyll Index (MTCI) and photochemical reflectance index (PRI) to biophysically assess vegetation status (Dash and Curran, 2004; Prasad et al., 2006; Frampton et al., 2013). More specifically, PRI estimated light or radiation use efficiency (as ratio of net $CO_2$ assimilation and PPFD or absorbed PPFD), photosynthetic efficiency or related isoprenoid emissions (Garbulsky et al., 2011; Peñuelas et al., 2013). NDVI is used for estimation of vegetation productivity and drought detection up to global scale using satellite data (Prasad et al., 2006; Vicente-Serrano et al., 2013). Second, fluorescence can be retrieved from the full reflectance spectrum by separating reflected sunlight from the fluorescence signal (Campbell et al., 2008; Rascher et al., 2015). Retrieval of fluorescence is required since the fluorescence signal contributes with only 2-5% to the total reflected sunlight at 740 nm (Campbell et al., 2008).

The full fluorescence spectrum can be directly measured under lab conditions when the excitation wavelengths are not in the range of fluorescence. The fluorescence spectrum consists of many overlaying peaks (Pancaldi et al., 2002). The two main peaks match the emission of the antennae of both photosystems: fluorescence spectrum of PSII antennae peaks at 685 nm and has a shoulder at 720 nm, whereas the PSI antennae emits fluorescence mainly at 720-740 nm forming the second peak (Bressan et al., 2016; Galka et al., 2012; Wei et al., 2016). The red shift of the second peak origins from special chlorophylls in the PSI antenna dimers absorbing effectively fluorescence at lower wavelengths (Morosinotto et al., 2003; Vacek et al., 1977; Wientjes and Croce, 2011). Therefore, e.g. state transition of PSII antennae moving to PSI can be detected as relative increase of the PSI peak at 720-740 nm (Nellaepalli et al., 2012). Reported fluorescence of PSI in the range of 685 nm are most likely artefacts produced by isolation of the antennae complexes as pointed out by Croce and van Amerongen (2013) or misinterpretation of fluorescence signal (fluorescence intensity taken as $F_m$ signal) as in Franck et al. (2002). The fluorescence intensity is highly dependent on light intensity, temperature and chlorophyll content (Schreiber, 2004; van der Tol et al., 2009). Under natural conditions, sun-induced fluorescence (SIF) signal is sensitive to PPFD, diurnal course, seasonal changes of the vegetation and its architecture (Damm et al., 2015; Rascher et al., 2015; Wieneke et al., 2016). SIF in the 760 nm range shows a diurnal pattern highly correlated with PPFD with some deviation related to NPQ (Pinto et al., 2016; Wieneke et al., 2016). The relation of SIF to electron transport or $CO_2$ assimilation is difficult (Wieneke et al., 2016). Possibly by using DCMU as reference, the SIF values could be used to calculate $F_q'/F_m$ (Pinto et al., 2016). The ratio of different wavelength of the full fluorescence emission spectrum bares information about various stress conditions (Agati et al., 2000; Baldisserotto et al., 2013; Wahadoszamen et al., 2012; Zubik et al., 2013), e.g. it has been shown that decreasing temperature

increased F685 and F735 fluorescence in different species while decreasing F685/ F735 ratio (Agati et al., 1995, 2000). In summary, the passive retrieved fluorescence spectrum bares information about light absorption in the antennae which is not directly linked to photochemistry (van der Tol et al., 2014).

### 1.2.2 Active fluorescence methods

Active fluorescence methods were successfully used to detect a wide range of abiotic stresses (Kalaji et al., 2016). These methods allow to measure variable fluorescence due to $Q_A$ reduction by excluding background irradiation (Schreiber, 2004). The assumptions behind $F_v/F_m$ measurements are that fluorescence yield increase depends on progressively reduced $Q_A$ (Butler, 1978), and that individual fluorescence yield caused by single $Q_A$ does not change during the induction, e.g. due to increased heat dissipation (van Kooten and Snel, 1990). Variable fluorescence originates mostly from PSII, whereas PSI contribution is small and usually neglected (Schansker et al., 2005; Wientjes and Croce, 2012; Lazár, 2013). Variable fluorescence detected in the 680 nm range excludes PSI fluorescence signal, however the signal to noise ratio (S/N ratio) is lower due to higher reabsorption of the generated fluorescence signal (Schreiber, 2004). Since active fluorescence methods manipulate and compare $Q_A$ redox state, background irradiation needs to be excluded from the measuring signal. Background irradiation occurs when measuring in the light or during a SF. The fluorescence signal induced by the measuring beam is called fluorescence yield (Schreiber, 2004). Different methods have been developed to separate the background irradiation from the fluorescence yield (Kolber et al., 1998; Schreiber et al., 1986a; Strasser et al., 1995). In the pulse amplitude modulation (PAM) approach, this is achieved by amplifying the difference of the signal induced by the measuring beam and the signal a few µs *after* the measuring beam (Schreiber, 2004). It is noted that in all active fluorescence methods $F_o$ and $F_m$ are measured with the same measuring intensity allowing comparison of these values and calculation of $F_v/F_m$ (Kolber et al., 1998; Schreiber et al., 1986a; Strasser et al., 1995).

Two approaches using strong light pulses are widely accepted to reduce $Q_A$: single turn-over flash and SF. A single turn-over flash (100-200 µs at >12000 µmol photons $m^{-2}$ $s^{-1}$) allows, in theory, one charge separation and stabilization event in each PS II reaction center, returning a local maximum fluorescence yield ($F_mQ_A$) (Malkin and Kok, 1966; Samson and Bruce, 1996; Kolber et al., 1998; Kalaji et al., 2017). In contrast, $F_m$ is measured during multiple turnover of PS II reaction centers, in which $Q_A$ reduction is followed by reduction of PQ pool (Schansker et al., 2014). This requires a SF which is longer but less intense than a single turn-over flash (Ögren and Baker, 1985; Schreiber et al., 1986a; Schreiber, 2004). During a SF of 15000 µmol photons $m^{-2}$ $s^{-1}$ and 1 s length, both $F_mQ_A$ and $F_m$ can be recorded (Tóth et al., 2007a). An advantage of using single turn-over flashes is that they are less intrusive than SF, allowing higher time resolution and/or longer monitoring of the same measurement spots without affecting the PSII functioning (Osmond et al. 2017). Whereas $F_m$ measurement requires reduction of PQ pool or DCMU inhibition, $F_mQ_A$ is measured by a single turn-over flash when electron transport chain is mainly oxidized (Vernotte et al., 1979; Tóth et al., 2005). This allows standardized examination of fluorescence relaxation kinetics in the dark (Vass et al., 1999). After a single turn-over flash, reoxidation of $Q_A$ is coupled to fluorescence relaxation (Vass et al., 1999). Thus, electron transport from PS II can be studied by analyzing the time constants of $Q_A$ reoxidation (Vass et al., 1999). According to an exponential decay model with three time constants, fluorescence relaxes due to electron transport from $Q_A^-$ to $Q_B$ with a first time constant ($\tau_1$) of 0.1 to 0.2 ms when $Q_B$ site is protonated and occupied by a PQ (Bowes and Crofts, 1980; Vass et al., 1999; Shinkarev, 2004; Petrouleas and Crofts, 2005). The second exponential component represents the electron transfer from $Q_B$ to PQ and its time constant ($\tau_2$) is estimated to be between 2.2 and 10 ms when $Q_B$ site was

vacant (Vass et al., 1999; Eshaghi et al., 2000; Petrouleas and Crofts, 2005). The third component ($\tau_3$) is slow (500 ms to seconds) and interpreted as a backreaction from $Q_A$- to the reaction center and the donor side components of PSII in a dark-adapted state (Vass et al., 1999).

The light-induced fluorescence transient (LIFT) method is a unique approach to probe PS II from a distance under natural conditions (Kolber et al., 1998; Pieruschka et al., 2010; Osmond et al., 2017). The short measuring time of the LIFT method, taking no more than ~0.2 s per measurement, is ideal for integration into automated systems for high throughput phenotyping. In the LIFT standard protocol, $Q_A$ is reduced within 750 µs using fast repetition rate (FRR) subsaturating (actinic) measuring flashlets to induce $F_mQ_A$. Subsequently, a decreasing repetition rate of flashlets allows reoxidation of $Q_A$ which can be simultaneously monitored as fluorescence relaxation. The FRR method has long been applied in marine research (Kolber et al., 1998; Oxborough et al., 2012; Robinson et al., 2014; Suggett et al., 2001). For terrestrial plants, a previously developed LIFT system using a laser excitation source was able to measure fluorescence transients in leaves and canopy from a distance of 50 m (Pieruschka et al., 2010; Raesch et al., 2014). $F_q'/F_m'$ measured with this previous LIFT system correlated well with pulse amplitude modulation (PAM) measurements ($r^2$=0.89) and $CO_2$ assimilation rates ($r^2$=0.94) (Ananyev et al., 2005a; Pieruschka et al., 2010, 2014). Recently, the functional absorption cross section ($\sigma_{PSII}$) derived from the LIFT modeling software has been validated in leaves of barley and Arabidopsis mutants having an altered antenna size (Osmond et al. 2017). In summary, SF and single turn-over flashes are established to measure $F_v/F_m$ and kinetics of the fluorescence relaxation. The LIFT method uses FRR excitation flashlets for proximate sensing of both fluorescence induction and relaxation.

## 1.3 Knowledge gaps and objectives

Knowledge gaps in photosynthesis exist in the area of photosynthetic regulation under natural conditions. These gaps reflect the available methods which are handheld instruments favoring low-throughput measurements under controlled conditions. The following shortcuts were identified:

- Most knowledge was gained under controlled steady-state conditions limiting the understanding of photosynthesis in natural and fluctuating environment (Poorter et al., 2016; Vialet-Chabrand et al., 2017).
- The data sets in current studies are too small to disentangle photosynthetic responses to environmental processes, which are often autocorrelated, e.g. high temperature with high light intensity. Higher temporal data resolution is required to identify key factors, which determine photosynthesis.
- In field studies, only one condition, which is present at time of the measurement, is commonly evaluated. Photosynthetic traits interacting with environment are neglected which leads to unreliable photosynthesis models and inaccurate genotypic selections (Gage et al., 2016; Millet et al., 2016; Meacham et al., 2017).
- Measurements are often done on leaf level while photosynthetic performance is influenced by canopy effects (Evans, 2013; Kaiser et al., 2017). In addition, measuring on leaf level includes the danger that moving the leaf to the instrument affects the photosynthetic status, e.g. by changing the incoming light intensity on the leaf.
- Studies often focus on $F_v/F_m$ parameter, which cannot observe processes downstream of $Q_A$.

A critical step to close the mentioned gaps in knowledge is to understand diurnal and seasonal response of photosynthetic performance under fluctuating conditions (Evans, 2013; Vialet-Chabrand et al., 2017). Therefore, the objectives of this thesis were the following:

- Monitor photosynthesis interacting with fluctuating environmental factors as temperature, light, humidity and drought in high temporal resolution.
- Acquire a large fluorescence and environmental data set by establishing a high-throughput screening system in semi-field and field conditions. Then, identify key factors, which determine photosynthesis in fluctuating conditions. Analyze diurnal and seasonal photosynthesis patterns and determine the influence of spectral indices as NDVI and PRI.
- Assess and quantify the photosynthetic response of specific genotypes in controlled, stress and field conditions.
- Estimate photosynthetic performance on canopy level non-invasively and from the distance.
- Understand the LIFT signal and establish parameters for monitoring processes downstream of $Q_A$ which augment the information of the $F_v/F_m$ parameter.

Regulation and acclimation of photosynthesis in response to natural fluctuating environment was studied by carrying out large automated fluorescence screening in high spatio-temporal resolution (Figure 1). Fluorescence parameters reflecting interaction with the environment were identified and studied from controlled up to field conditions.

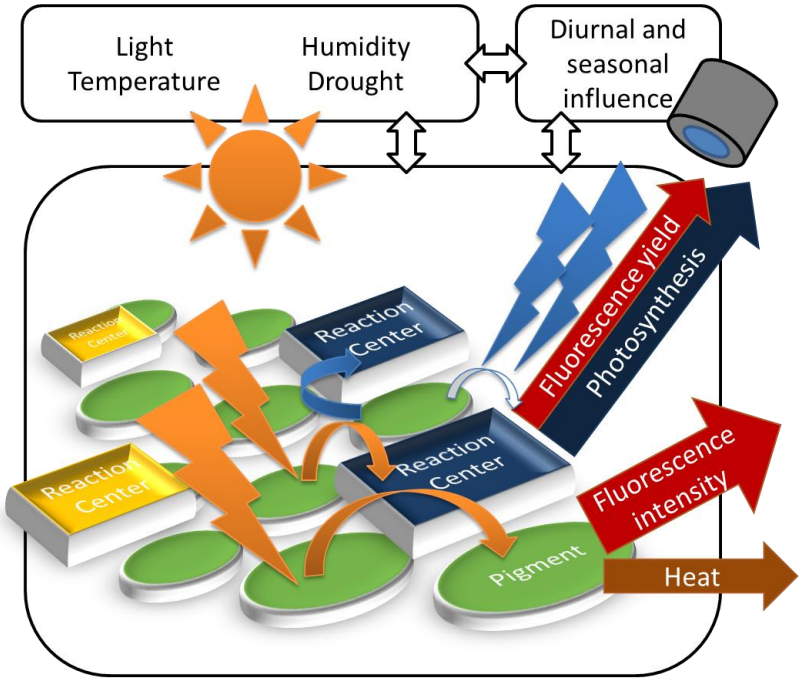


**Figure 1** Pigments organized in the light harvesting antennae of plant thylakoids absorb light energy. The energy is used in three competing pathways (1) stable charge separation reducing $Q_A$ and driving electron transport, (2) emission of absorbed light energy as chlorophyll fluorescence, and (3) dissipation of excess energy as heat (Butler, 1978). Plants optimize energy distribution to these three pathways aiming for maximal use of incoming light energy while protecting itself from excess energy. Acclimation response of photosynthesis to light, temperature, humidity and drought is well studied under steady state conditions. However, the interaction with the environment over diurnal and seasonal stages under natural conditions was often neglected. Therefore a high-throughput system was established inducing and measuring fluorescence yield from the distance while scanning crop canopy.

# 2 Material and methods

Fluorescence measurements were conducted from controlled up to field conditions on various crops and genotypes by using the LIFT method in high-throughput.

## 2.1 Light-induced fluorescence transient (LIFT) instrument

The newly developed compact LIFT instrument (Version LIFT-REM, Soliense Inc., New York, USA) is equipped with a blue LED (445 nm), a STS spectrometer (Ocean Optics, Florida, USA) and two RGB cameras (FLIR Integrated Imaging Solutions Inc., British Colombia, Canada). Subsaturating actinic LED flashlets in FRR induce the maximum fluorescence yield and monitor its relaxation with decreasing repetition rates (Figure 2). Fluorescence is detected at 685 (±10) nm. The excitation protocols are flexible in flashlet number in the reduction phase and flashlet time interval (Table 1). When measuring under ambient light, background irradiation in the range of the detector is determined between the flashlets and subtracted from the fluorescence yield of every flashlet.

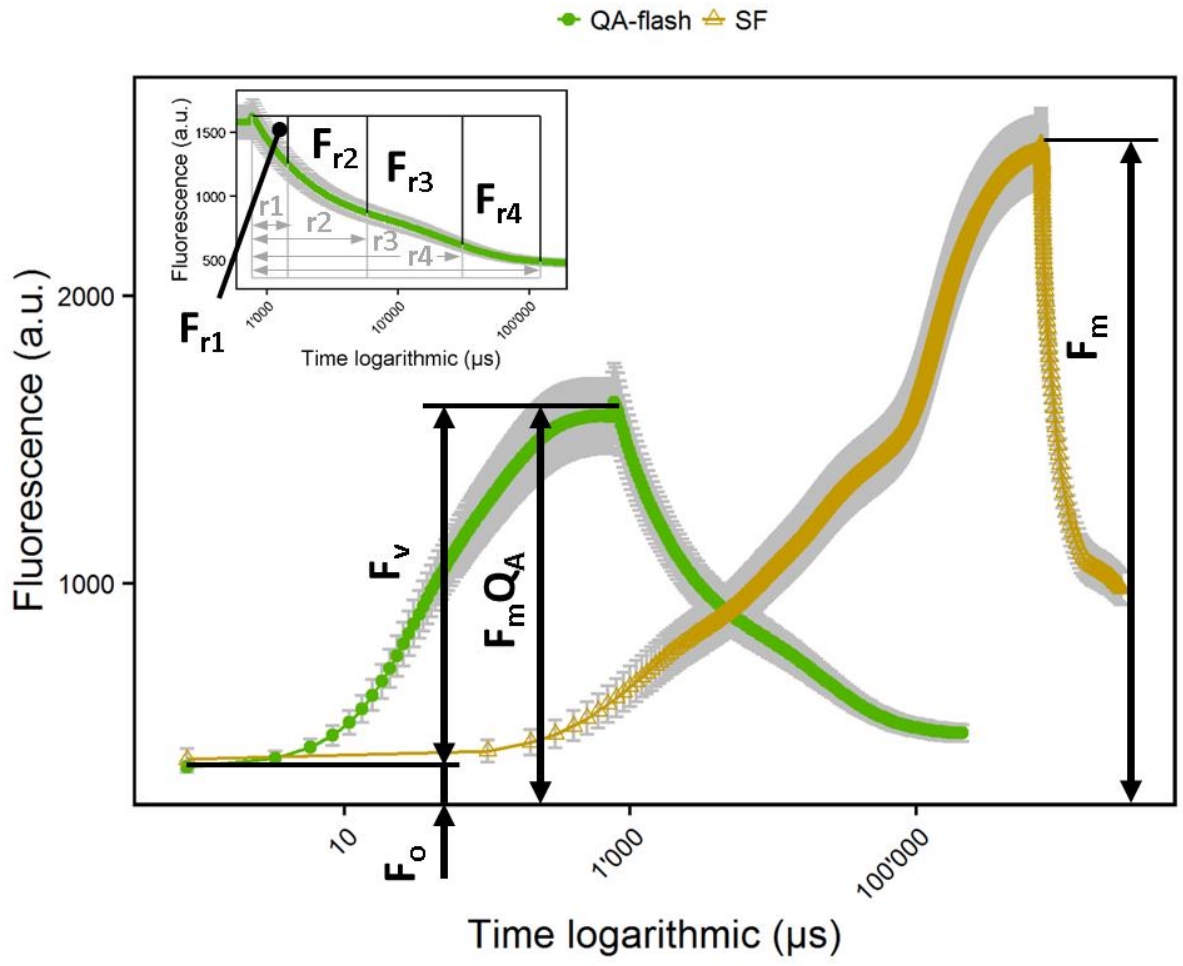


**Figure 2** Fluorescence transient induced by $Q_A$-flash (green circle) and the saturating flash (SF, yellow triangles) using two excitation protocols of the light-induced fluorescence transient (LIFT) device. $Q_A$-flash consists of 300 subsaturating flashlets in the first 0.75 ms following 127 flashes in lower repetition rate allowing relaxation of the fluorescence due to reoxidation of the electron transport chain. Minimum fluorescence ($F_o$), local maximum fluorescence ($F_mQ_A$) and variable fluorescence ($F_v$) out of $Q_A$-flash are used for calculation of quantum efficiency of photosystem II ($F_v/F_m$). The area above fluorescence relaxation curve ($F_{r1}$ to $F_{r4}$) between $F_mQ_A$ and indicated

time point (r1=0.65 ms, r2=5 ms, r3=30 ms and r4=120 ms after $F_mQ_A$ was reached; see inset) were used to calculate corresponding reoxidation efficiency ($F_{r1}/F_m$ to $F_{r4}/F_m$). The SF induces maximum fluorescence ($F_m$) by 7500 subsaturating flashlets within 750 ms. Error bars show standard deviation of n=6 spinach plants (modified from Keller et al. *submitted*).

### 2.1.1 Calibrations

In order to ensure consistent fluorescence yield during an excitation protocol, detected fluorescence signal is internally normalized against excitation power to compensate for small fluctuation of excitation power within the series of flashlets. Additionally, the fluorescence signal is corrected against a fluorescence reference standard to correct for detector noise. In order to determine the intensity of a given excitation power during FRR fluorescence induction, a calibration flash is required because the induction phase is too short to measure with a quantum sensor. This phase cannot be extended due to limitation in excitation power. Therefore, the FRR series is performed at 1% of excitation power which allows to extend the length of induction phase to a few seconds. Excitation power at specified distance was measured with a quantum sensor (LI-190R, LI-COR, Inc.) using the calibration flash and then extrapolated to 100%.

**Table 1** Fast repetition rate (FRR) excitation protocols are shown. In the reduction phase flashlet interval is constant for given amount of flashlets and interval, while it increases exponential in the relaxation phase to allow reoxidation of the primary quinone. Flashlet length is always 1.6 µs and has in all flashes the same specified excitation power.

| FRR protocol | Reduction phase (ms) | Number of flashlets in reduction phase | Flashlet interval reduction phase (µs) | Relaxation phase (ms) | Number of flashlets in relaxation phase | Flashlet length (µs) |
|---|---|---|---|---|---|---|
| QA flash | 0.75 | 300 | 2.5 | 209 | 127 | 1.6 |
| Prolonged QA flash | 2.5 | 1000 | 2.5 | 209 | 127 | 1.6 |
| Saturating flash | 750 | 7500 | 100 | 1975 | 127 | 1.6 |

### 2.1.2 Fluorescence data processing

The fluorescence transient data acquired by the LIFT $Q_A$-flash represent complex processes of $Q_A$ reduction and reoxidation. In order to quantify these main processes, the fluorescence transients were analyzed on empirical basis. The underlying mechanisms are determined by different S-states and $Q_B$ redox states which lead to 600 possible combinations of $Q_A^-$ reoxidation pathways (Rascher and Nedbal, 2006). These combination of pathways can only be assessed by modeling. The LIFT software offers the possibility to model the fluorescence transient by defining many parameters (based on Kolber et al. 1998; see http://soliense.com/LIFT_Terrestrial.php).

*Minimum and maximum fluorescence retrieval*

On an empirical basis, $F_v$ represents the difference between $F_o$ as the fluorescence yield of the first flashlet and $F_mQ_A$ as the averaged fluorescence yield of 301$^{st}$ and 302$^{nd}$ flashlet. The 300$^{th}$ flashlet is not representing $F_mQ_A$ due to quenching processes in the induction phase (Figure 3). $F_v/F_m$ was calculated using $F_mQ_A$, i.e. $(F_o - F_mQ_A)/F_mQ_A$. This will result in systematic lower $F_v/F_m$ values when calculated with $F_mQ_A$ compared to values calculated with $F_m$. However, the two approaches produced highly correlated values (Pieruschka et al., 2010; Keller et al., submitted).

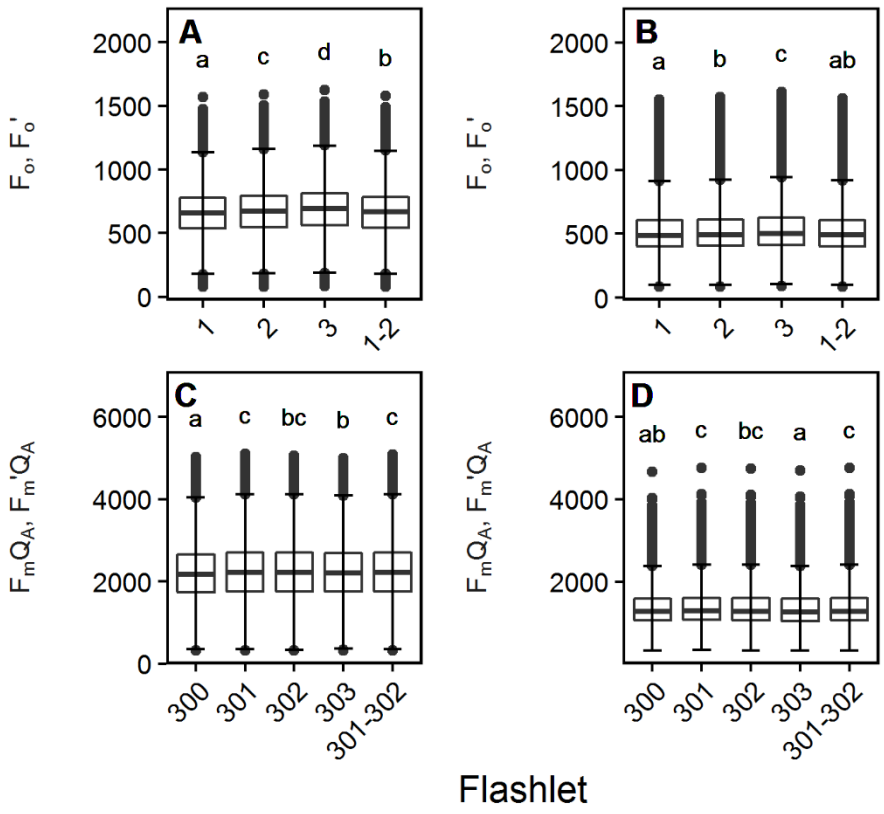


**Figure 3** Quantitative data showed the effect of flashlet number to fluorescence yield of $F_o$ (A, B) and $F_mQ_A$ (C, D) using $Q_A$-flash. Barley (A, C) and soybean (B, D) genotypes were measured diurnal at October 14 to 29, 2016 (n=26'574) and July 2 to 4, 2017 (n=32'630), respectively, in an unheated greenhouse. Box represents inter-quartile range, bold horizontal bar the median, the discontinuous lines the upper and lower quartile, and outlier data points (>1.5 × inter-quartile range) are depicted by a point. Means with different letters differ significantly using Tukey's multiple comparisons of means.

*$Q_A^-$ reoxidation efficiencies*

Efficiency of reoxidation after $Q_A$ reduction ($F_r/F_m$) is coupled to the kinetics of fluorescence relaxation. $F_r/F_m$ parameter was calculated as the area above the fluorescence curve in a specific time range (r) normalized with the area given by $F_m$ in that time range (Figure 2). For a detailed description, the reader is refered to Keller et al. *submitted*. Time ranges, r1 to r4, were chosen to catch reoxidation processes which have different time constants. The time ranges of r1 and r2 represent approximately the first and second exponential decay phases of fluorescence (Vass et al., 1999). This phases are pronounced in the dark when the photosynthetic apparatus is not active but are not visible in the light (Figure 4). Time ranges were the following:

r1 from 0.8 ms to 1.47 ms (0.65 ms)

r2 from 0.8 ms to 5.9 ms (5 ms)

r3 from 0.8 ms to 31 ms (30 ms)

r4 from 0.8 ms to 122 ms (121 ms).

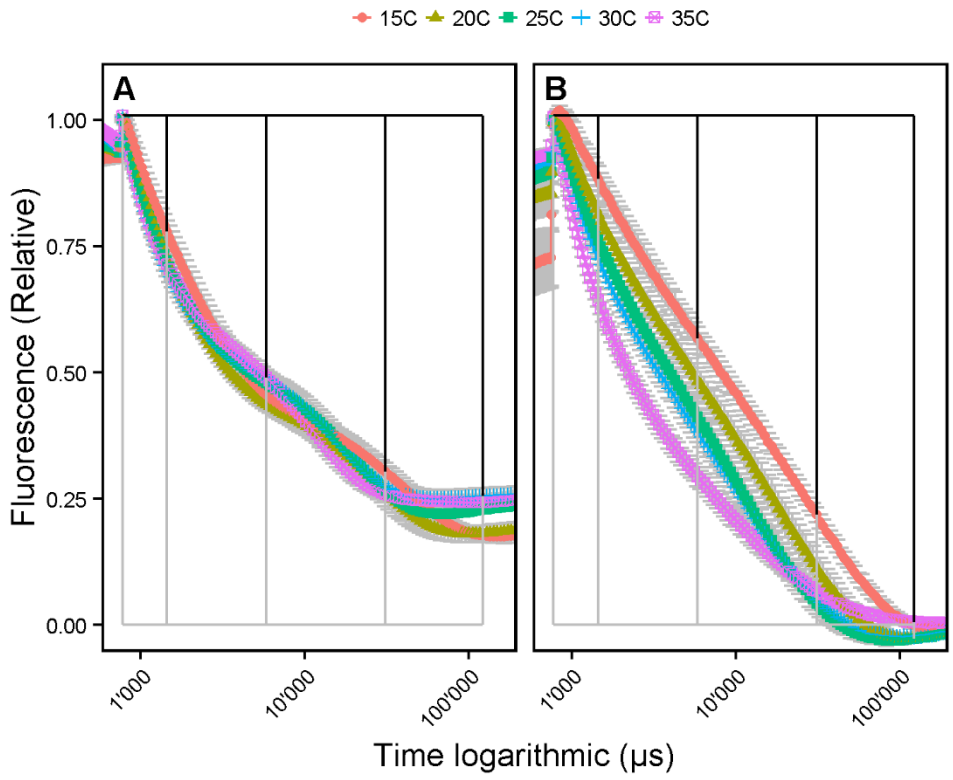


**Figure 4** Fluorescence relaxation of Arabidopsis leaves acquired in the dark (A) and under 100 µmol photons $m^{-2}$ $s^{-1}$ of blue light (B) using $Q_A$-flash. Fluorescence relaxation was faster with increasing temperatures. In the dark, different phases of fluorescence relaxation were visible whereas in the light the relaxation was more linear. Vertical lines indicate time points which were used to calculate reoxidation efficiencies. Error bars show standard deviation of n=6 plants.

*Further parameter retrieval*

Light absorption efficiency ($F_i/F_m$) was calculated as the mean of the fluorescence yield from 0 ms to 0.03 ms normalized with $F_m$. In this short initial time range, electron transport is assumed to be negligible (Shinkarev, 2004). Carotenoid quenching (carQ) was assessed as difference between $F_m$ and the mean of the fluorescence yield of flashlets number 299 and 300. This quenching manifested itself as an instantaneous fluorescence peak when the quenching relaxed upon changing from high- to low-repetition-rate flashes (Figure 4). The phenomena is attributed to carotenoids since carotenoid triplets quench fluorescence when operating with flashes at high excitation power (Schödel et al., 1999; Steffen et al., 2001; Braslavsky and Holzwarth, 2012). S/N ratio was calculated as the standard deviation of fluorescence yield from flashlets number 280 to 300 normalized with $F_m$. In this region the signal is expected to be stable since $Q_A$ is mainly reduced.

*Model settings*

The fluorescence transient data obtained by the LIFT instrument can be fitted to a model by which parameters like $\sigma_{PSII}$, $\tau_1$ to $\tau_3$ and $F_v/F_m$ can be derived using the LIFT software (based on Kolber et al. 1998; see http://soliense.com/LIFT_Terrestrial.php). The following settings were chosen to fit data obtained in the *Miniplot* facility:

$F_o$, $F_mQ_A$, $\sigma_{PSII}$, $\tau_1$ - $\tau_3$, oxidized size of PQ pool, the probability of energy transfer (p), and the amplitude of the backreaction of the back-reaction (Cx) from $Q_A$ to the reaction center (RC) and carQ were fitted by the model. The time constants of the backreaction was constrained to constant 400 ms in order to limit the degree of freedom in the fitting procedure, but allowing Cx to vary. Similarly, the amplitude of carQ was set to 80 and charge recombination ($fQ_B$) to zero. The $\tau_1$ was set to ≥100 µs and the minimal ratio of $\tau_2$ to $\tau_1$ was set to 0.1. Applying these constraints marginally affected the quality of the fit as judged from the $\chi^2$ and the distribution of residuals. Note that allowing all the chosen parameter to fit bears the danger of overfitting the model and increasing the standard deviation of the fitted values.

## 2.2 Controlled conditions

LIFT measurements were carried out under controlled conditions in the lab or growth chamber. Plants and isolated thylakoids were subjected to various treatments, which manipulate fluorescence induction and relaxation.

### 2.2.1 Spinach

In total, 36 spinach (*Spinacia oleracea*) plants of genotype Matador were grown in the greenhouse under 16 h/8 h day/night cycle at 20 °C/18 °C. Light intensity was between 60-300 µmol photons $m^{-2}$ $s^{-1}$. 400 ml pots were filled with a turf-clay substrate (ED73, Einheitserdewerke). Plants were watered automatically twice a day during cultivation for 28 or 32 days.

*Anaeorobiosis induction in nitrogen atmosphere*

Oxygen depletion inhibits the plastid terminal oxidase (PTOX) which in control conditions keeps PQ in a oxidized state in the dark (Bohme et al., 1971; Cournac et al., 2000; Feilke et al., 2014). Thus this treatment was used to study PQ reduction non-invasively on living plants (Tóth et al., 2007b)

LI-6400XT transparent chamber head (2x3 cm window, LI-COR, Inc., Nebraska USA) was used to create anoxic atmosphere. Air inflow into the chamber came either from the ambient air (as control, with 400 ppm $CO_2$) or from $N_2$ gas supply without oxygen (containing less than 1.5 ppm $CO_2$). A fully expanded leaf was measured with LIFT after 5-min exposure to control or $N_2$ atmosphere using 5 $Q_A$-flashes followed by one SF. After another 5 min leaves were measured again using 5 prolonged $Q_A$-flashes. Number of replicates was n=6 plants.

*DCMU treatment*

3-(3,4-dichlorophenyl)-1,1-dimethylurea (DCMU) inhibits reoxidation of $Q_A$ and was used to validate $F_m$ induction (Lazár, 1999). Plants were dark-adapted overnight, then a fully expanded leaf was left untreated or was subjected to 200 µM DCMU in 50 ml Milli-Q water (Tóth et al., 2005). 1% alcohol in distilled water showed no effect on $F_m$ but in the fluorescence rise of DCMU treated leaves compared to untreated leaves (Tóth et al., 2005). Therefore, control was left untreated and no alcohol was used in the DCMU solution to avoid side effects (Haldimann and Tsimilli-Michael, 2005). DCMU dissolved almost completely in water. One leaf per plant were left for 6 h in DCMU solution in the dark, then wiped, left for 30 minutes in the air and measured (n=6 plants).

*Measurements*

Measurements were carried out in control and anoxic conditions on control and DCMU treated plants (n=6 plants). Prior to measurements, plants were dark-adapted overnight. Then, light response curve consisting of 160 $Q_A$-flashes, 40 $Q_A$-flashes at each light intensity level in a 5 s interval, were conducted on the control plants. Light intensities were 30, 100, 300, 700 µmol $m^{-2}$ $s^{-1}$ (see also section 2.2.5).

### 2.2.2 Arabidopsis

The effect of temperature and far-red irradiation on the fluorescence relaxation was assessed in Arabidopsis *(Arabidopsis thaliana)* plants. Col-0 genotypes were grown at 23°C in 12/12 h day/night cycle in the growth chamber at around 150 µmol photons $m^{-2}$ $s^{-1}$. Plants were measured under increasing blue light intensities at different temperatures in a transparent LI-COR chamber head (LI-COR, Inc., Nebraska USA) in one experiment and with far-red background irradiation in a second experiment.

*Measurements*

Blue light curves at different temperatures were conducted 63 days after sowing (DAS). At 59 DAS, plants were subjected for four days to fluctuating temperature between 15-35°C. The temperature increased in the light and decreased in the dark. Temperature steps were 5°C in two hours intervals followed by 4 hours at 20°C. Then, plants were measured at 25°C, 35°C and the following day at 20°C, 15°C and 30°C. Plants were dark-adapted for 30 min prior to measurements (n=5 plants). The light response curve consisted of 160 $Q_A$-flashes, 40 $Q_A$-flashes at each light intensity level in a 1.5 s interval. Light intensities were 80, 100, 200, 400 µmol $m^{-2}$ $s^{-1}$. Transition between temperatures took about 20 min. The air humidity in the climate chamber was kept constant at around 50-70%. LI-COR sensor were matched at every temperature step and after every second measurement.

In the far-red experiment, Col-0 plants grew for 45 days. Plants were measured at room temperature after dark adaptation for 30 min and after 10 s exposure of blue light at 300 µmol photons $m^{-2}$ $s^{-1}$ using $Q_A$-flash. The measurements were done with and without approximately 1 µmol photons $m^{-2}$ $s^{-1}$ background irradiation of 740 nm wavelength (n= 5 plants).

### 2.2.3 Maize

The effect of drought on the fluorescence transient was assessed in maize (*Zea mays*) plants. 12 maize plants of genotype B73 and Mo17 were grown in the greenhouse under 16 h/8 h day/night cycle at 20 °C/18 °C. Light intensity was between 60-300 µmol photons $m^{-2}$ $s^{-1}$. 400 ml pots were filled with a turf-clay substrate (ED73, Einheitserdewerke). Plants were watered automatically twice a day during cultivation for 27 and 35 days for drought and control treatment, respectively. Drought treatment did not receive water for the last 8 days.

*Measurements*

The light response curve consisted of 200 $Q_A$-flashes, 50 $Q_A$-flashes at each light intensity level in a 1.5 s interval. Light intensities were 100, 300, 800, 2000 µmol $m^{-2}$ $s^{-1}$. Plants were dark-adapted for 30 min prior to measurements (n=4 plants). Before and after the light curve 50 $Q_A$-flashes were applied in the dark. The youngest fully expanded leaf was measured.

### 2.2.4 Isolation of thylakoids and particles

For isolation of spinach thylakoids and Berthold, Babcock, Yocum particles (BBY, PSII core particles), fresh spinach leaves were bought from a local supermarket and prepared as described in Berthold et al. (1981). For measurements with LIFT and FL3000, the final concentration of thylakoids was adjusted to equivalent chlorophyll *a* concentration of 10 µM (10 µg/mL).

*DCMU and DBMIB treatment*

DCMU and 2,5-dibromo-5-methyl-6-isopropyl-benzoquinone (DBMIB) which selectively inhibit reoxidation of $Q_A$ and PQ, respectively, were used to manipulate fluorescence relaxation in thylakoid samples (Lazár, 1999; Kurisu et al., 2003). Thylakoids were dark-adapted overnight, then 3 ml were

transferred to transparent plastic cuvettes. DCMU and DBMIB was added to final concentration of 5 µM (1.17 µg/mL) and 0.66 µM (0.213 µg/mL). Samples were stirred manually followed by either LIFT or FL3000 measurements. The number of technical replicates was 5, except for DBMIB, DCMU and thylakoid in the FL3000 method it was 3.

### 2.2.5 LIFT measurements

All measurements were done at 60 cm distance. For the DCMU and DBMIB experiment, the excitation power was approximately 20000 µmol photons $m^{-2}$ $s^{-1}$ for the fluorescence induction phase using the $Q_A$-flash protocol (Table 1). For intact plants excitation power was 40000, 24000 and 1000 µmol photons $m^{-2}$ $s^{-1}$ for the fluorescence induction phase using $Q_A$-flash, prolonged $Q_A$-flash and SF, respectively.

*Light response curves*

The blue LED of the LIFT instrument was used as actinic light source. The size of the illumination spot was around 3 $cm^2$. The intensity of the blue LED was calibrated by using a quantum sensor (LI-190R, LI-COR, Inc.) at 60 cm distance. Fluorescence spectrum (600-800 nm) is acquired after each $Q_A$-flash from the build in STS spectrometer (Ocean Optics, Florida, USA) between the measurements. Signal was corrected against detector noise recorded in the dark at each temperature.

A fully expanded leaf was placed into LI-6400XT transparent 2x3 cm chamber head (LI-COR, Inc., Nebraska USA) and measured with the LIFT instrument through the transparent film of the chamber. The air flow rate during the measurements was 300 µmol air $s^{-1}$ and block temperature was kept at 20°C. Measured leaf area was. $CO_2$ concentration in the air was controlled at 400 ppm and air flow was set to 400 µmol $s^{-1}$.

Electron transport rates (ETR) were calculated from gas exchange data with the formula:

$$ETR_{LI\text{-}COR} = (A+R_d)(4C_i+8T^*)/(C_i-T^*) \quad (1)$$

where A is $CO_2$ assimilation rate in µmol $m^{-2}$ $s^{-1}$, $R_d$ is respiratory photosynthesis measured in the dark in µmol $m^{-2}$ $s^{-1}$, $C_i$ is intercellular $CO_2$ in µmol $mol^{-1}$ and T* is the $CO_2$ compensation point in the absence of respiration in µmol $mol^{-1}$ (Bernacchi et al., 2001; Yamori et al., 2012). T* values were determined by Bernacchi et al. (2001). $ETR_{LI\text{-}COR}$ were corrected with a factor of 0.75 to roughly account for that the excitation area was smaller than the chamber. ETR derived by LIFT were calculated as:

$$ETR_{LIFT} = F_q'/F_m' * \text{blue light intensity} * 0.5 * 0.8 \quad (2).$$

**Figure 5** Experimental set-up of combined light-induced fluorescence transient (LIFT) and gas exchange measurements. The leaf was placed in a LI-COR chamber head which allowed measurements of $CO_2$ assimilation in a highly controlled environment. LIFT device was mounted to an tripod allowing perpendicular fluorescence measurements of Arabidopsis leaves at 60 cm distance. Measurements took place in the dark using the actinic blue light of the LIFT device as light source.

### 2.2.6 FL3000 measurements

Fluorescence relaxation after a single turn-over flash was monitored by weak, non-actinic measuring flashes in increasing time intervals (Trtilek et al., 1997; Vass et al., 1999). The double-modulated fluorescence measurements were performed with an FL3000 fluorometer (Photon Systems Instruments Ltd., Brno) (Trtilek et al., 1997). The instrument had red LEDs (639 nm) for both actinic (20 µs, excitation power 1020 µmol photons $m^{-2}$ $s^{-1}$ for actinic light) and measuring (8 µs) flashes, with a measuring delay of 7 µs. By using the double-modulation technique, changes in fluorescence yield can be measured in a very broad time range, from 100 µs to 100 s, during which reoxidation of $Q_A$ by both forward and backward reactions can be studied (Vass et al., 1999). The FL3000 method monitors the reoxidation phase after a short high light flash. Measurements were repeated on three biological replicates.

## 2.3 Semi-field conditions

The *Miniplot* facility equipped with an automated measuring platform is located in an unheated greenhouse without additional lighting (Thomas et al., submitted). The *Miniplot* facility hosts a total of 90 growth containers (111 x 71 x 61 cm) with a volume of 535 liters filled with soil from the CKA field site. Containers were watered with approximately 16 liters per week using drip irrigation. The amount was increased to up to 36 liters per week in hot weather conditions.

### 2.3.1 Maize

Different maize (*Zea mays*) genotypes were evaluated over two seasons including one drought treatment in 2016. Genotypes B73 and Mo17 were planted in 7 containers on May 13, 2016. These genotypes are the parental lines of a population often used for QTL studies (Lee et al., 2002; Benke et al., 2014). 12 plants per container were arrayed into two rows (40 cm row distance). On June 15, 30 g Hakaphos® yellow (COMPO EXPERT GmbH) per container was applied. At the same day, the drought treatment started in 2 plots of both genotypes reducing the watering to 10% compared to control. Additional genotypes of the German Plant Phenotyping Network (DPPN) reference collection, named B, D, I, F, K were sown on May 24, 2016. Genotypes were grown in 10 containers (2 replicates each). In 2017, 9 genotypes of the DPPN reference, named A, B, C, D, G, H, I, J and K were sown on May 30. Genotypes were grown in 18 containers (2 replicates each).

### 2.3.2 Soybean

Soybean (*Glycine max*) genotypes differing in cold tolerance were kindly provided from the Swiss soybean breeding program of Agroscope in Changins. Genotypes Amarok, Gallec and Tourmaline are tolerant to cold whereas 22216, S1 and Protibus are cold sensitive. S1 is registered in Canada, Amarok in Germany, 22216 is not registered yet and the others are registered in Switzerland (Bundesamt für Landwirtschaft, 2015; Bundessortenamt, 2017). MinnGold, Eiko (Asgrow, USA) and Bahia genotypes were provided by the University of Udine which selected them in the framework of the fluorescence explorer (FLEX) campaign.[1] The MinnGold genotype has a chlorophyll-deficient phenotype caused by a spontaneous mutation in the Mg-chelatase subunit gene (ChlI1a) (Campbell et al., 2015). In 2016, soybean genotypes were sown on August 19 directly into the containers of the *Miniplot*. Seeds were planted in two rows every 10 cm in about 3 cm depth (22 seeds per container, 40 cm row distance). 5 genotypes in 2 replicates and 1 genotypes in 4 replicates were planted in 14 containers. In September 20, each container was fertilized with 30g Hakaphos® blue (COMPO EXPERT GmbH). On October 5, drought treatment started in three containers reducing the amount of water to 10% compared to the control containers.

In 2017, 8 soybean genotypes were germinated in controlled greenhouse for 2 weeks at approximately 20°C. Then at March 23, plants were transplanted into containers in the *Miniplot*. 16 plants per container were arrayed into two rows (40 cm row distance). 6 genotypes in 4 replicates and 2 genotypes in 2 replicates were planted in 28 containers. 34 days after seeding (DAS), plants were fertilized using 24 g Hakaphos® blue (COMPO EXPERT GmbH) per plot (around 3.6 g N per plot or 0.2 g N per plant). LIFT instrument beam was focused at a measuring distance of 1.4 m until June 21, 2017 and then adjusted to 1.2 m.

*Height / distance experiment*

Leaves of genotype Tourmaline were fixed with three needles on top of a bamboo stick 30 cm above ground horizontal to the LIFT lens. Four leaves per plot in 4 plots were fixed (n=16). Automated platform measured changing the distance randomized from 120 cm in 15 cm steps to 75 cm. Every leave was measured with randomized distance in 14 min intervals allowing oxygen evolving complex to relax in the dark.

[1] http://www.esa.int/Our_Activities/Observing_the_Earth/FLEX_takes_on_mutants; visted on January 22, 2018

### 2.3.3 Barley

Publicly available barley (*Hordeum vulgare*) genotypes differing in powdery mildew were selected for detecting disease resistance against powdery mildew (Thomas et al., submitted). Irina and Eileen were selected as resistant genotypes, Milford and Gesine as intermediate and Grace and Tocada as susceptible (Bundessortenamt, 2013). Barley genotypes were grown in the *Miniplot* and inoculated with powdery mildew 46 DAS (Thomas et al., submitted). In 2015, the six barley genotypes were sown at November 9 into 12 containers (2 replicates). Inoculation with powdery mildew pathotype was at December 26. In 2016, the same six barley genotypes were sown at September 16 into 12 containers (2 replicates). Inoculation with powdery mildew pathotype was at November 2.

### 2.3.4 Wheat

For the wheat (*Triticum aestivum*) experiment with drought treatment, Brilhante, PF37 and PF62 genotypes were selected (Poersch-Bortolon et al., 2016). 50 seeds per meter in 15 cm row distance (5 rows per container) were sown on May 12, 2016. On June 15, 30 g Hakaphos® blue (COMPO EXPERT GmbH) per container was applied. On June 2, started the drought treatment in wheat reducing the amount of water to 10% compared to the control containers.

### 2.3.5 Rapeseed

Major and Sensation genotypes of Rrapeseed (*Brassica napus*) were germinated in the field in 2015 and transplanted to the Miniplot containers in early November 2015. About 16 plants per container were planted. The two genotype were grown in eight containers (four replicates per genotype).

### 2.3.6 Automated measurements

Fully automated measurements took place from December 2015 to August 2017 using the measuring platform of the *Miniplot* facility. Every hour, crop canopy of the containers was scanned by one or two LIFT devices in 3 x 300 mm steps at around 30 mm/s speed (Figure 6).

*Fluorescence screening*

The distance from the LIFT lens to soil was 1.5 m, focused at 1.4 m then focus was adjusted when plants were growing. Measuring spot was around 30 mm in diameter, hence about 700 $mm^2$. Excitation energy in the reduction phase of $Q_A$-flash protocol was about 40000 µmol photons $m^{-2}$ $s^{-1}$ in 60 cm distance. Fluorescence measurement took 210 ms, followed by spectral measurements with 1790 ms integration time. In that mode, every two seconds one measurement was acquired resulting in 5 to 7 measurements merged to the four positions per 300 mm step for both spectral and fluorescence measurements (Figure 7). In total, about 18 independent measurements were acquired for each row operating with one LIFT devices. Third measurement was excluded since it most likely measured the same spot due to the stop of the positioning system after 300 mm. For the experiments in 2017, it was about 36 measurements since two LIFT devices operated simultaneously hanging next to each other from the moving platform.

*Recovery from non-photochemical quenching (NPQ)*

Leaves were exposed to approximate 1000 µmol photons $m^{-2}$ $s^{-1}$ of blue light for three minutes to induce NPQ. The recovery of NPQ was monitored directly afterwards (after 2 and 10 s) as well as after 120 s, 420 s and 900 s. The time between the monitoring of the recovery was used to induce NPQ in new leaves at new position allowing around three times higher throughput.

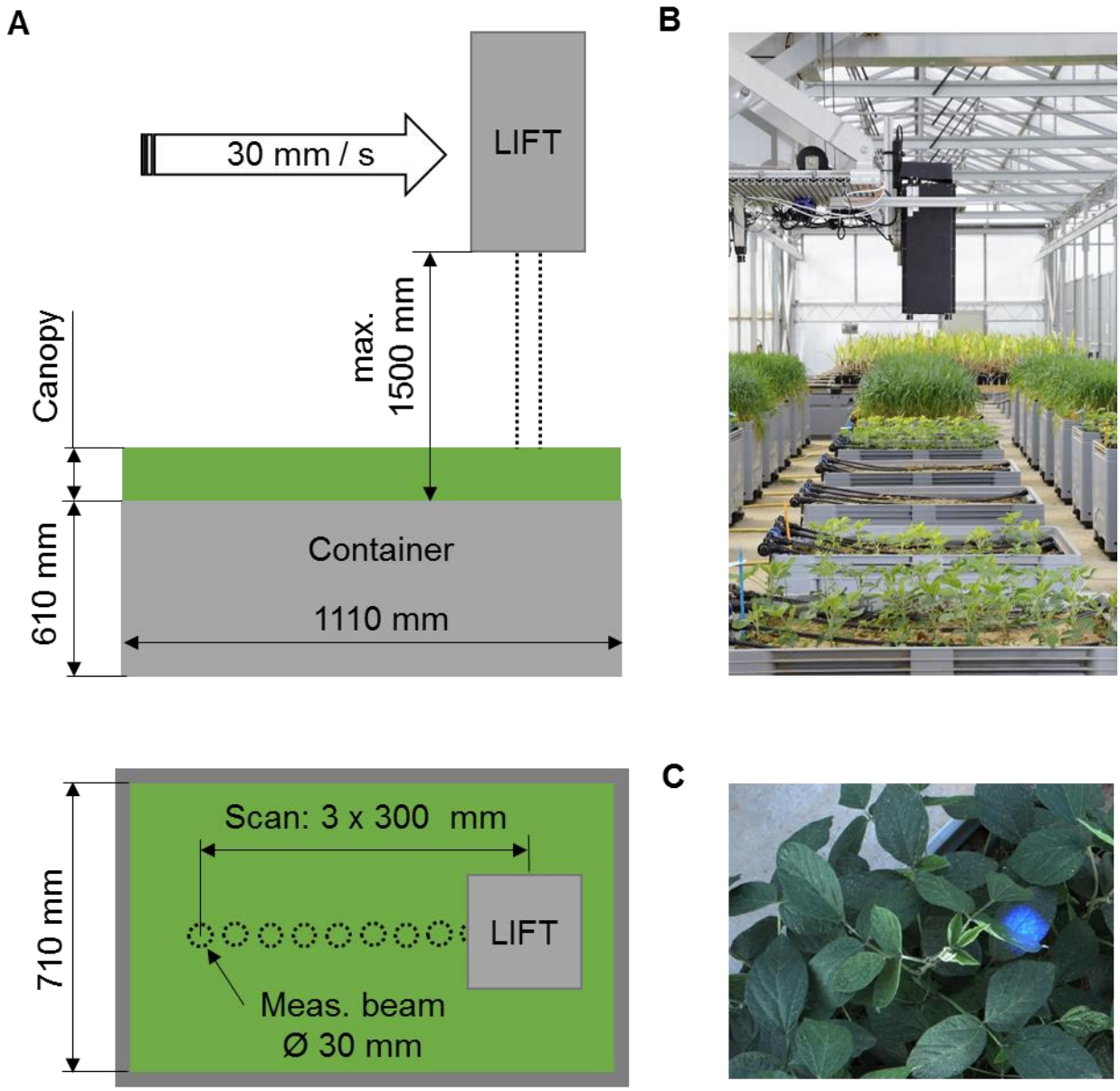


**Figure 6** High-throughput photosynthesis screening was realized using a light-induced fluorescence transient (LIFT) devices mounted to an automated positioning system. Fluorescence data is acquired from approximately 1 m distance while scanning over the crop canopy (A). The plants were grown in up to 90 containers (1110 x 710 x 610 mmm) in the *Miniplot* facility located in an unheated greenhouse (B). In order to retrieve the fluorescence signal, the measuring flashlets excite a circle of approximately 30 mm in diameter within 210 ms in an interval of 2 s (C). This results in a canopy measurement about every 60 mm and takes less than 1 min per container.

*Spectral measurements*

Spectral measurements were taken from 400 to 800 nm in 0.46 nm resolution. The detector temperature of the spectrometer was kept between 20 and 35°C. Raw digital numbers from the spectrometer output were averaged to even wavelengths and then used to calculate pseudo spectral indices. The pseudo spectral indices are marked with a *p* in the beginning of the abbreviation, e.g. pseudo normalized difference vegetation index (pNDVI). In addition, spectral indices were roughly corrected using a grey reference (50% reflectance of incoming irradiation) in the middle of every measuring round, i.e. once per hour. In that way, sunlight spectra were acquired from May 15 to 18,

2017 and merged to PPFD values recorded at the same time from an independent quantum sensor (see section 2.5). Reference spectra were averaged in steps of 10 PPFD in order to generate a look up table of reference spectra covering a range from 100 to 1350 µmol photons $m^{-2}$ $s^{-1}$ (Figure S 1). Finally, raw digital numbers of the spectral measurement were associated with PPFD value measured at the same time and corrected using closest reference spectra (Figure 8). NDVI, green normalized difference vegetation index (GNDVI), MTCI and PRI were calculated as the following:

NDVI = (R750-R706) / (R750+R706) adapted from Frampton et al. (2013)
NDVI_II = (R740-R680) / (R740+R680) adapted from Frampton et al. (2013)
MTCI = (R754-R710) / (R710+R680) adapted from Dash and Curran (2004)
PRI = (R530-R570) / (R530+R570) adapted from Gamon et al. (1992)
GNDVI = (R740-R540) / (R740+R540) adapted from Frampton et al. (2013)

where R indicates the used wavelength from the corrected signal. The same wavelengths were used to calculate the pseudo indices using the raw digital signal. The parameter called reflectance was calculated as the sum of the raw signals in all wavelengths. The parameter called absorbance was calculated based on corrected values as integral in the range from 500 to 700 nm subtracted from 100% reflectance given by the reference look up table.

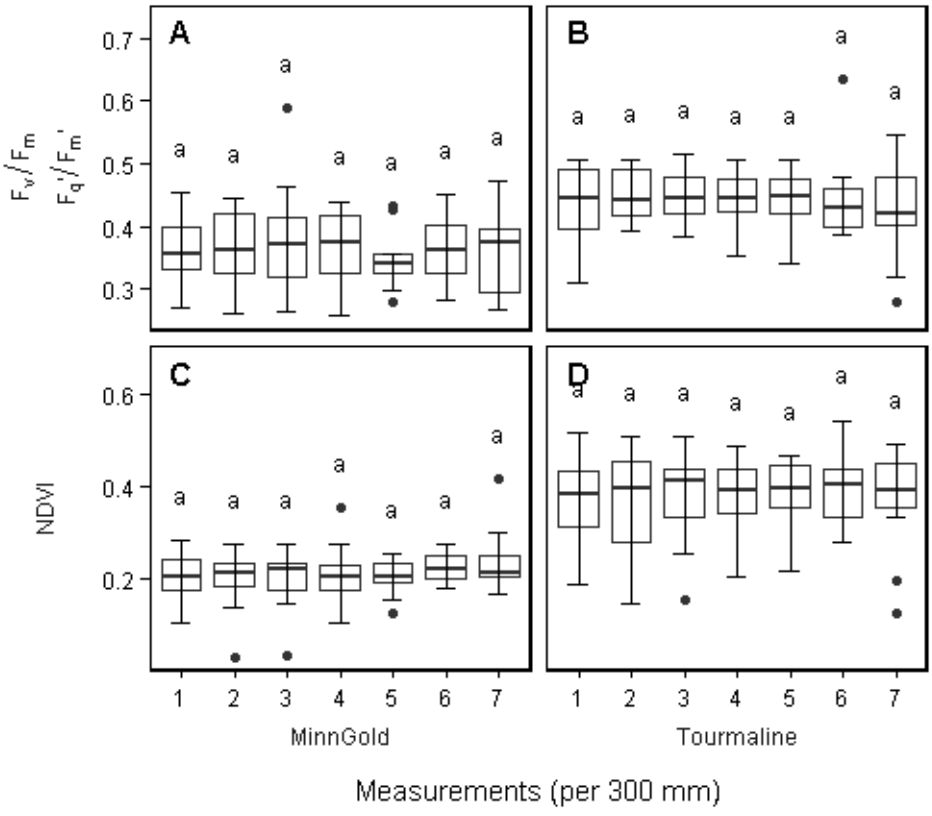


**Figure 7** Boxplot of quantum efficiency of the photosystem II ($F_v/F_m$ in the dark and $F_q'/F_m'$ in the light), and normalized difference vegetation index (NDVI) for genotype MinnGold (A, C) and Tourmaline (B, D) measured while scanning the crop canopy at May 12, 2017. Up to 7 measurements were taken at noon in 4 containers per genotype in 3 x 300 mm scans. Box represents inter-quartile range, bold horizontal bar the median, the discontinuous lines the upper and lower quartile, and outlier data points (>1.5 × inter-quartile range) are depicted by a point. Means with different letters differ significantly using Tukey's multiple comparisons of means (n=13 to 16).

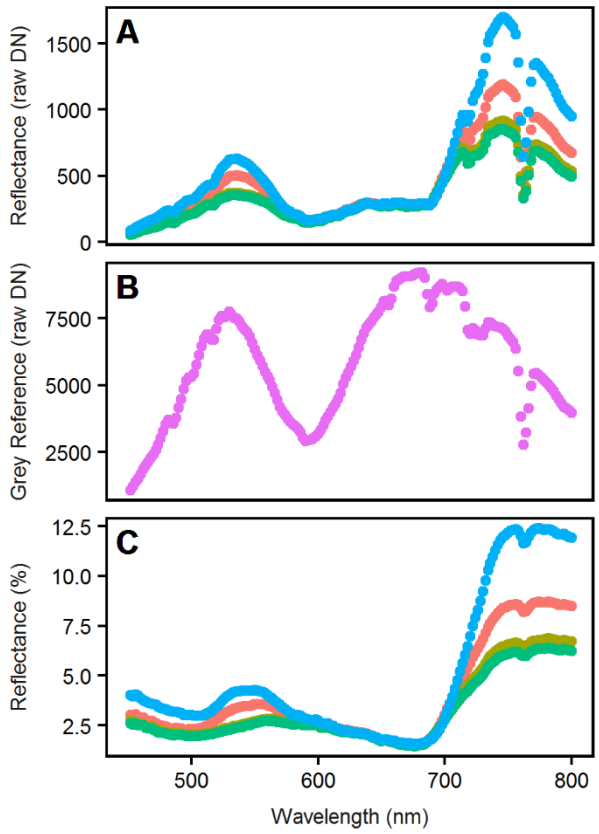


**Figure 8** Four examples of spectral measurements taken at noon over one plot showing uncorrected reflectance in raw digital numbers (A), the associated grey reference at the same light intensity (B) and the normalized reflectance spectra (C).

## 2.4 Field conditions

Field site was in Campus Klein Altendorf (University of Bonn, Germany, 50°37′ N, 6°59′ E) on a loamy-clay silt soil (luvisol) (Hecht et al., 2016). The field trial with drought treatment was carried out in Planaltina (Embrapa Cerrados, Brazil, 15°35' S and 47°42' W).

### 2.4.1 Maize

Maize was sown in 75 cm row distance and about 13 cm distance between plants resulting in about 10 seeds/$m^2$. Maize was sowed at 2016 May 6 and 2017 May 8 and 9.

In 2016, plant protection was applied at June 7, 1.5 l/ha Calaris and 1.25 l/ha Dual Gold. Field was fertilized with 120 kg N/ha on April 21, 36 kg N/ha on May 6, 92 kg $P_2O_5$/ha on May 8, 100 kg $P_2O_5$ on May 11, 140 kg $K_2O$/ha together with 21 kg MgO/ha on May 12 and 31 kg $P_2O_5$/ha, 245 kg MgO/ha and 1330 kg CaO/ha on August 14.

In 2017, plant protection was applied at June 1, 1.5 l/ha Calaris and 1.25 l/ha Dual Gold. Field was fertilized with 110 kg N/ha on April 27, 36 kg N/ha together with 92 kg $P_2O_5$/ha on May 5, 140 kg $K_2O$/ha together with 21 kg MgO/ha on July 22 and 90 kg $P_2O_5$/ha on July 27.

### 2.4.2 Soybean

Soybean was sown in 21 cm row distance and about 5 cm distance between plants resulting in about 100 seeds/$m^2$. In 2016 and 2017, soybean was sowed at May 12 and May 30, respectively. Plant protection, 2 l/ha Stomp Aqua, was applied at May 12, 2016 and May 31 in 2017. Plants were not fertilized.

*Field trial with irrigation gradient*

The soybean seeding in Planaltina was on June 7, 2016. Plants were thinned to achieve five plants per row meter. For the first 30 days after emergence, plants were irrigated homogenous (total 136 mm). Then, drought treatment was induced by an irrigation gradient (Rodolfo Junior et al., 2016). 100% (well-watered), 70% (watered), 25% (dry) and 1% (very dry) from July 5 to September 13, 2016. Ranging from total 626 mm for well-watered to 143 mm for very dry treatment. Three soybean genotypes, BRS-5980, NA-5909 and BRS-7280, were measured in total 72 plots (6 replicates).

### 2.4.3 Measurements

The LIFT instrument was mounted to a self-built phenotyping bike (*field4cycle*) with a track width of 3 m or to an autonomous field robot with a boom allowing top of canopy measurements in a distance from 60 to 80 cm (Figure 9). The *field4cycle* was manually driven with an approximate speed of 10 cm/s. At around the same speed, the field robot (Raussendorf GmbH, Obergurig) with a flexible boom (Lüttich Ingenieure GmbH, Dohna OT Borthen) allowed measurements from up to 4 m in height and 3.8 m next to the machine track. Actual measuring distance was between 50 and 80 cm. The field robot was only used for the measurements in soybean at August 15, 2016.

$Q_A$-flash protocol was executed in 1 to 2 second interval with excitation of about 40000 µmol photons $m^{-2}$ $s^{-1}$ in 60 cm distance. Spectral measurements with 200 ms integration time were acquired in between the $Q_A$-flashes. Pseudo spectral indices were calculated as described in section 2.3.6. Depending on plot length 10 to 30 measurements were acquired while moving the phenotyping bike across one plot.


**Figure 9** High-throughput photosynthesis screening was realized using a light-induced fluorescence transient (LIFT) devices mounted to an phenotyping bike (A) or autonomous field robot (B). The bike was manually driven over the plots in constant speed of around 10 cm/s. The field robot followed programmed GPS data and is able to measure up to 3.8 meter next to the machine track. Fluorescence data was acquired from the distance while scanning over the crop canopy. In order to retrieve the fluorescence signal, the measuring flashlets excited a circle of approximately 30 mm in diameter in an interval of 1 to 2 s from 50 to 80 cm distance.

## 2.5 Environmental parameters

Combined sensors in the *Miniplot* facility as well as in the field recorded environmental data every minute and uploaded it to an SQL database. The sensors measured soil temperature (DS18B20, Maxim Integrated, San Jose USA), soil moisture (EC-5, Decagon Devices, Inc., Pullman, USA), PPFD (LI-190, LI-COR Inc., Nebraska USA), air temperature and humidity (Vaisala, HMP110, Helsinki, Finland).

## 2.6 Data analysis

Fluorescence transients were discarded when S/N ratio was lower than 50 in case of maize, rapeseed and soybean or lower than 100 in barley and wheat. Fluorescence transients were also excluded when $F_v/F_m$ respective $F_q'/F_m'$ and $F_r/F_m$ respective $F_r'/F_m'$ were lower than 0 or higher than 1.

Values from spectral indices were removed when PPFD at that time was <30 µmol photons $m^{-2}$ $s^{-1}$ due to low signal to noise ratio at low light intensities. Outliers or measurement errors of spectral indices, for example when soil was targeted, were removed when the value was >1.5 times and <1.5 times the second and third quantile of all data, respectively.

### 2.6.1 Identifying influencing parameter and linear modeling

PCA was performed using *FactoMineR* package of the R program. Missing values were imputed by the *missMDA* package. Least absolute shrinkage and selection operator (Lasso) regression was performed to identify influencing parameters on phenotype using *glmnet* package of R program. The λ value was determined by cross-validation. Parameters were PPFD, temperature, humidity, VPD, total reflectance, reflectance at 685 nm, absorbance, NDVI, PRI, MTCI, age of plants in DAS, measuring date, date in seconds (TimeSec), daytime, treatment and genotype were tested. Selected parameters were then used for linear modeling.

### 2.6.2 Post hoc tests

Post hoc tests were performed either on the mean or on the slope of phenotype with covariate interaction using Scheffé test of the *agricolae* R package or pairwise comparison of the *lsmeans* R package, respectively. For comparison of paired means one or two way ANOVA was conducted followed by Tukey's test.

# 3 Results

Dynamic regulation of photosynthesis under fluctuating natural conditions was assessed by a high-throughput LIFT system. Proximal sensing of $F_v/F_m$ respective $F_q'/F_m'$, $F_{r2}/F_m$ respective $F_{r2}'/F_m'$ was established and interactions with environmental factors were analyzed and quantified by linear models.

## 3.1 Controlled conditions

The signal of the LIFT method was studied and validated under controlled conditions using various treatments which manipulates reoxidation efficiency of $Q_A^-$. DCMU and anoxic $N_2$ treatment inhibit reoxidation of $Q_A^-$ and of PQ pool in the dark, respectively. In contrast, far-red light which excites only PSI antennae supports reoxidation of the electron transport chain. In addition, influence of light intensity and temperature was measured in the lab under tightly controlled conditions.

### 3.1.1 Fluorescence induction and relaxation

Depending on the length of the excitation flash and the status of the electron transport chain, either $F_m$ or $F_mQ_A$ was measured. The $Q_A$-flash protocol induced $F_mQ_A$ when electron transport was functioning. In contrast, $Q_A$-flash induced $F_m$ when electron transport was blocked by DCMU treatment (Figure 10A). In order to study the induction of $F_m$, the excitation protocol was extend to an SF (Table 1). The SF induced $F_m$ in control leaves which was confirmed by DCMU treatment (Figure 10B). In order to confirm that the $F_mQ_A$ is indeed a maximum, a prolonged $Q_A$-flash protocol was used. This showed a clear $F_mQ_A$ after around 750 µs on dark-adapted control leaves (Figure 10C). When PQ pool was reduced under anoxic conditions, the $F_mQ_A$ was not reached. In the relaxation phase, control leaves showed fastest fluorescence relaxation followed by anoxic $N_2$ and DCMU treatment. The fluorescence induction and relaxation phase depends on the function of electron transport and reduction level of PQ pool (Keller et al., submitted).

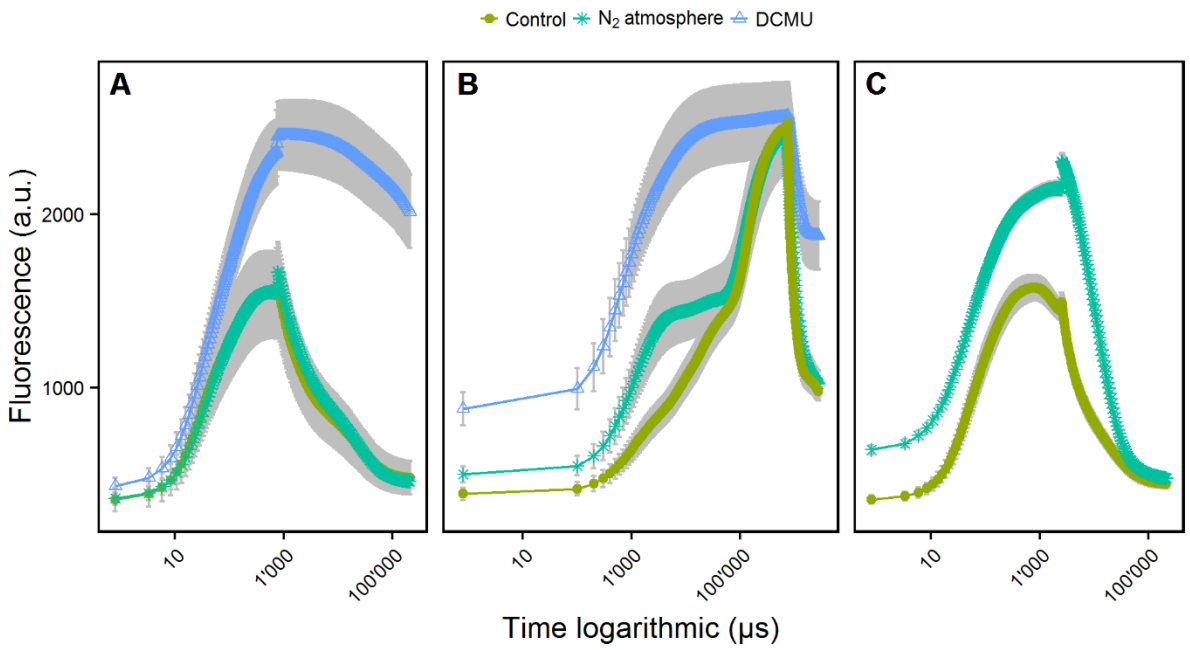


**Figure 10** Dark-adapted spinach leaves were subjected to 3-(3,4-dichlorophenyl)-1,1-dimethylurea (DCMU) treatment and nitrogen ($N_2$) atmosphere which prevent reoxidation of quinone A ($Q_A$) and plastoquinone (PQ) pool, respectively. Under those treatments, the following excitation protocols of the light-induced fluorescence

transient (LIFT) instrument were used to study fluorescence induction and relaxation: $Q_A$-flash (A), saturating flash (B) and prolonged $Q_A$-flash (C). $Q_A$-flash was performed after 5 min in control or $N_2$ atmosphere (for DCMU treatment see Material and methods). Saturating flash was performed after $Q_A$-flash. Prolonged $Q_A$-flash was performed after additional 5 min in control or $N_2$ atmosphere. Error bars showing standard deviation of the mean (n=6 plants, modified from Keller et al. *submitted*).

A second example of PQ pool influence on fluorescence transient is shown in Figure 11. Weak far-red (740 nm) background irradiation was used to excite PSI antennae and facilitate reoxidation of $Q_A^-$. The transient with 740 nm background irradiation was faster in the induction phase in the dark compared to control due to quenching of $F_mQ_A$ (Figure 11A). This response was not caused by NPQ since it was similar in the NPQ deficient Arabidopsis mutant (*npq4*, data not shown). Then, leaves were exposed for 10 s of blue light to reduce PQ pool (Figure 11B). After blue light exposure, the fluorescence relaxation phase with far-red light was faster in the first phase compared to control (Figure 11C). This showed also the coupling of fluorescence relaxation and electron transport towards PSI. Interestingly, the end of transient is lower in the control than the far red treatment after blue light exposure.

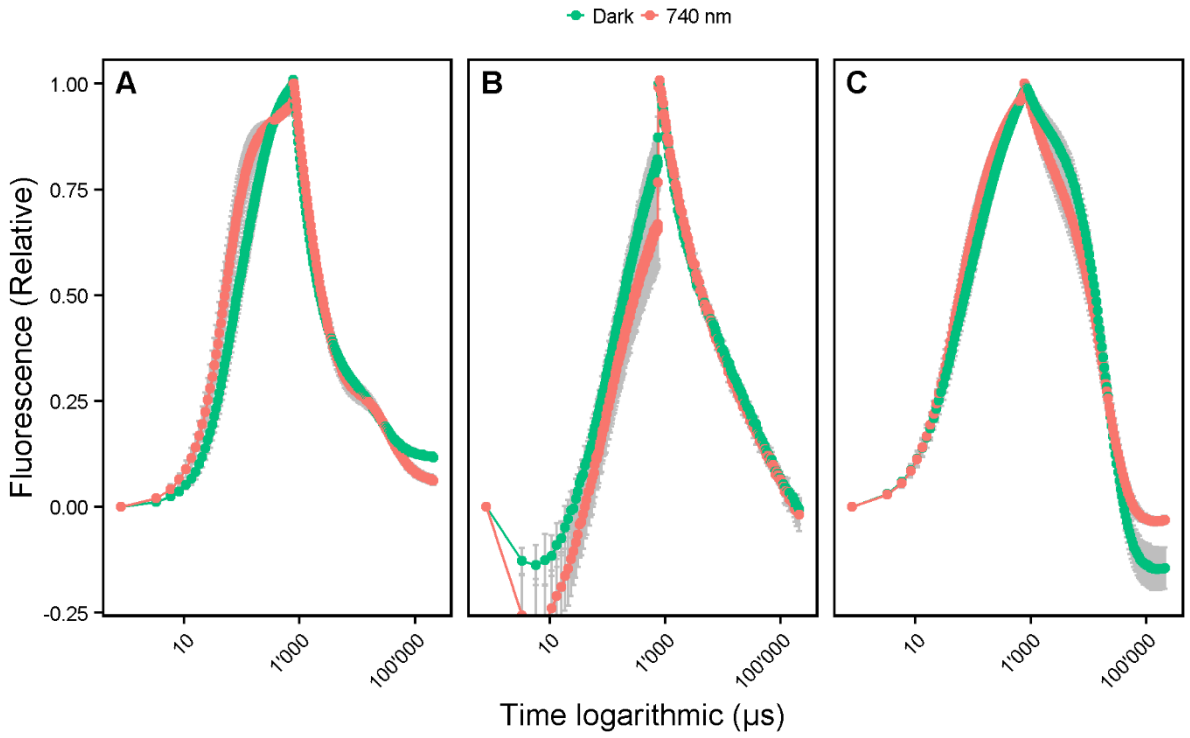


**Figure 11** Fluorescence transient of Arabidopsis leaves influenced by weak far-red background light (740 nm) in dark-adapted state (A) within 10 s of blue light at 300 µmol photons $m^{-2}$ $s^{-1}$ (B) and after blue light interference (C). Light-induced fluorescence transient (LIFT) method was used with $Q_A$- flash from 60 cm distance. Error bars showing standard deviation of the mean (n=5 plants).

In order to further validate fluorescence relaxation kinetics, FL3000 and LIFT methods were compared using thylakoids with impaired electron transport and BBY particles. DCMU and DBMIB blocks reoxidation at $Q_A$ and PQ, respectively (Lazár, 1999; Kurisu et al., 2003). Consequently, the treated thylakoids showed significant slower fluorescence relaxation kinetics compared to control (Figure 12). BBY lacks PSI and therefore showed slower fluorescence relaxation kinetics compared to control

thylakoids. The methods showed similar results regarding the raw fluorescence signal. The FL3000 showed slightly faster fluorescence kinetics in the first phase.

Looking at the retrieved parameters, $F_v/F_m$ measured by the LIFT method was ranging between 0.58 (±0.01) for BBY and 0.7 (±0.02) for thylakoids (Figure 13A). The FL3000 method showed general lower $F_v/F_m$: The lowest $F_v/F_m$ of 0.31 (±0.04) was measured for BBY particles, which was significantly decreased compared to thylakoids with $F_v/F_m$ of 0.49 (±0.02) (Figure 13B). $F_{r1}/F_m$, which measures the efficiency of $Q_A$- reoxidation, detected significant differences between all treatments in both methods (Figure 13C, D). For the LIFT method $F_{r1}/F_m$ ranged from 0.21 (±0.008) for thylakoids to 0.11 (±0.015) for the DBMIB treatment and 0.04 (±0.008) for BBY. $F_{r1}/F_m$ measured by the FL3000 method was in general higher: 0.34 (±0.025) for thylakoids, 0.17 (±0.009) for the DBMIB treatment and 0.1 (±0.013) for BBY (Figure 13D). In both methods, $F_{r4}/F_m$ showed increasing discrepancy between the control and treatments, which impaired electron transport (Figure 13E, D). In summary, $F_{r1}/F_m$ and $F_{r4}/F_m$ in both methods responded specifically to the treatments, which block electron transport at different steps.

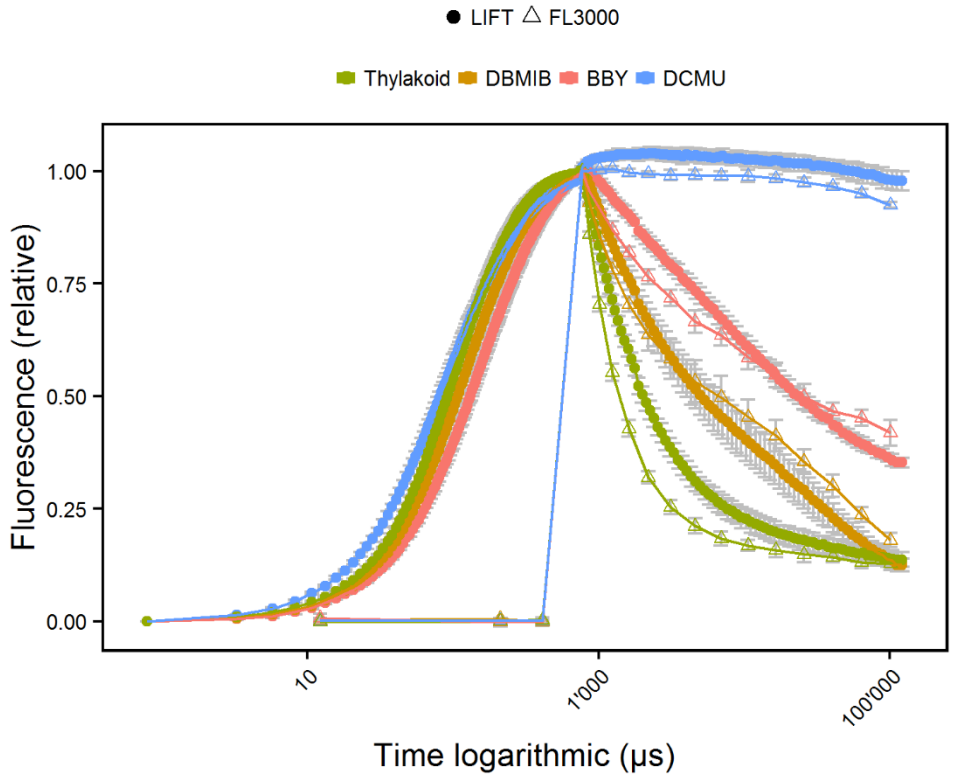


**Figure 12** Fluorescence transients measured in isolated spinach thylakoids and photosystem II particles (BBY). The measurements were performed either by the light-induced fluorescence transient (LIFT) instrument (closed circles) or with the double-modulated (FL3000) fluorometer (open triangles). Thylakoid samples (10 µg chlorophyll /mL) were either untreated, or treated with 5 µM 3-(3,4-dichlorophenyl)-1,1-dimethylurea (DCMU) or 0.66 µM 2,5-dibromo-5-methyl-6-isopropyl-benzoquinone (DBMIB). Fluorescence signals are double normalized so that the signal starts from 0 for measured minimum fluorescence ($F_o$), and has a total amplitude of 1. Chemicals were added in the dark and samples were dark-adapted for 3 min before measurement. Error bars showing standard deviation of the mean (n=5, except DCMU FL3000 and DBMIB FL3000 n=3, modified from Keller et al. *submitted*).

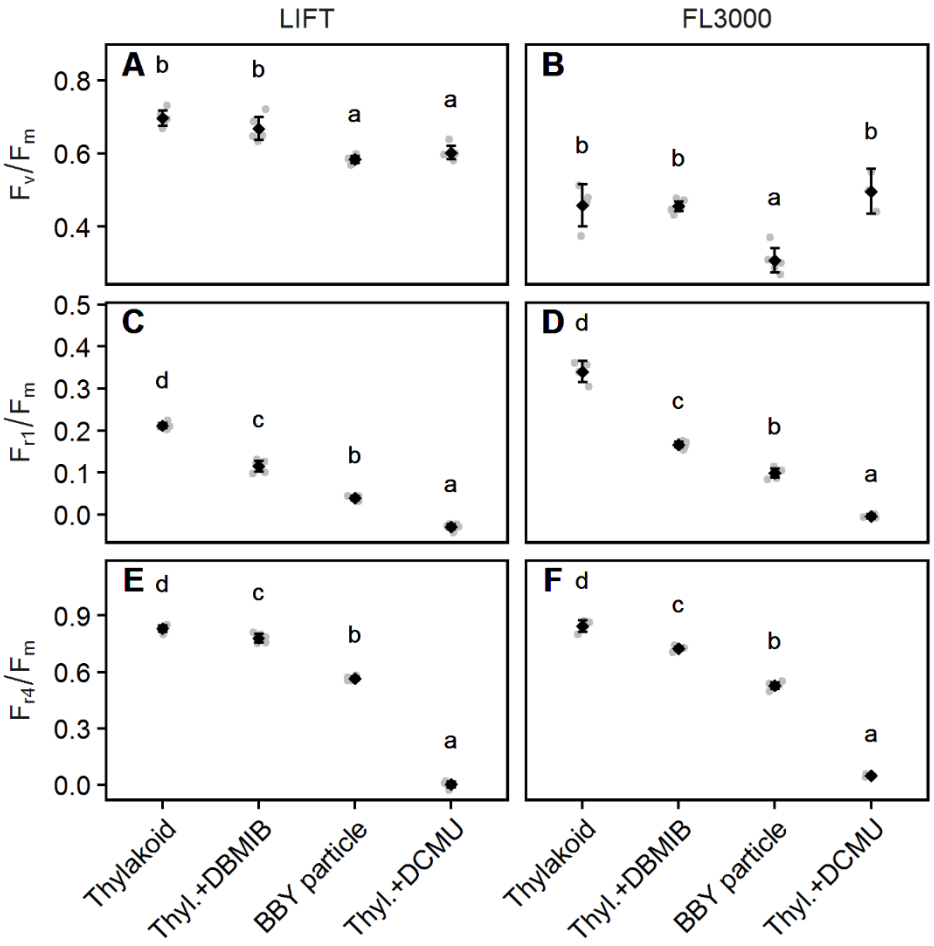


**Figure 13** Comparison of photosystem II quantum efficiency ($F_v/F_m$, A, B) and efficiency of reoxidation ($F_{r1}/F_m$ and $F_{r4}/F_m$, C-F) acquired by light-induced fluorescence transient (LIFT) and double-modulated (FL3000) measurements in isolated spinach thylakoids and BBY particles. Thylakoid samples (10 µg chlorophyll /mL) were either untreated, or treated with 5 µM 3-(3,4-dichlorophenyl)-1,1-dimethylurea (DCMU) or 0.66 µM 2,5-dibromo-5-methyl-6-isopropyl-benzoquinone (DBMIB) resulting in different fluorescence relaxation as shown in Figure 12. Black diamonds show mean values and error bars indicate the 95% confidence intervals. Individual data points are depicted by a grey point (n=5, except DCMU FL3000 and DBMIB FL3000 n=3). Means labeled with different letters differ significantly from each other according to Tukey's multiple comparisons of means (modified from Keller et al. *submitted*).

### 3.1.2 Response to light and temperature

Temperature and light changes, e.g. during a day, have large influence of photosynthetic regulation. The influence of this environmental changes to LIFT parameters were estimated on Arabidopsis plants subjected to increasing blue light intensities under different temperatures. Following PCA, temperature and PPFD were highly correlated with PC1 (x-axis) and PC2 (y-axis), respectively. Therefore, data variance was controlled by temperature which can be assigned to the x-axis (explaining 41.2% of variance) and light intensity which can be assigned to the y-axis (explaining 28.8% of variance). $F_r/F_m$ and $F_v/F_m$ showed high correlation with those axes, hence with temperature and light, respectively (Figure 14).

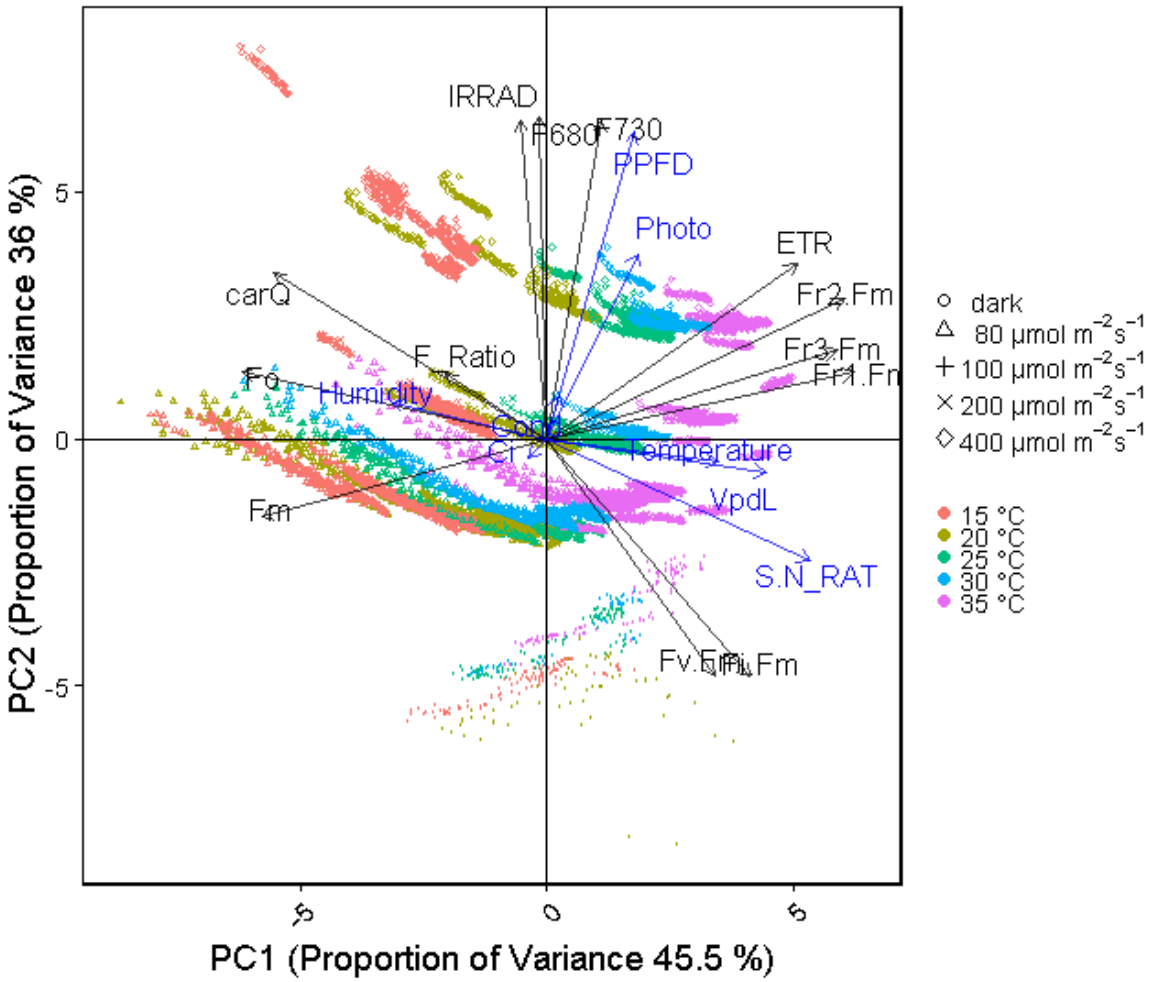


**Figure 14** Principal component analysis (PCA) of light-induced fluorescence transient (LIFT) and gas exchange parameter acquired from Arabidopsis leaves in the dark, under increasing blue light intensities and under different temperatures. Fluorescence was measured from 60 cm distance through a transparent chamber head which enclosed the leaf, controlled the temperature and measured $CO_2$ assimilation. The x-axis clearly represents temperature and the y-axis light intensities.

In the following the effect of temperature to fluorescence relaxation was analyzed more in detail. Fluorescence relaxation subjected to different temperatures in the dark and under 100 µmol photons $m^{-2}$ $s^{-1}$ of blue light is shown in Figure 4. The response of fluorescence relaxation to temperature was distinct until r1 time point (0.65 ms) and r4 = 120 ms in the dark and light, respective. Hence, $F_{r1}/F_m$ parameter was sensitive to temperature in the dark in contrast to $F_{r3}/F_m$ (Figure S 2). $F_{r1}/F_m$ and $F_v/F_m$ were similar in their response to temperature in the dark as well as in the light. The full fluorescence spectrum in response to different temperatures at 200 µmol photons $m^{-2}$ $s^{-1}$ of blue light in steady state conditions is shown in Figure 15. At this light intensity, the fluorescence intensity was invers correlated with temperature.

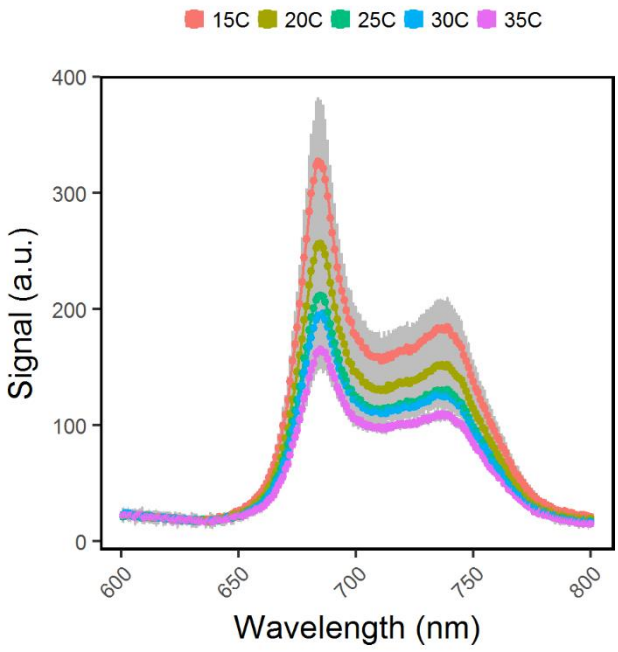


**Figure 15** Response of full fluorescence spectrum to different temperatures (15 to 35°C ) measured by the light-induced fluorescence transient (LIFT) devices at 200 µmol photons $m^{-2}$ $s^{-1}$ of blue light (445 nm). Spectrum was acquired from Arabidopsis leaves by a separate built in spectrometer. The spectral integration time was 1.5 ms. Error bars show standard deviation of n=6 leaves.

The full light response curve of *A. thaliana* leaves under different temperatures are shown in Figure 16. $F_v/F_m$ respective $F_q'/F_m'$ and F680 are sensitive to light intensities. In contrast, $F_r/F_m$ respective $F_r'/F_m'$ parameters and F680/F730 ratio responded more to temperature. The effect of increasing light intensities seems to vanish at longer reoxidation times (r3 and r4), especially at higher temperature. With exception at 15°C, $F_{r4}/F_m$ was separated from $F_{r4}'/F_m'$ values.

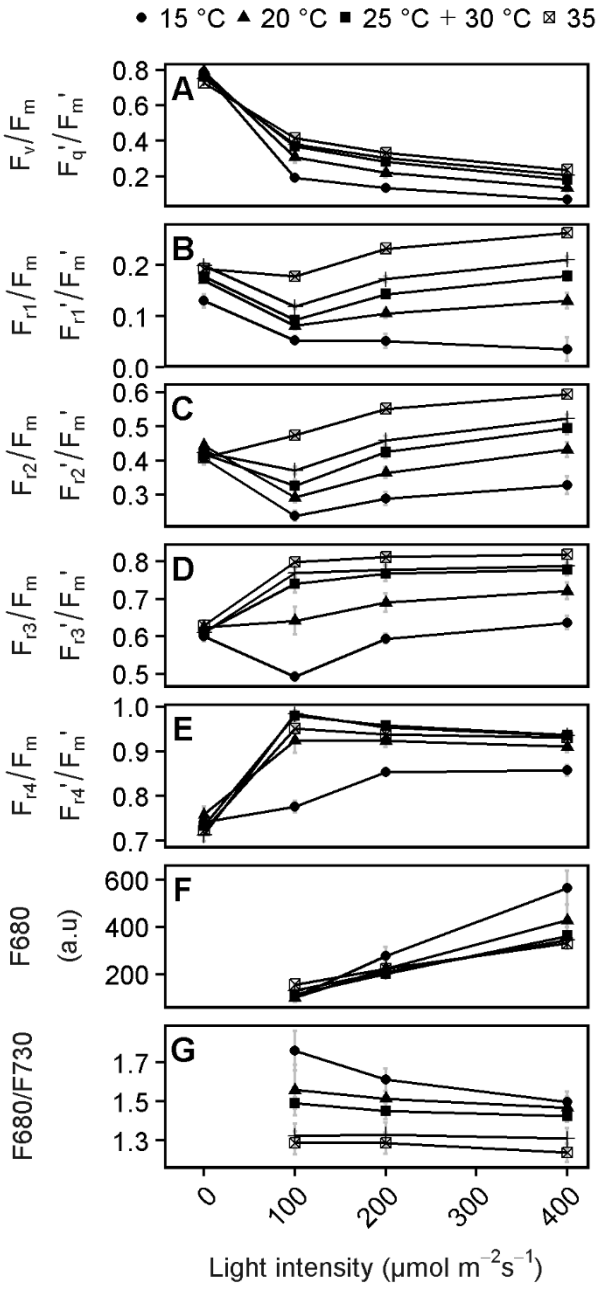


**Figure 16** Light response at different temperatures (15 to 35°C ) measured by the light-induced fluorescence transient (LIFT) instrument based on active and passive induced fluorescence at 0, 80, 100, 200 and 400 µmol $m^{-2}$ $s^{-1}$ of blue light. Quantum efficiency of the photosystem II ($F_v/F_m$ in the dark and $F_q'/F_m'$ in the light) (A), efficiency of electron transport 0.65 ms ($F_{r1}/F_m$ in the dark, $F_{r1}'/F_m'$ in the light) (B), 5 ms ($F_{r2}/F_m$ in the dark, $F_{r2}'/F_m'$ in the light) (C), 30 ms ($F_{r3}/F_m$ in the dark, $F_{r3}'/F_m'$ in the light) (D) and 120 ms ($F_{r4}/F_m$ in the dark, $F_{r4}'/F_m'$ in the light) (E) after reduction of primary quinone ($Q_A$) are shown regarding active fluorescence parameters. Then, passive fluorescence intensity at 680 nm (F) and the ration of 680 nm and 730 nm wavelength (G) were recorded in-between $Q_A$-flashes. Attached Arabidopsis leaves (n=6) were measured dark-adapted and in steady state at each light intensity. Black dots show mean values and error bars indicate the 95% confident interval.

ETR based on measured $F_q'/F_m'$ correlated well with ETR derived by gas exchange measuring $CO_2$ assimilation at all light and temperature steps (Figure 17). The ETR at all temperatures were highly correlated between fluorescence paramter and gas exchange data. The ratio of ETR values from both methods was almost 1:1, with the exception of the treatment at 15°C where the fluorescence based values were underestimated compared to measured $CO_2$ assimilation.

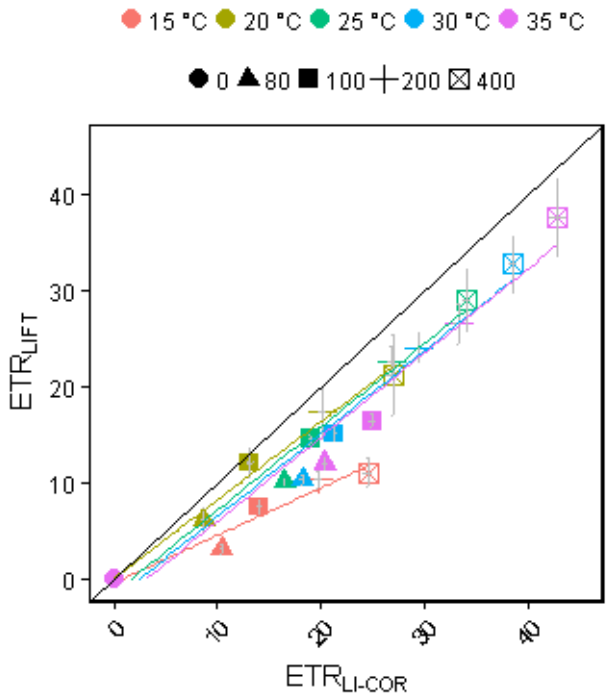


**Figure 17** Photosynthesis was measured based on $CO_2$ and $H_20$ gas exchange using LI-COR 6400 and fluorescence using light-induced fluorescence transient (LIFT) instrument. Derived electron transport rate (ETR) were compared at different temperature and light intensities. Arabidopsis leaves were measured with 0, 80, 100, 200 and 400 µmol $m^{-2}$ $s^{-1}$ of blue light at steady state conditions (data of $37^{th}$ to $40^{th}$ $Q_A$ flash averaged). ETRs were calculated as the following: $ETR_{LI-COR} = (A+R_d)(4C_i+8T^*)/(C_i-T^*)$, whereas A is $CO_2$ assimilation rate in µmol $m^{-2}$ $s^{-1}$, $R_d$ is respiratory photosynthesis measured in the dark in µmol $m^{-2}$ $s^{-1}$, $C_i$ is intercellular $CO_2$ in µmol $mol^{-1}$ and T* is the $CO_2$ compensation point in the absence of respiration in µmol $mol^{-1}$ (Bernacchi et al., 2001; Yamori et al., 2012) and $ETR_{LIFT} = F_q'/F_m'$ * blue light intensity * 0.5 * 0.8 whereas $F_q'/F_m'$ is the operating efficiency of the photosystem II.

### 3.1.3 Response to drought

Response to drought was detected in the B73 genotype compared to control when exposed to increasing blue light intensities and in the recovery phase followed by the blue light (Figure 18). In contrast, the Mo17 genotype was not affected in the drought compared to its control (Figure 19). Mo17 showed in control and drought conditions significant lower $F_q'/F_m'$ or $F_{r2}'/F_m'$ compared to B73. Probably, growth conditions for Mo17 genotype were not optimal in both conditions. B73 showed faster recovery of $F_{r2}/F_m$ after light exposure in control than drought treatment whereas the recovery in NPQ was the same.

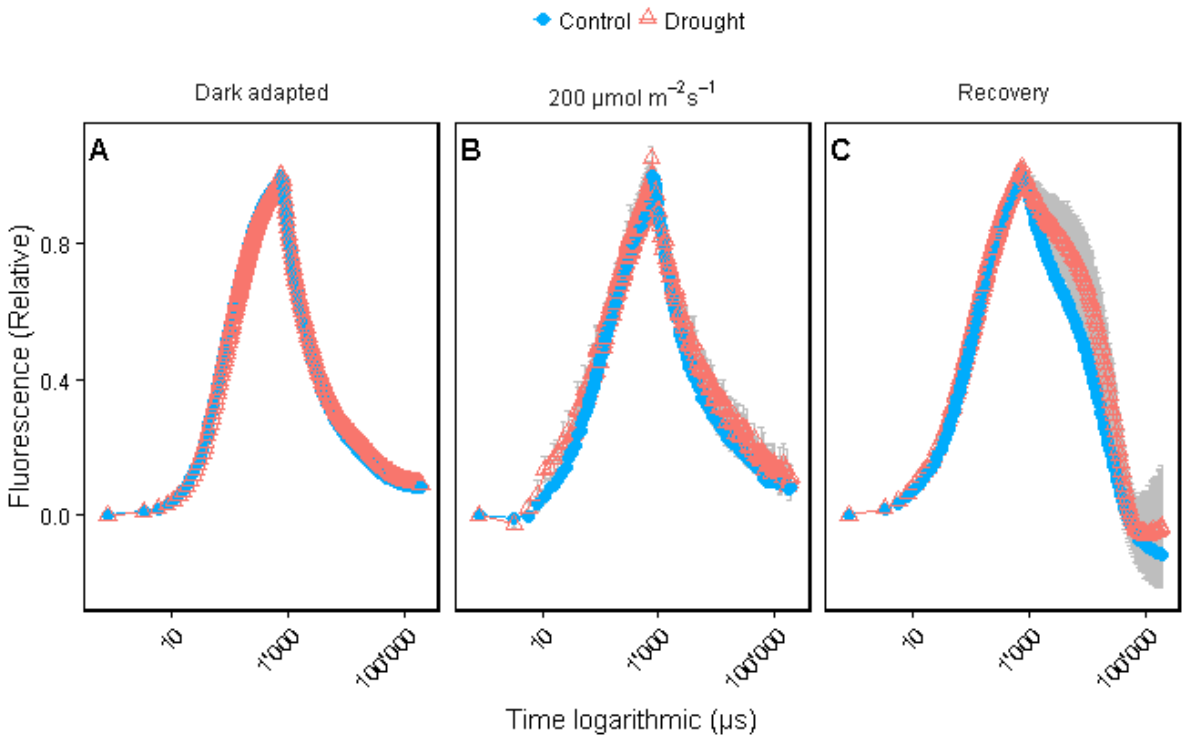


**Figure 18** Fluorescence transient of leaves from the maize B73 genotype subjected to drought in dark-adapted state (A) at 200 µmol photons $m^{-2}$ $s^{-1}$ in steady state (B) and the recovery 2 s after blue light (C) compared to control conditions. Light-induced fluorescence transient (LIFT) method was used with $Q_A$-flash from 60 cm distance. Error bars showing standard deviation of the mean (n=4 plants).

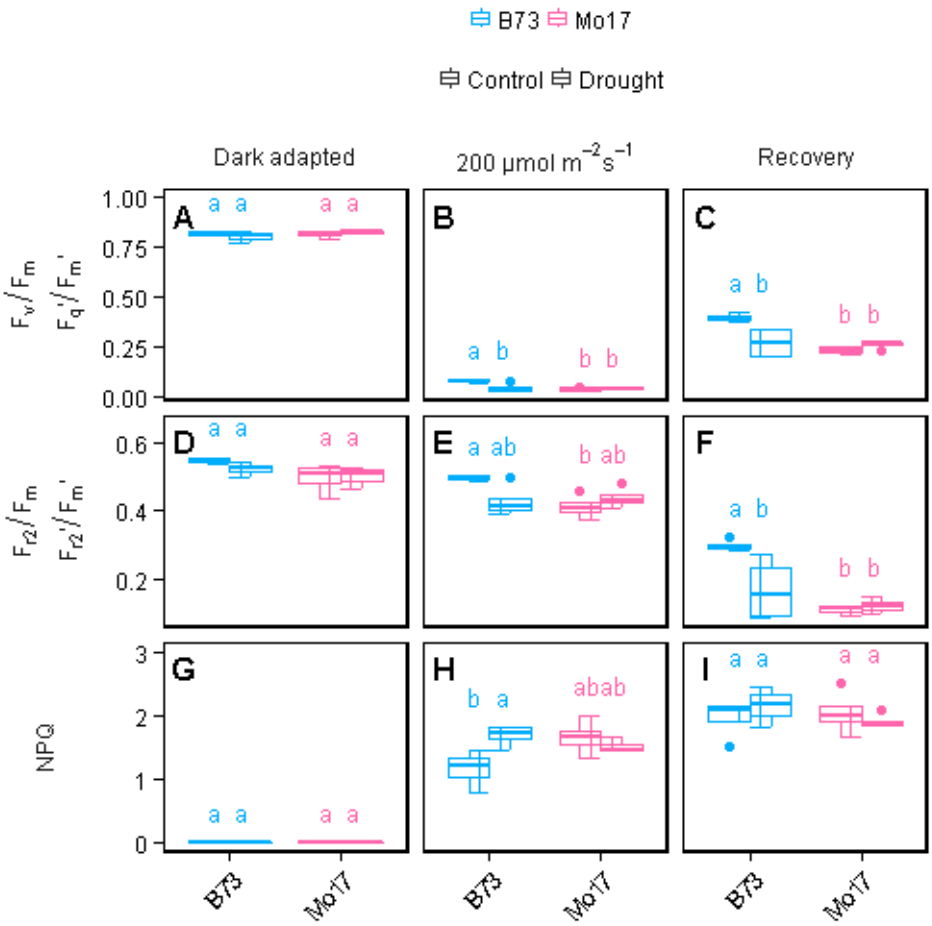


**Figure 19** Boxplot of quantum efficiency of the photosystem II ($F_v/F_m$ in the dark and $F_q'/F_m'$ in the light, A to C), reoxidation efficiency 5 ms after primary quinone ($Q_A$) reduction ($F_{r2}/F_m$ in the dark, $F_{r2}'/F_m'$ in the light, D to F) and non-photochemical quenching (NPQ, G to I) of maize B73 and Mo17 genotype. Genotypes subjected to drought were compared to control conditions in dark-adapted state (A, D, G) in steady state at 200 µmol photons $m^{-2}$ $s^{-1}$ (B, E, H) and the recovery 2 s after blue light (C, F, I). Box represents inter-quartile range, bold horizontal bar the median, the discontinuous lines the upper and lower quartile, and outlier data points (>1.5 × inter-quartile range) are depicted by a point. Means with different letters differ significantly using Scheffé's multiple comparisons of means (n=4 plants).

### 3.1.4 Summary: Controlled conditions

Fluorescence induction and relaxation was studied under a wide range of physiological conditions. When electron transport was intact, $F_mQ_A$ and $F_m$ were induced by $Q_A$-flash and SF, respectively (Figure 10). SF reached $F_m$ due to the longer excitation phase (0.75 s) of the flash reducing $Q_A$ and PQ pool. The shorter $Q_A$-flash detected reduction level of PQ prior to measurement (Figure 10A, C) and electron transport through PQ pool towards PSI based on kinetics of the fluorescence relaxation (Figure 11 and Figure 12). The newly established parameter, $F_{r2}/F_m$, detected inhibition of the electron transport chain (Figure 13) and drought stress (Figure 19). $F_q'/F_m'$ showed close correlation to $CO_2$ assimilation under different light intensities and temperatures (Figure 17). Whereas $F_v/F_m$ respective $F_q'/F_m'$ was sensitive to PPFD, $F_{r2}/F_m$ respective $F_{r2}'/F_m'$ was influenced by temperature (Figure 16).

## 3.2 Semi-field conditions

Over two years, 1078383 measurements were acquired in five different crops using the automated LIFT system in the *Miniplot* facility (Keller et al., in prep.). Barley, maize and soybean were monitored for two growing seasons. Rapeseed and wheat were monitored for one growing seasons. The growth conditions covered a wide range of environmental fluctuation. The highly dynamic regulation of photosynthesis parameter $F_v/F_m$ respective $F_q'/F_m'$ and $F_{r2}/F_m$ respective $F_{r2}'/F_m'$ in response to the natural fluctuating environment, e.g. in light intensity and temperature, is shown in Figure 20.

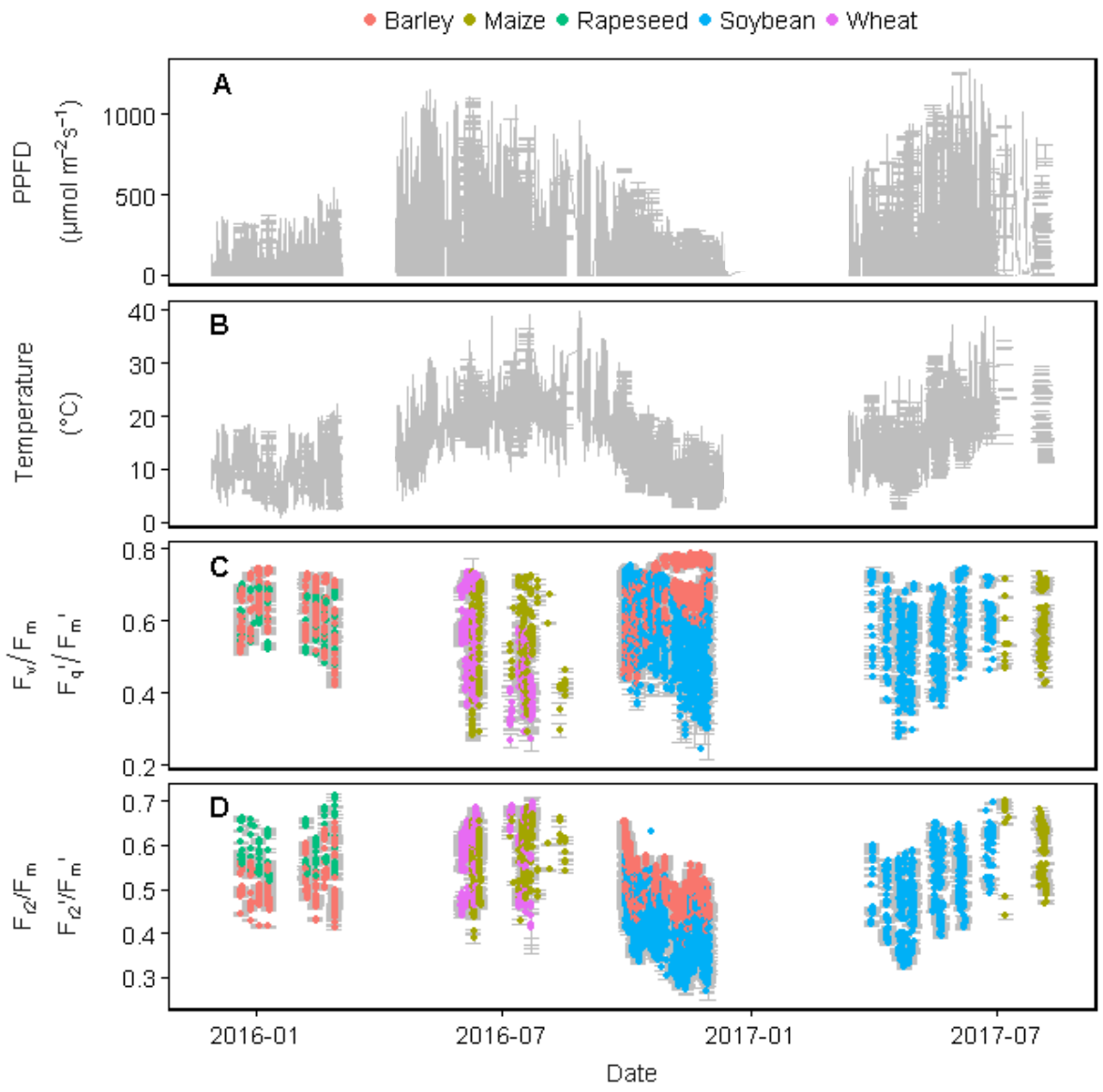


**Figure 20** Photosynthetic performance was assessed in a fluctuating environment over two years. Photosynthetic photon flux density (PPFD, A) temperature (B), quantum efficiency of the photosystem II ($F_v/F_m$ in the dark and $F_q'/F_m'$ in the light, C) and reoxidation efficiency 5 ms after primary quinone ($Q_A$) reduction ($F_{r2}/F_m$ in the dark and $F_{r2}'/F_m'$ in the light, D) is shown over time. Fluorescence data was acquired by up to two light-induced fluorescence transient (LIFT) devices scanning crop canopy simultaneously from an automated platform. Environmental conditions as PPFD were recorded by up to three stations distributed in the unheated greenhouse. Measurements took place from December 2015 to August 2017 in barley, maize, rapeseed, soybean and wheat genotypes. Grey error bars show standard error of several hundred independent measurements taken per hour (n=1078383, modified from Keller et al., in prep.).

### 3.2.1 Parameters determining data variance

PCA analysis was conducted in order to get an overview over all data collected (n=1092841, missing values imputed) in the *Miniplot* facility (Figure 21). In PCA, dimension 1 accounts for the largest possible variability in the data set. Dimension 1 and 2 explained 46.3% and 20.1% of the total variance in the data set. Spectral indices to each other and $F_r/F_m$ parameters to each other were highly correlated. $F_{r2}/F_m$ respective $F_{r2}'/F_m'$, $F_{r3}/F_m$ respective $F_{r3}'/F_m'$, NDVI, pNDVI, NDVI_II and MTCI did contribute most to the variance in the data (over 16%). Dimension 3 and 4 explained 9% and 5.3%, respectively, with PRI, $F_i/F_m$, carQ, $F_v/F_m$ respective $F_q'/F_m'$ and $F_{r1}/F_m$ respective $F_{r1}'/F_m'$ as important variables (not shown). Based on that, the following analysis will focus on $F_q'/F_m'$ and $F_{r2}/F_m$ respective $F_{r2}'/F_m'$.

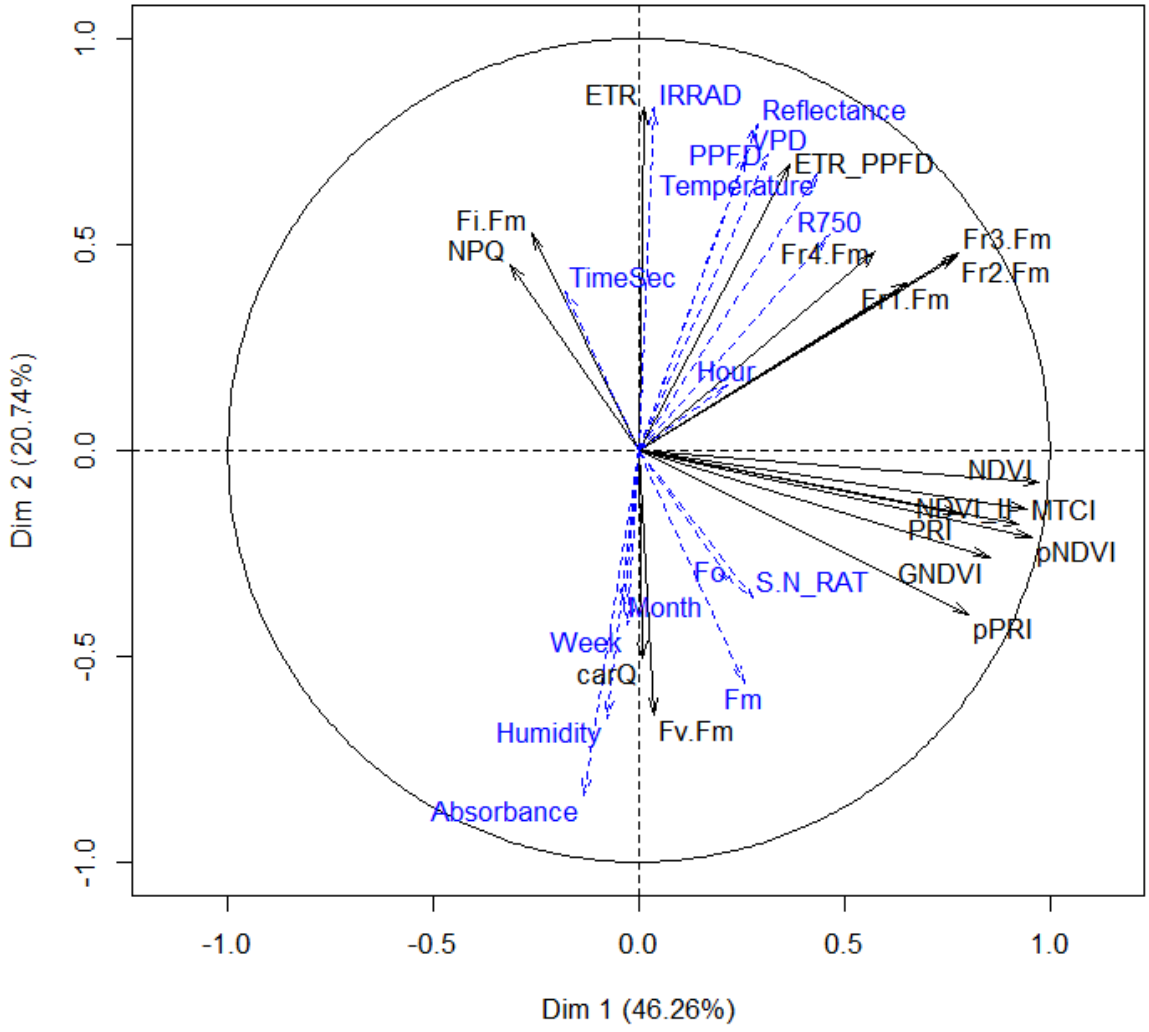


**Figure 21** Principal component analysis (PCA) of fluorescence and spectral data from barley, maize, rapeseed, soybean and wheat genotypes. Measurements took place from December 2015 to August 2017 using the light-induced fluorescence transient (LIFT) device. The first two dimensions (Dim) are shown which explain together 67% of the total data variance (n=1092841, missing values imputed). Environmental data was recorded by external sensors and merged to the measurements.

### 3.2.2 Factors influencing $F_v/F_m$ respective $F_q'/F_m'$

In order to understand the fluctuating response of $F_v/F_m$ respective $F_q'/F_m'$ to environmental factors, the main factors causing the fluctuation were identified by using Lasso regression. As expected, $F_v/F_m$ respective $F_q'/F_m'$ is mainly determined by PPFD ($R^2$=0.38, Figure S 3). For further analysis, values acquired during the night were discarded to avoid a heavy tail in data distribution and the analysis was performed with only light-adapted measurements (PPFD>30). According to Lasso regression, $F_q'/F_m'$ was dependent on PPFD, pNDVI, PRI, crop species and humidity. These factors were then selected for linear modeling. PPFD explained in total 26% of all variance in $F_q'/F_m'$ (including the square root term, Table 2). Uncorrected pNDVI followed with 15.5%. Further influencing variables were PRI, crop species and humidity explaining 3.8%, 1.7% and 0.9% of all variance in the data, respectively. Based on Lasso regression, diurnal, seasonal and development stage did not significantly affect $F_q'/F_m'$.

**Table 2** Liner model of photosystem II operating efficiency ($F_q'/F_m'$) measured in five crop species over two seasons in an unheated greenhouse (n= 441915 measurements). Depending factors or covariates were photosynthetic photon flux density (PPFD), pseudo normalized difference vegetation index (pNDVI), photochemical reflectance index (PRI), crop species and humidity. Descriptors of the linear model are degree of freedom (Df), sum of squares (Sum Sq), mean of squares (Mean Sq), ratio of Mean Sq and Mean Sq error (F value), the associated p value (Pr(>F)) and the explained Sum Sq per factor (ExpVar).

| | Df | Sum Sq | Mean Sq | F value | Pr(>F) | ExpVar |
|---|---|---|---|---|---|---|
| Residuals | 441905 | 2678.6 | 0.01 | NA | NA | 52.1 |
| PPFD | 1 | 1156.49 | 1156.49 | 190792.6 | 0 | 22.5 |
| pNDVI | 1 | 794.44 | 794.44 | 131062.9 | 0 | 15.5 |
| PRI | 1 | 193.6 | 193.6 | 31939.2 | 0 | 3.8 |
| $PPFD^{0.5}$ | 1 | 177.85 | 177.85 | 29340.8 | 0 | 3.5 |
| Crop | 4 | 88.87 | 22.22 | 3665.5 | 0 | 1.7 |
| Humidity | 1 | 48.39 | 48.39 | 7983.5 | 0 | 0.9 |

Grouping $F_q'/F_m'$ values into pNDVI ranges improved the explained variance to up to 34% (Figure 22). Since NDVI bares information about plant growth status and canopy architecture, it may explain the rather high influence to $F_q'/F_m'$. When all influencing factors identified by Lasso regression were included into a linear model, the model explained 47.9% of all variance in $F_q'/F_m'$.

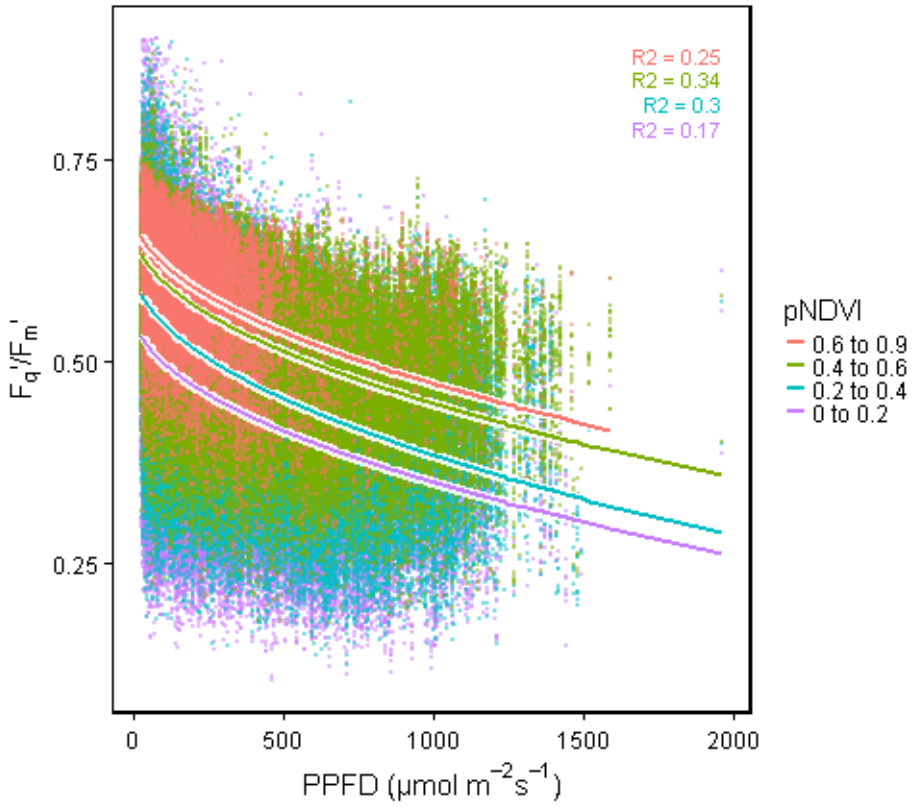


**Figure 22** Photosynthetic performance was assessed in a fluctuating environment over two years. Photosystem II operating efficiency ($F_q'/F_m'$) was correlated to photosynthetic photon flux density (PPFD) and grouped after pseudo normalized difference vegetation index (pNDVI) values. PPFD and pNDVI had the highest effect on $F_q'/F_m'$ according to Lasso regression analysis. Fluorescence and spectral data was acquired by a light-induced fluorescence transient (LIFT) device scanning the crop canopy from an automated moving platform. Environmental conditions as PPFD and temperature were recorded every minute by three stations distributed in the unheated greenhouse and merged to the measurements done in the same minute. Measurements took place from December 2015 to August 2017 in barley, maize, rapeseed, soybean and wheat genotypes. White intervals show 95% confidence intervals for the mean of $F_q'/F_m'$ fitted to a linear model depending on PPFD (square root transformed, n=444824 measurements).

### 3.2.3 Factor influencing $F_{r2}/F_m$ respective $F_{r2}'/F_m'$

Lasso regression was used to identify the factors causing the fluctuation in $F_{r2}/F_m$ respective $F_{r2}'/F_m'$. This parameter was largely determined by temperature explaining 61% of the variance over all crops and seasons (Figure S 4). According to Lasso regression, temperature, date and crop species influenced $F_{r2}/F_m$ respective $F_{r2}'/F_m'$. These factors were then selected for linear modeling. Temperature alone explained over 60% of all variance (Table 2). The different dates accounted for 11% of all variance. The different crop species accounted for 4.1% of all variance, which was relatively low considering that winter and summer crops were monitored. In contrast to $F_q'/F_m'$, the NDVI did not contribute to variation in the data. The unexplained variance was 21%.

**Table 3** Liner model of reoxidation efficiency 5 ms after primary quinone ($Q_A$) reduction ($F_{r2}/F_m$ in the dark and $F_{r2}'/F_m'$ in the light) measured in five crop species over two seasons in an unheated greenhouse (n= 1085175 measurements). Depending factors or covariates were temperature, crop species and normalized difference vegetation index (NDVI). Descriptors of the linear models are degree of freedom (Df), sum of squares (Sum Sq),

mean of squares (Mean Sq), ratio of Mean Sq and Mean Sq error (F value), the associated p value (Pr(>F)) and the explained Sum Sq per factor (ExpVar).

| | Df | Sum Sq | Mean Sq | F value | Pr(>F) | ExpVar |
|---|---|---|---|---|---|---|
| Temperature | 1 | 6645.54 | 6645.54 | 3273879 | 0 | 63.4 |
| Residuals | 1085411 | 2203.24 | 0 | NA | NA | 21 |
| Date | 43 | 1154.46 | 26.85 | 13226.4 | 0 | 11 |
| Crop | 4 | 433.69 | 108.42 | 53413.8 | 0 | 4.1 |
| Temperature$^{0.5}$ | 1 | 44.68 | 44.68 | 22009 | 0 | 0.4 |

Grouped into crop species, the R square increased further, e.g. up to 0.77 in soybean (Figure 23). Interestingly, rapeseed showed much higher $F_{r2}/F_m$ respective $F_{r2}'/F_m'$ in colder temperature than soybean or wheat. Barley compared to soybean showed high efficiency in colder temperature but less in warmer conditions.

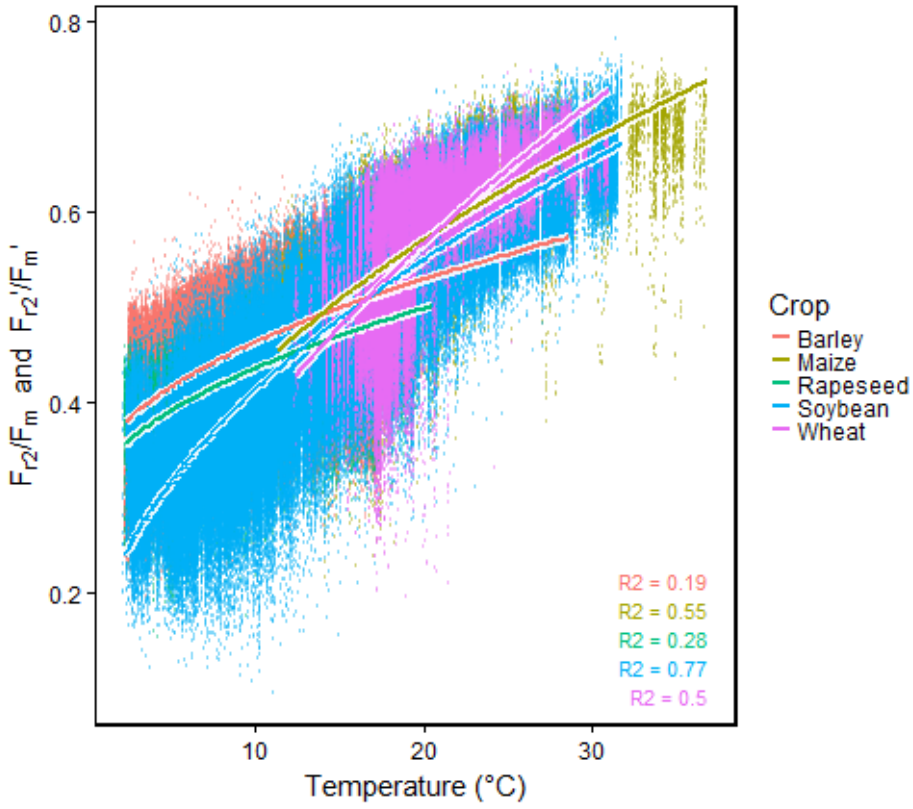


**Figure 23** Photosynthetic performance was assessed in a fluctuating environment over two years. Reoxidation efficiency 5 ms after primary quinone ($Q_A$) reduction ($F_{r2}/F_m$ in the dark and $F_{r2}'/F_m'$ in the light) was correlated to temperature and grouped after crop species. Fluorescence data was acquired by a light-induced fluorescence transient (LIFT) device scanning the crop canopy from an automated moving platform. Environmental conditions as PPFD and temperature were recorded every minute by three stations distributed in the unheated greenhouse and merged to the measurements done in the same minute. Measurements took place from December 2015 to August 2017 in barley, maize, rapeseed, soybean and wheat genotypes. White intervals show 95% confidence intervals for the mean of $F_{r2}/F_m$ respective $F_{r2}'/F_m'$ fitted to a linear model depending on temperature (square root transformed, n= 1085175 measurements).

### 3.2.4 Maize

Photosynthetic performance in maize was assessed over two seasons under fluctuating environmental conditions in the *Miniplot* facility. The fluorescence response in 7 genotypes during summer 2016 and in 9 genotypes during summer 2017 is shown in Figure 24. Clear diurnal patterns of $F_v/F_m$ respective $F_q'/F_m'$ and $F_{r2}/F_m$ respective $F_{r2}'/F_m'$ are visible. The experiment in 2016 included a drought treatment for B73 and Mo17 genotypes starting on June 15. In the week of July 18, the effect of drought was clearly visible in $F_q'/F_m'$ and $F_{r2}'/F_m'$ on B73 genotype in the afternoon.

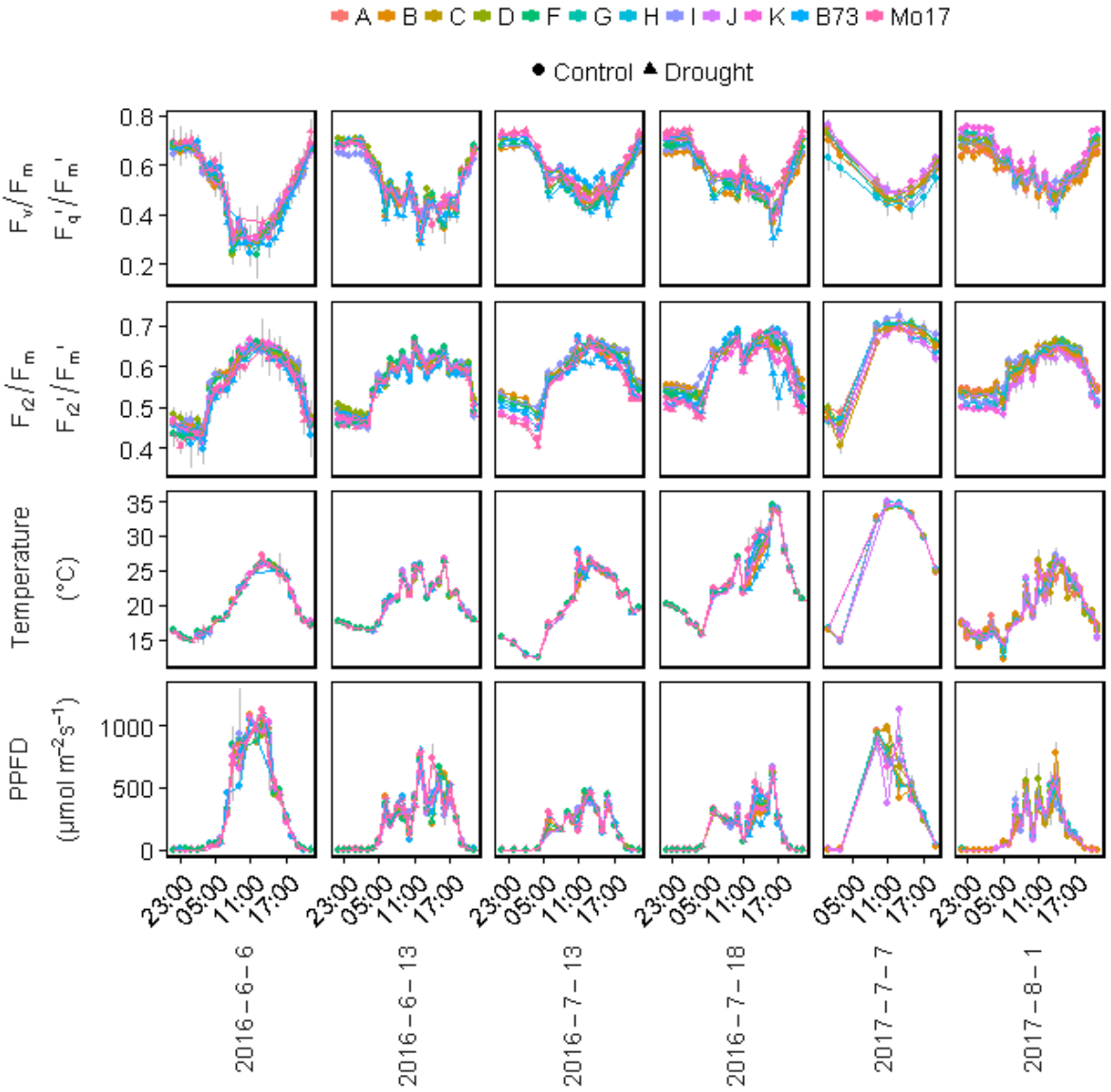


**Figure 24** Response of quantum efficiency of the photosystem II ($F_v/F_m$ in the dark and $F_q'/F_m'$ in the light), reoxidation efficiency 5 ms after primary quinone ($Q_A$) reduction ($F_{r2}/F_m$ in the dark and $F_{r2}'/F_m'$ in the light) in maize genotypes, associated temperature and photosynthetic photon flux density (PPFD) averaged per hour and week. Fluorescence data was acquired by automated light-induced fluorescence transient (LIFT) device scanning crop canopy. Environmental conditions as temperature were recorded every minute by three stations distributed in the unheated greenhouse and merged to the measurements done in the same minute. Grey error bars show 95% confidence interval. Experiment included 7 genotypes and a drought treatment in 2016 and 9 genotypes in 2017.

Ranking of genotypes according to statistical analysis showed consistent results over the season (Figure 25). For example, genotype D was in both years best performing in $F_v/F_m$ respective $F_q'/F_m'$ and in $F_{r2}/F_m$ respective $F_{r2}'/F_m'$. Genotype I showed the same $F_{r2}/F_m$ respective $F_{r2}'/F_m'$ as genotype D. Genotypes B and K were less consistent in the ranking indicating conditions where they could not maintain the photosynthetic performance as high as genotype D. In July, drought stress is clearly visible in B73 genotype regarding $F_v/F_m$ respective $F_q'/F_m'$ and in both genotypes, B73 and Mo17 regarding $F_{r2}/F_m$ respective $F_{r2}'/F_m'$. There were some significant differences in the temperature and PPFD when the different genotypes were measured indicating unequal conditions at that measuring period.

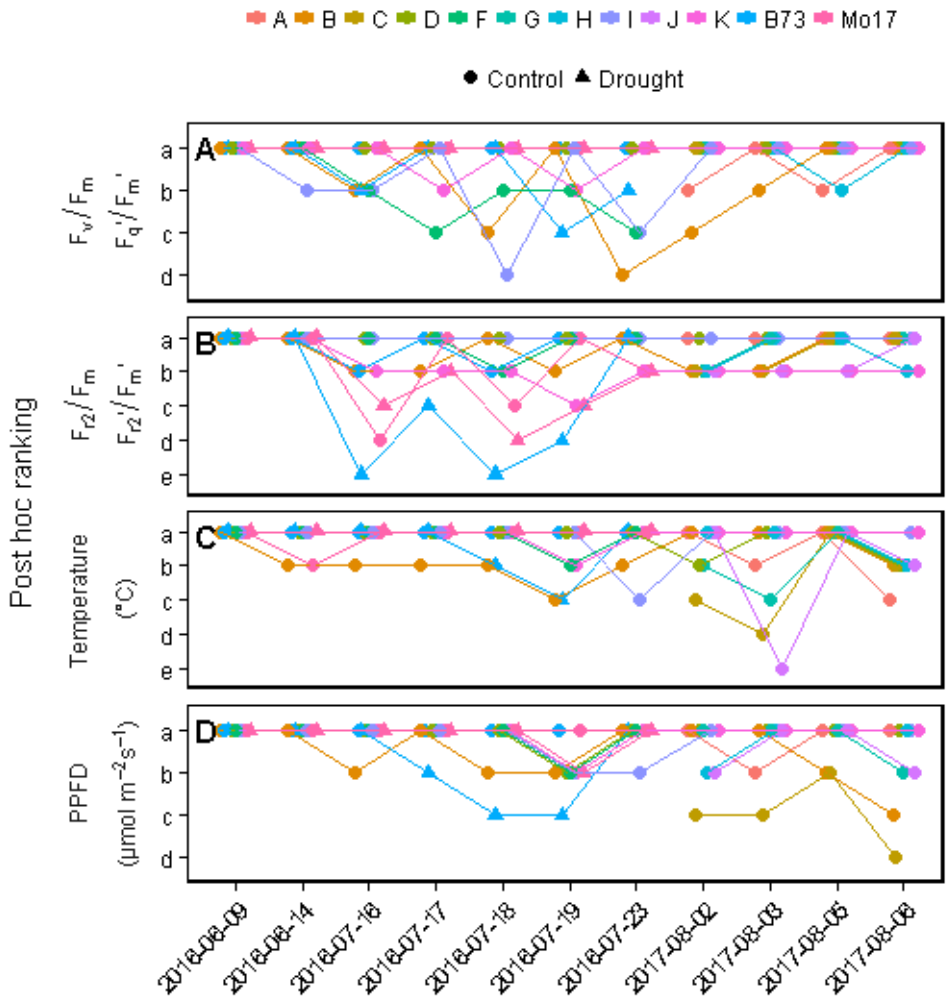


**Figure 25** Analysis of variance (ANOVA) followed by Scheffé test for maize genotypes was performed daily for quantum efficiency of the photosystem II ($F_v/F_m$ in the dark and $F_q'/F_m'$ in the light, A), reoxidation efficiency 5 ms after primary quinone ($Q_A$) reduction ($F_{r2}/F_m$ in the dark and $F_{r2}'/F_m'$ in the light, B) and associated temperature (C) and photosynthetic photon flux density (PPFD, D). Data was averaged per hour and week. Fluorescence data was acquired by automated light-induced fluorescence transient (LIFT) device which scans the crop canopy. Environmental conditions as temperature were recorded every minute by three stations distributed in the unheated greenhouse and merged to the measurements done in the same minute.

*Factors influencing $F_q'/F_m'$*

The data of the maize experiment in 2016 and 2017 was combined to identify influencing factors causing the fluctuation in $F_q'/F_m'$. In the light (PPFD>30 µmol photons $m^{-2}$ $s^{-1}$), the response of $F_q'/F_m'$ was mainly influenced by PPFD, PRI and VPD according to Lasso regression. The relation of this parameters to $F_q'/F_m'$ is shown in Figure S 5. The response of $F_q'/F_m'$ to the two factors with highest effect, PPFD and PRI, is shown in Figure 26. The explained variance ranged from 29% at high PRI values to 40% at low PRI values in the linear model with square root transformed PPFD as covariate.

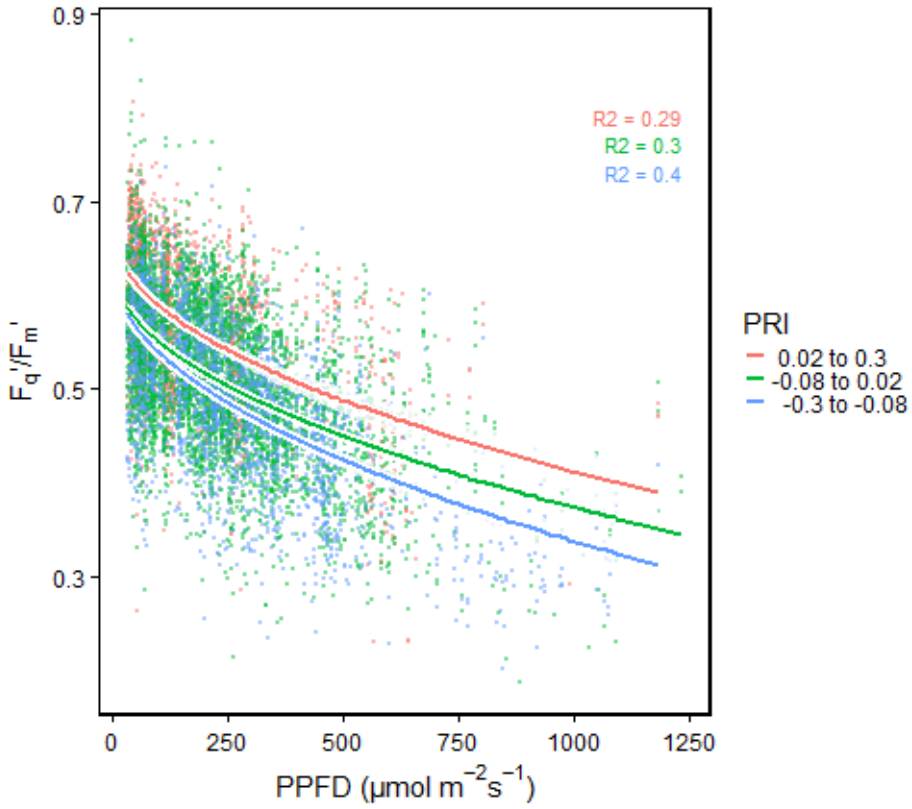


**Figure 26** Photosystem II operating efficiency ($F_q'/F_m'$) of maize genotypes was correlated to photosynthetic photon flux density (PPFD) and grouped after photochemical reflectance index (PRI) values. PPFD and PRI influenced $F_q'/F_m'$ highest according to lasso regression. Fluorescence and spectral data was acquired by automated light-induced fluorescence transient (LIFT) device scanning the crop canopy. Environmental conditions as PPFD and temperature were recorded every minute by three stations distributed in the unheated greenhouse and merged to the measurements done in the same minute. Measurements include two independent maize experiments in 2016 and 2017 with in total 12 genotypes. White intervals show 95% confidence intervals for the mean of $F_q'/F_m'$ fitted to a linear model depending on PPFD (square root transformed, n=10157 measurements).

In the following, genotypic performance regarding $F_q'/F_m'$ were summarized per year using the adjusted mean only or including PPFD or PRI as covariates. Regarding the mean, Genotypes B, I and K showed in both years consistently significant different $F_q'/F_m'$ (Figure 27). From these three genotypes, genotype K showed the highest mean of $F_q'/F_m'$ and Genotype B the lowest. When interaction with PPFD was considered, Genotypes B performed significant lower compared to genotype K and D in both years. Genotype I showed high interaction with PRI values in both years. However, the photosynthetic

response of genotypes remains complex since genotypes performed different when interaction with different environmental factors were considered.

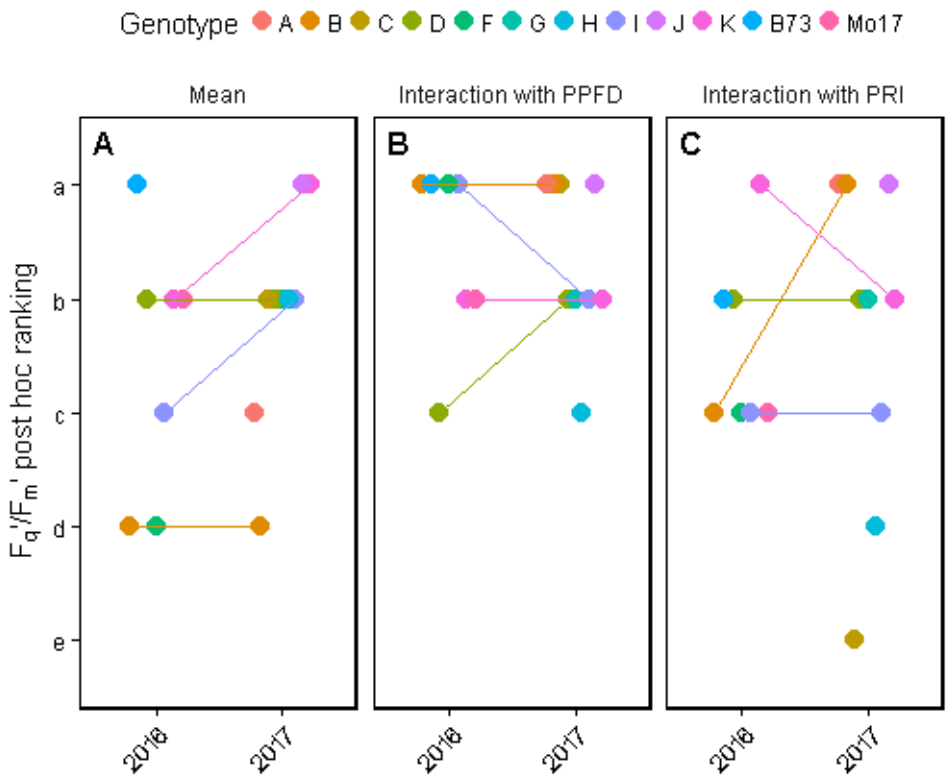


**Figure 27** Ranking of photosystem II operating efficiency ($F_q'/F_m'$) of maize genotypes based on mean (A), interaction with photosynthetic photon flux density (PPFD, B) and photochemical reflectance index (PRI, C) over two years. Different letters indicate significant different means or interactions according to analysis of variance (ANOVA) followed by pairwise comparison. Five maize genotypes were monitored from June to July 2016 and nine genotypes from July to August 2017 in an unheated greenhouse (n=22395 total and ranging from 416 to 3044 per year and genotype).

*Factor influencing $F_{r2}/F_m$ respective $F_{r2}'/F_m'$*

Lasso regression was performed to identify the important factors which influence $F_{r2}/F_m$ respective $F_{r2}'/F_m'$. After temperature which explained 55% of the variance, $F_{r2}/F_m$ respective $F_{r2}'/F_m'$ was influenced by daytime (Figure 28). The influence of daytime was rather small and not systematic probably more associated to environmental conditions at this daytime. NDVI or PPFD did not have a significant influence on $F_{r2}/F_m$ respective $F_{r2}'/F_m'$ according to Lasso regression (not shown).

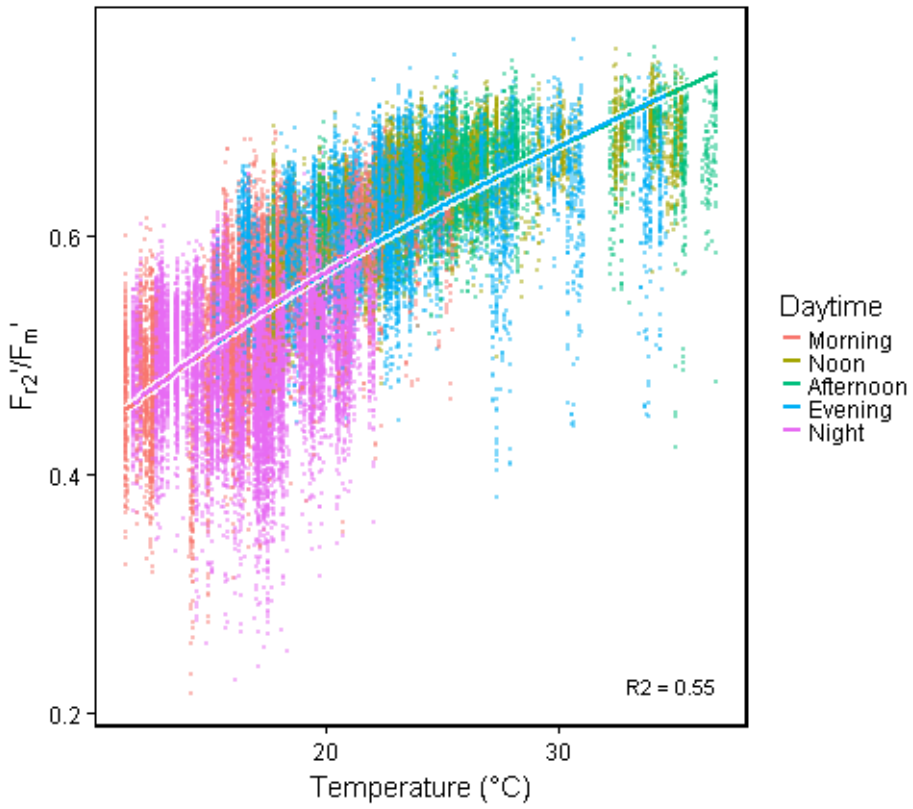


**Figure 28** Reoxidation efficiency 5 ms after primary quinone ($Q_A$) reduction ($F_{r2}/F_m$ in the dark and $F_{r2}'/F_m'$ in the light) of maize genotypes was correlated to temperature and grouped after daytime. Temperature and measurements at specific daytime influenced $F_{r2}/F_m$ respective $F_{r2}'/F_m'$ highest according to lasso regression. Fluorescence data was acquired by automated light-induced fluorescence transient (LIFT) device scanning the crop canopy. Environmental conditions as temperature were recorded every minute by three stations distributed in the unheated greenhouse and merged to the measurements done in the same minute. Measurements include two independent maize experiments in 2016 and 2017 with in total 12 genotypes. White intervals show 95% confidence intervals for the mean of $F_{r2}/F_m$ respective $F_{r2}'/F_m'$ fitted to a linear model depending on temperature (square root transformed, n=47151 measurements).

Similar as with the $F_q'/F_m'$ parameter, genotypic performance regarding $F_{r2}/F_m$ respective $F_{r2}'/F_m'$ were summarized per year using the mean only or including temperature as covariates. Regarding the mean, Genotypes B, D and K showed in both years consistently significant different $F_{r2}/F_m$ respective $F_{r2}'/F_m'$ (Figure 29). From these three genotypes, genotype D showed the highest mean of $F_{r2}/F_m$ respective $F_{r2}'/F_m'$ and Genotype K the lowest. Regarding interaction with temperature, genotype D showed in both experiments higher $F_{r2}/F_m$ respective $F_{r2}'/F_m'$ compared to genotypes K and I.

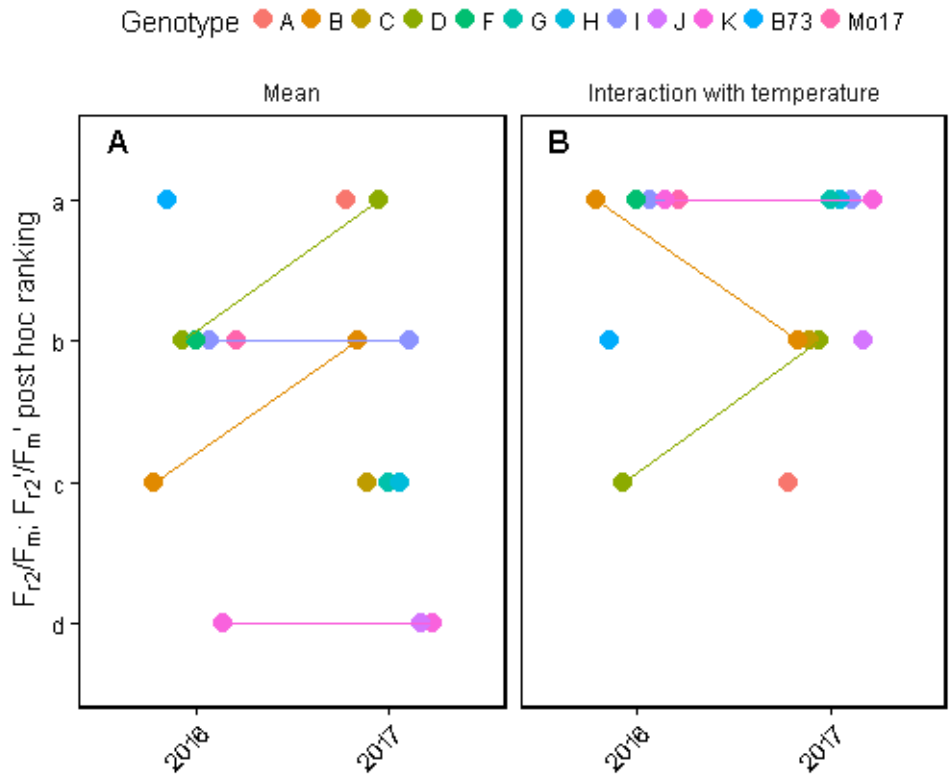


**Figure 29** Reoxidation efficiency 5 ms after primary quinone ($Q_A$) reduction ($F_{r2}/F_m$ in the dark and $F_{r2}'/F_m'$ in the light) of maize genotypes based on mean (A) and interaction (B) with temperature over two years. Different letters indicate significant different means or interactions according to analysis of variance (ANOVA) followed by pairwise comparison. Five maize genotypes were monitored from June to July 2016 and nine genotypes from July to August 2017 in an unheated greenhouse (n=40978 total, ranging from 869 to 4486 per year and genotype).

*Response to drought at selected time points*

Drought stress response in B73 and Mo17 was analyzed by selecting measurements acquired from 14.00 h to 18.00 h when the stress response seemed to be highest (Figure 30). Significant differences in fluorescence parameters were observed around one month after starting drought treatment. On June 14 before the drought treatment started, there was no significant difference between the treatments in each genotype (Figure 30). Under increasing drought stress on July 16 and 19, $F_q'/F_m'$ was in both genotypes significantly decreased compared to control. $F_{r2}'/F_m'$ was on July 19 significantly decreased in both genotypes compared to control. The response of NDVI to drought stress differed significantly on July 16 in B73. However, this response of NDVI was not consistent in the measurements three days later. Comparing both genotypes in drought tolerance, B73 showed more severe stress response in all parameters than Mo17. PPFD and temperature associated to each measurement did not significantly differ between genotypes and treatment (data not shown).

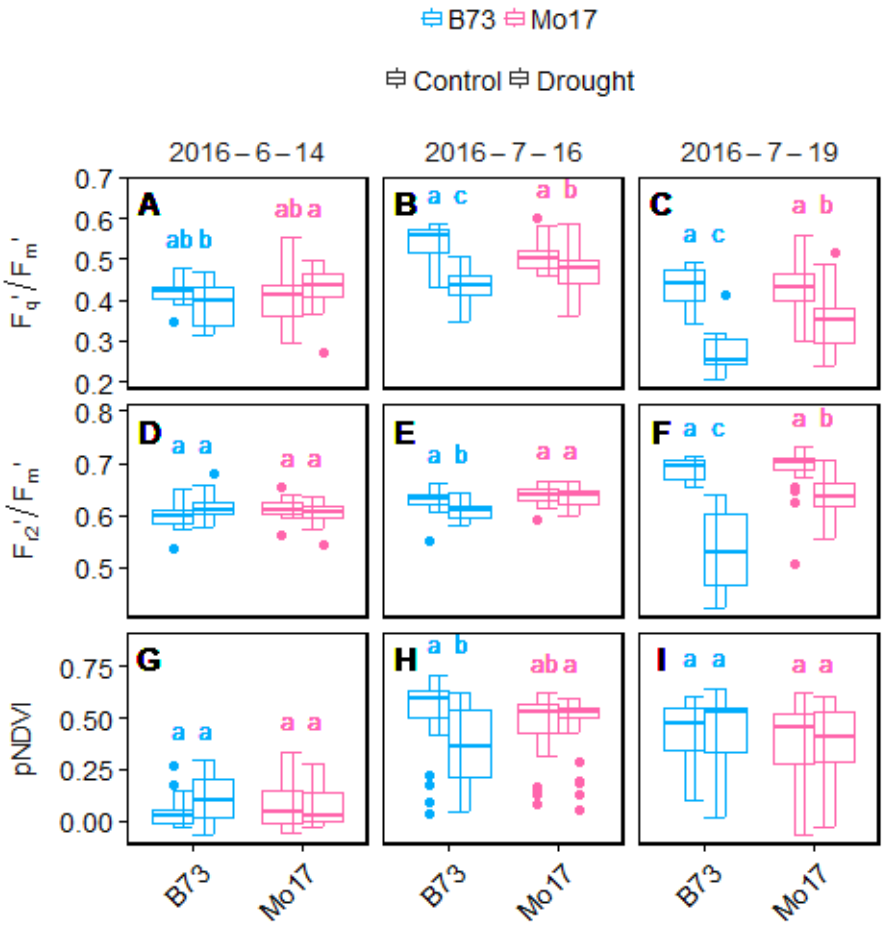


**Figure 30** Boxplot of photosystem II operating efficiency ($F_q'/F_m'$, A to C), reoxidation efficiency 5 ms after primary quinone ($Q_A$) reduction ($F_{r2}'/F_m'$, D to F) and pseudo normalized difference vegetation index (pNDVI, G to I) of three selected days before and within drought stress development (2016-06-14, 2016-07-16 and 2016-07-19, measurements averaged from 14.00 h to 18.00 h). B73 and Mo17 genotypes grew in 7 containers whereas 4 plots were subjected to drought treatment starting June 16, 2016. Box represents inter-quartile range, bold horizontal bar the median, the discontinuous lines the upper and lower quartile, and outlier data points (>1.5 × inter-quartile range) are depicted by a point. Means with different letters differ significantly using Tukey's multiple comparisons of means (n=10 to 40 measurements).

*Response to drought including environmental interaction*

Response to drought was also detected analyzing the interaction of the fluorescence parameters with PPFD and temperature using all available data. The interaction of $F_q'/F_m'$ with PPFD in control and drought treatment over time is shown in Figure 31. The light response curves in both genotypes decreased with increasing drought stress. Based on the slope of the light response curve pairwise comparison was conducted (Figure 32). Both genotypes ended with significant different interaction with PFFD under drought stress compared to control. The detection using interaction of $F_q'/F_m'$ with PPFD was more consistent than comparing the means of both treatments. In interaction with PPFD, Mo17 was more sensitive than B73. In contrast, the $F_q'/F_m'$ means of B73 were lower compared to Mo17

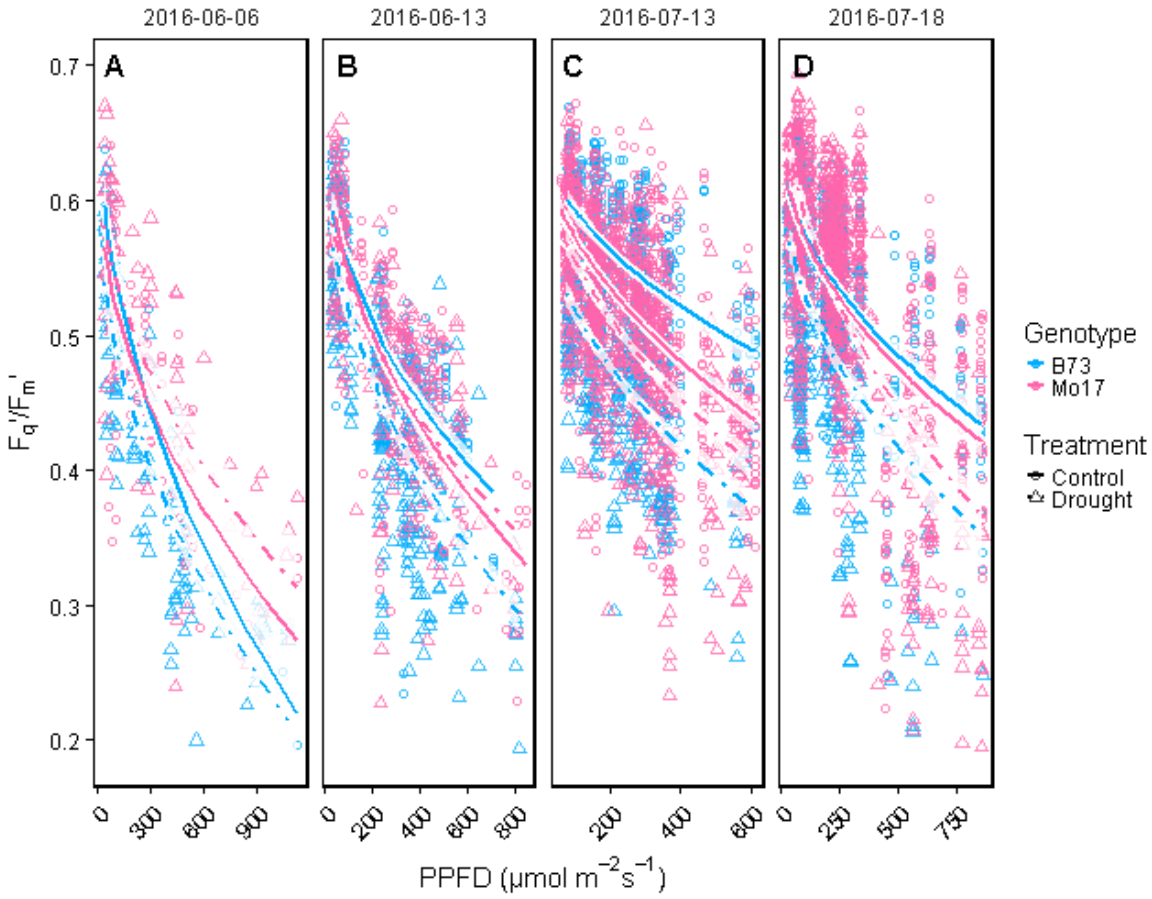


**Figure 31** Photosystem II operating efficiency ($F_q'/F_m'$) was correlated to photon flux density (PPFD), grouped after genotype and treatment and split into four dates (A to D). The date represents all measurements taken in the same week of the indicated date. Fluorescence data was acquired by automated light-induced fluorescence transient (LIFT) device scanning the crop canopy. Environmental conditions as PPFD and temperature were recorded every minute by three stations distributed in the unheated greenhouse and merged to the measurements done in the same minute. B73 and Mo17 genotypes grew in 7 containers whereas two plots of each genotype were subjected to drought treatment starting June 16, 2016. White intervals show 95% confidence intervals for the mean of $F_q'/F_m'$ fitted to a linear model depending on PPFD (square root transformed, n=5192 measurements total, ranging from 28 to 654 measurements per treatment and genotype).

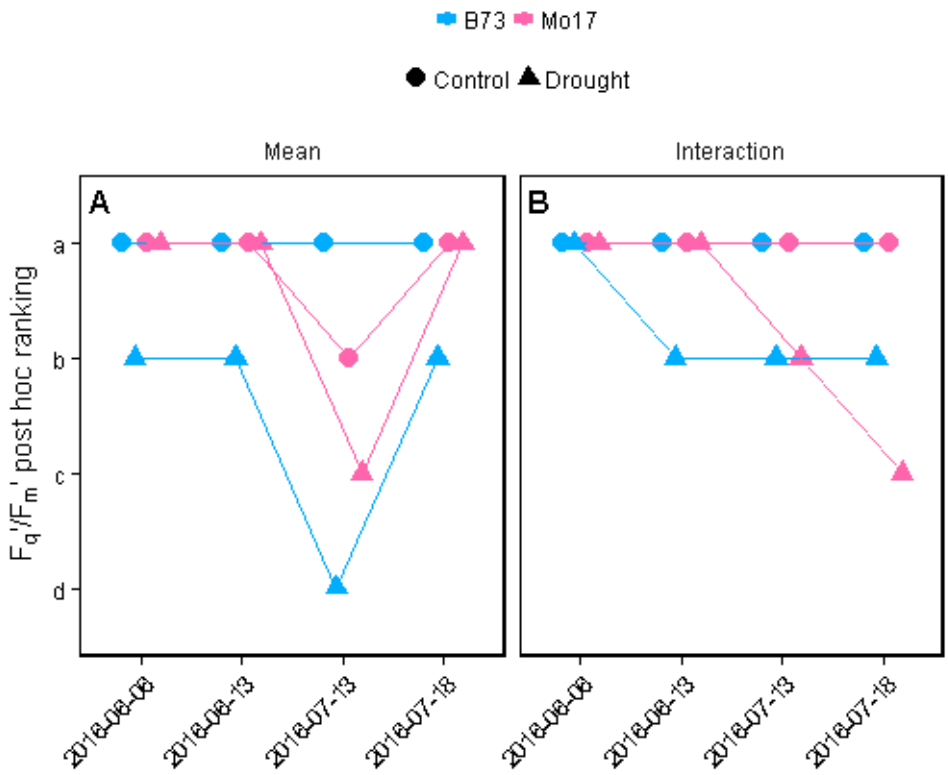


**Figure 32** Ranking of photosystem II operating efficiency ($F_q'/F_m'$) of B73 and Mo17 maize genotypes based on mean (A) and interaction (B) with photon flux density (PPFD) and pseudo normalized difference vegetation index (NDVI) in control and drought conditions. Different letters indicate significant different means or interactions according to analysis of variance (ANOVA) followed by pairwise comparison. Analysis was done with measurements bulked per week from the indicated date (n=5192 total and ranging from 28 to 654 per treatment and genotype). Drought treatment started on June 16, 2016.

Similar as in $F_q'/F_m'$, response to drought was detected analyzing the interaction of $F_{r2}/F_m$ respective $F_{r2}'/F_m'$ with temperature in control and drought treatment over time (Figure 33). Increasing drought stress clearly affected the response of $F_{r2}/F_m$ respective $F_{r2}'/F_m'$ to temperature. Based on the mean and the slope of the temperature response curve pairwise comparisons were conducted (Figure 34). In both genotypes, the mean of $F_{r2}/F_m$ respective $F_{r2}'/F_m'$ and the interaction with temperature separated drought and control treatment. Focusing on the interaction with temperature, differences of genotypes and treatments were developing with increasing drought stress. At the end of the treatment, B73 showed a more sensitive response to drought than Mo17 in interaction with temperature.

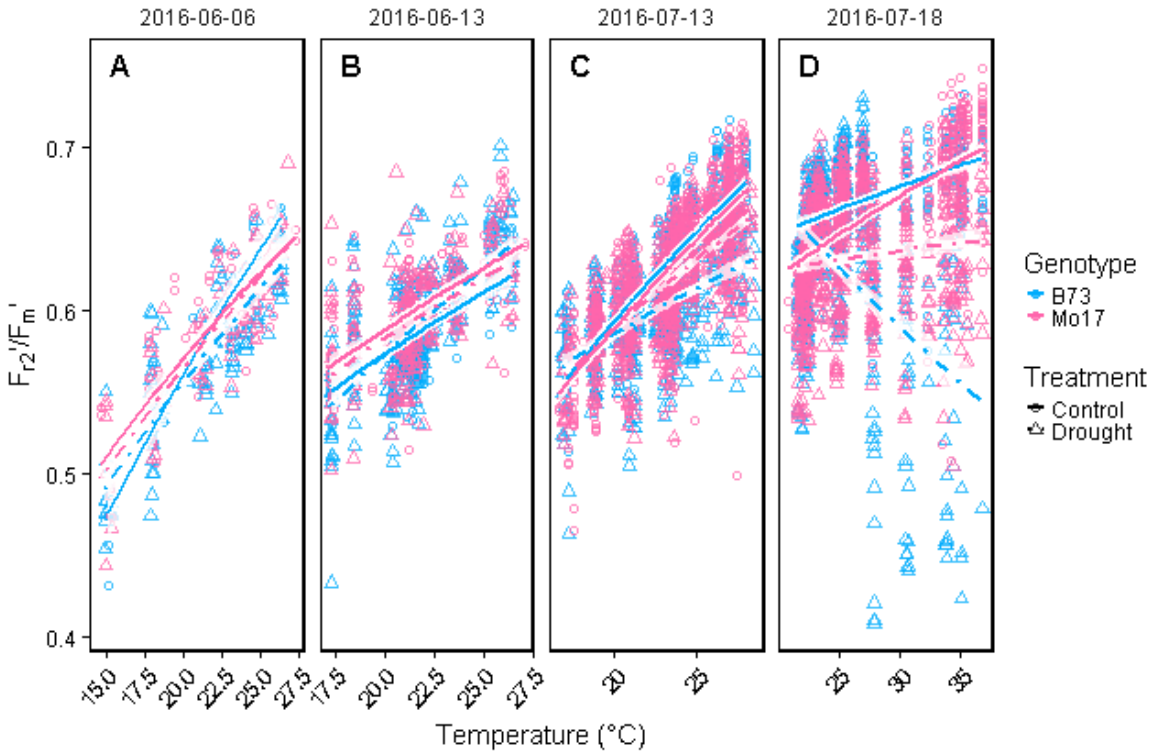


**Figure 33** Reoxidation efficiency 5 ms after primary quinone ($Q_A$) reduction ($F_{r2}'/F_m'$) was correlated to temperature, grouped after genotype and treatment and split into four dates (A to D). The date represents all measurements taken in the same week of the indicated date. Fluorescence data was acquired by automated light-induced fluorescence transient (LIFT) device scanning the crop canopy. Environmental conditions as temperature were recorded every minute by three stations distributed in the unheated greenhouse and merged to the measurements done in the same minute. B73 and Mo17 genotypes grew in 7 containers whereas two plots of each genotype were subjected to drought treatment starting June 16, 2016. White intervals show 95% confidence White intervals show 95% confidence intervals for the mean of $F_{r2}/F_m$ respective $F_{r2}'/F_m'$ fitted to a linear model depending on temperature (square root transformed, n=5'192 measurements total, ranging from 28 to 654 measurements per treatment and genotype).

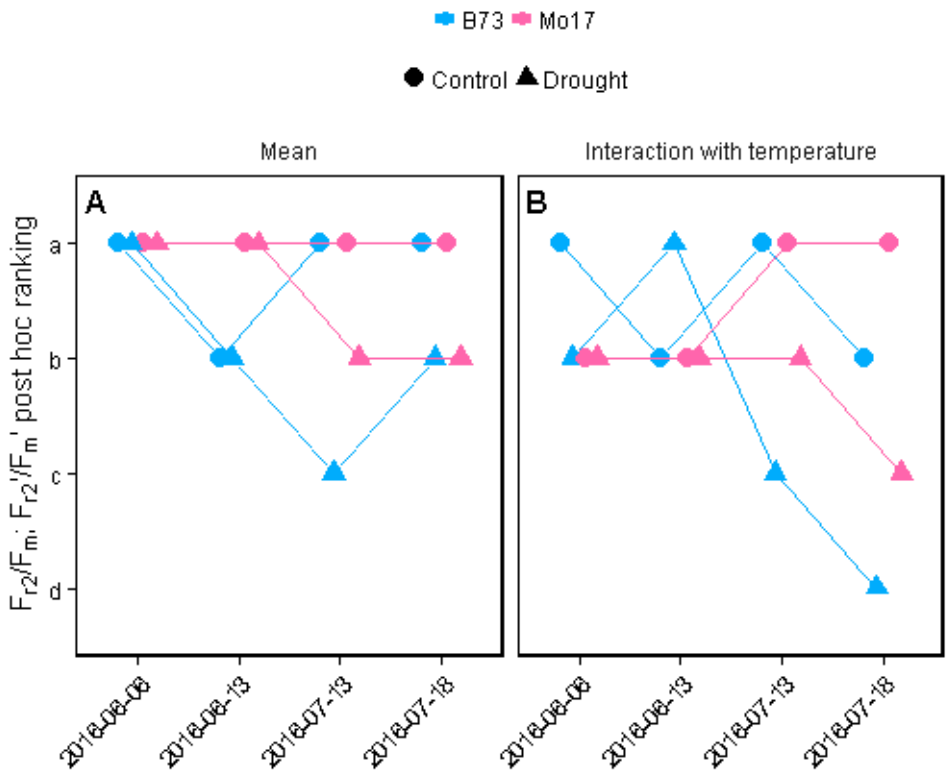


**Figure 34** Ranking of reoxidation efficiency 5 ms after primary quinone ($Q_A$) reduction ($F_{r2}/F_m$ in the dark and $F_{r2}'/F_m'$ in the light) of B73 and Mo17 maize genotypes based on mean (A) and interaction with temperature (B) in control and drought conditions. Different letters indicate significant different means or interactions according to analysis of variance (ANOVA) followed by pairwise comparison. Analysis was done with measurements bulked per week from the indicated date (n=5192 total and ranging from 28 to 654 per treatment and genotype). Drought treatment started on June 16, 2016.

*Modeling*

In order to get a mechanistic understanding of processes linked to $Q_A$ reduction and reoxidation, fluorescence transient data were fitted to the LIFT model. The same raw data as in Figure 30 was taken for modeling of the fluorescence transient using the LIFT software (see section 2.1.2). The fluorescence transients and model fits are shown in Figure 35. Although the model fitted the data well, some derived parameter values showed high influence and leverage on statistical analysis (Cook's distance four times bigger than the average) and were therefore removed from the data set. As expected, modeled $F_q'/F_m'$ and $\tau_2$ showed the same pattern as $F_q'/F_m'$ and $F_{r2}'/F_m'$ which were directly retrieved from the raw data (Figure 36).

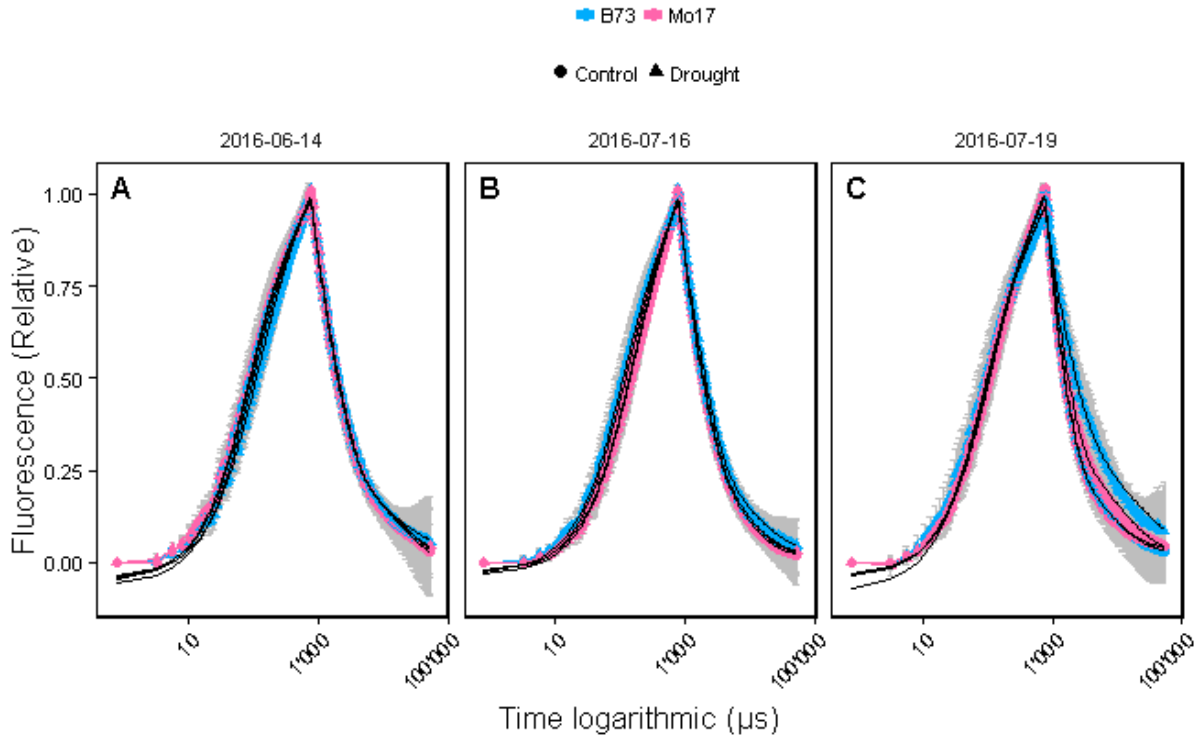


**Figure 35** Fluorescence transient of maize canopy of three selected days before and with increasing drought stress (measurements were selected and averaged from 14.00 h to 18.00 h). B73 and Mo17 genotypes grew in 7 containers. Four containers were subjected to drought starting from June 16. Light-induced fluorescence transient (LIFT) method with $Q_A$- flash excitation protocol was used to measure from about 60 to 80 cm distance. Error bars showing standard deviation of the mean (n=10 to 40 measurements).

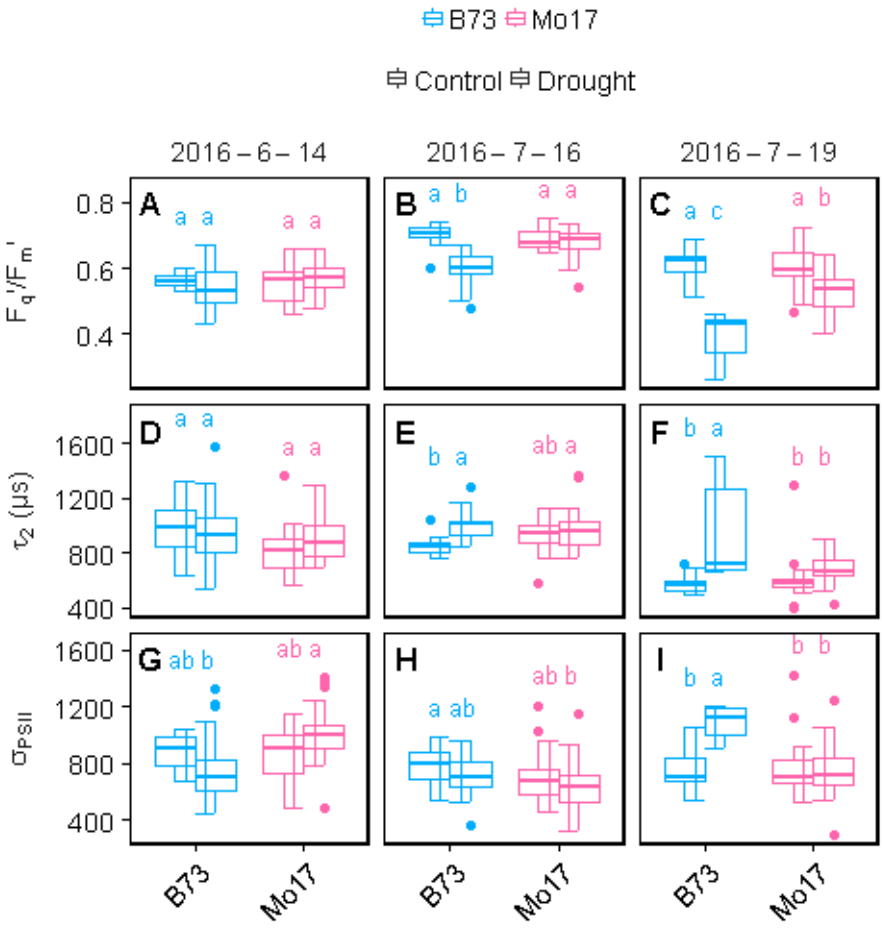


**Figure 36** Boxplot of modeled operating efficiency of the photosystem II ($F_q'/F_m'$, A to C), electron transport time constants ($\tau_2$, D to F) and functional absorption cross section of photosystem II ($\sigma_{PSII}$, G to I) of three selected days before and within drought stress development (2016-06-14, 2016-07-16 and 2016-07-19, measurements averaged from 14.00 h to 18.00 h). B73 and Mo17 genotypes are shown growing in 7 containers. Highly influencing data points (Cook's distance > 4 x average of Cook's distance) were removed. 4 containers were subjected to drought treatment starting June 16. Box represents inter-quartile range, bold horizontal bar the median, the discontinuous lines the upper and lower quartile, and outlier data points (>1.5 × inter-quartile range) are depicted by a point. Means with different letters differ significantly using Tukey's multiple comparisons of means (n=6 to 38 measurements).

### 3.2.5 Soybean

Photosynthetic performance in soybean was assessed over two seasons under fluctuating environmental conditions in the *Miniplot* facility. Figure 37 shows data from six soybean genotypes acquired in 2016. The diurnal pattern of $F_v/F_m$ respective $F_q'/F_m'$ and $F_{r2}/F_m$ respective $F_{r2}'/F_m'$ was again clearly detected. Three genotypes were subjected to drought treatment on October 5, resulting in higher variance of those genotypes. Possibly, that wilting plants caused a higher variation in data while the S/N ratio was not affected and therefore those data was not removed. Pots-hoc ANOVA ranking showed consistent significant lower $F_q'/F_m'$ of Gallec and Amarok compared to the other genotypes in the beginning in October 2016 (Figure 38). In this time period, Tourmaline showed also significant lower $F_{r2}/F_m$ respective $F_{r2}'/F_m'$ compared to the other genotypes. Temperature and PPFD values were mostly the same during measurements of the different genotypes.

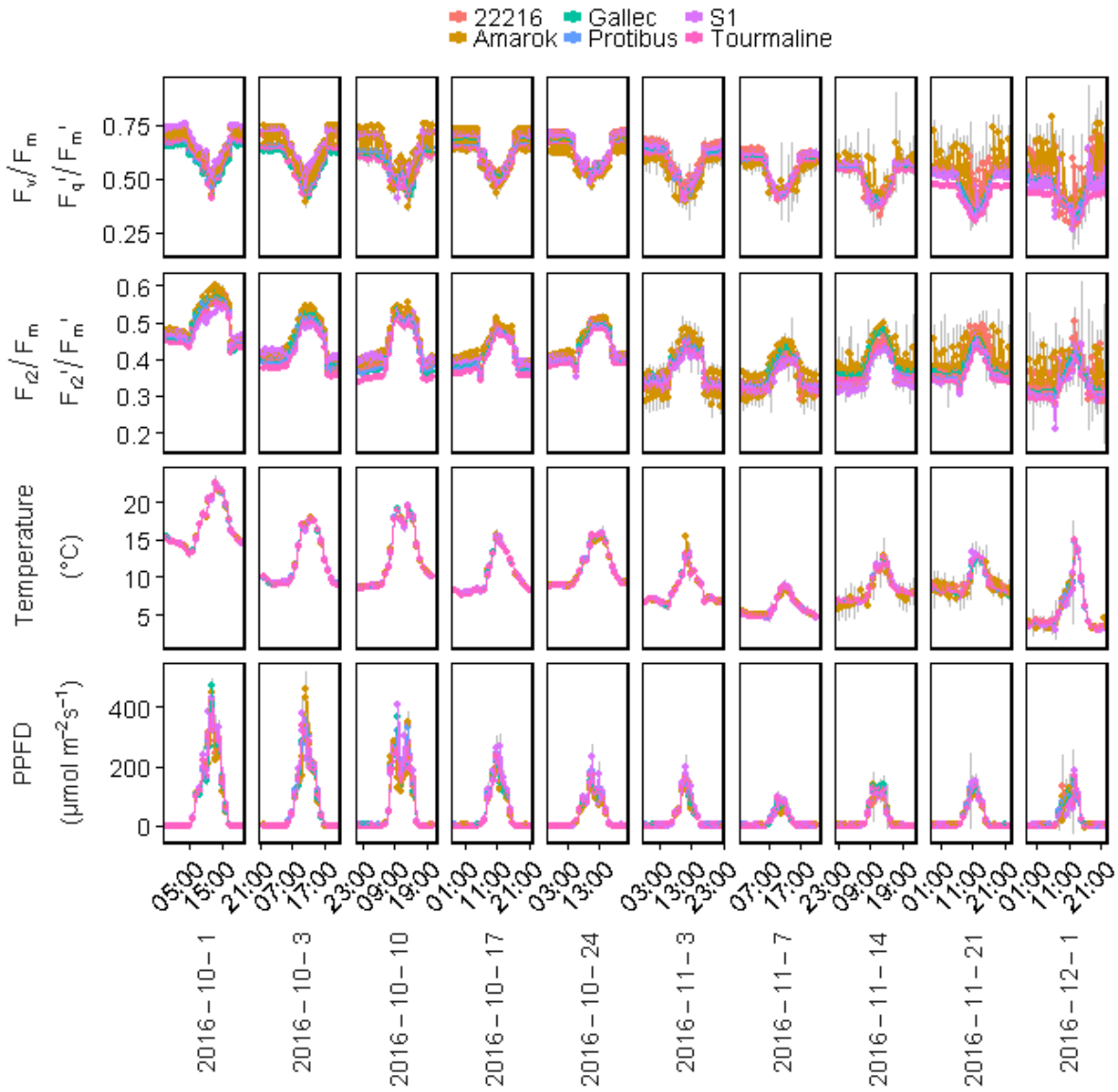


**Figure 37** Response of quantum efficiency of the photosystem II ($F_v/F_m$ in the dark and $F_q'/F_m'$ in the light), reoxidation efficiency 5 ms after primary quinone ($Q_A$) reduction ($F_{r2}/F_m$ in the dark and $F_{r2}'/F_m'$ in the light) of soybean genotypes, associated temperature and photosynthetic photon flux density (PPFD) averaged per hour and week. Fluorescence data was acquired by automated light-induced fluorescence transient (LIFT) device scanning crop canopy. Environmental conditions as temperature were recorded every minute by three stations distributed in the unheated greenhouse and merged to the measurements done in the same minute. Grey error bars show 95% confidence interval (n=177165 in total). Six soybean genotypes were monitored in 15 plots. Drought treatment started at October 5, 2016 in four plots.

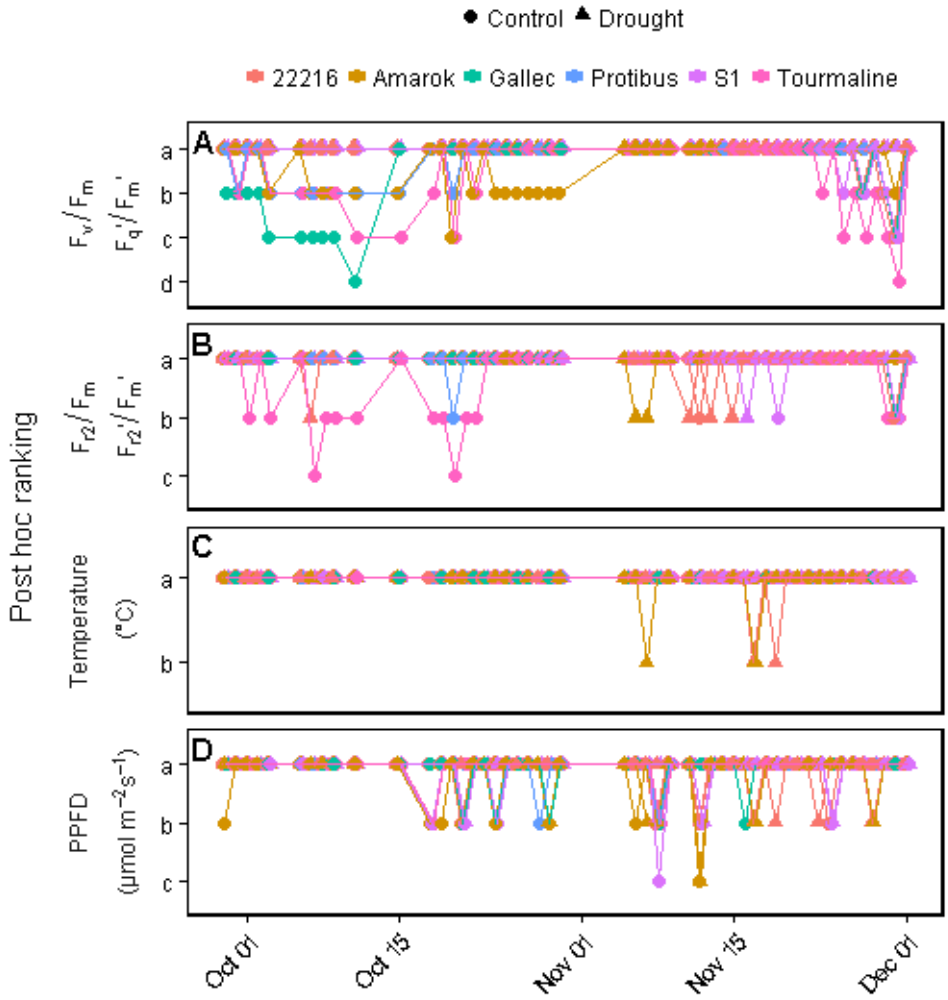


**Figure 38** Analysis of variance (ANOVA) followed by Scheffé test for 6 soybean genotypes was performed daily for quantum efficiency of the photosystem II ($F_v/F_m$ in the dark and $F_q'/F_m'$ in the light, A), reoxidation efficiency 5 ms after primary quinone ($Q_A$) reduction ($F_{r2}/F_m$ in the dark and $F_{r2}'/F_m'$ in the light, B) and associated temperature (C) and photosynthetic photon flux density (PPFD, D). Data was averaged per hour and day. Fluorescence data was acquired by automated light-induced fluorescence transient (LIFT) device scanning crop canopy. Environmental conditions as temperature were recorded every minute by three stations distributed in the unheated greenhouse and merged to the measurements done in the same minute. Six soybean genotypes were monitored in 15 plots. Drought treatment started at October 5, 2016 in four plots.

*Factors influencing $F_q'/F_m'$*

Lasso regression was performed to identify the factors determining $F_q'/F_m'$. PRI, PPFD and measuring date were highest correlated to $F_q'/F_m'$ explaining 20.9%, 17.8% (15.3% in the linear relation and additional 2.5% for the square root response) and 8.5% of the variance, respectively (Table S 1). PPFD explained up to 29% of the variance when measurements were grouped after different ranges of PRI (Figure 39).

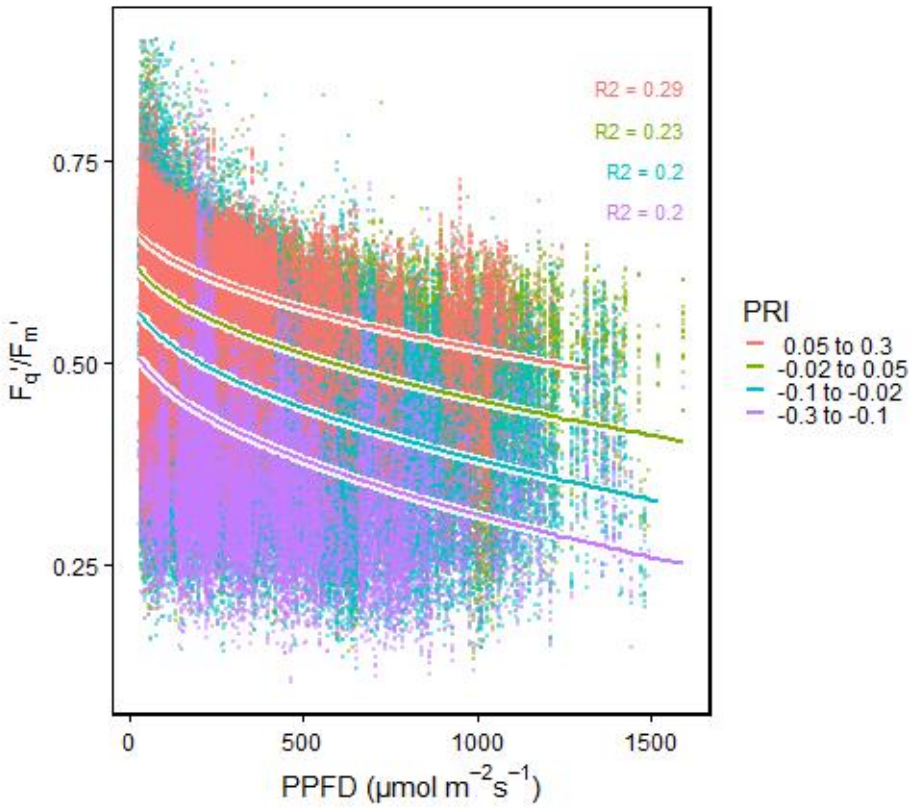


**Figure 39** Photosystem II operating efficiency ($F_q'/F_m'$) of soybean genotypes was correlated to photosynthetic photon flux density (PPFD) and grouped after photochemical reflectance index (PRI) values. Light-induced fluorescence transient (LIFT) devices scanned canopy of up to 28 containers automatically acquiring fluorescence and spectral data every hour throughout a measuring day. $F_q'/F_m'$ was highest influenced by PRI followed by PPFD according to lasso regression. PPFD was recorded by up to three stations distributed in an unheated greenhouse. Measurements took place from September 2016 to August 2017 in 9 soybean genotypes. White intervals show 95% confidence intervals for the mean of $F_q'/F_m'$ fitted to a linear model depending on PPFD (square root transformed, n=279523 measurements, modified from Keller et al., in prep.).

Genotypic differences explained 0.7% of the variance (Table S 1). Still, significant differences could be detected between genotypes using mean and interaction with PPFD and PRI (Figure 40). The analysis on the mean is not very consistent comparing the two years whereas analyzing the interaction with PPFD and PRI improves the consistency. For example, regarding the interaction of $F_q'/F_m'$ with PRI the genotypes 22216 and Amarok showed in both years consistent significant lower interaction than the other genotypes.

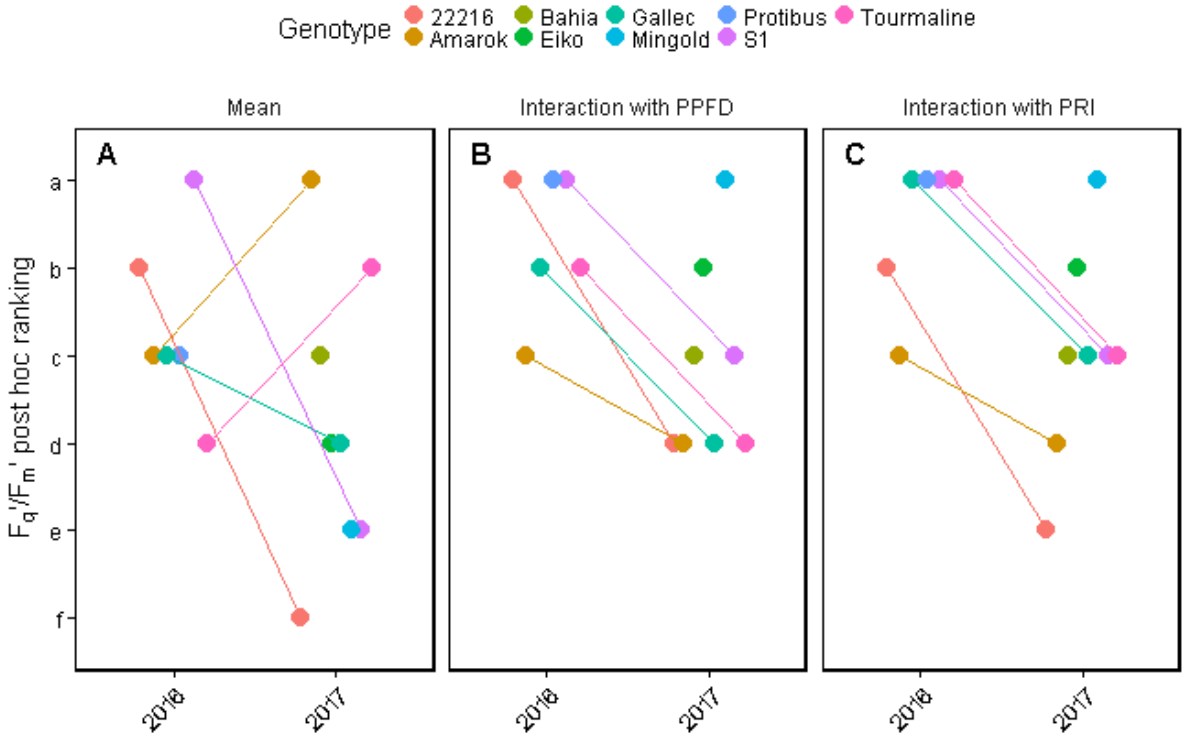


**Figure 40** Ranking of photosystem II operating efficiency ($F_q'/F_m'$) of soybean genotypes based on mean (A), interaction with photosynthetic photon flux density (PPFD, B) and photochemical reflectance index (PRI, C) over two years. Different letters indicate significant different means or interactions according to analysis of variance (ANOVA) followed by pairwise comparison. Six genotypes were monitored from September to November 2016 and eight genotypes from March to August 2017 in an unheated greenhouse (n= 270661 total, ranging from 2331 to 38854 per year and genotype).

*Factors influencing $F_{r2}/F_m$ respective $F_{r2}'/F_m'$*

According to the results of Lasso regression, $F_{r2}/F_m$ respective $F_{r2}'/F_m'$ was linear modeled with selected parameters, Temperature and plant age. Temperature was best correlated with $F_{r2}/F_m$ respective $F_{r2}'/F_m'$ explaining 77% of the variance (square root transformed, n=625774 measurements) (Figure 23). The age of the plant and therefore increasing height of the plant did contribute with less than 0.1% to the explained variance (not shown).

Differences of $F_{r2}/F_m$ respective $F_{r2}'/F_m'$ were analyzed for the cold tolerant and sensitive genotypes. Significant influence of specific genotypes in response to temperature were detected (Figure 41). Although, the differences in $F_{r2}/F_m$ respective $F_{r2}'/F_m'$ were small, they were significant and rather consistently measured over two seasons. Considering interaction with temperature the consistency of genotypic differences over two seasons was even higher (Figure 42). Regarding the mean of $F_{r2}/F_m$ respective $F_{r2}'/F_m'$, MinnGold genotype showed highest values in the one season it was measured. Only genotype Tourmaline separated significant and consistent over two seasons from the other genotypes. When interaction with temperature was considered, genotype S1, Tourmaline and 22216 separated consistently from each other. Regarding cold tolerance, the three genotypes Gallec, Amarok and Tourmaline known for cold tolerance did not differ systematically from the others in the response of $F_{r2}/F_m$ respective $F_{r2}'/F_m'$ to temperature (Figure S 8).

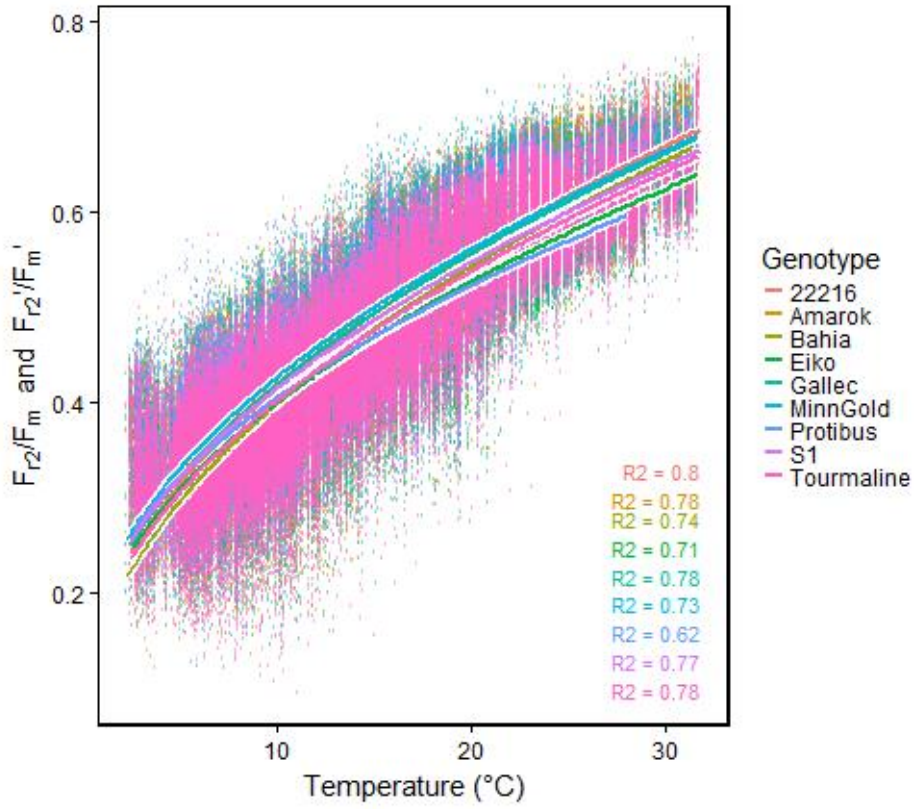


**Figure 41** Reoxidation efficiency 5 ms after primary quinone ($Q_A$) reduction ($F_{r2}/F_m$ in the dark and $F_{r2}'/F_m'$ in the light) in 9 soybean genotypes showed high correlation with temperature. Fluorescence data was acquired by a light-induced fluorescence transient (LIFT) device scanning crop canopy from an automated moving platform. Environmental conditions as temperature were recorded every minute by three stations distributed in the greenhouse and merged to the measurements done in the same minute. Six genotypes were monitored from September to November 2016 and eight genotypes from March to August 2017 in an unheated greenhouse. White intervals show 95% confidence intervals for the mean $F_{r2}/F_m$ respective $F_{r2}'/F_m'$ which was fitted to a linear model depending on temperature (square root transformed, n= 585520 measurements ranging from 28385 to 97889 per genotypes, modified from Keller et al., in prep.).

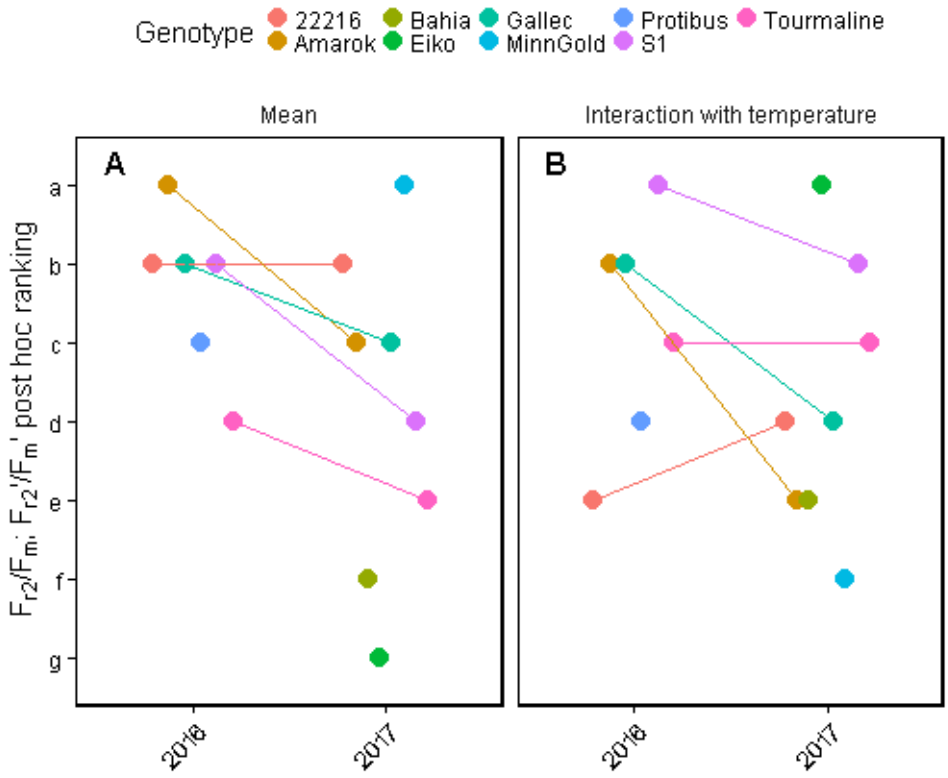


**Figure 42** Reoxidation efficiency 5 ms after primary quinone ($Q_A$) reduction ($F_{r2}/F_m$ in the dark and $F_{r2}'/F_m'$ in the light) of soybean genotypes based on mean (A) and interaction (B) with temperature over two years. Different letters indicate significant different means or interactions according to analysis of variance (ANOVA) followed by pairwise comparison. Six genotypes were monitored from September to November 2016 and eight genotypes from March to August 2017 in an unheated greenhouse (n= 585520 total, ranging from 12086 to 70440 per year and genotype).

*Response to drought at selected time point*

Drought treatment which started on October 5, showed significant differences in $F_{r2}'/F_m'$ in the beginning of November when data from the whole day was averaged (Figure 38). Detailed comparison of measurements acquired at noon between the end of September and end of October showed tendency of lower $F_{r2}'/F_m'$ and NDVI values in S1 genotypes compared to control (Figure S 7). However, these differences were only significant comparing 22216 control to S1 drought treatment. Regarding $F_q'/F_m'$ and NPQ, no significant effect of drought in S1 and 22216 genotype were detected.

*Influence of plant height and leaf angle*

Variance introduced by leaf angle and distance ranging from 750 to 1200 mm is shown in Figure 43. At noon and night, LIFT signal was not significantly affected by changes of the measuring distance in the dynamic range of 150 mm.

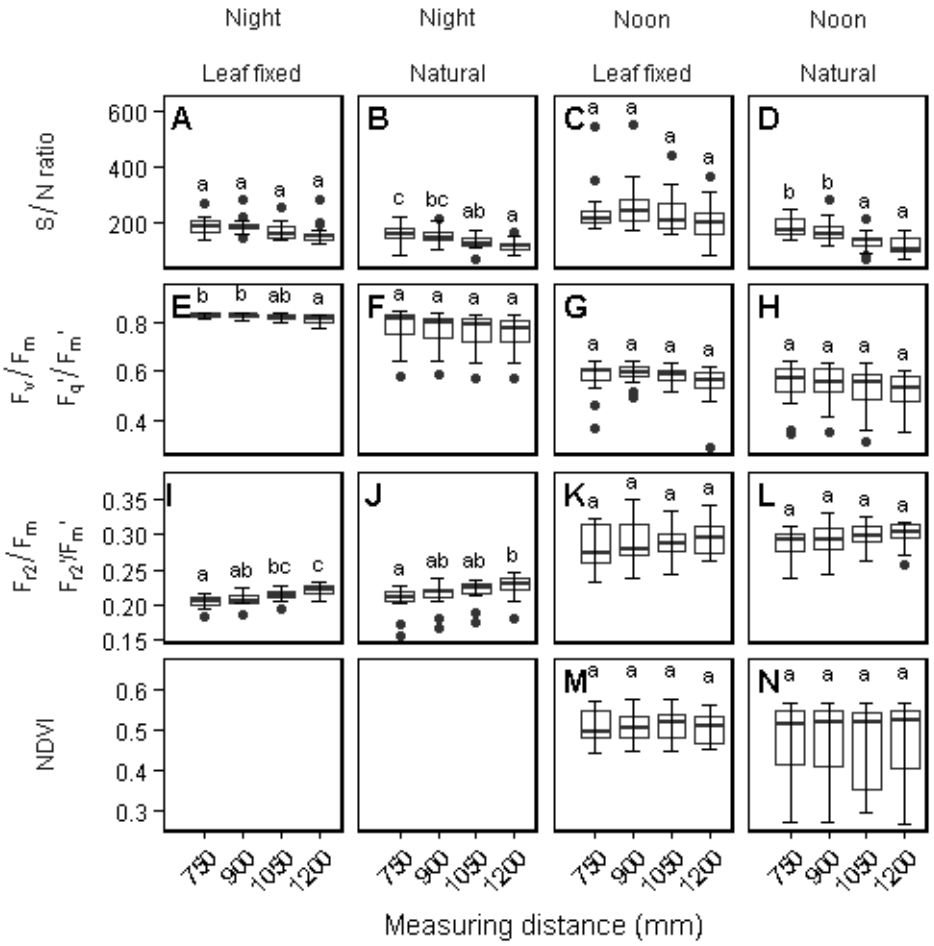


**Figure 43** Boxplot of signal to noise ratio (S/N ratio, A to D), operating efficiency of the photosystem II ($F_v/F_m$ in the dark and $F_q'/F_m'$ in the light, E to H), reoxidation efficiency 5 ms after primary quinone ($Q_A$) reduction ($F_{r2}/F_m$ in the dark and $F_{r2}'/F_m'$ in the light, I to L) and normalized difference vegetation index (NDVI, M, N) with measuring distance ranging from 750 mm to 1200 mm and fixed or natural leaf angle as treatments. Measurements were carried out at night or at noon (n=14 to 16). Box represents inter-quartile range, bold horizontal bar the median, the discontinuous lines the upper and lower quartile, and outlier data points (>1.5 × inter-quartile range) are depicted by a point. Means with different letters differ significantly using Tukey's multiple comparisons of means.

However, decreasing measuring distance, i.e. when the target gets out of the range where the measuring beam is focused, influenced the signal more strongly. According to one way ANOVA, the effect of whole distance range from 750 to 1200 mm to $F_v/F_m$ and $F_{r2}/F_m$ accounted for about 1.4% and 19.3% of the variance during night measurements, respectively (Table S 4). In contrast, leaf angle affected more $F_v/F_m$ (23.6% of explained variance) than $F_{r2}/F_m$ (2.2 % of explained variance). At noon, the explained variance for $F_q'/F_m'$, $F_{r2}'/F_m'$ and NDVI is not bigger than 8% (Table 4). Regarding S/N ratio, fixing the leaf angle explained 29.7% of the variance, thus did improve the measuring signal. Interaction of leaf angle and distance accounted for not more than 1% of variance during day or night.

**Table 4** Analysis of variance (ANOVA) was carried out for signal to noise ratio (S/N ratio), operating efficiency of the photosystem II ($F_q'/F_m'$), reoxidation efficiency 5 ms after primary quinone ($Q_A$) reduction ($F_{r2}'/F_m'$) and normalized difference vegetation index (NDVI) with distance from 750 mm to 1200 mm and fixed or natural leaf angle as depending factors. ANOVA is described by degree of freedom (Df), sum of squares (Sum Sq), mean of squares (Mean Sq), ratio of Mean Sq and Mean Sq error (F value), the associated p value (Pr(>F)) and the explained Sum Sq per factor (ExpVar). Measurements were done at noon (n=124).

| | Variable | Df | Sum Sq | Mean Sq | F value | Pr(>F) | ExpVar |
|---|---|---|---|---|---|---|---|
| Distance | S/N ratio | 3 | 62982.91 | 20994.3 | 5 | 0.00252 | 7.9 |
| Leaf angle | | 1 | 236366.82 | 236366.82 | 56.8 | 0 | 29.7 |
| Residuals | | 119 | 495334.64 | 4162.48 | NA | NA | 62.3 |
| Distance | $F_q'/F_m'$ | 3 | 0.02 | 0.01 | 1.3 | 0.26894 | 3 |
| Leaf angle | | 1 | 0.06 | 0.06 | 10.6 | 0.00145 | 8 |
| Residuals | | 119 | 0.64 | 0.01 | NA | NA | 89.1 |
| Distance | $F_{r2}'/F_m'$ | 3 | 0 | 0 | 1.9 | 0.13955 | 4.5 |
| Leaf angle | | 1 | 0 | 0 | 0.8 | 0.37409 | 0.6 |
| Residuals | | 119 | 0.07 | 0 | NA | NA | 94.9 |
| Distance | NDVI | 3 | 0 | 0 | 0 | 0.99166 | 0.1 |
| Leaf angle | | 1 | 0.04 | 0.04 | 7.8 | 0.00605 | 6.2 |
| Residuals | | 119 | 0.6 | 0.01 | NA | NA | 93.8 |

*Recovery from non-photochemical quenching (NPQ)*

After three minutes of exposure to strong blue light (approximate 1000 µmol photons $m^{-2}$ $s^{-1}$), the recovery of Eiko and MinnGold was monitored over 15 min (Figure 44). $F_v/F_m$ was the same in both genotypes in the dark-adapted state, but differed significantly after exposure to blue light. NPQ developed less strongly in MinnGold directly after exposure compared to Eiko genotype. MinnGold reached almost initial levels of NPQ after 120 s (mean of 0.076 (±0.128)) whereas Eiko showed still a mean of 0.285 (±0.183).

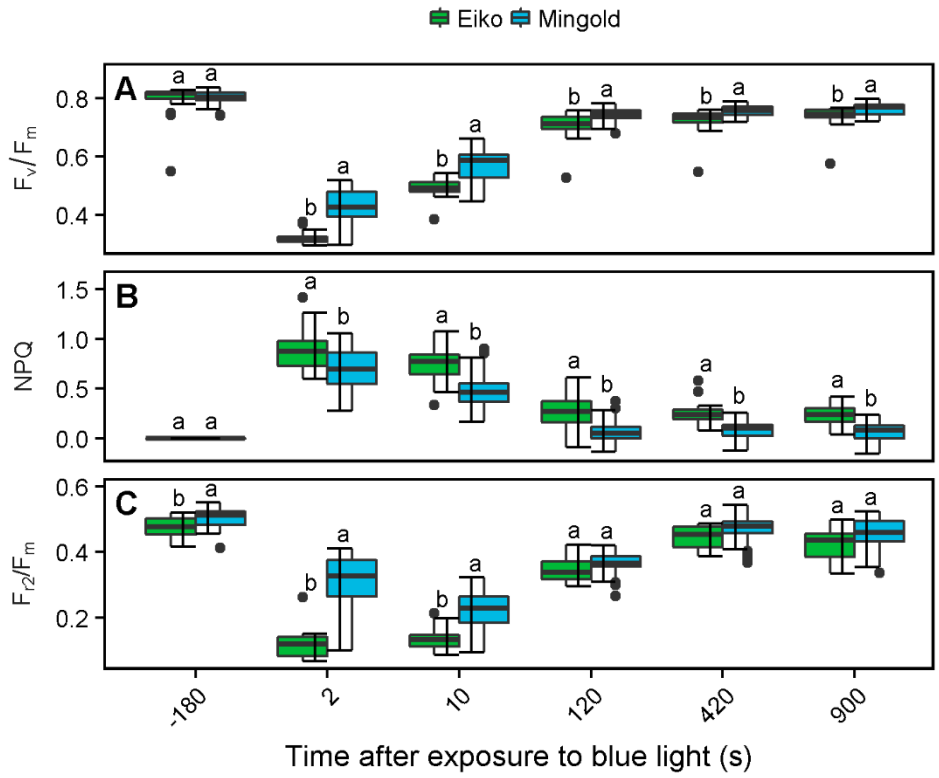


**Figure 44** Recovery of maximum quantum efficiency of the photosystem II ($F_v/F_m$), non-photochemical quenching (NPQ) and reoxidation efficiency 5 ms after primary quinone ($Q_A$) reduction ($F_{r2}/F_m$) in the dark after 180 s of blue light exposure in two soybean genotypes. Blue light intensity (445 nm) was approximate 1000 µmol photons $m^{-2}$ $s^{-1}$ for three minutes on one spot. Excitation light was provided by a light-induced fluorescence transient (LIFT) devices mounted to a platform which automatically moved between several excited spots to monitor recovery from the blue light providing a higher-throughput. Measurements were done in one night in an unheated greenhouse (n=13 for Eiko and 30 for MinnGold). Box represents inter-quartile range, bold horizontal bar the median, the discontinuous lines the upper and lower quartile, and outlier data points (>1.5 × inter-quartile range) are depicted by a point. Means with different letters differ significantly between genotypes at the indicated time step.

### 3.2.6 Barley

Six barley genotypes were monitored in control conditions and subjected to powdery mildew infection in 2015 and 2016 using the automated LIFT system (Figure 45). About two weeks after infection, infected genotypes Grace, Gesine and Milford showed significant lower $F_v/F_m$ respective $F_q'/F_m'$ compared to control at specific days (Figure 46). Interestingly, the infected resistant cultivars Irina and Eileen seemed not to be affected in $F_v/F_m$ respective $F_q'/F_m'$ but decreased in $F_{r2}/F_m$ respective $F_{r2}'/F_m'$ compared to control. As expected, temperature and PPFD at the time of the measurements were in general the same for all genotypes. It means influence of these environmental factors averaged to the same level over the measurements during the day.

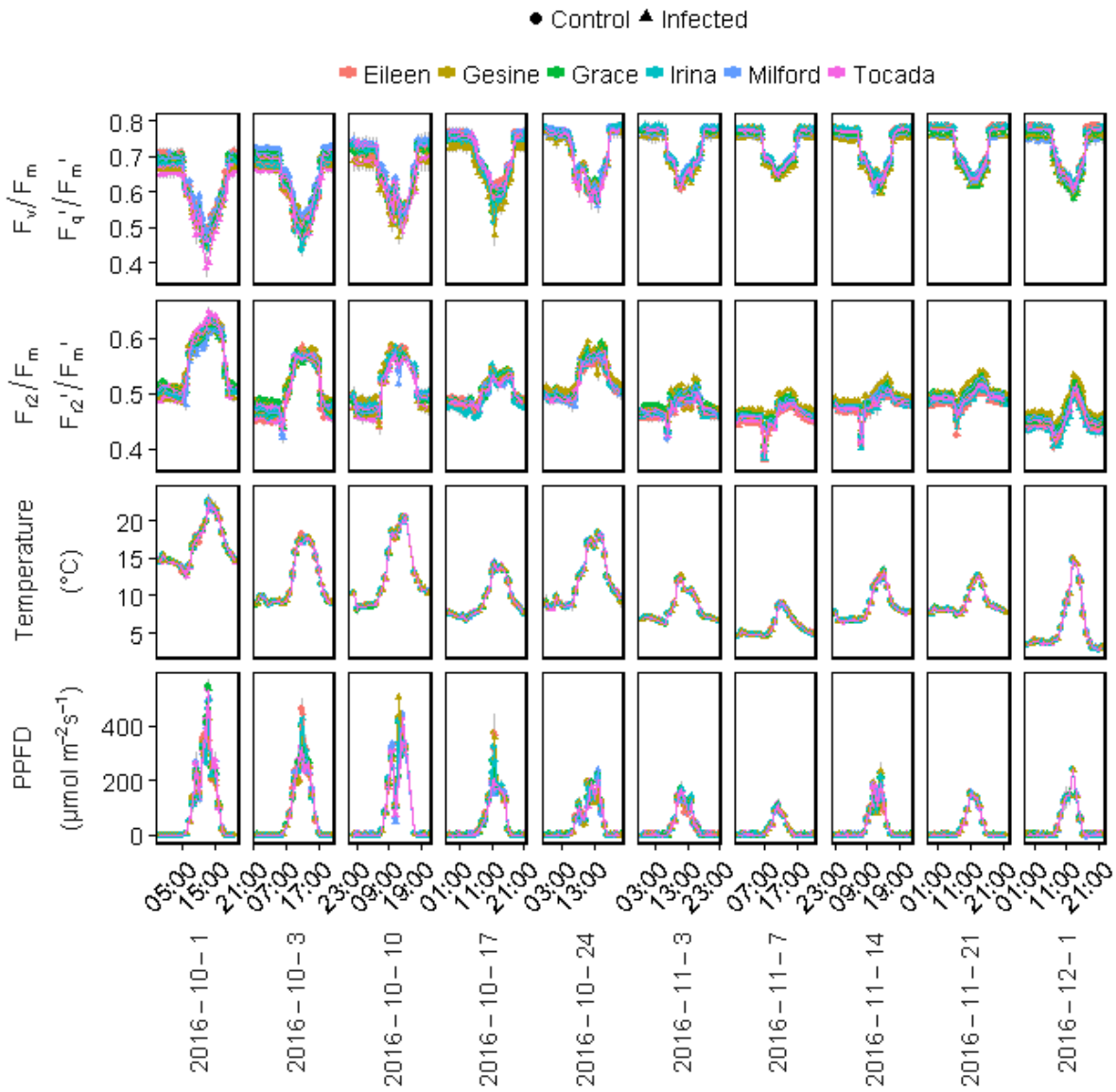


**Figure 45** Quantum efficiency of the photosystem II ($F_v/F_m$ in the dark and $F_q'/F_m'$ in the light), reoxidation efficiency 5 ms after primary quinone ($Q_A$) reduction ($F_{r2}/F_m$ in the dark and $F_{r2}'/F_m'$ in the light) of barley genotypes, associated temperature and photosynthetic photon flux density (PPFD) were averaged per hour and week. Fluorescence data was acquired by automated light-induced fluorescence transient (LIFT) device scanning crop canopy. Environmental conditions as temperature were recorded every minute by three stations distributed in the unheated greenhouse and merged to the measurements done in the same minute. Grey error bars show 95% confidence interval. Six barley genotypes were monitored from October to December 2016 in 12 plots. 6 plots were infected with powdery mildew on November 2.

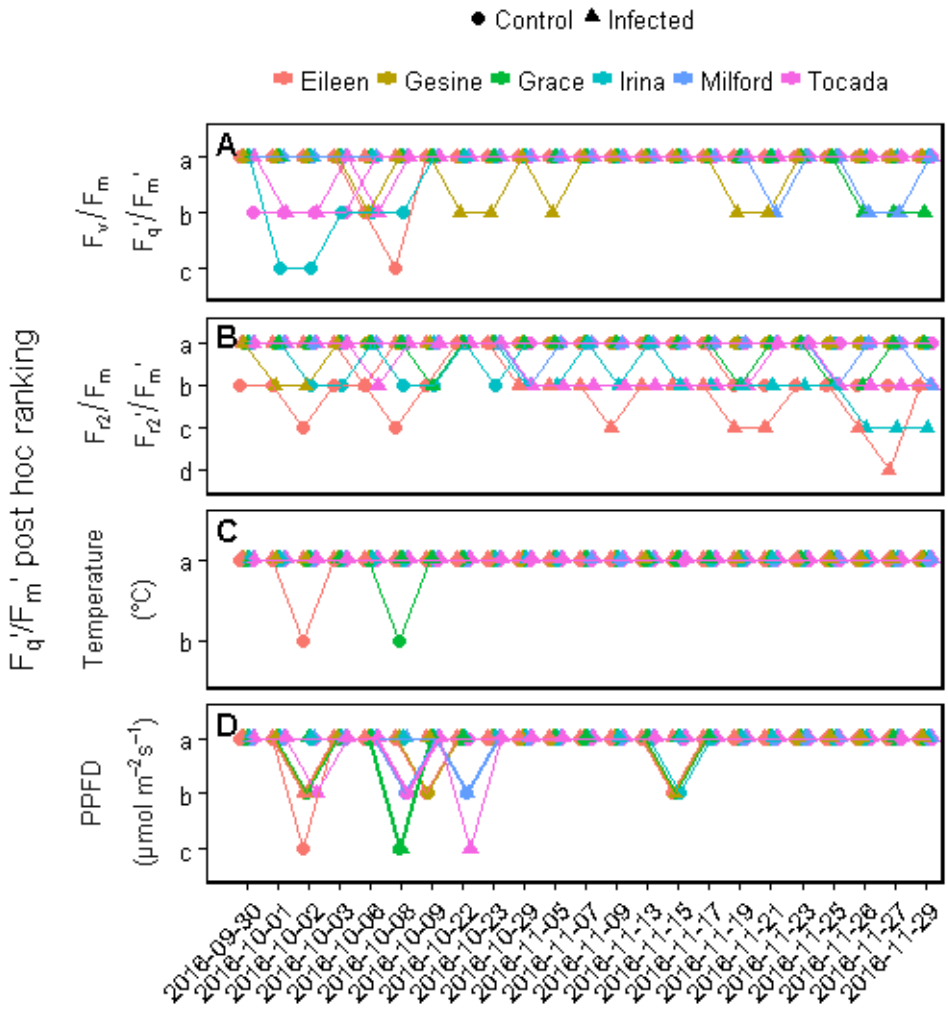


**Figure 46** Analysis of variance (ANOVA) followed by Scheffé test for barley genotypes was performed daily for quantum efficiency of the photosystem II ($F_v/F_m$ in the dark and $F_q'/F_m'$ in the light, A), reoxidation efficiency 5 ms after primary quinone ($Q_A$) reduction ($F_{r2}/F_m$ in the dark and $F_{r2}'/F_m'$ in the light, B) and associated temperature (C) and photosynthetic photon flux density (PPFD, D). Data was averaged per hour and day. Fluorescence data was acquired by automated light-induced fluorescence transient (LIFT) device which scans the crop canopy. Environmental conditions as temperature were recorded every minute by three stations distributed in the unheated greenhouse and merged to the measurements done in the same minute. Six barley genotypes were monitored from October to December 2016 in 12 plots. 6 plots were infected with powdery mildew on November 2.

*Disease resistance on selected time points*

For the detection of powdery mildew infection three dates were selected covering the plant before the infection and the disease progress. Gesine cultivar showed already five days after infection (DAI) significant decreased $F_q'/F_m'$ compared to control. This is remarkable since visual scoring detected first symptoms three days later at 8 DAI (Stefan Thomas, personal communication). 23 DAI, $F_q'/F_m'$ of Grace decreased significantly compared to control. $F_q'/F_m'$ of Irina was not affected. In agreement, Irina is classified as powdery mildew resistant (Bundessortenamt, 2013). A clear response of $F_{r2}'/F_m'$, NPQ and pNDVI to infection is not visible on that selected dates until 23 DAI. PPFD and temperature merged to measurements did not significantly differ between genotypes and treatment (data not shown).

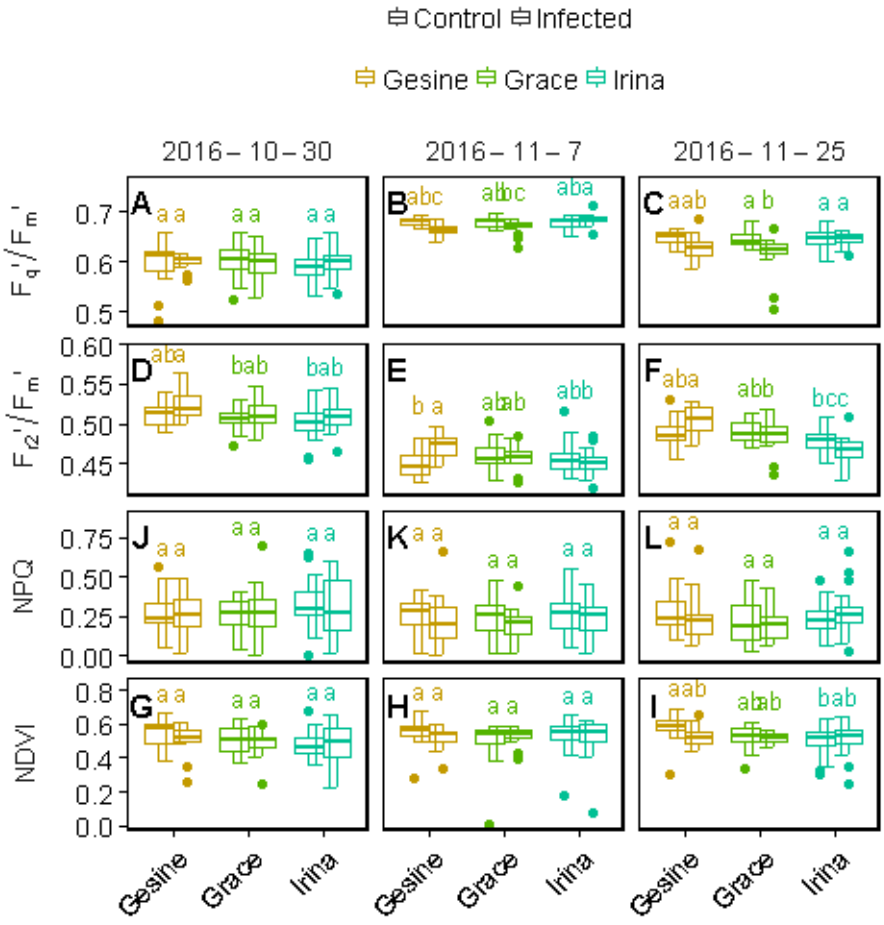


**Figure 47** Boxplot of photosystem II operating efficiency ($F_q'/F_m'$, A, B), reoxidation efficiency 5 ms after primary quinone ($Q_A$) reduction ($F_{r2}'/F_m'$, C,D), non-photochemical quenching (NPQ, G,H) and pseudo normalized difference vegetation index (NDVI, E,F) of three selected days before and within disease progression (2016-10-29, 2016-11-97 and 2016-11-25, measurements averaged from 11.00 h to 16.00 h). Three selected barley genotypes are shown growing in 6 plots (n=16 to 23 measurements). 3 plots were infected with powdery mildew on November 2. Box represents inter-quartile range, bold horizontal bar the median, the discontinuous lines the upper and lower quartile, and outlier data points (>1.5 × inter-quartile range) are depicted by a point. Means with different letters differ significantly using Scheffé's multiple comparisons of means.

*Factors influencing $F_q'/F_m'$*

Lasso regression was performed to identify the important factors which influence $F_q'/F_m'$ of control and infected barley. After PPFD, $F_q'/F_m'$ was mainly influenced by pNDVI. Consequently, $F_q'/F_m'$ was correlated to PPFD and grouped into pNDVI ranges. This resulted in an explained variance of $F_q'/F_m'$ of up to 59% in measurements associated with high pNDVI values (Figure 48).

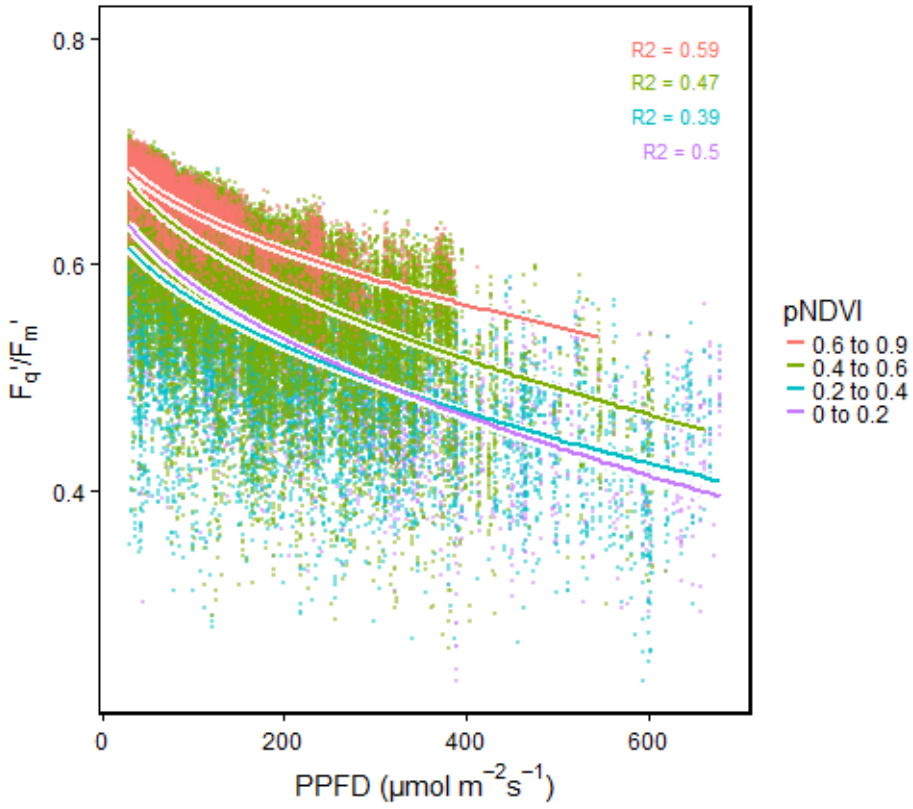


**Figure 48** Photosystem II operating efficiency ($F_q'/F_m'$) of barley genotypes was correlated to photosynthetic photon flux density (PPFD) and grouped after pseudo normalized difference vegetation index (pNDVI) values. PPFD and pNDVI influenced $F_q'/F_m'$ highest according to lasso regression. Fluorescence and spectral data was acquired by automated light-induced fluorescence transient (LIFT) device scanning the crop canopy. Environmental conditions as PPFD and temperature were recorded every minute by three stations distributed in the unheated greenhouse and merged to the measurements done in the same minute. Measurements include two independent barley experiments with powdery mildew infection. White intervals show 95% confidence intervals for the mean based on linear model with PPFD as covariate (n=70'785 measurements, 6 genotypes in 12 containers).

*Genotypic response of $F_q'/F_m'$ to powdery mildew infection*

The interaction of $F_q'/F_m'$ with PPFD in plants infected with powdery mildew and the control is shown in Figure 49. The response of $F_q'/F_m'$ to PPFD in infected plants did not show consistent differences in all genotypes compared to control plants. In addition, genotype Gesine and Tocada showed already differences in light response before the infection. This was probably caused by block effects which favored growth conditions in specific containers. Following pairwise comparison of the $F_q'/F_m'$ slope, no consistent pattern was visible either regarding mean nor interaction with PPFD (Figure 50). The response was not consistent over both experiments either. The exception were Genotype Milford and Gesine which showed significant lower interaction of $F_q'/F_m'$ with PPFD of the infected plants compared

to the control in both experiments. In both experiments, genotype Grace showed already decreased $F_q'/F_m'$ interaction in the plots before the infection started compared to control plots. However, this differences vanished after the infection in both experiments, meaning that infection relatively lowered $F_q'/F_m'$ compared to before the infection.

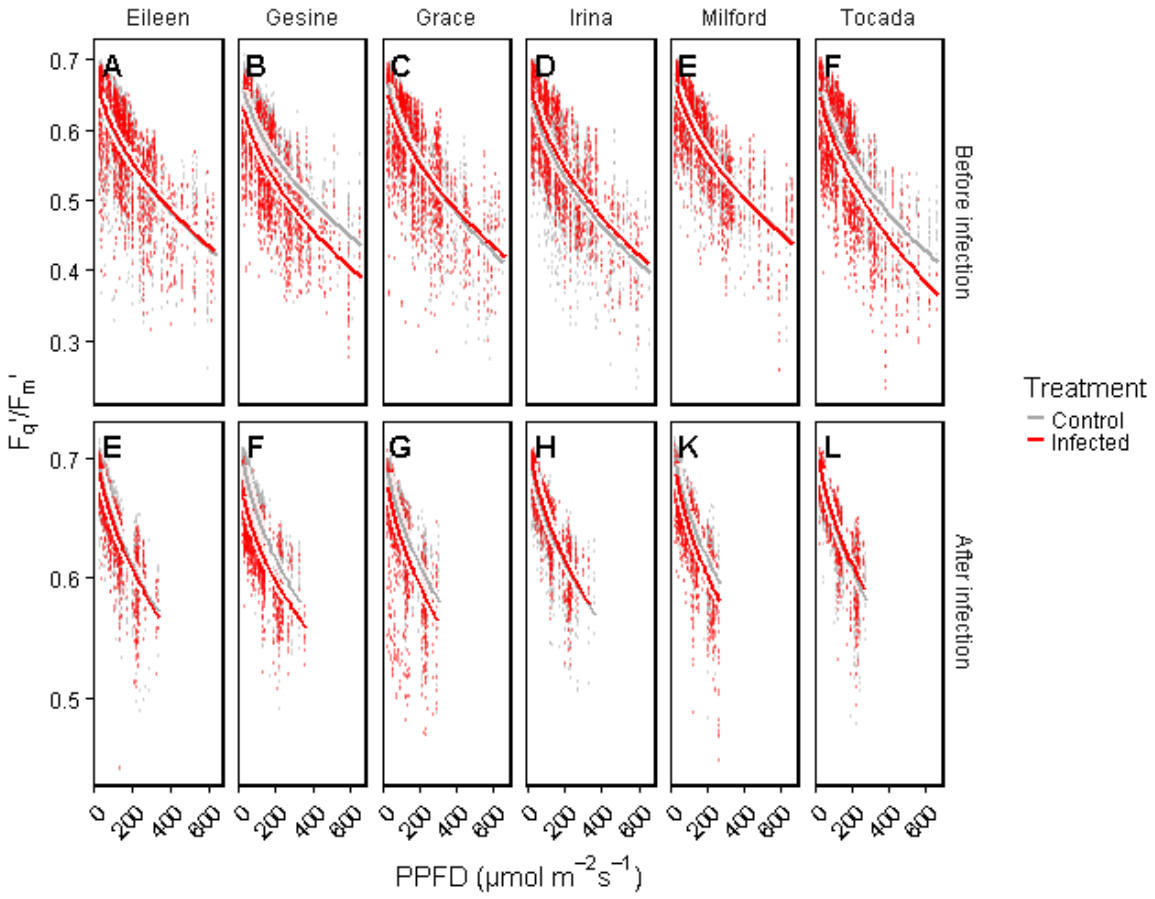


**Figure 49** Photosystem II operating efficiency ($F_q'/F_m'$) values were grouped into different barley genotypes as well as in measurements before (A to F) and after (G to L) powdery mildew infection. $F_q'/F_m'$ was fitted to a linear model depending on photon flux density (PPFD) and grouped after treatment. Light-induced fluorescence transient (LIFT) devices scanned canopy automatically acquiring fluorescence data every hour throughout a measuring day. PPFD was recorded every minute by three stations distributed in the unheated greenhouse and merged to the measurements done in the same minute. Measurements were derived from the second barley experiments October to December 2016. White intervals show 95% confidence intervals for the mean (n= 1608 to 2009, in total 45331 measurements, 6 genotypes in 12 containers).

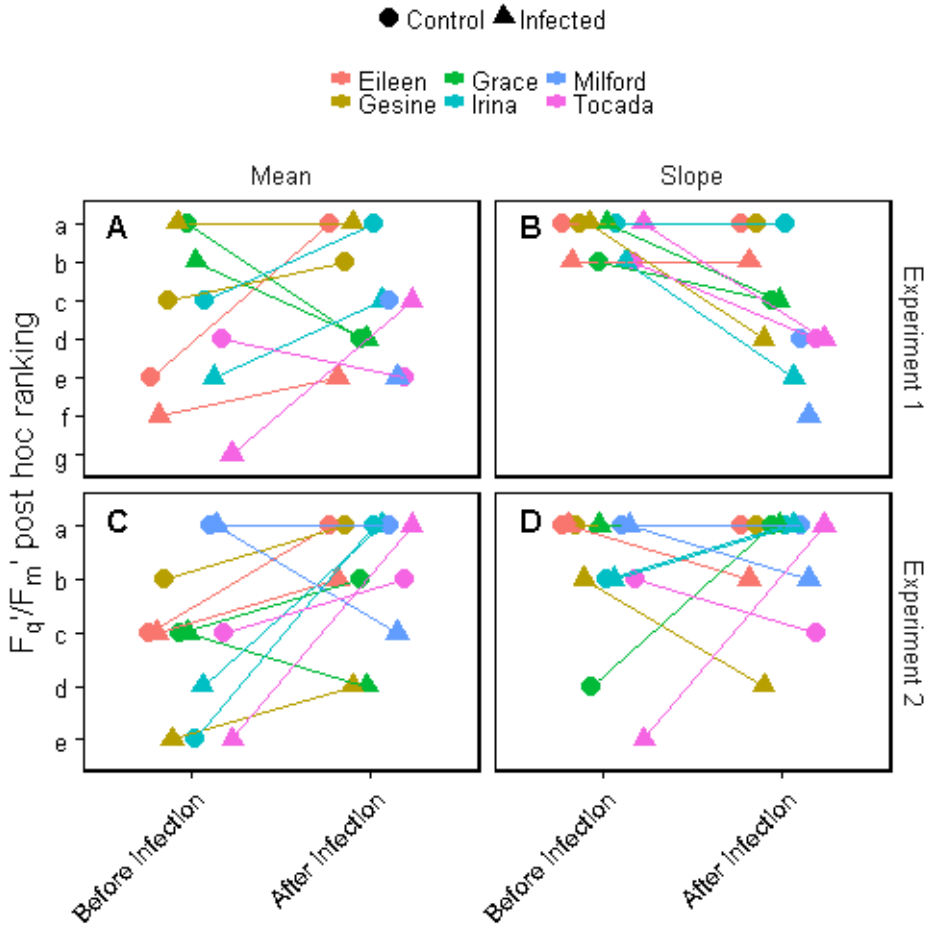


**Figure 50** Ranking of photosystem II operating efficiency ($F_q'/F_m'$) of barley genotypes based on mean (A, C) and interaction (B, D) with photon flux density (PPFD) and pseudo normalized difference vegetation index (pNDVI). Measurements were acquired in two independent experiments (A, B and C, D) and grouped in measurements done before and after infection of powdery mildew. Different letters indicate significant different means or interactions according to analysis of variance (ANOVA) followed by pairwise comparison. Six barley genotypes were monitored from September 2015 to February 2016 and October to December 2016 in 12 plots. Half of the plots were infected with powdery mildew (n=316 to 2328).

*Factors influencing $F_{r2}/F_m$ respective $F_{r2}'/F_m'$*

Lasso regression was performed to identify the important factors which influence $F_{r2}/F_m$ respective $F_{r2}'/F_m'$. After temperature which explained 55% of the variance, $F_{r2}/F_m$ respective $F_{r2}'/F_m'$ was influenced by DAS (Figure 51). It cannot be excluded here that the effect of increasing height with increasing DAS contributed to the variance. NDVI or PPFD did not have a significant influence on $F_{r2}/F_m$ respective $F_{r2}'/F_m'$ according to Lasso regression.

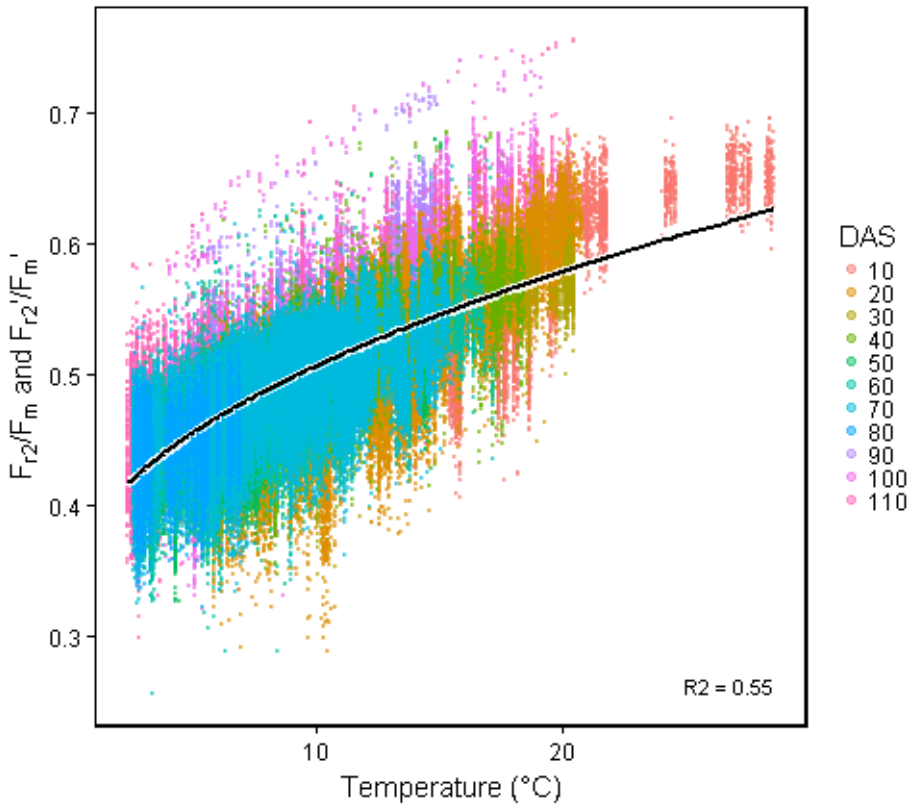


**Figure 51** Reoxidation efficiency 5 ms after primary quinone ($Q_A$) reduction ($F_{r2}/F_m$ in the dark and $F_{r2}'/F_m'$ in the light) of barely genotypes was correlated to temperature and grouped after days after sowing (DAS). $F_{r2}/F_m$ respective $F_{r2}'/F_m'$ highest was highest affected by temperature and DAS according to lasso regression. Fluorescence and spectral data was acquired by automated light-induced fluorescence transient (LIFT) device scanning the crop canopy. Environmental conditions as temperature were recorded every minute by three stations distributed in the unheated greenhouse and merged to the measurements done in the same minute. Measurements include two independent barley experiments with powdery mildew infection. White intervals show 95% confidence intervals of the mean based on linear model with temperature as covariate (n=264'337 measurements, 6 genotypes in 12 containers).

*Genotypic response of $F_{r2}/F_m$ respective $F_{r2}'/F_m'$ to powdery mildew infection*

The response of $F_{r2}/F_m$ respective $F_{r2}'/F_m'$ to temperature before and after infection of powdery mildew is shown in Figure 52. The interaction of $F_{r2}/F_m$ respective $F_{r2}'/F_m'$ with temperature between infected and control genotypes were similar. Therefore, the post hoc test on the mean and interaction term did not show a consistent response in infected and control plants with the exception of Milford and Tocada (Figure 53). Interestingly, response to infection in the genotype Tocada could not be detected using $F_q'/F_m'$ parameter but using the response of $F_{r2}/F_m$ respective $F_{r2}'/F_m'$.

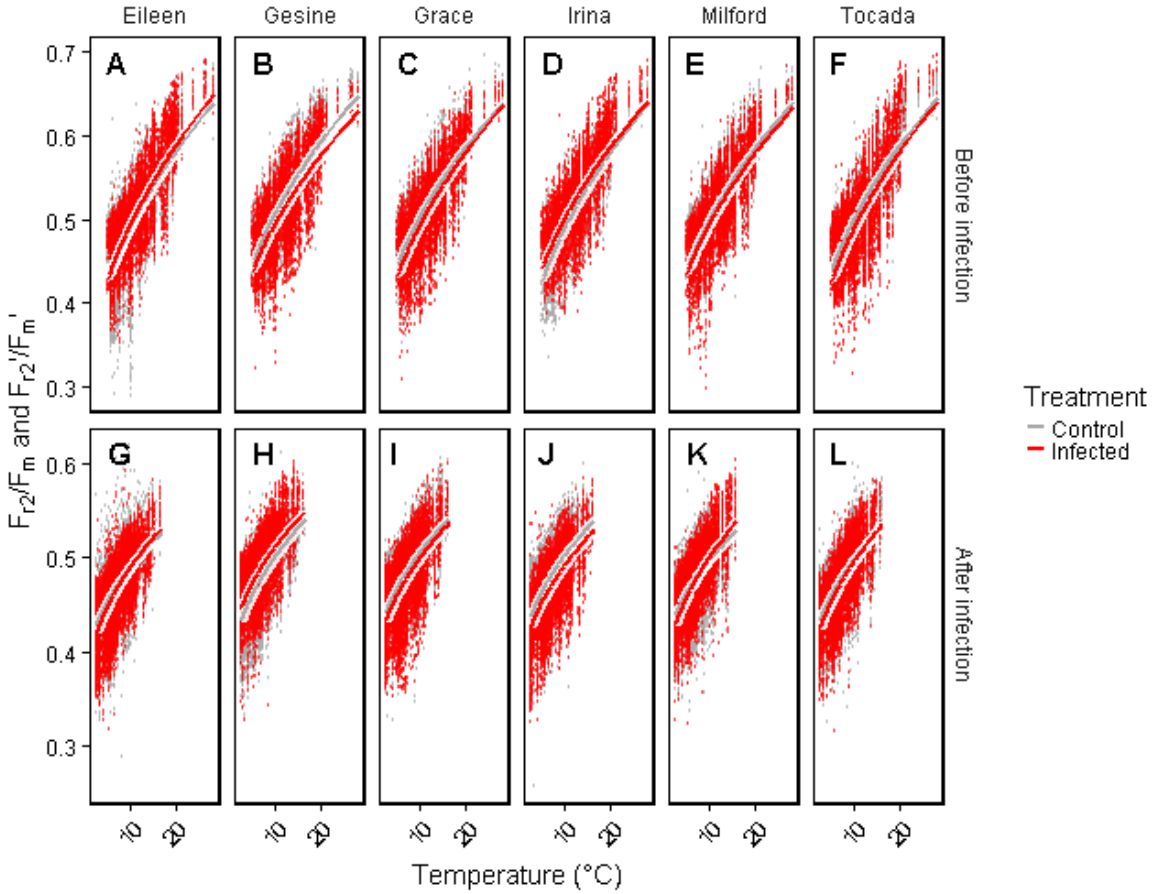


**Figure 52** Reoxidation efficiency 5 ms after primary quinone ($Q_A$) reduction ($F_{r2}/F_m$ in the dark and $F_{r2}'/F_m'$ in the light) values were grouped into different barley genotypes as well as in measurements before (A to F) and after (G to L) powdery mildew infection. $F_{r2}/F_m$ respective $F_{r2}'/F_m'$ was fitted to a linear model depending on temperature and grouped after treatment. Light-induced fluorescence transient (LIFT) devices scanned canopy automatically acquiring fluorescence data every hour throughout a measuring day. PPFD was recorded every minute by three stations distributed in the unheated greenhouse and merged to the measurements done in the same minute. Measurements were derived from the second barley experiments October to December 2016. White intervals show 95% confidence intervals for the mean of (n= 5658 to 10210, total 192012 measurements, 6 genotypes in 12 containers).

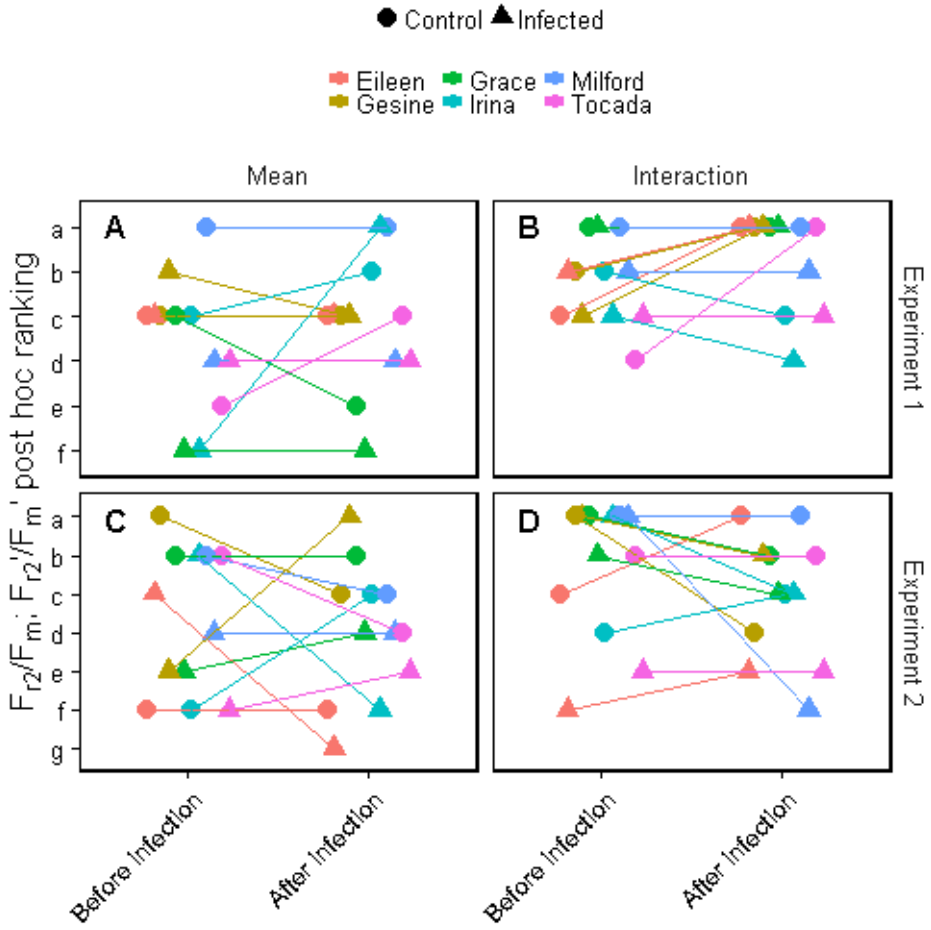


**Figure 53** Reoxidation efficiency 5 ms after primary quinone ($Q_A$) reduction ($F_{r2}/F_m$ in the dark and $F_{r2}'/F_m'$ in the light) of barley genotypes based on mean (A, C) and interaction (B, D) with temperature. Measurements were acquired in two independent experiments (A, B and C, D) and grouped in measurements done before and after infection of powdery mildew. Different letters indicate significant different means or interactions according to analysis of variance (ANOVA) followed by pairwise comparison. Six barley genotypes were monitored from September 2015 to February 2016 and October to December 2016 in 12 plots. Half of the plots were infected with powdery mildew (n=79 to 10210).

### 3.2.7 Summary: Semi-field conditions

Five species grown in the *Miniplot* facility were monitored in high spatio-temporal resolution using automated LIFT system. Investigated photosynthesis parameters showed a dynamic response under the natural fluctuating environment resulting in a clear diurnal pattern (e.g. Figure 24). Over all species, $F_v/F_m$ respective $F_q'/F_m'$ was mainly dependent on PPFD explaining 26% of all variance in $F_q'/F_m'$ (Table 2). Further important factors were pNDVI and PRI. A linear model including these factors accounted for almost 50% of the variance in $F_q'/F_m'$. In soybean, also the measuring date showed influence to $F_q'/F_m'$, but it was not significant considering all species (Table S 1 and Table 2). The variance in $F_q'/F_m'$ was caused additionally by the inhomogeneous canopy while measurements on the leaf level showed smaller variance (Figure 43E to H). $F_{r2}/F_m$ respective $F_{r2}'/F_m'$ was mainly dependent on temperature across all species. In soybean, temperature explained 77% of all variance in $F_{r2}/F_m$ respective $F_{r2}'/F_m'$ (Figure 23). No second factor, which has an effect on this parameter, was consistently identified. Plant height seemed to affect $F_{r2}'/F_m'$ and especially $F_{r2}/F_m$ (Figure 43I to L). However, the effect of different

plant height, e.g. when plants grow higher over the season, was negligible compared to the response to temperature (Figure 51). Both parameters, $F_q'/F_m'$ and $F_{r2}/F_m$ (respective $F_{r2}'/F_m'$) detected genotypic differences in control and stress conditions. In maize, B73 was identified as more tolerant to drought than Mo17 (Figure 30). The response to drought of $F_q'/F_m'$ and $F_{r2}/F_m$ (respective $F_{r2}'/F_m'$) was more consistently detected when instead of the mean interaction with PPFD and temperature was considered, respectively (Figure 32 and Figure 34). In soybean, genotype S1 showed over both seasons the smallest interaction of $F_q'/F_m'$ and $F_{r2}/F_m$ respective $F_{r2}'/F_m'$ with PPFD and temperature, respectively. In barley, the approach of including environmental interaction for disease detection did not work (Figure 50 and Figure 53). However using $F_q'/F_m'$ at selected time period, response to powdery mildew infection in sensitive genotype Gesine was detected already five DAI (Figure 47). Photosynthetic response in a fluctuating environment and stress tolerant genotypes were successfully detected by analyzing the LIFT paramters using their interaction with environmental covariates or the mean of selected time periods.

## 3.3 Field conditions

Photosynthesis was measured in the field in CKA in Germany and Planaltina in Brazil. In Planaltina, plants were measured under different levels of drought stress induced by an irrigation gradient

### 3.3.1 Maize and Soybean

In order to assess photosynthetic dynamic in the field, LIFT data was collected over two field seasons in maize and soybean. Figure 54 shows the response of $F_v/F_m$ respective $F_q'/F_m'$, and $F_{r2}/F_m$ respective $F_{r2}'/F_m'$ under fluctuating field environment measured at the field site of CKA.

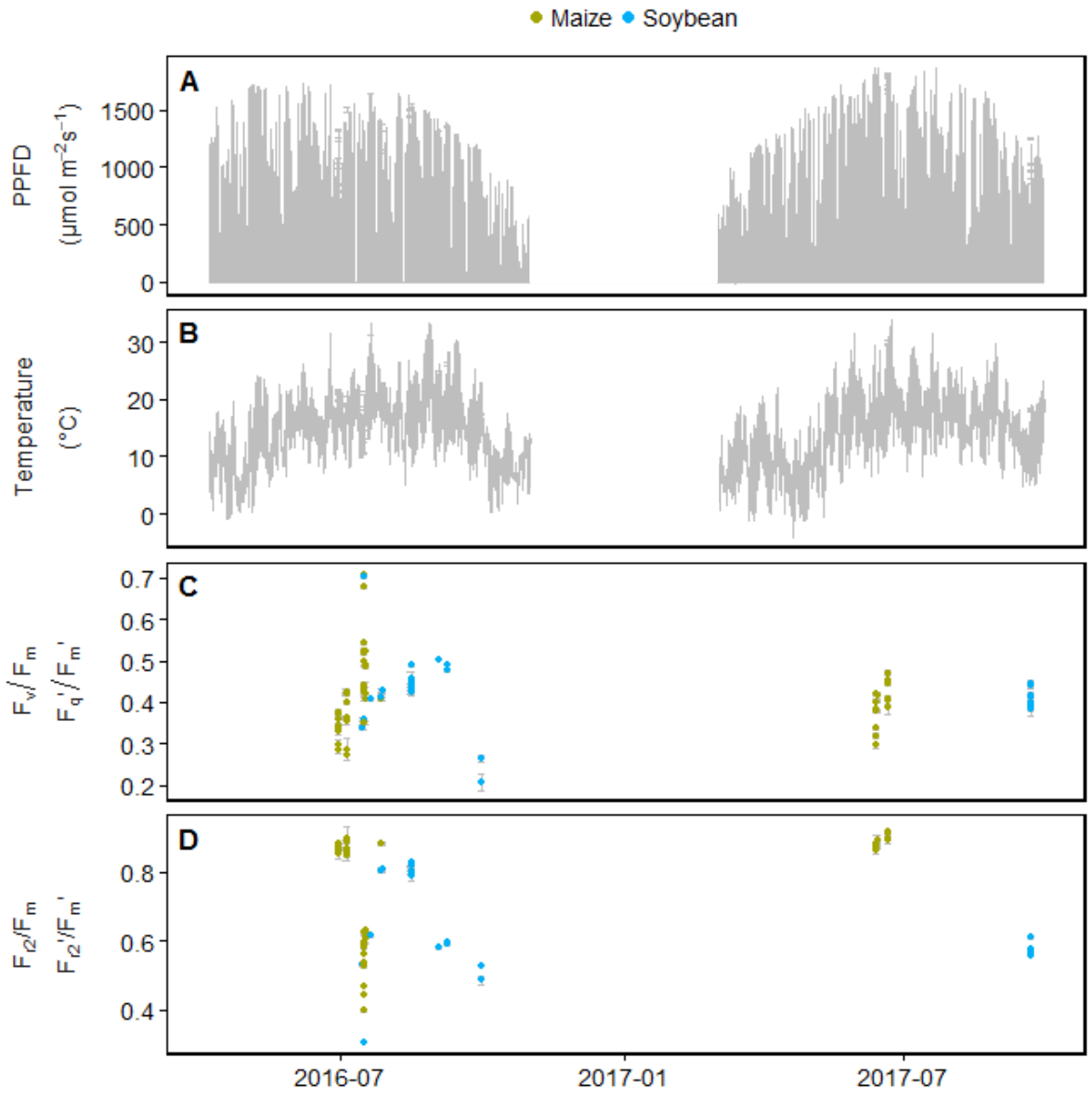


**Figure 54** Photosynthetic performance was assessed in the field over two years. Photosynthetic photon flux density (PPFD, A) temperature (B), response of quantum efficiency of the photosystem II ($F_v/F_m$ in the dark and $F_q'/F_m'$ in the light, C) and reoxidation efficiency 5 ms after primary quinone ($Q_A$) reduction ($F_{r2}/F_m$ in the dark and $F_{r2}'/F_m'$ in the light, D) is shown over time. Fluorescence data was acquired by a light-induced fluorescence transient (LIFT) devices scanning crop canopy from an manually driven field bike or an autonomous robot. Environmental conditions as PPFD were recorded by up to three stations distributed in field. Measurements took place from June 2016 to September 2017 in different maize and soybean genotypes. Grey error bars show standard error of several hundred independent measurements taken per hour.

*Factors influencing $F_v/F_m$ respective $F_q'/F_m'$*

In order to explain the fluctuating response, variables which determined $F_v/F_m$ respective $F_q'/F_m'$ were selected by Lasso regression. According to the results of Lasso regression, $F_q'/F_m'$ was linear modeled with those selected parameters (Table S 2). In contrast to Miniplot data, not PPFD but light reflectance at 685 nm on the target leaf was best correlated with $F_q'/F_m'$. This relationship explained 30% of the variance in the light and 45% when night measurements were included (Figure 55). The influence of the date of measurement explained about 12 % of all variance in $F_q'/F_m'$ (Table S 2). The measurements probably clustered due to differences in light intensity at the time of measurement. Weather conditions at one specific date did not vary much since the duration of measurement was in general only about 2 hours and not a full diurnal cycle as in the *Miniplot* facility.

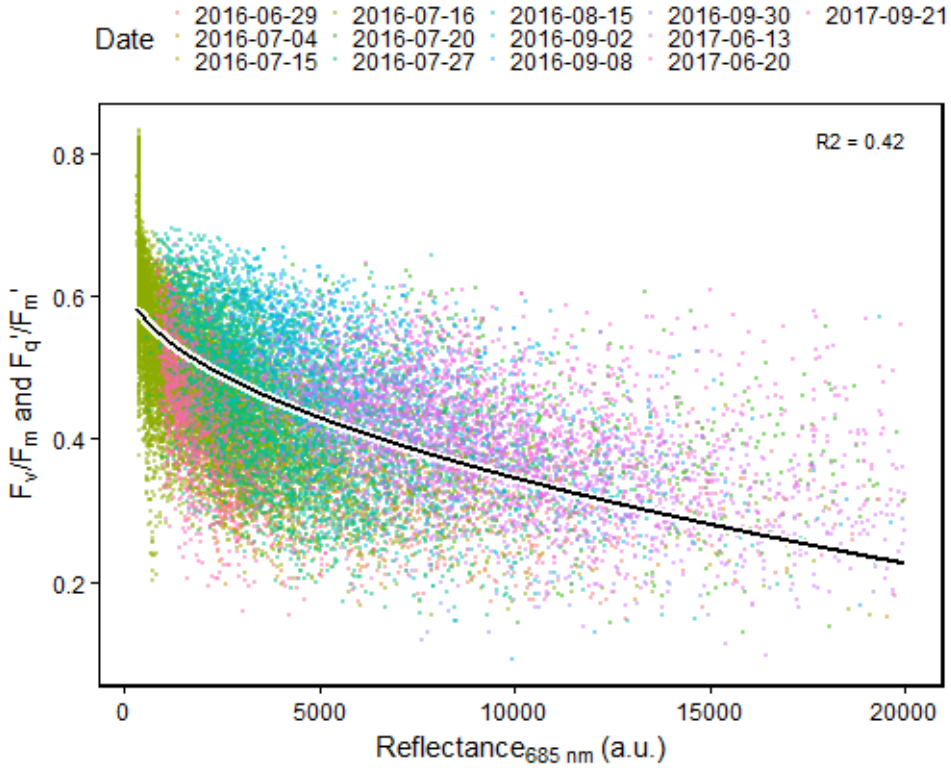


**Figure 55** Quantum efficiency of the photosystem II ($F_v/F_m$ in the dark and $F_q'/F_m'$ in the light) measured in the field was mainly determined by the leaf sunlight reflectance of the measured leaf at 685 nm. Different measuring dates were identified as second important factor determining $F_q'/F_m'$ according to linear modelling. Fluorescence data was acquired by a light-induced fluorescence transient (LIFT) devices scanning crop canopy from an manually driven phenotyping bike or an automated robot. Measurements took place from June 2016 to September 2017 in different maize and soybean genotypes. White intervals show 95% confidence intervals for the mean of the $F_v/F_m$ respective $F_q'/F_m'$ which was fitted to a linear model depending on reflectance at 685 nm (square root transformed, n=22886 measurements).

*Factor influencing $F_{r2}/F_m$ respective $F_{r2}'/F_m'$*

According to the results of Lasso regression, $F_{r2}/F_m$ respective $F_{r2}'/F_m'$ was linear modeled with selected determining parameters (Table S 3). In agreement with *Miniplot* data, temperature was best correlated with $F_{r2}/F_m$ respective $F_{r2}'/F_m'$ explaining 35.2% of variance in the linear relation and additional 6.8% through the curvature factor. Grouped after the crop species, which was the second important factor, up to 79% of variance in the field was explained (Figure 56).

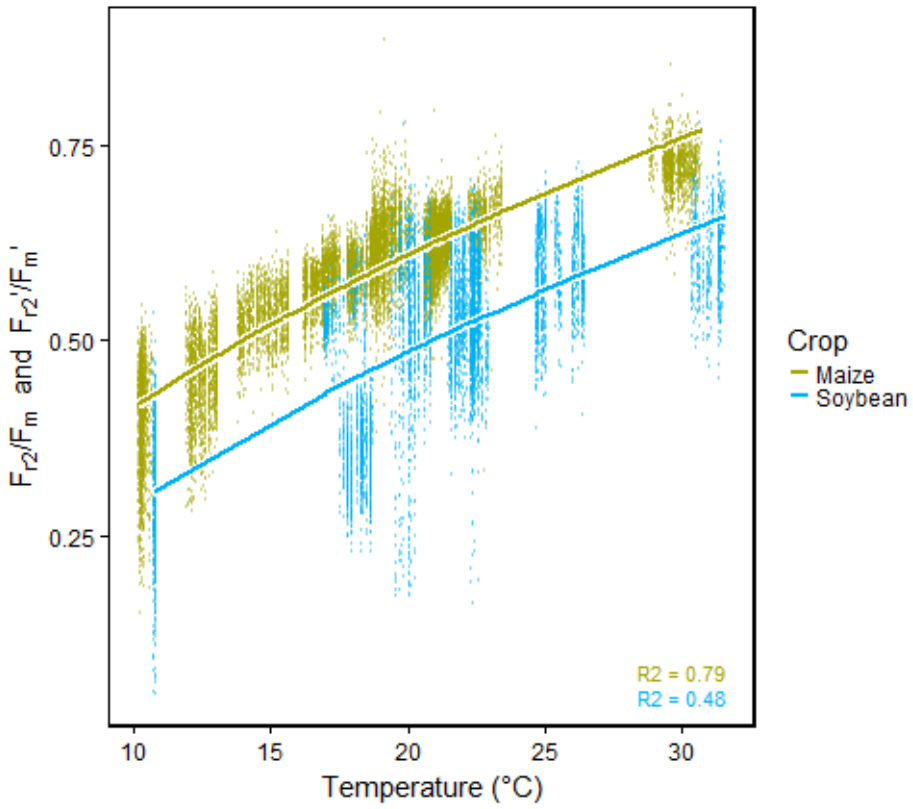


**Figure 56** Reoxidation efficiency 5 ms after primary quinone ($Q_A$) reduction ($F_{r2}/F_m$ in the dark and $F_{r2}'/F_m'$ in the light) was correlated to temperature and grouped after crop species. Fluorescence data was acquired by a light-induced fluorescence transient (LIFT) devices scanning crop canopy from an manually driven phenotyping bike or an automated robot. Environmental conditions as temperature were recorded every minute by three stations distributed in the field and merged to the measurements done in the same minute. Measurements took place from June 2016 to September 2017 in different maize and soybean genotypes. White intervals show 95% confidence intervals for the mean $F_{r2}/F_m$ respective $F_{r2}'/F_m'$ which was fitted to a linear model depending on temperature (square root transformed, n=20116 measurements).

*Genotypic differences in maize under field conditions*

In maize, 13 genotypes were measured over two years in the field site in CKA: four times over the season in 2016, including one full diurnal cycle inclusive night measurements on the June 16, and twice in 2017 on June 13 and 20 (Figure 57). Typical diurnal response from $F_v/F_m$ respective $F_q'/F_m'$ and $F_{r2}/F_m$ respective $F_{r2}'/F_m'$ to PPFD and temperature, respectively, are also visible in the field.

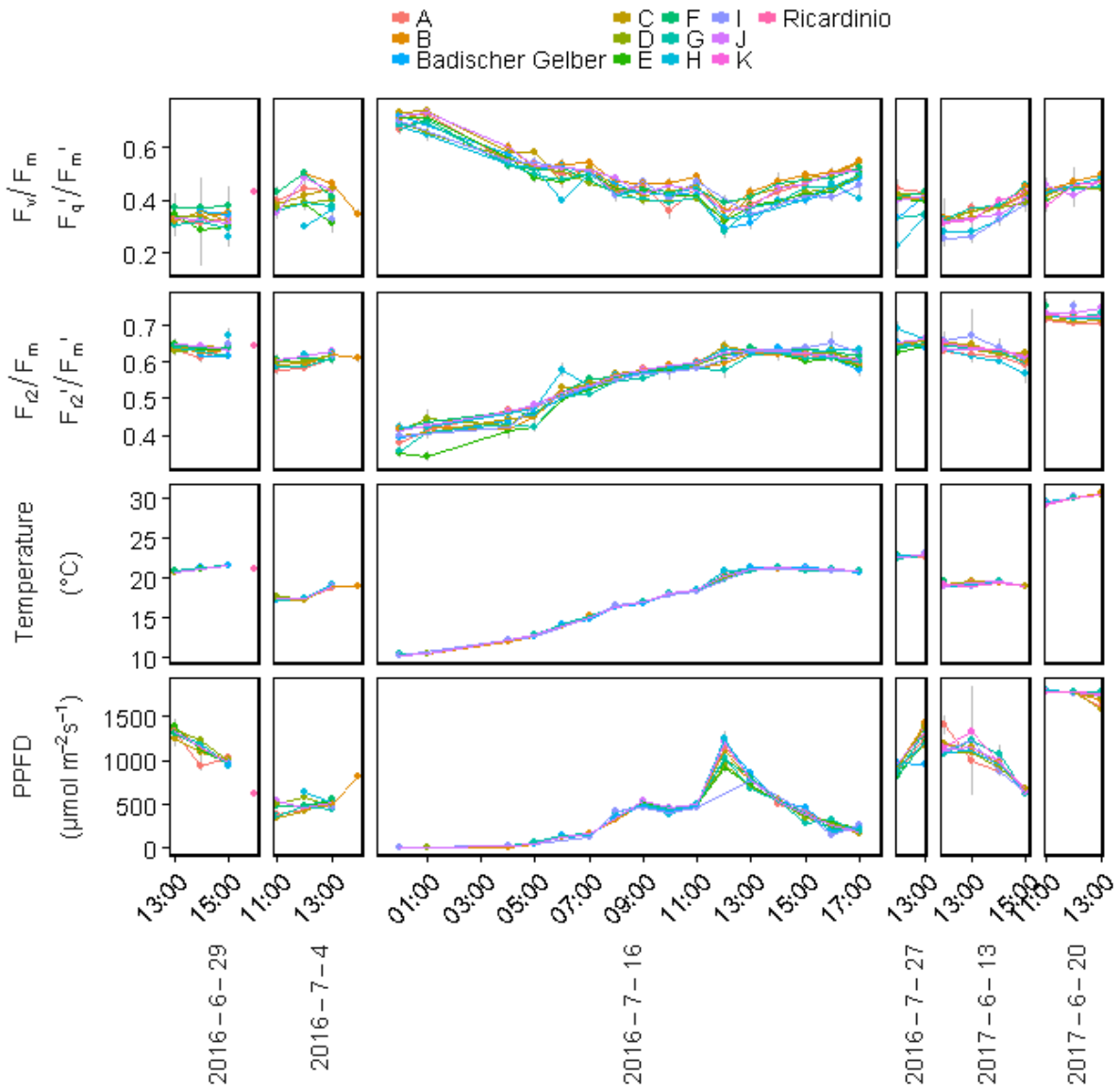


**Figure 57** Response of quantum efficiency of the photosystem II ($F_v/F_m$ in the dark and $F_q'/F_m'$ in the light), reoxidation efficiency 5 ms after primary quinone ($Q_A$) reduction ($F_{r2}/F_m$ in the dark and $F_{r2}'/F_m'$ in the light) of maize genotypes, associated temperature and photosynthetic photon flux density (PPFD) is shown over time averaged by hour and week. Fluorescence data was acquired by light-induced fluorescence transient (LIFT) device scanning crop canopy. Environmental conditions as PPFD and temperature were recorded every minute by three stations distributed in the field and merged to the measurements done in the same minute. Grey error bars show 95% confidence interval. Experiment included 13 genotypes in 2016 and a subset of 10 genotypes in 2017.

According to the results of Lasso regression, $F_q'/F_m'$ of maize genotypes was linear modeled with the most determining parameters which were reflectance at 685 nm and plot number explaining 38.3% and 4.2%, respectively (Figure S 11). On genotypic level, Genotype B and C showed over both years consistently significant higher means of $F_q'/F_m'$ compared to genotypes D, H and J (Figure 58). In contrast, genotypes A and B differed in interaction with reflectance at 685 nm significant from genotypes C, D and I.

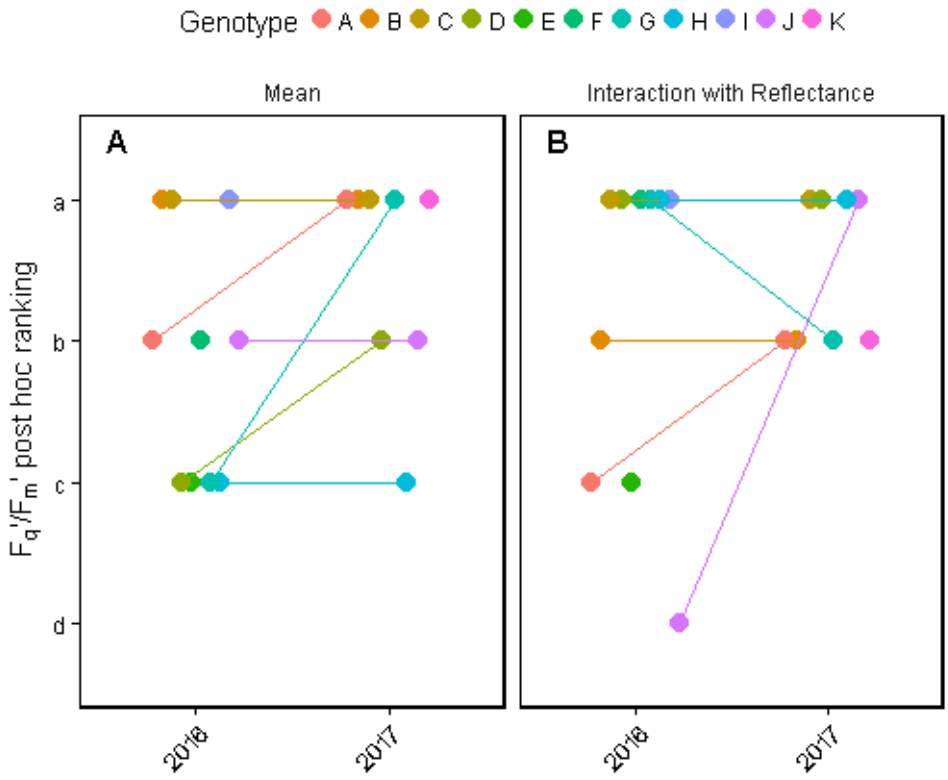


**Figure 58** Ranking of photosystem II operating efficiency ($F_q'/F_m'$) of maize genotypes based on mean (A) and interaction (B) with reflectance at 685 nm over two years. Different letters indicate significant different means or interactions according to analysis of variance (ANOVA) followed by pairwise comparison. Five maize genotypes were monitored from June to July 2016 and nine genotypes from July to August 2017 in the field (n= 11310 total ranging from 156 to 1367 per year and genotype).

Response of $F_{r2}/F_m$ respective $F_{r2}'/F_m'$ to temperature explained 79% of all variance in the Maize data (Figure 55). This indicated accurate determination of this parameter with only a small variance controlled by additional factors or noise. Regarding genotypic differences, genotype E, H and G differed significantly from most of the other genotypes regarding mean and interaction of $F_{r2}/F_m$ respective $F_{r2}'/F_m'$ with temperature, respectively (Figure 59).

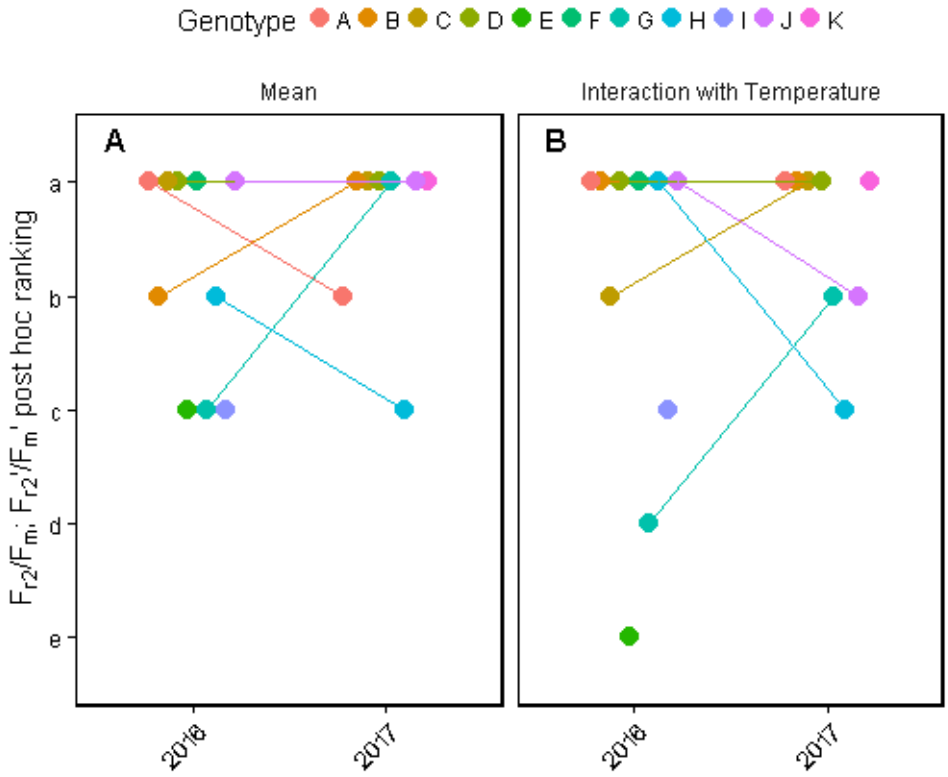


**Figure 59** Ranking of reoxidation efficiency 5 ms after primary quinone ($Q_A$) reduction ($F_{r2}/F_m$ in the dark and $F_{r2}'/F_m'$ in the light) of maize genotypes based on mean (A) and interaction (B) with temperature over two years. Different letters indicate significant different means or interactions according to analysis of variance (ANOVA) followed by pairwise comparison. Five maize genotypes were monitored from June to July 2016 and nine genotypes from July to August 2017 in the field (n= 22395 total and ranging from 416 to 3044 per year and genotype).

### 3.3.2 Soybean: Response to drought

Three soybean genotypes were phenotyped in the field in Planaltina (Brazil) within an irrigation gradient at different times of four days (Figure 60). Comparing the 1%- and 100%-irrigation level, differences in $F_q'/F_m'$ and $F_{r2}'/F_m'$ were already visible when data was averaged to the hour of measurement.

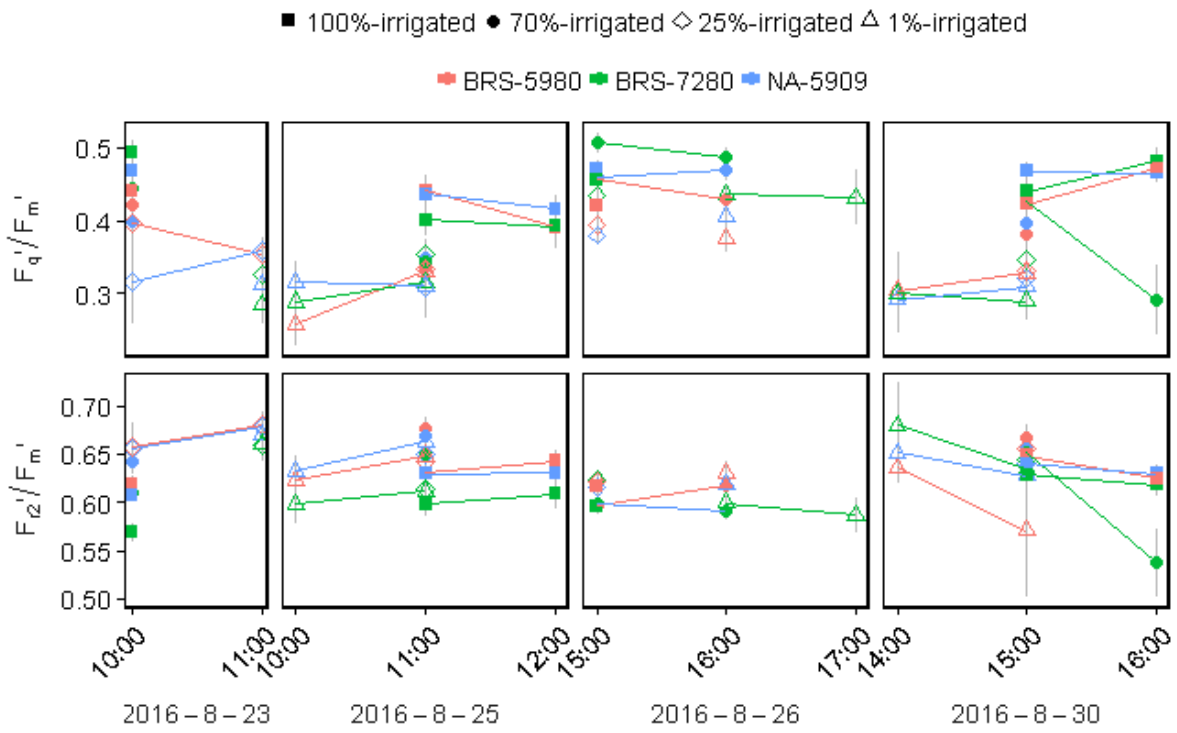


**Figure 60** Response of quantum efficiency of the photosystem II ($F_q'/F_m'$) and reoxidation efficiency 5 ms after primary quinone ($Q_A$) reduction ($F_{r2}'/F_m'$) of three soybean genotypes grown in the field in Planaltina, Brazil, subjected to different levels of drought stress. Fluorescence data was acquired on four different days by the light-induced fluorescence transient (LIFT) device mounted to a phenotyping bike scanning crop canopy. Grey error bars show 95% confidence interval of the mean.

Figure 61 shows the fluorescence transients of the first measuring day at August 23 in 2016. Drought treatment did affect the initial phase of fluorescence induction as well as the fluorescence relaxation. Taken the data of all four measuring days into account, the response to drought in $F_q'/F_m'$ and NDVI decreased significantly with decreasing levels of irrigation (Figure 62). $F_{r2}'/F_m'$ showed a significant increase with increasing drought stress. Between the three measured genotypes significant differences could only be detected in the NDVI parameter (data not shown).

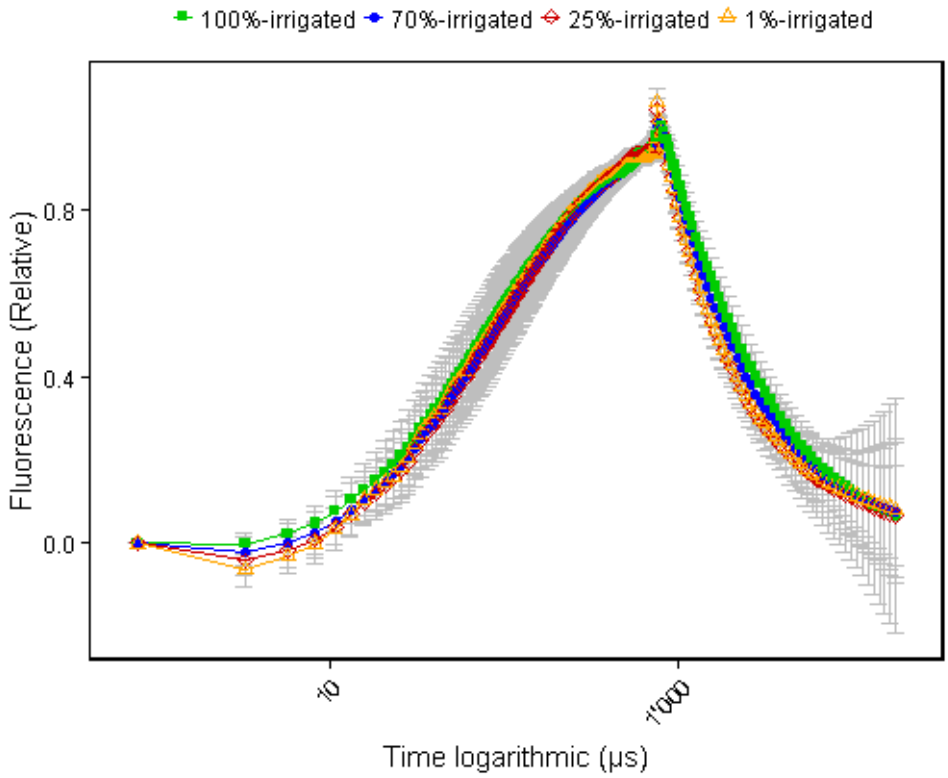


**Figure 61** Fluorescence transient of soybean canopy with different irrigation levels measured at September 23, 2016 in the field in Planaltina, Brazil. Fluorescence data was acquired by the light-induced fluorescence transient (LIFT) device mounted to a field phenotyping bike scanning crop canopy. $Q_A$- flash excitation protocol was used from 60-80 cm distance. Error bars showing standard deviation of the mean (n= 31 to 343 measurements).

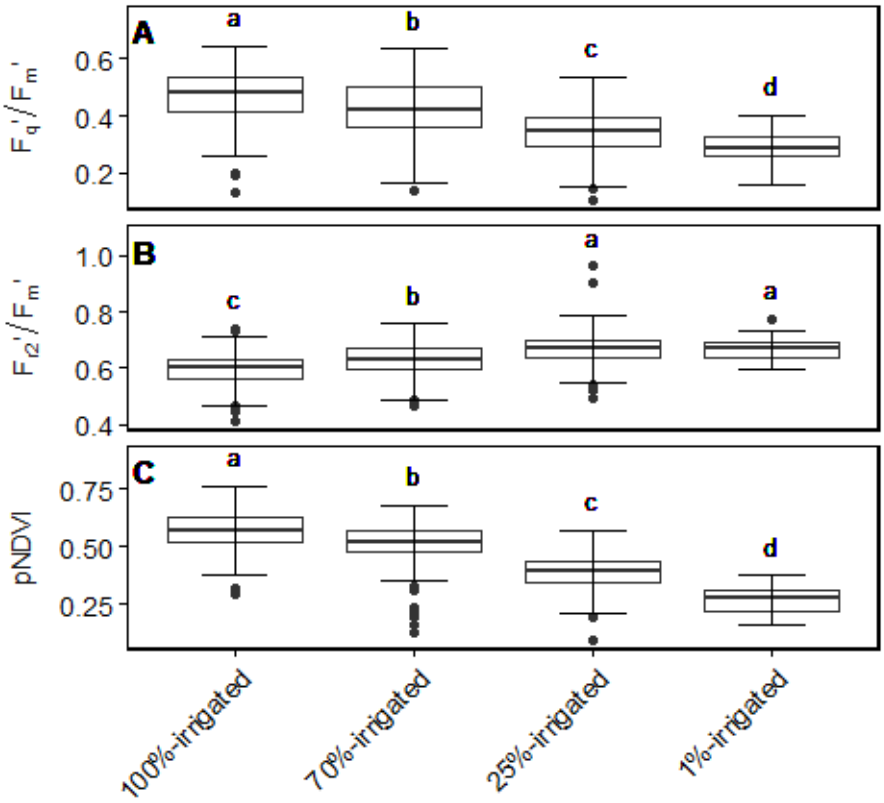


**Figure 62**Boxplot of quantum efficiency of the photosystem II ($F_q'/F_m'$), reoxidation efficiency 5 ms after primary quinone ($Q_A$) reduction ($F_{r2}'/F_m'$) and pseudo normalized difference vegetation index (pNDVI) of soybean genotypes in response to different levels of drought stress. Fluorescence data was acquired on September 23, 2016 by the light-induced fluorescence transient (LIFT) device mounted to a field phenotyping bike scanning crop canopy. Box represents inter-quartile range, bold horizontal bar the median, the discontinuous lines the upper and lower quartile, and outlier data points (>1.5 × inter-quartile range) are depicted by a point. Means with different letters differ significantly using Scheffé's multiple comparisons of means (n= 31 to 343 measurements).

### 3.3.3 Summary: Field conditions

Photosynthetic parameters, $F_v/Fm$ respective $F_q'/F_m'$ and $F_{r2}/F_m$ respective $F_{r2}'/F_m'$, were investigated under field conditions. Both parameters showed a dynamic response following a diurnal pattern (Figure 57). As under semi-field conditions, $F_q'/F_m'$ was dependent on PPFD but was even higher correlated to leaf reflectance of sunlight at 685 nm (Figure 55). $F_{r2}/F_m$ respective $F_{r2}'/F_m'$ was again dependent on temperature (Figure 56). In maize, this relation explained already 79% of the variance in $F_{r2}/F_m$ respective $F_{r2}'/F_m'$. Genotypic differences were detected in both parameters separating specific genotypes consistently over two field seasons from each other. Regarding the means of $F_q'/F_m'$ and $F_{r2}/F_m$ respective $F_{r2}'/F_m'$, maize genotype H showed low values compared to the other genotypes in both seasons (Figure 58 and Figure 59). When interaction of $F_q'/F_m'$ with PPFD was considered, genotype A and B separated consistently over both seasons from other genotypes. When interaction of $F_{r2}'/F_m'$ with temperature was considered, genotype G separated consistently over both seasons from the other genotypes. However, these genotype specific results in maize under field conditions were not consistent with results observed under semi-field conditions. In soybean, drought stress was successfully detected which resulted in significant decreased $F_q'/F_m'$ and increased $F_{r2}'/F_m'$ compared to well-watered conditions (Figure 62).

# 4 Discussion

Fluorescence transient were studied in controlled conditions regarding fluorescence induction and relaxation phase. From these phases, $F_v/F_m$ and $F_r/F_m$ parameters were derived and shown to be coupled to $Q_A$ reduction and reoxidation, respectively. Then, for the first time, these photosynthesis parameters were monitored in diurnal and seasonal time scale in high enough throughput to analyze interactions with fluctuating environmental factors. The LIFT derived parameters showed consistent response to temperature, light intensity and drought from the lab up to field conditions.

## 4.1 Fluorescence rise by the LIFT method

In order to retrieve accurate $F_v/F_m$ values, induction of $F_m$ and $F_mQ_A$ were studied by different excitation protocols of the LIFT instrument. $F_v/F_m$ respective $F_q'/F_m'$ was then measured in fluctuating environment and showed high dependency on PPFD and spectral indices.

### 4.1.1 $F_m$ and $F_mQ_A$ induction

Experiments on dark-adapted spinach leaves confirmed $F_m$ and $F_mQ_A$ induction using SF and prolonged $Q_A$-flash, respectively (Figure 10). In the literature it is still debated if $F_m$ or $F_mQ_A$ represent fully reduced $Q_A$ (Vernotte et al., 1979; Falkowski et al., 2004; Tóth et al., 2005; Schansker et al., 2014; Osmond et al., 2017). In this thesis, $F_m$ was induced in intact plants (no DCMU treatment) only after PQ reduction which requires multiple turn overs of $Q_A$ reduction within about 0.5 seconds (Schansker et al., 2014). In contrast, $F_mQ_A$ was reached when $Q_B$ was still reducing but possibly exceeding the capacities of electron donation from the OEC in dark-adapted state (Figure 10C). This indicated that $F_mQ_A$ is a dynamic equilibrium of $Q_A$ reduction and reoxidation. In agreement, far-red treatment in the dark quenched $F_mQ_A$ due to enhanced $Q_A^-$ reoxidation by facilitating electron transport towards PSI (Figure 11).

Fluorescence rise during a SF applied by LIFT was polyphasic when plotted against logarithmic time scale (Figure 2). Polyphasic fluorescence rise during a saturating light pulse was described as OJIP-curve and separated into three phases (Strasser et al., 1995). In addition, in OJIP curves obtained at high light intensities (15000 µmol photons $m^{-2}$ $s^{-1}$) the J-step forms a local fluorescence maximum similar to $F_mQ_A$ (Tóth et al., 2007a, Osmond et al. 2017). In the LIFT method, $F_mQ_A$ is induced by $Q_A$-flash, which has a high excitation power (above 20000 µmol photons $m^{-2}$ $s^{-1}$). $F_mQ_A$ in Figure 10C as well as the J-step were sensitive to PQ pool reduction (Tóth et al., 2007b). Additionally, $F_mQ_A$ at around 1 ms was detected in OJIP curves using pre-flashed sample (not in $s_1$-state) or high excitation power which overload the capacity of the OEC (Strasser, 1997; Tóth et al., 2007b). $F_mQ_A$ was also detected in heat treated samples due to inactivation of OEC (Strasser, 1997; Tóth et al., 2007a). However, this was caused by acceptor side limitation and therefore occurred already after 0.3 ms (Strasser, 1997). $F_mQ_A$ or J-step were not clearly detected in a SF of the LIFT instrument due to less excitation power compared to $Q_A$-flash or OJIP SF. We conclude that $F_mQ_A$ is related to the J-step and their formation is caused by OEC and PQ pool capacities influencing $Q_A$ redox state.

Under standard conditions, $F_m$ and $F_mQ_A$ were shown to be highly correlated and $F_v/F_m$ can be calculated with $F_m$ or $F_mQ_A$ (Keller et al., submitted). In agreement, LIFT derived $F_v/F_m$ values using $F_mQ_A$ were systematic lower compared to PAM derived values (Pieruschka et al., 2008, 2010). Electron transport rates (ETR) based on $F_q'/F_m'$ derived by the LIFT method correlated to ETR derived by LI-COR with a slight offset (Figure 17).

### 4.1.2 $F_v/F_m$ and $F_q'/F_m'$ interactions with fluctuating environment

In steady state conditions, $F_v/F_m$ respective $F_q'/F_m'$ are well documented fluorescence parameters linked to electron transport and $CO_2$ assimilation (Genty et al., 1989; Baker, 2008). Under natural conditions, $F_v/F_m$ respective $F_q'/F_m'$ follow a diurnal pattern (Adams and Demmig-Adams, 1995; Ribeiro et al., 2004; Pieruschka et al., 2008; Moura dos Santos et al., 2013). Similar results in much higher time resolution over whole seasons were presented in this study (e.g. Figure 24 and Figure 37). For the first time, the dynamic of these parameters under natural fluctuating conditions was analyzed by identifying the environmental factors causing the dynamic photosynthetic response. $F_v/F_m$ respective $F_q'/F_m'$ were largely determined by light intensity and NDVI (Table 2). In contrast to measurements on leaf level, the variance in $F_q'/F_m'$ is additionally influenced by canopy structure captured by the top of canopy measurements (Figure 43E to H). Taken the variance related to PPFD and NDVI into account, $F_q'/F_m'$ did not respond significantly to diurnal, seasonal or development stage.

The influence of light intensity in steady state conditions is well studied and accurately modeled (Niyogi et al., 1998; Von Caemmerer, 2000). Modeled light response curves, however, differ when measured under control and natural conditions (Rascher et al., 2000; Meacham et al., 2017). The curvature factor as well as the light saturation point was reported to be reduced under natural light conditions (Rascher et al., 2000; Meacham et al., 2017). In agreement, $F_q'/F_m'$ and ETR light response curve measured in the *Miniplot* facility and field did not fit to traditional model. The data obtained under natural conditions in the *Miniplot* facility and field showed only a square root response with no saturation at high light. This was probably caused by much higher NPQ levels under natural fluctuating sunlight than under short-term acclimation to controlled actinic light (Jia et al., 2013; Meacham et al., 2017).

After PPFD, $F_q'/F_m'$ was determined by NDVI including all five measured species (Figure 22). NDVI was linked to vegetation productivity therefore may well be an indicator of photosynthesis (Prasad et al., 2006). NDVI can vary in the field canopy and was related to canopy structure (Rascher et al., 2015; Cordon et al., 2016). Also in this study, scans of natural canopy showed highly variable NDVI values (Figure 43N). Therefore, with NDVI also $F_q'/F_m'$ was indirectly influenced by the canopy measurements. NDVI was closely related to $F_q'/F_m'$ in barley, whereas in soybean and maize PRI was the second important factor (e.g. Figure 39). In agreement, NDVI relation to $F_q'/F_m'$ was found to be specific to certain species whereas PRI showed an overall relation to $F_q'/F_m'$ in different species (Rascher et al., 2007; Cordon et al., 2016).

Canopy structure was assessed by comparing leaves fixed to a horizontal angle with leaves in the natural canopy. $F_v/F_m$ and $F_q'/F_m'$ were rather largely affected by this treatment which explained 23.6% and 8% of all variance in the data, respectively. This showed that $F_v/F_m$ respective $F_q'/F_m'$ values are heterogeneous within the top of canopy measurements (Figure 43F, H). In agreement, an avocado plant showed higher $F_q'/F_m'$ in the upper canopy which is more exposed to incoming light than the lower canopy region (Rascher and Pieruschka, 2008). In addition, bottom leaves in shaded plants contributed more to photosynthesis than in unshaded control plants (Mu et al., 2010). Total chlorophyll content as well as leaf area index was reduced in shaded plants compared to control and therefore allowed increased light interception into the canopy (Mu et al., 2010). Furthermore, steep angles from the targeted leaf surface to the LIFT lens (>60°) decreased $F_q'/F_m'$ (Wyber et al., 2017). This reasons can explain the variation in $F_q'/F_m'$ observed in the derived LIFT data from canopy scans. Although, top of canopy measurements hit mainly outer canopy layers, it is not excluded that some measurements penetrate deeper into the canopy. As discussed above, part of the $F_q'/F_m'$ variation due to canopy structure is already taken into account by NDVI varying simultaneously and correlated with

$F_q'/F_m'$ in the canopy. This variation in $F_q'/F_m'$ reflects the screening result as a canopy information which likely explains plant performance in the field more accurate than measurements of selected leaves only (Evans, 2013).

Given the heterogeneous canopy structure, a light intensity estimation on the measured leaf would give more accurate estimation of photosynthetic performance and electron transport. This could be achieved by using light reflectance of the measured leaf as light intensity. Indeed, light reflectance on target at 685 nm was highly correlated ($R^2 > 0.9$) with PPFD (Wyber et al., 2017). Also in this study, light reflectance at 685 nm was better correlated to $F_q'/F_m'$ than PPFD measured on top of canopy (Figure 55). This indicated more realistic assessment of light intensity on the targeted leaf by using reflectance. However, this approximation did not work in the greenhouse, probably due to light scattering by the greenhouse glasses. In summary, $F_v/F_m$ respective $F_q'/F_m'$ interacted mainly with PPFD and spectral indices whereas the variance of these parameters add information about canopy structure in terms of light interception or leaf angle distribution.

## 4.2 Fluorescence relaxation indicates electron transport towards photosystem I

Fluorescence relaxation was influenced by chemicals, by anoxic treatment and far-red irradiation which inhibit electron transport, reduces PQ pool and facilitate electron transport through PSI, respectively. This showed the coupling of fluorescence relaxation with $Q_A^-$ reoxidation and electron transport. In the dark, the fluorescence relaxation was separated into different time phases reflecting steps in the electron transport (Vass et al., 1999). The used time constant for $F_{r1}/F_m$ (r1=0.65 ms) indicates that the electron transport from $Q_A$ to $Q_B$ has completed and the electron is transferred by the PQ (Bowes and Crofts, 1980; Petrouleas and Crofts, 2005). In agreement, impairment of $Q_A$ and PQ pool reoxidation using DCMU and DBMIB, respectively, was detected by $F_{r1}/F_m$ (Figure 13). $F_{r2}/F_m$ probably represents further levels of PQ pool reduction. The used time constant for $F_{r2}/F_m$ (r2=5 ms) matches the time constant for electron transport from $Q_A$ to a vacant $Q_B$, i.e. a PQ molecule needs to be bound first (Vass et al., 1999; Petrouleas and Crofts, 2005). Consequently, $F_{r2}/F_m$ reflects further electron transport towards PQ pool detecting processes beyond $Q_A$. Using $Q_A$-flash on dark-adapted plant, the reoxidation capacity of PQ pool exceeds the capacity of OEC to reduce $Q_A$ (see section 4.1.1). Therefore in the dark, $F_{r2}/F_m$ was determined by reduction kinetics of PQ pool which should represent standard measurement conditions. Since plastoquinol ($PQH_2$) carries the electrons through the thylakoid membrane, its fluidity in low temperatures may be critical (Nolan and Smillie, 1976; Barber et al., 1984). In agreement, fluorescence relaxation was measured for the first time in a quantitative study in the field revealing its close relation to temperature. Highly reproducible response of $F_{r2}/F_m$ respective $F_{r2}'/F_m'$ to temperature was measured under controlled, greenhouse and field conditions (Figure 16, Figure 23 and Figure 56). Cold tolerance of genotypes was not directly linked to $F_{r2}/F_m$ respective $F_{r2}'/F_m'$. However, genotypic differences and drought stress were efficiently detected using this newly established parameter. In response to drought, cyclic electron transport probably increased the reduction level of PQ pool resulting in lower $F_{r2}'/F_m'$ (Finazzi et al., 1999; Munekage et al., 2004; Zivcak et al., 2013). In the light, the fluorescence relaxation did not show different relaxation phases (Figure 4). $F_{r1}'/F_m'$ and $F_{r2}'/F_m'$ seemed to reflect gradually electron transport from $Q_A$ towards PSI. In addition, $F_{r2}'/F_m'$ was less sensitive to increasing light intensities indicating the measurement of maximum capacity in electron transport (Figure 16).

### 4.2.1 $F_{r2}/F_m$ and $F_{r2}'/F_m'$ interactions with fluctuating environment

The parameter based on fluorescence relaxation, $F_{r2}/F_m$ respective $F_{r2}'/F_m'$, showed high correlation with temperature explaining up to 79% of variance in the field (Figure 56). It was shown that membrane fluidity is dependent on temperature (Nolan and Smillie, 1976; Barber et al., 1984). This could affect electron transport since PQ is mediating the transport through the thylakoid membrane. Indeed, reoxidation kinetics of $Q_A^-$ was dependent on temperature acclimatization altering electron transport between PSII and PSI (Yamasaki et al., 2002). Another indication of direct or indirect impairment of electron transport under cold stress was the decrease in net photosynthesis related to membrane composition after exposure to low temperature (Liu et al., 2013). $F_{r2}/F_m$ respective $F_{r2}'/F_m'$ might therefore be linked to electron transport and membrane fluidity. This is potentially useful for screening of tolerant genotypes maintaining high electron transport at given temperature. In this study, significant differences between genotypes could be detected consistently over two seasons indicating a highly heritable trait (Figure 42).

The high correlation of $F_{r2}/F_m$ respective $F_{r2}'/F_m'$ to temperature is promising for screening for cold tolerant genotypes. It was already proposed that the fluorescence signal can be used to screen for chilling tolerance (Strauss et al., 2006). However, the proof for screening application was missing in that article since the response to chilling was based on only two genotypes (Strauss et al., 2006). In that case, cold tolerant response was detected focusing on the first phase of fluorescence induction (J-step) which indicates light absorption and conversion of energy for charge separation (Strauss et al., 2006; Krüger et al., 2014). In another study, reoxidation of $Q_A$ was impaired under cold stress when only the shoot but not roots were acclimated to cold (Suzuki et al., 2011). Similarly, plants grown at high temperature were limited by electron transport and carboxylation rate at low temperature (Yamori et al., 2008). In this study, the focus of the analysis was the temperature sensitive part of $Q_A^-$ reoxidation after $Q_A$ reduction. Although the eight tested soybean genotypes showed variation in interaction of $F_{r2}/F_m$ respective $F_{r2}'/F_m'$ with temperature, a consistent difference between cold tolerant and sensitive genotypes could not be observed, e.g. the two extreme genotypes in temperature response, 22216 and S1, are both cold sensitive (Figure 42).

Accounting for the measuring distance in the range of 450 mm explained 19% of all variance in $F_{r2}/F_m$ (Figure 43I). This might reflect excitation power of LIFT flashlets which decrease with increasing measuring distance allowing fluorescence faster to relax. In the light, $F_{r2}'/F_m'$ is less affected of plant height compared to the dark. In contrast, leaf angle had only minor effect on $F_{r2}/F_m$ and $F_{r2}'/F_m'$. In summary, $F_{r2}/F_m$ respective $F_{r2}'/F_m'$ is highly influenced by temperature and stress response probably linked to membrane fluidity and enhanced cyclic electron transport, respectively.

## 4.3 Response to drought stress

The response to drought was detected by the LIFT signal from controlled conditions (Figure 18), to semi-field conditions (Figure 35), up to field conditions (Figure 61). In all those conditions, $F_q'/F_m'$ was decreased under drought stress compared to well-watered conditions. Decreased $F_v/F_m$ and $F_q'/F_m'$ in response to drought conditions was reported in other studies (Wang et al., 2012b; Jedmowski et al., 2013; de Miguel et al., 2014). In this study, $F_v/F_m$ measured under controlled conditions was not affected by drought stress (Figure 19). Similarly, $F_v/F_m$ was less affected from drought conditions than net $CO_2$ assimilation (Wang et al., 2012b). It was suggested that drought stress increases the cyclic electron transport whereas linear electron transport and therefore $F_v/F_m$ or $F_q'/F_m'$ is less affected (Zivcak et al., 2013). In agreement, response to drought was successful detected using methods which measure electron transport beyond $Q_A$ (Zivcak et al., 2008; Jedmowski et al., 2013; Kalaji et al., 2016).

Consequently, drought stress was also detected using $F_{r2}/F_m$ respective $F_{r2}'/F_m'$ which were decreased in maize genotypes subjected to drought (Figure 33). In contrast, the soybean genotypes in the field responded with an increase of $F_{r2}'/F_m'$ to increased levels of drought stress (Figure 62). This might be an effect of soybean which reacts different than maize under drought conditions. Furthermore, carQ seemed to be increased under drought conditions and may improve the detection of drought stress (Figure 61). In natural fluctuating conditions, the interaction of $F_{r2}/F_m$ respective $F_{r2}'/F_m'$ with temperature increased the accuracy of drought detection (Figure 34). In agreement, the response of maize genotypes to drought and heat conditions was predicted more accurate when environmental factors were included (Millet et al., 2016). This resulted in more consistent identification of QTL related to drought and heat stress (Millet et al., 2016). The importance of field measurements was stressed when drought tolerant maize lines identified under controlled conditions did not result in improved performance of these lines in the field (Ziyomo and Bernardo, 2013). In this study, response to drought was detected efficiently in photosynthetic electron transport beyond $Q_A$ using interaction of $F_{r2}/F_m$ respective $F_{r2}'/F_m'$ with temperature. In contrast, NDVI was not able to detect drought response under semi-field conditions. The possibility to measure in high-throughput using the LIFT device directly in the field has potential to improve selection for drought tolerance. The higher temporal resolution in the measurements will allow to analyze $F_q'/F_m'$ and $F_{r2}'/F_m'$ and their environmental interactions.

## 4.4 Method accuracy and relevance for the future

Response curves to temperature and light intensity persisted in different environmental conditions. In soybean, the response to temperature explained 77% of all variance in $F_{r2}/F_m$ respective $F_{r2}'/F_m'$ measured over two seasons in the *Miniplot* facility (Figure 23). This indicated accurate measurements and highly consistent trait response in-between and between seasons. For the first time, interactions with environmental factors were quantified over seasons resulting in different response of genotypes to different factors (e.g. Figure 27). Genotypic differences could be detected consistently over two seasons regarding mean and interactions. However, considering interaction with environmental factors often resulted in more consistent results, e.g. observed in soybean genotypes (Figure 40 and Figure 42). The mean of measured parameter is dependent on dominant environmental conditions at the time period of the measurements leading to biased and hardly reproducible results. The relative ranking of genotypes in $F_q'/F_m'$ and $F_{r2}/F_m$ respective $F_{r2}'/F_m'$ often differed, e.g. maize genotype A and B under field conditions (Figure 58 and Figure 59) or barley genotype Tocada in response to disease infection (Figure 50 and Figure 53). This emphasizes the potential of using interaction of $F_{r2}/F_m$ respective $F_{r2}'/F_m'$ with temperature to screen for new traits adapted to specific environmental conditions.

The automated LIFT system facilitated also time consuming measurements as NPQ recovery. Chlorophyll-deficient MinnGold genotype showed faster NPQ recovery compared to Bahia as control using the automated screening system (Figure 44). This result was confirmed in another study using handheld PAM device (Sakowska et al., submitted). Chlorophyll-deficient mutants can maintain same photosynthetic rates as wild types, e.g. a rice mutant with approximately 65% reduced chlorophyll was still able to capture 70% of the intercepted light (Li et al., 2013). This efficiency in light use is promising for genetic plant improvement. The faster NPQ recovery and lower induction level might be explained by the reduced carotenoid content which was found in the chlorophyll-deficient rice mutant (Li et al., 2013). Under fluctuating natural conditions, plants seem to maintain a higher NPQ level which protects from photodamage but lowers the productivity (Long et al., 2006). Maintaining low rates of NPQ at high light or faster recovery from NPQ are promising traits in plant breeding (Kromdijk et al., 2016;

Meacham et al., 2017). Automated screening of NPQ recovery provided reliable results and about three times higher throughput by alternating between NPQ induction with actinic light and monitoring the NPQ recovery in different plants.

Although the LIFT system is established and functioning in a high-throughput mode, there are some shortcuts. The following improvements will allow further exploitation of the LIFT method potential. Improving the LED power of the excitation beam will allow to operate in a bigger measuring range where the excitation beam is still focused. This will further decrease the signal dependency of different plant height affecting especially $F_{r2}/F_m$ signal. As second improvement, a bigger excitation spot would increase the S/N ratio and averaging out variability in the signal due to canopy structure. An upgrade on the built in spectrometer with higher resolution, higher S/N ratio and a second optic which records incoming irradiation would allow to retrieve passive fluorescence data in the field. It would also solve the problems with the reference spectrum to correct the spectral indices. In order to increase statistical power of data obtained in the *Miniplot* facility, the containers could be planted with different genotypes in a split plot design (Altman and Krzywinski, 2015). Although the contribution of the individual container to whole variance reached only a few percent, e.g. 2.8 % in soybean regarding $F_q'/F_m$ (Table S 1), split plots would help to further control this variance. The optimal number of measurements or replicates to catch the variance per genotype and its canopy structure in given growth conditions is to estimate further. Any positioning system including autonomous field robots are suitable for high-throughput screening in the field as long as they maintain constant low speed (not faster than 10 cm/s). In summary, the potential of the LIFT method to provide consistent fluorescence information about photosynthetic performance in high spatio-temporal resolution in natural environment was proofed and can be further optimized.

$F_v/F_m$ respective $F_q'/F_m$ and the newly established $F_{r2}/F_m$ respective $F_{r2}'/F_m'$ were able to detect genotypic differences under natural fluctuating environment in controlled and stressed growth conditions. $F_q'/F_m$ together with PPFD provided the *actual* electron transport rate at $Q_A$. In contrast, $F_{r2}/F_m$ respective $F_{r2}'/F_m'$ was rather independent from PPFD and reflected electron transport *capacity* through PQ pool and towards PSI. Therefore, $F_{r2}/F_m$ respective $F_{r2}'/F_m'$ was more dependent on temperature and efficiently detected drought stress response which enhances cyclic electron transport (Zivcak et al., 2013). Due to the high spatio-temporal resolution of the data, not only measured means under specific conditions but also the interaction with environmental factors could be analyzed. This provided more detailed information regarding estimation of photosynthetic performance under natural fluctuating conditions and the tolerance to this fluctuation. The available information about photosynthetic performance under field conditions was extended which could improve genotypic selection in breeding programs or modelling approaches. In that perspective, the $\sigma_{PSII}$ modeled from the LIFT signal was able to detect antennae size of the PSII providing additional information about light harvesting (Osmond et al., 2017). $F_i/F_m$ derived directly from the initial LIFT signal in the first few µs potentially bares similar information. Further parameters derived from the LIFT signal as carQ are open for investigation to determine and predict photosynthetic performance in greater detail.

# 5 Conclusions

The LIFT method was validated for fluorescence induction and relaxation. Based on that, established $F_v/F_m$ parameter and a newly introduced parameter, $F_{r2}/F_m$, were analyzed in different crop species and genotypes from controlled lab conditions up to field conditions. The LIFT method demonstrated the ability to carry out large fluorescence screening in high spatio-temporal resolution. The acquired data allowed to analyze interactions of the fluorescence parameters with the fluctating environment. PPFD and temperature mainly determined $F_v/F_m$ and $F_{r2}/F_m$ parameter under fluctuating conditions causing a diurnal pattern, respectively. Consequently, $F_v/F_m$ parameter was mainly sensitive to light intensity and quantified the light-use efficiency of plant photosynthesis. In contrast, temperature sensitive parameter, $F_r/F_m$, complemented the physiological observations by identifying temperature-use efficienct photosysnthetic phenotypes. In addition to the parameter means, response curves to PPFD and temperature detected (1) differences in genotypes consistently over two seasons under fluctuating conditions, (2) various stress conditions like drought or disease infection, and (3) differences in NPQ recovery. The LIFT method has potential application in selection of photosynthetic superior genotypes for plant breeding and in improving models for photosynthesis under fluctuating conditions.

# 6 Acknowledgments

At first, I would like to give my sincerest thanks to Professor Uwe Rascher and Dr. Onno Muller for guidance through the whole PhD thesis. I also would like to thank my further supervisors Dr. Shizue Matsubara, Dr. Roland Pieruschka and Professor Frank Hochholdinger for advices and critical questions. Special thanks go to Angelina Steier for great automation work, Dr. Zbigniew Kolber for introduction to the fluorometer with its 24 hours support and to the whole shoot dynamics group for the great support. I sincerely thank Lars Zimmerman for many field measurement, Benedikt Janssen for operating the autonomous field robot, Dr. Maria Lucrécia Gerosa Ramos and Dr. Walter Quadros Ribeiro Junior for making the measurements in Brasília possible, Dr. Imre Vass and Dr. Kenny Paul for measurements on the double modulated fluorometer, Dr. Christoph Jedmowski and Dr. Anke Schickling for discussion of the results, Stefan Thomas for allowing measurements in his barley experiment, and Prof. Barry Osmond, Prof. Sharon Robinson and Rhys Wyber for measurements and discussion in Wollongong and Canberra. Many thanks go to people managing the *Miniplot* facility and field experiments on the campus Klein-Altendorf, especially Ines Munoz-Fernandez, Tim Schiffer, Karl-Josef Wiesel, Dr. Thorsten Kraska and Hubert Kühn. Furthermore, I would like to acknowledged Beate Uhlig, Marcel Schneider, Katharina Wolter-Heinen and Christian Jungmann to ensure optimal plant growth conditions in the greenhouses.

# 7 References

Adams, W.W., and Demmig-Adams, B. (1995). The xanthophyll cycle and sustained thermal energy dissipation activity in Vinca minor and Euonymus kiautschovicus in winter. Plant Cell Environ. *18*, 117–127.

Adams III, W.W., Zarter, C.R., Mueh, K.E., Amiard, V., and Demmig-Adams, B. (2006). Energy Dissipation and Photoinhibition: A Continuum of Photoprotection. In Photoprotection, Photoinhibition, Gene Regulation, and Environment, B. Demmig-Adams, W.W. Adams, and A.K. Mattoo, eds. (Dordrecht: Springer Netherlands), pp. 49–64.

Agati, G., Mazzinghi, P., Fusi, F., and Ambrosini, I. (1995). The F685/F730 Chlorophyll Fluorescence Ratio As A Tool in Plant Physiology - Response to Physiological and Environmental-Factors. J. PLANT Physiol. *145*, 228–238.

Agati, G., Cerovic, Z.G., and Moya, I. (2000). The Effect of Decreasing Temperature up to Chilling Values on the in vivo F685/F735 Chlorophyll Fluorescence Ratio in Phaseolus vulgaris and Pisum sativum: The Role of the Photosystem I Contribution to the 735 nm Fluorescence Band ¶. Photochem. Photobiol. *72*, 75–84.

Alexandratos, N., and Bruinsma, J. (2012). World agriculture towards 2030/2050: the 2012 revision (Food and Agricultural Organization (FAO)).

Al-Shoaibi, A.A. (2008). Photosynthetic Response to the Low Temperature in Elephant Grass (Pennisetum purpureum) and Zea mays. Int. J. Bot. *4*, 309–314.

Altman, N., and Krzywinski, M. (2015). Points of Significance: Split plot design. Nat. Methods *12*, 165.

Ananyev, G., Kolber, Z.S., Klimov, D., Falkowski, P.G., Berry, J.A., Rascher, U., Martin, R., and Osmond, B. (2005a). Remote sensing of heterogeneity in photosynthetic efficiency, electron transport and dissipation of excess light in Populus deltoides stands under ambient and elevated CO2 concentrations, and in a tropical forest canopy, using a new laser-induced fluorescence transient device. Glob. Change Biol. *11*, 1195–1206.

Baker, N.R. (2008). Chlorophyll fluorescence: A probe of photosynthesis in vivo. Annu. Rev. Plant Biol. *59*, 89–113.

Baldisserotto, C., Ferroni, L., Pantaleoni, L., and Pancaldi, S. (2013). Comparison of photosynthesis recovery dynamics in floating leaves of Trapa natans after inhibition by manganese or molybdenum: Effects on Photosystem {II}. Plant Physiol. Biochem. *70*, 387–395.

Barber, J., Ford, R.C., Mitchell, R.A.C., and Millner, P.A. (1984). Chloroplast thylakoid membrane fluidity and its sensitivity to temperature. Planta *161*, 375–380.

Bassham, J.A. (2003). Mapping the carbon reduction cycle: a personal retrospective. Photosynth. Res. *76*, 35–52.

Belgio, E., Johnson, M.P., Jurić, S., and Ruban, A.V. (2012). Higher Plant Photosystem II Light-Harvesting Antenna, Not the Reaction Center, Determines the Excited-State Lifetime—Both the Maximum and the Nonphotochemically Quenched. Biophys. J. *102*, 2761–2771.

Benke, A., Urbany, C., Marsian, J., Shi, R., Wiren, N., and Stich, B. (2014). The genetic basis of natural variation for iron homeostasis in the maize IBM population. BMC Plant Biol. *14*, 12.

Bernacchi, C., Singsaas, E., Pimentel, C., Portis, A., and Long, S. (2001). Improved temperature response functions for models of Rubisco-limited photosynthesis. PLANT CELL Environ. *24*, 253–259.

Berthold, D.A., Babcock, G.T., and Yocum, C.F. (1981). A highly resolved, oxygen-evolving photosystem II preparation from spinach thylakoid membranes: EPR and electron-transport properties. FEBS Lett. *134*, 231–234.

Bilger, W., and Björkman, O. (1990). Role of the xanthophyll cycle in photoprotection elucidated by measurements of light-induced absorbance changes, fluorescence and photosynthesis in leaves of Hedera canariensis. Photosynth. Res. *25*, 173–185.

Bohme, H., Reimer, S., and Trebst, A. (1971). The Effect of Dibromothymoquinone, an Antagonist of Plastoquinone, on Non Cyclic and Cyclic Electron Flow Systems in Isolated Chloroplasts. Z. Naturforschung Part B-Chem. Biochem. Biophys. Biol. Verwandten Geb. *B 26*, 341–+.

Bowes, J.M., and Crofts, A.R. (1980). Binary oscillations in the rate of reoxidation of the primary acceptor of Photosystem II. Biochim. Biophys. Acta BBA - Bioenerg. *590*, 373–384.

Braslavsky, S.E., and Holzwarth, A.R. (2012). Role of Carotenoids in Photosystem II (PSII) Reaction Centers. Int. J. Thermophys. *33*, 2021–2025.

Bressan, M., Dall'Osto, L., Bargigia, I., Alcocer, M.J.P., Viola, D., Cerullo, G., D'Andrea, C., Bassi, R., and Ballottari, M. (2016). LHCII can substitute for LHCI as an antenna for photosystem I but with reduced light-harvesting capacity. Nat. Plants *2*, 16131.

Bundesamt für Landwirtschaft (2015). Verordnung des BLW über Sortenkataloge und Sortenlisten landwirtschaftlich genutzter Pflanzenarten (Sortenverordnung) (Bern: Bundesamt für Landwirtschaft (BLW)).

Bundessortenamt (2013). Beschreibende Sortenliste - Sortenliste Getreide, Mais, Öl- und Faserpflanzen, Leguminosen, Rüben, Zwischenfrüchte (Hannover).

Bundessortenamt (2017). Beschreibende Sortenliste - Sortenliste Getreide, Mais, Öl- und Faserpflanzen, Leguminosen, Rüben, Zwischenfrüchte (Hannover).

Butler, W.L. (1978). Energy distribution in the photochemical apparatus of photosynthesis. Annu. Rev. Plant Physiol. *29*, 345–378.

Campbell, B.W., Mani, D., Curtin, S.J., Slattery, R.A., Michno, J.-M., Ort, D.R., Schaus, P.J., Palmer, R.G., Orf, J.H., and Stupar, R.M. (2015). Identical Substitutions in Magnesium Chelatase Paralogs Result in Chlorophyll-Deficient Soybean Mutants. G3 GenesGenomesGenetics *5*, 123–131.

Campbell, P.K.E., Middleton, E.M., Corp, L.A., and Kim, M.S. (2008). Contribution of chlorophyll fluorescence to the apparent vegetation reflectance. Sci. Total Environ. *404*, 433–439.

Cordon, G., Lagorio, M.G., and Paruelo, J.M. (2016). Chlorophyll fluorescence, photochemical reflective index and normalized difference vegetative index during plant senescence. J. Plant Physiol. *199*, 100–110.

Cournac, L., Redding, K., Ravenel, J., Rumeau, D., Josse, E.M., Kuntz, M., and Peltier, G. (2000). Electron flow between photosystem II and oxygen in chloroplasts of photosystem. J. Biol. Chem. *275*, 17256–17262.

Croce, R. (2015). PsbS is the plants' pick for sun protection. Nat Struct Mol Biol *22*, 650–652.

Croce, R., and van Amerongen, H. (2013). Light-harvesting in photosystem I. Photosynth. Res. *116*, 153–166.

Croce, R., and van Amerongen, H. (2014). Natural strategies for photosynthetic light harvesting. Nat Chem Biol *10*, 492–501.

Czyczylo-Mysza, I., Tyrka, M., Marcinska, I., Skrzypek, E., Karbarz, M., Dziurka, M., Hura, T., Dziurka, K., and Quarrie, S.A. (2013). Quantitative trait loci for leaf chlorophyll fluorescence parameters, chlorophyll and carotenoid contents in relation to biomass and yield in bread wheat and their chromosome deletion bin assignments. Mol. Breed. *32*, 189–210.

Damm, A., Guanter, L., Verhoef, W., Schläpfer, D., Garbari, S., and Schaepman, M.E. (2015). Impact of varying irradiance on vegetation indices and chlorophyll fluorescence derived from spectroscopy data. Remote Sens. Environ. *156*, 202–215.

Dash, J., and Curran, P.J. (2004). The MERIS terrestrial chlorophyll index. Int. J. Remote Sens. *25*, 5403–5413.

Delosme, R., and Joliot, P. (2002). Period four oscillations in chlorophyll a fluorescence. Photosynth. Res. *73*, 165–168.

Demmig-Adams, B., Cohu, C.M., Muller, O., and Adams, W.W., III (2012). Modulation of photosynthetic energy conversion efficiency in nature: from seconds to seasons. Photosynth. Res. *113*, 75–88.

Driever, S.M., Lawson, T., Andralojc, P.J., Raines, C.A., and Parry, M.A.J. (2014). Natural variation in photosynthetic capacity, growth, and yield in 64 field-grown wheat genotypes. J. Exp. Bot. *65*, 4959–4973.

Eshaghi, S., Turcsányi, E., Vass, I., Nugent, J., Andersson, B., and Barber, J. (2000). Functional characterization of the PS II–LHC II supercomplex isolated by a direct method from spinach thylakoid membranes. Photosynth. Res. *64*, 179–187.

Evans, J.R. (2013). Improving Photosynthesis. Plant Physiol. *162*, 1780–1793.

Falkowski, P.G., Koblfzek, M., Gorbunov, M., and Kolber, Z. (2004). Development and Application of Variable Chlorophyll Fluorescence Techniques in Marine Ecosystems. In Chlorophyll a Fluorescence: A Signature of Photosynthesis, G.C. Papageorgiou, and Govindjee, eds. (Dordrecht: Springer Netherlands), pp. 757–778.

FAO (2016). The State of Food and Agriculture - Climate change, Agriculture and Food Security (Rome: Food and Agricultural Organization (FAO)).

Feilke, K., Yu, Q., Beyer, P., Sétif, P., and Krieger-Liszkay, A. (2014). In vitro analysis of the plastid terminal oxidase in photosynthetic electron transport. Biochim. Biophys. Acta BBA - Bioenerg. *1837*, 1684–1690.

Finazzi, G., Furia, A., Barbagallo, R.P., and Forti, G. (1999). State transitions, cyclic and linear electron transport and photophosphorylation in Chlamydomonas reinhardtii. Biochim. Biophys. Acta BBA - Bioenerg. *1413*, 117–129.

Foroozanfar, M., Exbrayat, S., Gentzbittel, L., Bertoni, G., Maury, P., Naghavie, M.R., Peyghambari, A., Badri, M., Ben, C., Debelle, F., et al. (2014). Genetic variability and identification of quantitative trait loci affecting plant growth and chlorophyll fluorescence parameters in the model legume Medicago truncatula under control and salt stress conditions. Funct. Plant Biol. *41*, 983–1001.

Frampton, W.J., Dash, J., Watmough, G., and Milton, E.J. (2013). Evaluating the capabilities of Sentinel-2 for quantitative estimation of biophysical variables in vegetation. ISPRS J. Photogramm. Remote Sens. *82*, 83–92.

Franck, F., Juneau, P., and Popovic, R. (2002). Resolution of the Photosystem I and Photosystem II contributions to chlorophyll fluorescence of intact leaves at room temperature. Biochim. Biophys. Acta BBA - Bioenerg. *1556*, 239–246.

Furbank, R.T., and Tester, M. (2011). Phenomics - technologies to relieve the phenotyping bottleneck. Trends Plant Sci. *16*, 635–644.

Gage, S.H., Davey Smith, G., Ware, J.J., Flint, J., and Munafò, M.R. (2016). G = E: What GWAS Can Tell Us about the Environment. PLOS Genet. *12*, e1005765.

Galka, P., Santabarbara, S., Thi Thu Huong, K., Degand, H., Morsomme, P., Jennings, R.C., Boekema, E.J., and Caffarri, S. (2012). Functional Analyses of the Plant Photosystem I-Light-Harvesting Complex II Supercomplex Reveal That Light-Harvesting Complex II Loosely Bound to Photosystem II Is a Very Efficient Antenna for Photosystem I in State II. Plant Cell *24*, 2963–2978.

Gamon, J.A., Peñuelas, J., and Field, C.B. (1992). A narrow-waveband spectral index that tracks diurnal changes in photosynthetic efficiency. Remote Sens. Environ. *41*, 35–44.

Garbulsky, M.F., Peñuelas, J., Gamon, J., Inoue, Y., and Filella, I. (2011). The photochemical reflectance index (PRI) and the remote sensing of leaf, canopy and ecosystem radiation use efficiencies: A review and meta-analysis. Remote Sens. Environ. *115*, 281–297.

Genty, B., Briantais, J.-M., and Baker, N.R. (1989). The relationship between the quantum yield of photosynthetic electron transport and quenching of chlorophyll fluorescence. Biochim. Biophys. Acta BBA - Gen. Subj. *990*, 87–92.

Guanter, L., Zhang, Y., Jung, M., Joiner, J., Voigt, M., Berry, J.A., Frankenberg, C., Huete, A.R., Zarco-Tejada, P., Lee, J.-E., et al. (2014). Global and time-resolved monitoring of crop photosynthesis with chlorophyll fluorescence. Proc. Natl. Acad. Sci. U. S. A. *111*, E1327–E1333.

Guo, P.G., Baum, M., Varshney, R.K., Graner, A., Grando, S., and Ceccarelli, S. (2008). QTLs for chlorophyll and chlorophyll fluorescence parameters in barley under post-flowering drought. Euphytica *163*, 203–214.

Haldimann, P., and Tsimilli-Michael, M. (2005). Non-photochemical quenching of chlorophyll a fluorescence by oxidised plastoquinone: new evidences based on modulation of the redox state of the endogenous plastoquinone pool in broken spinach chloroplasts. Biochim. Biophys. Acta BBA - Bioenerg. *1706*, 239–249.

Haritha, G., Vishnukiran, T., Yugandhar, P., Sarla, N., and Subrahmanyam, D. (2017). Introgressions from Oryza rufipogon Increase Photosynthetic Efficiency of KMR3 Rice Lines. Rice Sci. *24*, 85–96.

Hecht, V.L., Temperton, V.M., Nagel, K.A., Rascher, U., and Postma, J.A. (2016). Sowing Density: A Neglected Factor Fundamentally Affecting Root Distribution and Biomass Allocation of Field Grown Spring Barley (Hordeum Vulgare L.). Front. Plant Sci. *7*, 944.

Iba, K. (2002). ACCLIMATIVE RESPONSE TO TEMPERATURE STRESS IN HIGHER PLANTS: Approaches of Gene Engineering for Temperature Tolerance. Annu. Rev. Plant Biol. *53*, 225–245.

Jedmowski, C., Ashoub, A., and Brueggemann, W. (2013). Reactions of Egyptian landraces of Hordeum vulgare and Sorghum bicolor to drought stress, evaluated by the OJIP fluorescence transient analysis. ACTA Physiol. Plant. *35*, 345–354.

Jia, H., Foerster, B., Chow, W.S., Pogson, B.J., and Osmond, C.B. (2013). Decreased Photochemical Efficiency of Photosystem II following Sunlight Exposure of Shade-Grown Leaves of Avocado: Because of, or in Spite of, Two Kinetically Distinct Xanthophyll Cycles? Plant Physiol. *161*, 836–852.

Joiner, J., Yoshida, Y., Vasilkov, A.P., Yoshida, Y., Corp, L.A., and Middleton, E.M. (2011). First observations of global and seasonal terrestrial chlorophyll fluorescence from space. Biogeosciences *8*, 637–651.

Kaiser, E., Matsubara, S., Harbinson, J., Heuvelink, E., and Marcelis, L.F.M. (2017). Acclimation of photosynthesis to lightflecks in tomato leaves: interaction with progressive shading in a growing canopy. Physiol. Plant.

Kalaji, H.M., Jajoo, A., Oukarroum, A., Brestic, M., Zivcak, M., Samborska, I.A., Cetner, M.D., Łukasik, I., Goltsev, V., and Ladle, R.J. (2016). Chlorophyll a fluorescence as a tool to monitor physiological status of plants under abiotic stress conditions. Acta Physiol. Plant. *38*, 102.

Kalaji, H.M., Schansker, G., Brestic, M., Bussotti, F., Calatayud, A., Ferroni, L., Goltsev, V., Guidi, L., Jajoo, A., Li, P., et al. (2017). Frequently asked questions about chlorophyll fluorescence, the sequel. Photosynth. Res. *132*, 13–66.

Kautsky, H., and Hirsch, A. (1931). Neue Versuche zur Kohlensäureassimilation. Naturwissenschaften *19*, 964–964.

Keller, B., Vass, I., Matsubara, S., Paul, K., Jedmowski, C., Pieruschka, R., Rascher, U., and Muller, O. (submitted). Maximum fluorescence and electron transport kinetics determined by light induced fluorescence transients (LIFT) for photosynthesis phenotyping. Photosynth. Res.

Keller, B., Matsubara, S., Rascher, U., Pieruschka, R., Steier, A., Kraska, T., and Muller, O. (in prep.). Genotype specific photosynthesis x environment interactions captured by automated fluorescence canopy scans over two seasons under fluctuating conditions.

Kim, K., and Portis, A.R. (2005). Temperature Dependence of Photosynthesis in Arabidopsis Plants with Modifications in Rubisco Activase and Membrane Fluidity. Plant Cell Physiol. *46*, 522–530.

Kolber, Z.S., Prasil, O., and Falkowski, P.G. (1998). Measurements of variable chlorophyll fluorescence using fast repetition rate techniques: defining methodology and experimental protocols. Biochim. Biophys. Acta-Bioenerg. *1367*, 88–106.

Kono, M., and Terashima, I. (2014). Long-term and short-term responses of the photosynthetic electron transport to fluctuating light. J. Photochem. Photobiol. B *137*, 89–99.

van Kooten, O., and Snel, J.F. (1990). The use of chlorophyll fluorescence nomenclature in plant stress physiology. Photosynth. Res. *25*, 147–150.

Kromdijk, J., Głowacka, K., Leonelli, L., Gabilly, S.T., Iwai, M., Niyogi, K.K., and Long, S.P. (2016). Improving photosynthesis and crop productivity by accelerating recovery from photoprotection. Science *354*, 857.

Krüger, G.H.J., De Villiers, M.F., Strauss, A.J., de Beer, M., van Heerden, P.D.R., Maldonado, R., and Strasser, R.J. (2014). Inhibition of photosystem II activities in soybean (Glycine max) genotypes differing in chilling sensitivity. South Afr. J. Bot. *95*, 85–96.

Kurisu, G., Zhang, H.M., Smith, J.L., and Cramer, W.A. (2003). Structure of the cytochrome b(6)f complex of oxygenic photosynthesis: Tuning the cavity. Science *302*, 1009–1014.

Lawson, T., Oxborough, K., Morison, J., and Baker, N. (2002). Responses of photosynthetic electron transport in stomatal guard cells and mesophyll cells in intact leaves to light, CO2, and humidity. PLANT Physiol. *128*, 52–62.

Lazár, D. (1999). Chlorophyll a fluorescence induction. Biochim. Biophys. Acta-Bioenerg. *1412*, 1–28.

Lazár, D. (2013). Simulations show that a small part of variable chlorophyll a fluorescence originates in photosystem I and contributes to overall fluorescence rise. J. Theor. Biol. *335*, 249–264.

Lee, M., Sharopova, N., Beavis, W.D., Grant, D., Katt, M., Blair, D., and Hallauer, A. (2002). Expanding the genetic map of maize with the intermated B73 x Mo17 (IBM) population. Plant Mol Biol *48*, 453–461.

Li, Y., Ren, B., Gao, L., Ding, L., Jiang, D., Xu, X., Shen, Q., and Guo, S. (2013). Less Chlorophyll Does not Necessarily Restrain Light Capture Ability and Photosynthesis in a Chlorophyll-Deficient Rice Mutant. J. Agron. Crop Sci. *199*, 49–56.

Liu, X.Y., Teng, Y.B., Li, B., and Meng, Q.W. (2013). Enhancement of low-temperature tolerance in transgenic tomato plants overexpressing Lefad7 through regulation of trienoic fatty acids. Photosynthetica *51*, 238–244.

Long, S.P., Zhu, X.-G., Naidu, S.L., and Ort, D.R. (2006). Can improvement in photosynthesis increase crop yields? Plant Cell Environ. *29*, 315–330.

Malkin, S., and Kok, B. (1966). Fluorescence induction studies in isolated chloroplasts I. Number of components involved in the reaction and quantum yields. Biochim. Biophys. Acta BBA - Biophys. Photosynth. *126*, 413–432.

Marutani, Y., Yamauchi, Y., Kimura, Y., Mizutani, M., and Sugimoto, Y. (2012). Damage to photosystem II due to heat stress without light-driven electron flow: involvement of enhanced introduction of reducing power into thylakoid membranes. Planta *236*, 753–761.

Mathur, S., Agrawal, D., and Jajoo, A. (2014). Photosynthesis: Response to high temperature stress. Stress Photosynth. *137*, 116–126.

Meacham, K., Sirault, X., Quick, W.P., von Caemmerer, S., and Furbank, R. (2017). Diurnal Solar Energy Conversion and Photoprotection in Rice Canopies. Plant Physiol. *173*, 495–508.

de Miguel, M., Cabezas, J.A., de Maria, N., Sanchez-Gomez, D., Guevara, M.A., Velez, M.D., Saez-Laguna, E., Diaz, L.M., Mancha, J.A., Barbero, M.C., et al. (2014). Genetic control of functional traits related to photosynthesis and water use efficiency in Pinus pinaster Ait. drought response: integration of genome annotation, allele association and QTL detection for candidate gene identification. Bmc Genomics *15*.

Millet, E., Welcker, C., Kruijer, W., Negro, S., Nicolas, S., Praud, S., Ranc, N., Presterl, T., Tuberosa, R., Bedo, Z., et al. (2016). Genome-wide analysis of yield in Europe: allelic effects as functions of drought and heat scenarios. Plant Physiol.

Morison, J.I.L., and Gifford, R.M. (1983). Stomatal Sensitivity to Carbon Dioxide and Humidity. Plant Physiol. *71*, 789–796.

Morosinotto, T., Breton, J., Bassi, R., and Croce, R. (2003). The Nature of a Chlorophyll Ligand in Lhca Proteins Determines the Far Red Fluorescence Emission Typical of Photosystem I. J. Biol. Chem. *278*, 49223–49229.

Moura dos Santos, C., Verissimo, V., Filho, H.C. de L.W., Ferreira, V.M., Cavalcante, P.G. da S., Rolim, E.V., and Endres, L. (2013). Seasonal variations of photosynthesis, gas exchange, quantum efficiency of photosystem II and biochemical responses of Jatropha curcas L. grown in semi-humid and semi-arid areas subject to water stress. Ind. Crops Prod. *41*, 203–213.

Mu, H., Jiang, D., Wollenweber, B., Dai, T., Jing, Q., and Cao, W. (2010). Long-term Low Radiation Decreases Leaf Photosynthesis, Photochemical Efficiency and Grain Yield in Winter Wheat. J. Agron. Crop Sci. *196*, 38–47.

Munekage, Y., Hashimoto, M., Miyake, C., Tomizawa, K., Endo, T., Tasaka, M., and Shikanai, T. (2004). Cyclic electron flow around photosystem I is essential for photosynthesis. Nature *429*, 579–582.

Murchie, E.H., Pinto, M., and Horton, P. (2009). Agriculture and the new challenges for photosynthesis research. New Phytol. *181*, 532–552.

Nellaepalli, S., Kodru, S., Tirupathi, M., and Subramanyam, R. (2012). Anaerobiosis Induced State Transition: A Non Photochemical Reduction of PQ Pool Mediated by NDH in Arabidopsis thaliana. PLOS ONE *7*, e49839.

Nilkens, M., Kress, E., Lambrev, P., Miloslavina, Y., Müller, M., Holzwarth, A.R., and Jahns, P. (2010). Identification of a slowly inducible zeaxanthin-dependent component of non-photochemical quenching of chlorophyll fluorescence generated under steady-state conditions in Arabidopsis. Biochim. Biophys. Acta BBA - Bioenerg. *1797*, 466–475.

Niyogi, K.K., Grossman, A.R., and Björkman, O. (1998). Arabidopsis Mutants Define a Central Role for the Xanthophyll Cycle in the Regulation of Photosynthetic Energy Conversion. Plant Cell *10*, 1121.

Nolan, W.G., and Smillie, R.M. (1976). Multi-temperature effects on Hill reaction activity of barley chloroplasts. Biochim. Biophys. Acta BBA - Bioenerg. *440*, 461–475.

Ögren, E., and Baker, N.R. (1985). Evaluation of a technique for the measurement of chlorophyll fluorescence from leaves exposed to continuous white light. Plant Cell Environ. *8*, 539–547.

Osmond, B., Chow, W.S., Wyber, R., Zavafer, A., Keller, B., Pogson, B.J., and Robinson, S.A. (2017). Relative functional and optical absorption cross sections of PSII and other photosynthetic parameters monitored in situ, at a distance with a time resolution of a few seconds, using a prototype Light Induced Fluorescence Transient (LIFT) device. Funct. Plant Biol.

Oxborough, K., Moore, C.M., Suggett, D.J., Lawson, T., Chan, H.G., and Geider, R.J. (2012). Direct estimation of functional PSII reaction center concentration and PSII electron flux on a volume basis: a new approach to the analysis of Fast Repetition Rate fluorometry (FRRf) data. Limnol. Oceanogr.-Methods *10*, 142–154.

Pancaldi, S., Baldisserotto, C., Ferroni, L., Bonora, A., and Fasulo, M.P. (2002). Room temperature microspectrofluorimetry as a useful tool for studying the assembly of the PSII chlorophyll–protein complexes in single living cells of etiolated Euglena gracilis Klebs during the greening process. J. Exp. Bot. *53*, 1753–1763.

Parry, M.A.J., Flexas, J., and Medrano, H. (2005). Prospects for crop production under drought: research priorities and future directions. Ann. Appl. Biol. *147*, 211–226.

Parry, M.A.J., Reynolds, M., Salvucci, M.E., Raines, C., Andralojc, P.J., Zhu, X.-G., Price, G.D., Condon, A.G., and Furbank, R.T. (2011). Raising yield potential of wheat. II. Increasing photosynthetic capacity and efficiency. J. Exp. Bot. *62*, 453–467.

Passioura, J. (2007). The drought environment: physical, biological and agricultural perspectives. J. Exp. Bot. *58*, 113–117.

Peñuelas, J., Marino, G., LLusia, J., Morfopoulos, C., Farré-Armengol, G., and Filella, I. (2013). Photochemical reflectance index as an indirect estimator of foliar isoprenoid emissions at the ecosystem level. *4*, 2604.

Pérez-Navarro, M., Neese, F., Lubitz, W., Pantazis, D.A., and Cox, N. (2016). Recent developments in biological water oxidation. Biocatal. Biotransformation Bioinorg. Chem. *31*, 113–119.

Peterson, R.B. (1990). Effects of Water Vapor Pressure Deficit on Photochemical and Fluorescence Yields in Tobacco Leaf Tissue. Plant Physiol. *92*, 608–614.

Petrouleas, V., and Crofts, A. (2005). The Iron-Quinone Acceptor Complex. In Photosystem II, T. Wydrzynski, K. Satoh, and J. Freeman, eds. (Springer Netherlands), pp. 177–206.

Pieruschka, R., Klimov, D., Rascher, U., Kolber, Z., and Berry, J. (2008). Remote Monitoring of Photosynthetic Efficiency Using Laser Induced Fluorescence Transient (LIFT) Technique. In Photosynthesis. Energy from the Sun, J. Allen, E. Gantt, J. Golbeck, and B. Osmond, eds. (Springer Netherlands), pp. 1539–1543.

Pieruschka, R., Klimov, D., Kolber, Z.S., and Berry, J.A. (2010). Monitoring of cold and light stress impact on photosynthesis by using the laser induced fluorescence transient (LIFT) approach. Funct. Plant Biol. *37*, 395–402.

Pieruschka, R., Albrecht, H., Muller, O., Berry, J.A., Klimov, D., Kolber, Z.S., Malenovský, Z., and Rascher, U. (2014). Daily and seasonal dynamics of remotely sensed photosynthetic efficiency in tree canopies. Tree Physiol. *34*, 674–685.

Pinto, F., Damm, A., Schickling, A., Panigada, C., Cogliati, S., Müller-Linow, M., Balvora, A., and Rascher, U. (2016). Sun-induced chlorophyll fluorescence from high-resolution imaging spectroscopy data to quantify spatio-temporal patterns of photosynthetic function in crop canopies. Plant Cell Environ. *39*, 1500–1512.

Poersch-Bortolon, L.B., Scagliusi, S.M.M., Yamazaki-Lau, E., and Bodanese-Zanettini, M.H. (2016). Androgenic response of Brazilian wheat genotypes to different pretreatments of spikes and to a gelling agent. Pesqui. AgropecuÃria Bras. *51*, 1839–1847.

Poorter, H., Fiorani, F., Pieruschka, R., Wojciechowski, T., van der Putten, W.H., Kleyer, M., Schurr, U., and Postma, J. (2016). Pampered inside, pestered outside? Differences and similarities between plants growing in controlled conditions and in the field. New Phytol. *212*, 838–855.

Prasad, A.K., Chai, L., Singh, R.P., and Kafatos, M. (2006). Crop yield estimation model for Iowa using remote sensing and surface parameters. Int. J. Appl. Earth Obs. Geoinformation *8*, 26–33.

Raesch, A., Muller, O., Pieruschka, R., and Rascher, U. (2014). Field Observations with Laser-Induced Fluorescence Transient (LIFT) Method in Barley and Sugar Beet. Agriculture *4*, 159–169.

Rascher, U., and Nedbal, L. (2006). Dynamics of photosynthesis in fluctuating light - Commentary. Curr. Opin. Plant Biol. *9*, 671–678.

Rascher, U., and Pieruschka, R. (2008). Spatio-temporal variations of photosynthesis: the potential of optical remote sensing to better understand and scale light use efficiency and stresses of plant ecosystems. Precis. Agric. *9*, 355–366.

Rascher, U., Liebig, M., and Lüttge, U. (2000). Evaluation of instant light-response curves of chlorophyll fluorescence parameters obtained with a portable chlorophyll fluorometer on site in the field. Plant Cell Environ. *23*, 1397–1405.

Rascher, U., Nichol, C.J., Small, C., and Hendricks, L. (2007). Monitoring spatio-temporal dynamics of photosynthesis with a portable hyperspectral imaging system. Photogramm. Eng. Remote Sens. *73*, 45–56.

Rascher, U., Alonso, L., Burkart, A., Cilia, C., Cogliati, S., Colombo, R., Damm, A., Drusch, M., Guanter, L., Hanus, J., et al. (2015). Sun-induced fluorescence – a new probe of photosynthesis: First maps from the imaging spectrometer HyPlant. Glob. Change Biol. *21*, 4673–4684.

Ribeiro, R., dos Santos, M., Souza, G., Machado, E., de Oliveira, R., Angelocci, L., and Pimentel, C. (2004). Environmental effects on photosynthetic capacity of bean genotypes. Pesqui. Agropecu. Bras. *39*, 615–623.

Robinson, C., Suggett, D.J., Cherukuru, N., Ralph, P.J., and Doblin, M.A. (2014). Performance of Fast Repetition Rate fluorometry based estimates of primary productivity in coastal waters. J. Mar. Syst. *139*, 299–310.

Rochaix, J.D. (2014). Regulation and Dynamics of the Light-Harvesting System. Annu. Rev. Plant Biol. Vol 65 *65*, 287–309.

Rodolfo Junior, F., Ribeiro Júnior, W., Ramos, M., Rocha, O., Maria Teles BATISTA, L., Macena, F., and Pesquisas Agrárias e Ambientais, N. (2016). Produtividade e qualidade de variedades de cana-de-açúcar de terceira soca sob regime hídrico variável/ Productivity and quality of third ratoon sugarcane varieties under variable hydrological regime.

Ruban, A.V., Johnson, M.P., and Duffy, C.D.P. (2012). The photoprotective molecular switch in the photosystem II antenna. Biochim. Biophys. Acta *1817*, 167–181.

Sakowska, K., Alberti, G., Genesio, L., Peressotti, A., Delle Vedove, G., Gianelle, D., Colombo, R., Rodeghiero, M., Panigada, C., Juszczak, R., et al. (submitted). Leaf and canopy photosynthesis of a chlorophyll deficient soybean mutant.

Samson, G., and Bruce, D. (1996). Origins of the low yield of chlorophyll a fluorescence induced by single turnover flash in spinach thylakoids. Biochim. Biophys. Acta-Bioenerg. *1276*, 147–153.

Schansker, G., Tóth, S.Z., and Strasser, R.J. (2005). Methylviologen and dibromothymoquinone treatments of pea leaves reveal the role of photosystem I in the Chl a fluorescence rise OJIP. Biochim. Biophys. Acta BBA - Bioenerg. *1706*, 250–261.

Schansker, G., Tóth, S., Holzwarth, A., and Garab, G. (2014). Chlorophyll a fluorescence: beyond the limits of the QA model. Photosynth. Res. *120*, 43–58.

Schickling, A., Matveeva, M., Damm, A., Schween, J.H., Wahner, A., Graf, A., Crewell, S., and Rascher, U. (2016). Combining Sun-Induced Chlorophyll Fluorescence and Photochemical Reflectance Index Improves Diurnal Modeling of Gross Primary Productivity. Remote Sens. *8*.

Schödel, R., Irrgang, K.-D., Voigt, J., and Renger, G. (1999). Quenching of Chlorophyll Fluorescence by Triplets in Solubilized Light-Harvesting Complex II (LHCII). Biophys. J. *76*, 2238–2248.

Schreiber, U. (2004). Pulse-Amplitude-Modulation (PAM) Fluorometry and Saturation Pulse Method: An Overview. In Chlorophyll a Fluorescence: A Signature of Photosynthesis, G.C. Papageorgiou, and Govindjee, eds. (Dordrecht: Springer Netherlands), pp. 279–319.

Schreiber, U., Schliwa, U., and Bilger, W. (1986a). Continuous recording of photochemical and non-photochemical chlorophyll fluorescence quenching with a new type of modulation fluorometer. Photosynth. Res. *10*, 51–62.

Sharkey, T.D., and Schrader, S.M. (2006). High temperature stress. In Physiology and Molecular Biology of Stress Tolerance in Plants, K.. Madhava Rao, A.S. Raghavendra, and K. Janardhan Reddy, eds. (Dordrecht: Springer Netherlands), pp. 101–129.

Shinkarev, V. (2004). Photosystem II: Oxygen Evolution and Chlorophyll a Fluorescence Induced by Multiple Flashes. In Chlorophyll a Fluorescence, G. Papageorgiou, and Govindjee, eds. (Springer Netherlands), pp. 197–229.

Steffen, R., Christen, G., and Renger, G. (2001). Time-resolved monitoring of flash-induced changes of fluorescence quantum yield and decay of delayed light emission in oxygen-evolving photosynthetic organisms. Biochemistry (Mosc.) *40*, 173–180.

Strasser, B.J. (1997). Donor side capacity of Photosystem II probed by chlorophyll a fluorescence transients. Photosynth. Res. *52*, 147–155.

Strasser, R.J., Srivastava, A., and Govindjee (1995). Polyphasic chlorophyll a fluorescence transient in plants and cyanobacteria. Photochem. Photobiol. *61*, 32–42.

Strauss, A.J., and van Heerden, P.D.R. (2011). Effects on both the roots and shoots of soybean during dark chilling determine the nature and extent of photosynthesis inhibition. Environ. Exp. Bot. *74*, 261–271.

Strauss, A.J., Krüger, G.H.J., Strasser, R.J., and Heerden, P.D.R.V. (2006). Ranking of dark chilling tolerance in soybean genotypes probed by the chlorophyll a fluorescence transient O-J-I-P. Environ. Exp. Bot. *56*, 147–157.

Suggett, D., Kraay, G., Holligan, P., Davey, M., Aiken, J., and Geider, R. (2001). Assessment of photosynthesis in a spring cyanobacterial bloom by use of a fast repetition rate fluorometer. Limnol. Oceanogr. *46*, 802–810.

Sui, N. (2015). Photoinhibition of Suaeda salsa to chilling stress is related to energy dissipation and water-water cycle. Photosynthetica *53*, 207–212.

Suzuki, K., Ohmori, Y., and Ratel, E. (2011). High Root Temperature Blocks Both Linear and Cyclic Electron Transport in the Dark During Chilling of the Leaves of Rice Seedlings. Plant Cell Physiol. *52*, 1697–1707.

Tardieu, F., Cabrera-Bosquet, L., Pridmore, T., and Bennett, M. (2017). Plant Phenomics, From Sensors to Knowledge. Curr. Biol. *27*, R770–R783.

Thomas, S., Behmann, J., Steier, A., Kraska, T., Muller, O., Rascher, U., and Mahlein, A.-K. (submitted). Quantitative assessment of disease severity and rating of barley cultivars based on hyperspectral imaging in a non-invasive, automated phenotyping platform.

van der Tol, C., Verhoef, W., Timmermans, J., Verhoef, A., and Su, Z. (2009). An integrated model of soil-canopy spectral radiances, photosynthesis, fluorescence, temperature and energy balance. Biogeosciences *6*, 3109–3129.

van der Tol, C., Berry, J.A., Campbell, P.K.E., and Rascher, U. (2014). Models of fluorescence and photosynthesis for interpreting measurements of solar-induced chlorophyll fluorescence. J. Geophys. Res. Biogeosciences *119*, 2312–2327.

Tóth, S.Z., Schansker, G., Garab, G., and Strasser, R.J. (2007a). Photosynthetic electron transport activity in heat-treated barley leaves: The role of internal alternative electron donors to photosystem II. Biochim. Biophys. Acta BBA - Bioenerg. *1767*, 295–305.

Tóth, S.Z., Schansker, G., and Strasser, R.J. (2007b). A non-invasive assay of the plastoquinone pool redox state based on the OJIP-transient. Photosynth. Res. *93*, 193.

Tóth, S.Z., Schansker, G., and Strasser, R.J. (2005). In intact leaves, the maximum fluorescence level (FM) is independent of the redox state of the plastoquinone pool: A DCMU-inhibition study. Biochim. Biophys. Acta BBA - Bioenerg. *1708*, 275–282.

Townsend, A.J., Retkute, R., Chinnathambi, K., Randall, J.W., foulkes, john, Carmo-Silva, E., and Murchie, E.H. (2017). Suboptimal acclimation of photosynthesis to light in wheat canopies. Plant Physiol.

Trtilek, M., Kramer, D.M., Koblizek, M., and Nedbal, L. (1997). Dual-modulation LED kinetic fluorometer. J. Lumin. *72–4*, 597–599.

Upchurch, R.G. (2008). Fatty acid unsaturation, mobilization, and regulation in the response of plants to stress. Biotechnol. Lett. *30*, 967–977.

Vacek, K., Wong, D., and Govindjee, G. (1977). Absorption and fluorescence properties of highly enriched reaction center particles of photosystem I and of artificial systems. Photochem. Photobiol. *26*, 269–276.

Van Heerden, P.D.R., Tsimilli-Michael, M., Krüger, G.H.J., and Strasser, R.J. (2003). Dark chilling effects on soybean genotypes during vegetative development: parallel studies of CO2 assimilation, chlorophyll a fluorescence kinetics O-J-I-P and nitrogen fixation. Physiol. Plant. *117*, 476–491.

Vass, I., Kirilovsky, D., and Etienne, A.L. (1999). UV-B radiation-induced donor- and acceptor-side modifications of photosystem II in the cyanobacterium Synechocystis sp PCC 6803. Biochemistry (Mosc.) *38*, 12786–12794.

Vernotte, C., Etienne, A.L., and Briantais, J.M. (1979). Quenching of the System II chlorophyll fluorescence by the plastoquinone pool. Biochim. Biophys. Acta *545*, 519–527.

Vialet-Chabrand, S.R., Matthews, J.S., Simkin, A., Raines, C.A., and Lawson, T. (2017). Importance of fluctuations in light on plant photosynthetic acclimation. Plant Physiol.

Vicente-Serrano, S.M., Gouveia, C., Camarero, J.J., Beguería, S., Trigo, R., López-Moreno, J.I., Azorín-Molina, C., Pasho, E., Lorenzo-Lacruz, J., Revuelto, J., et al. (2013). Response of vegetation to drought time-scales across global land biomes. Proc. Natl. Acad. Sci. U. S. A. *110*, 52–57.

Von Caemmerer, S. (Susanne) (2000). Biochemical models of leaf photosynthesis (Collingwood, Vic. : CSIRO Publishing).

Wahadoszamen, M., Berera, R., Ara, A.M., Romero, E., and van Grondelle, R. (2012). Identification of two emitting sites in the dissipative state of the major light harvesting antenna. Phys. Chem. Chem. Phys. PCCP *14*, 759–766.

Wang, Y., Ye, Q., Zhang, M., and Yang, C. (2012a). Involvement of Arabidopsis CPR5 in thermotolerance. Acta Physiol. Plant. *34*, 2093–2103.

Wang, Z.X., Chen, L., Ai, J., Qin, H.Y., Liu, Y.X., Xu, P.L., Jiao, Z.Q., Zhao, Y., and Zhang, Q.T. (2012b). Photosynthesis and activity of photosystem II in response to drought stress in Amur Grape (Vitis amurensis Rupr.). Photosynthetica *50*, 189–196.

Warren, C., and Dreyer, E. (2006). Temperature response of photosynthesis and internal conductance to CO2: results from two independent approaches. J. Exp. Bot. *57*, 3057–3067.

Wei, X., Su, X., Cao, P., Liu, X., Chang, W., Li, M., Zhang, X., and Liu, Z. (2016). Structure of spinach photosystem II–LHCII supercomplex at 3.2 Å resolution. Nature *534*, 69–74.

Wieneke, S., Ahrends, H., Damm, A., Pinto, F., Stadler, A., Rossini, M., and Rascher, U. (2016). Airborne based spectroscopy of red and far-red sun-induced chlorophyll fluorescence: Implications for improved estimates of gross primary productivity. Remote Sens. Environ. *184*, 654–667.

Wientjes, E., and Croce, R. (2011). The light-harvesting complexes of higher-plant Photosystem I: Lhca1/4 and Lhca2/3 form two red-emitting heterodimers. Biochem. J. *433*, 477–485.

Wientjes, E., and Croce, R. (2012). PMS: Photosystem I electron donor or fluorescence quencher. Photosynth. Res. *111*, 185–191.

Will, R.E., Wilson, S.M., Zou, C.B., and Hennessey, T.C. (2013). Increased vapor pressure deficit due to higher temperature leads to greater transpiration and faster mortality during drought for tree seedlings common to the forest-grassland ecotone. New Phytol. *200*, 366–374.

Wise, R.R., Olson, A.J., Schrader, S.M., and Sharkey, T.D. (2004). Electron transport is the functional limitation of photosynthesis in field-grown Pima cotton plants at high temperature. Plant Cell Environ. *27*, 717–724.

Wyber, R., Osmond, B., Ashcroft, M.B., Malenovsky, Z., and Robinson, S.A. (2017). Remote monitoring of dynamic canopy photosynthesis with high time resolution light-induced fluorescence transients. Tree Physiol.

Yamasaki, T., Yamakawa, T., Yamane, Y., Koike, H., Satoh, K., and Katoh, S. (2002). Temperature acclimation of photosynthesis and related changes in photosystem II electron transport in winter wheat. Plant Physiol. *128*, 1087–1097.

Yamori, W., Noguchi, K., Kashino, Y., and Terashima, I. (2008). The role of electron transport in determining the temperature dependence of the photosynthetic rate in spinach leaves grown at contrasting temperatures. Plant Cell Physiol. *49*, 583–591.

Yamori, W., Masumoto, C., Fukayama, H., and Makino, A. (2012). Rubisco activase is a key regulator of non-steady-state photosynthesis at any leaf temperature and, to a lesser extent, of steady-state photosynthesis at high temperature. Plant J. *71*, 871–880.

Yamori, W., Hikosaka, K., and Way, D.A. (2014). Temperature response of photosynthesis in C3, C4, and CAM plants: temperature acclimation and temperature adaptation. Photosynth. Res. *119*, 101–117.

Yin, Z.T., Meng, F.F., Song, H.N., He, X.H., Xu, X.M., and Yu, D.Y. (2010). Mapping quantitative trait loci associated with chlorophyll a fluorescence parameters in soybean (Glycine max (L.) Merr.). Planta *231*, 875–885.

Zhang, D., Du, Q., Zhang, Z., Jiao, X., Song, X., and Li, J. (2017). Vapour pressure deficit control in relation to water transport and water productivity in greenhouse tomato production during summer. Sci. Rep. *7*, 43461.

Zhu, X.G., Long, S.P., and Ort, D.R. (2010). Improving Photosynthetic Efficiency for Greater Yield. Annu. Rev. Plant Biol. Vol 61 *61*, 235–261.

Ziska, L.H., Bunce, J.A., Shimono, H., Gealy, D.R., Baker, J.T., Newton, P.C.D., Reynolds, M.P., Jagadish, K.S.V., Zhu, C., Howden, M., et al. (2012). Food security and climate change: on the potential to adapt global crop production by active selection to rising atmospheric carbon dioxide. Proc. R. Soc. B Biol. Sci. *279*, 4097–4105.

Zivcak, M., Brestic, M., Olsovska, K., and Slamka, P. (2008). Performance index as a sensitive indicator of water stress in Triticum aestivum L. PLANT SOIL Environ. *54*, 133–139.

Zivcak, M., Brestic, M., Balatova, Z., Drevenakova, P., Olsovska, K., Kalaji, H.M., Yang, X., and Allakhverdiev, S.I. (2013). Photosynthetic electron transport and specific photoprotective responses in wheat leaves under drought stress. Photosynth. Res. *117*, 529–546.

Ziyomo, C., and Bernardo, R. (2013). Drought Tolerance in Maize: Indirect Selection through Secondary Traits versus Genomewide Selection. Crop Sci. *53*, 1269–1275.

Zubik, M., Luchowski, R., Puzio, M., Janik, E., Bednarska, J., Grudzinski, W., and Gruszecki, W.I. (2013). The negative feedback molecular mechanism which regulates excitation level in the plant photosynthetic complex LHCII: Towards identification of the energy dissipative state. Biochim. Biophys. Acta BBA - Bioenerg. *1827*, 355–364.

# 8 Supplemental material

## 8.1 Supplemental figures

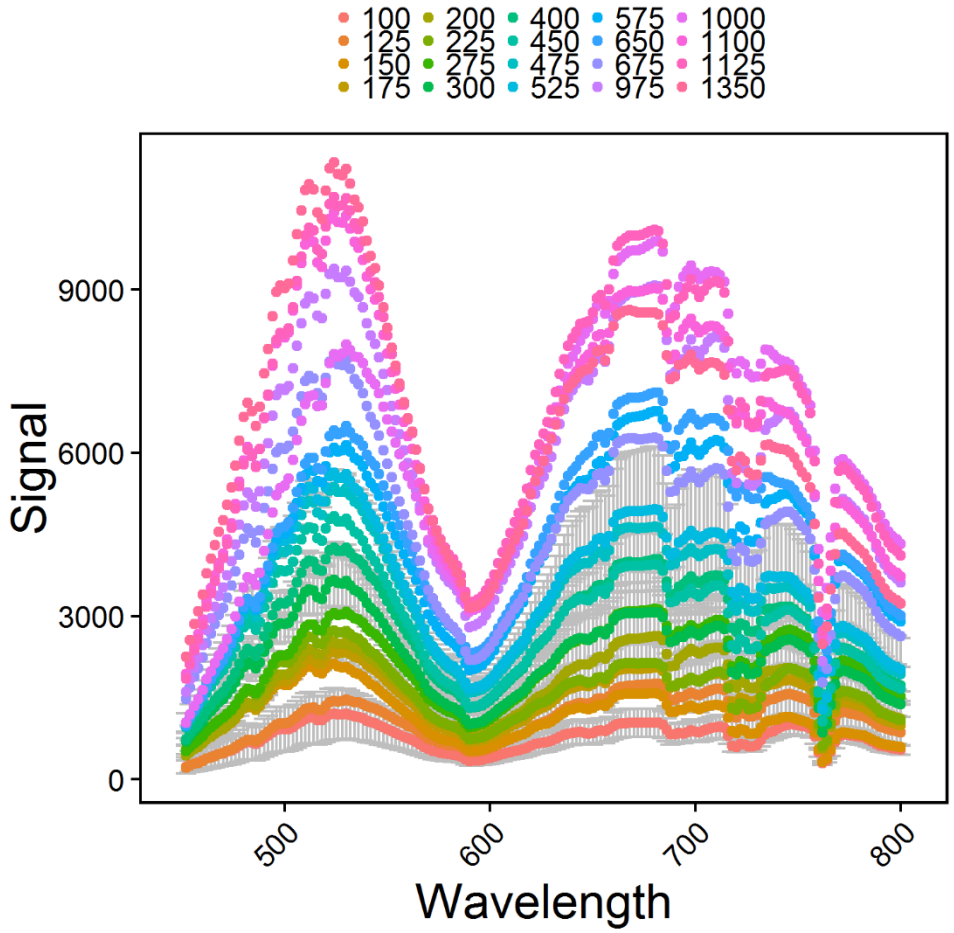


**Figure S 1** Look-up table for grey reference spectras for light intensityies from 100 to 1350 µmol photons $m^{-2}$ $s^{-1}$. Every measurement was merged to photosynthetic photon flux density (PPFD) value measured from environmental stations distributed in the greenhouse. Reference spectra at indicated light intensities were used to correct spectral measurements of plants taken at the same light intensities. This look up table was done as proxy correction because reference could not be simultaneously measured. Reference spectra measurements were carried out from May 15 to 18, 2017.

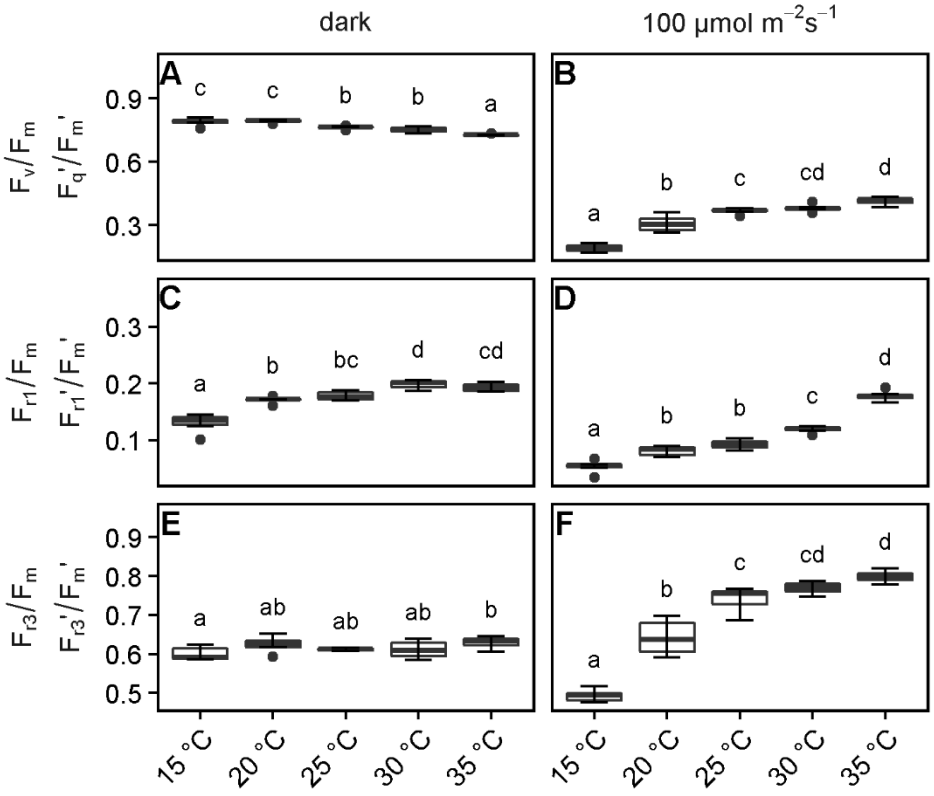


**Figure S 2** Light response at different temperatures (15 to 35°C ) measured by the light-induced fluorescence transient (LIFT) in the dark and at steady state 100 µmol photons $m^{-2}$ $s^{-1}$ of blue light. Quantum efficiency of the photosystem II ($F_v/F_m$ in the dark and $F_q'/F_m'$ in the light) (A), efficiency of electron transport after 0.65 ms ($F_{r1}/F_m$ in the dark, $F_{r1}'/F_m'$ in the light) and after 30 ms ($F_{r3}/F_m$ in the dark, $F_{r3}'/F_m'$ in the light) (D) is shown. Attached Arabidopsis leaves were measured (n=5-6). Box represents inter-quartile range, bold horizontal bar the median, the discontinuous lines the upper and lower quartile, and outlier data points (>1.5 × inter-quartile range) are depicted by a point. Means with different letters differ significantly using Tukey's multiple comparisons of means.

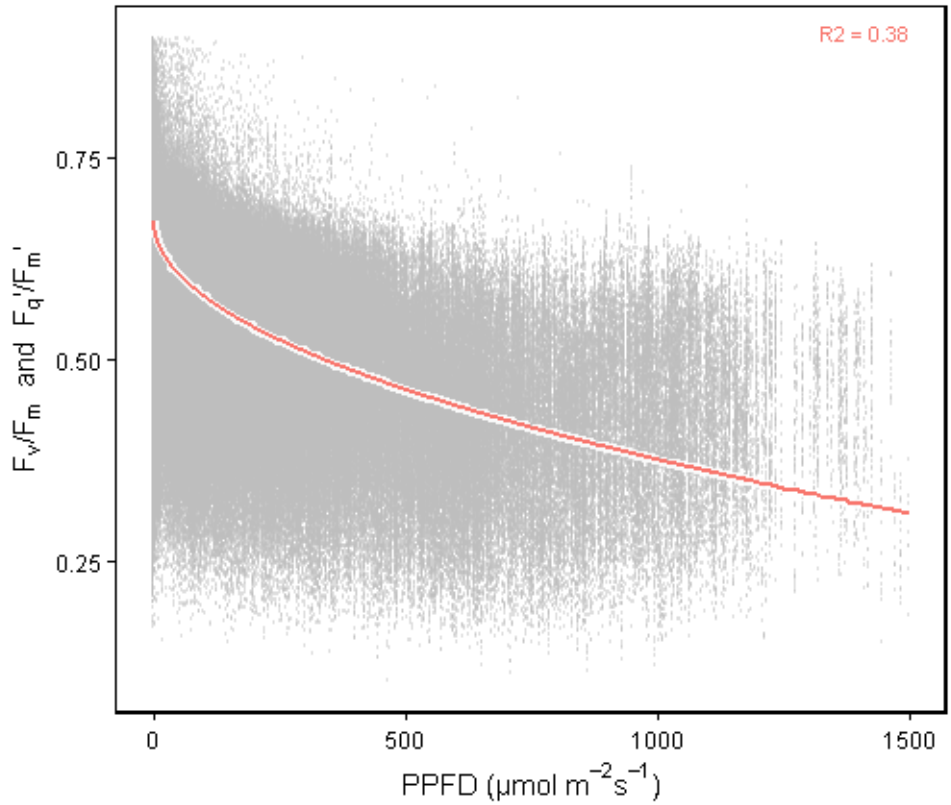


**Figure S 3** Response of quantum efficiency of the photosystem II ($F_v/F_m$ in the dark and $F_q'/F_m'$ in the light) to photosynthetic photon flux density (PPFD). Fluorescence data was acquired by up to two light-induced fluorescence transient (LIFT) devices scanning crop canopy simultaneously from an automated moving platform. Environmental conditions as PPFD were recorded by up to three stations distributed in the unheated greenhouse. Measurements took place from December 2015 to August 2017 in barley, maize, rapeseed, soybean and wheat genotypes ($F_q'/F_m' \sim PPFD^{0.5}$ with n=1086056 measurements).

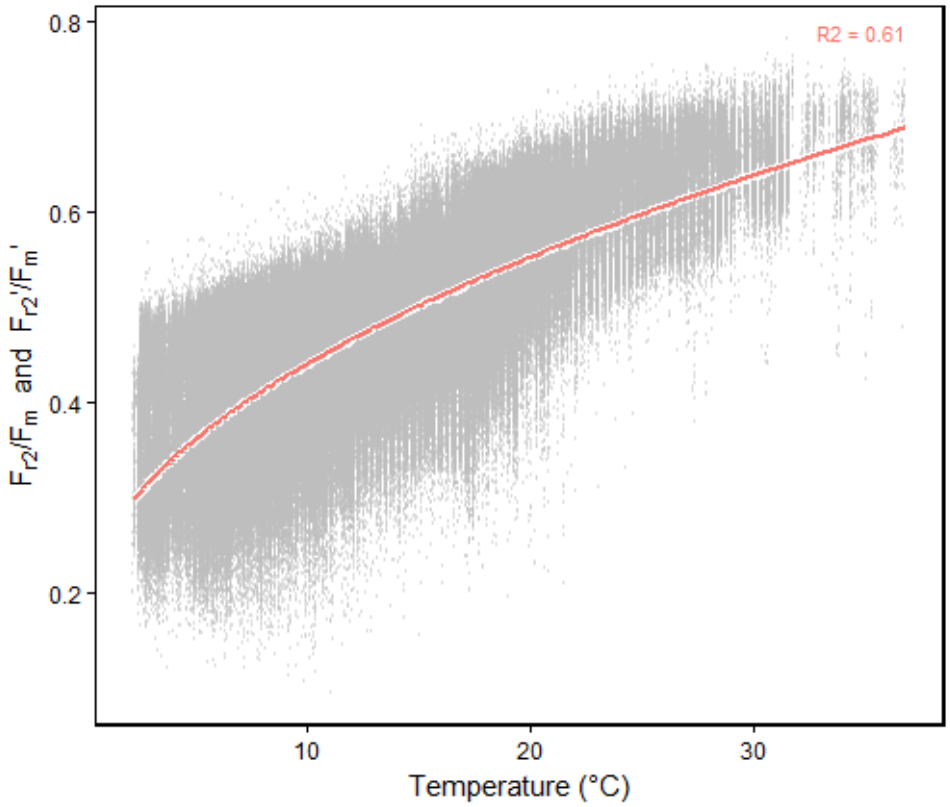


**Figure S 4** Reoxidation efficiency 5 ms after primary quinone ($Q_A$) reduction ($F_{r2}'/F_m'$) showed high correlation with temperature. Fluorescence data was acquired by up to two light-induced fluorescence transient (LIFT) devices scanning crop canopy simultaneously from an automated moving platform. Environmental conditions as temperature were recorded by up to three stations distributed in the unheated greenhouse. Measurements took place from December 2015 to August 2017 in barley, maize, rapeseed, soybean and wheat genotypes. White intervals show 95% confidence intervals for the mean of the $F_{r2}'/F_m'$ ~ Temperature regression with n=1078383 measurements.

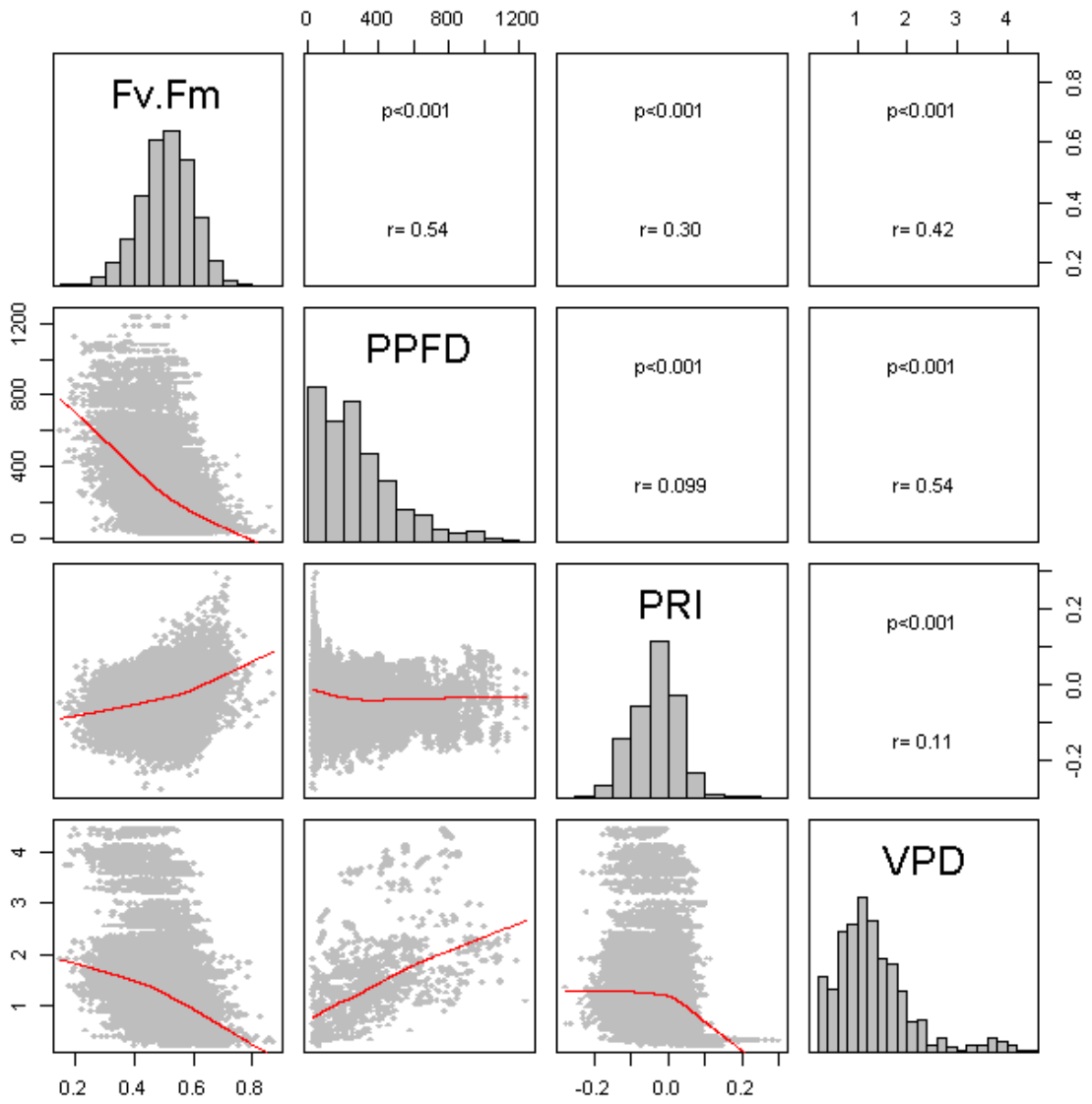


**Figure S 5** Correlations of photosystem II operating efficiency ($F_q'/F_m'$) in Maize genotypes with its influencing parameters photon flux density (PPFD), photochemical reflectance index (PRI) and vapor pressure deficit (VPD) are shown. In the diagonal histograms visualize distribution of the data, below the diagonal scatterplots with best linear fit (red line) and above the Pearson correlation with p value and R square. Parameters were per-selected based on lasso regression.

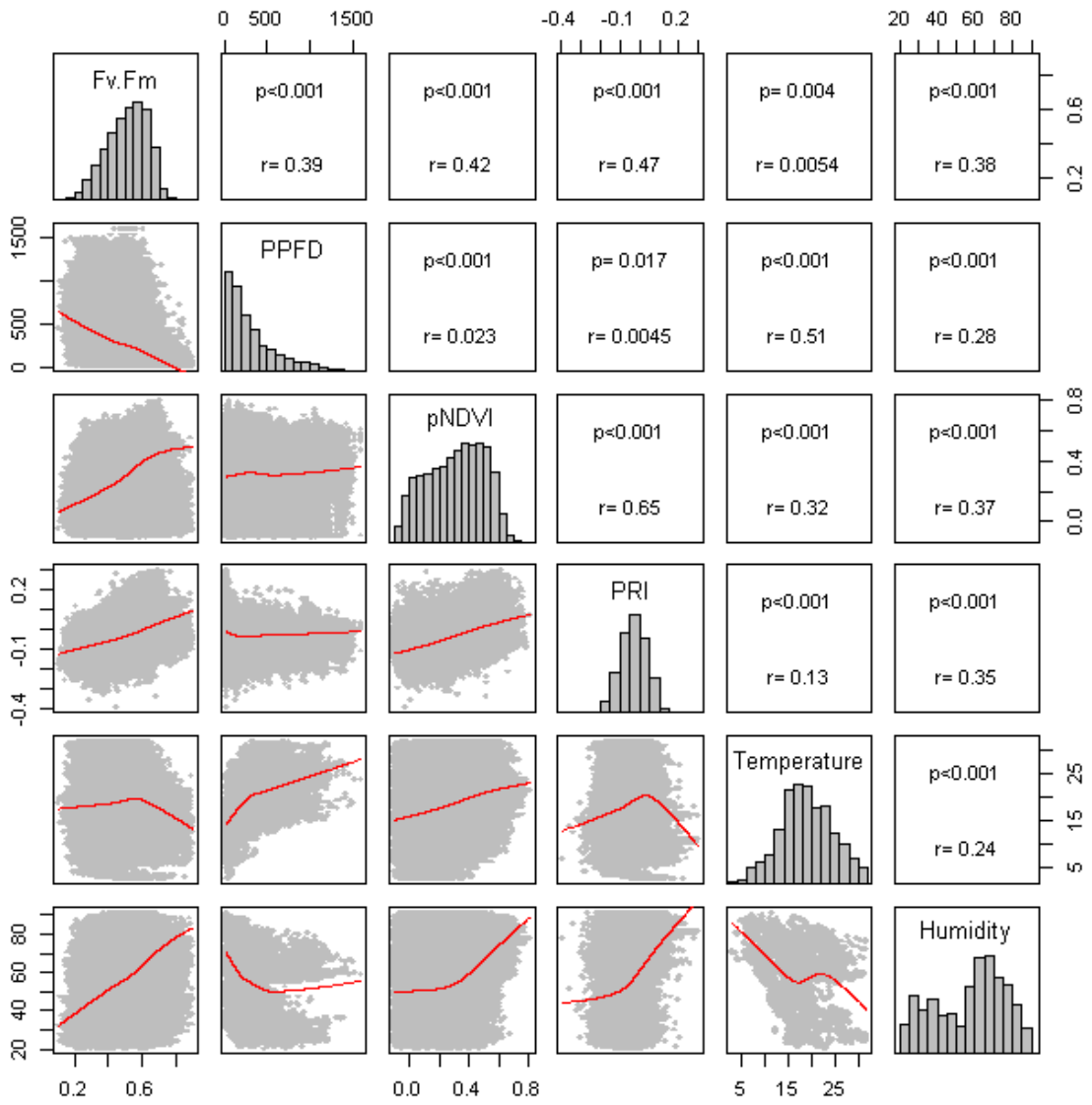


**Figure S 6** Correlations of photosystem II operating efficiency ($F_q'/F_m'$) with its influencing parameters photon flux density (PPFD), pseudo normalized difference vegetation index (pNDVI), photochemical reflectance index (PRI), temperature and humidity are shown. In the diagonal histograms visualize distribution of the data, below the diagonal scatterplots with best linear fit (red line) and above the Pearson correlation with p value and R square. Parameters were per-selected based on lasso regression.

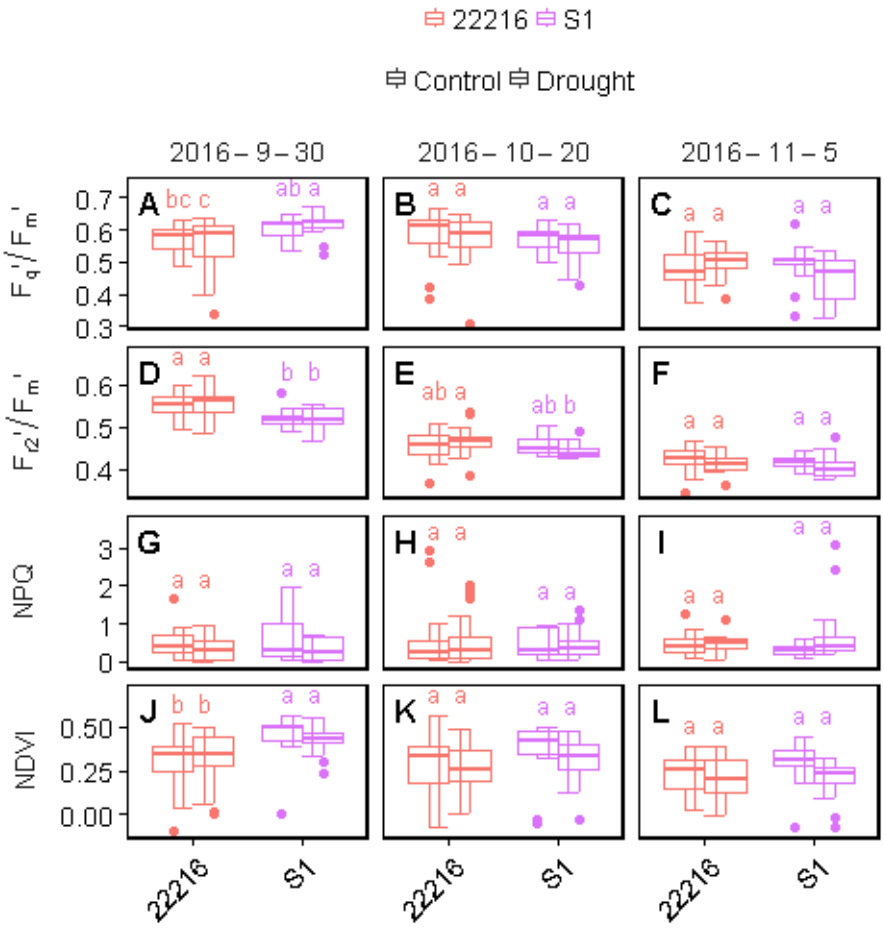


**Figure S 7** Boxplot of photosystem II operating efficiency ($F_q'/F_m'$, A, B), reoxidation efficiency 5 ms after primary quinone ($Q_A$) reduction ($F_{r2}'/F_m'$, C,D), non-photochemical quenching (NPQ, G,H) and normalized difference vegetation index (NDVI, E,F) of two selected days before and within drought treatment (2016-9-30, 2016-10-20 and 2016-11-5, measurements from 10 am to 12 am averaged). Six soybean genotypes were monitored in 15 plots. Drought treatment started at October 5$^{th}$ in four plots. Box represents inter-quartile range, bold horizontal bar the median, the discontinuous lines the upper and lower quartile, and outlier data points (>1.5 × inter-quartile range) are depicted by a point. Means with different letters differ significantly using Scheffé's multiple comparisons of means (n= 5 to 39).

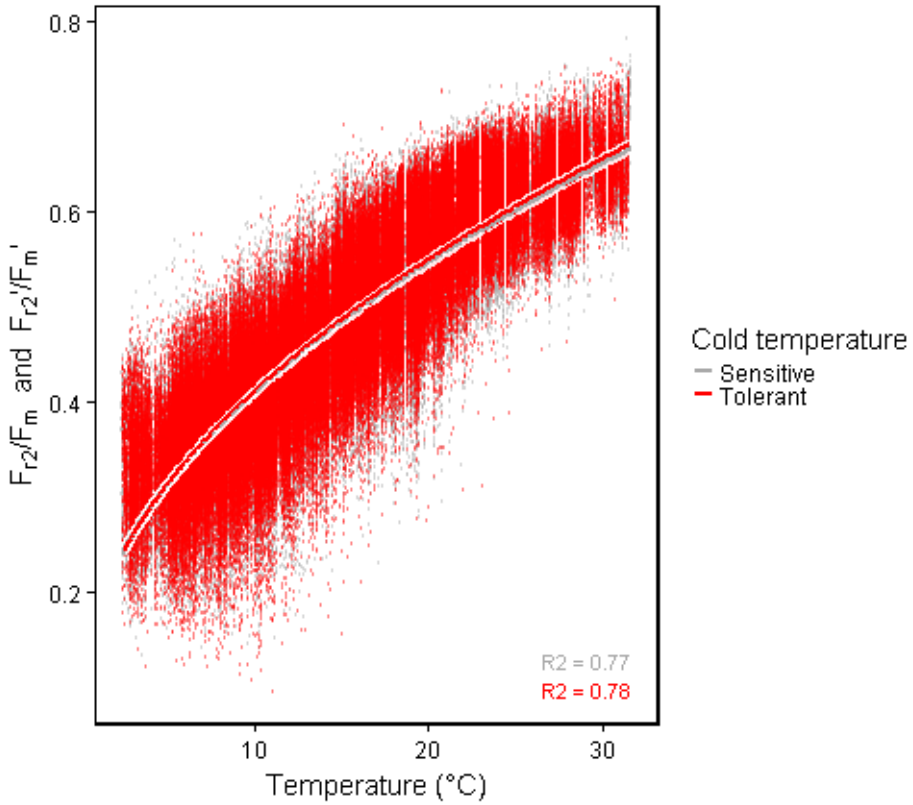


**Figure S 8** Reoxidation efficiency 5 ms after primary quinone ($Q_A$) reduction ($F_{r2}/F_m$ in the dark and $F_{r2}'/F_m'$ in the light) in 9 genotypes differing in cold tolerance showed high correlation with temperature. Fluorescence data was acquired by a light-induced fluorescence transient (LIFT) devices scanning crop canopy from an automated moving platform. Environmental conditions as temperature were recorded every minute by three stations distributed in the greenhouse and merged to the measurements done in the same minute. Six genotypes were monitored from September to November 2016 and eight genotypes from March to August 2017 in an unheated greenhouse. White intervals show 95% confidence intervals for the mean $F_{r2}/F_m$ respective $F_{r2}'/F_m'$ which was fitted to a linear model depending temperature (square root transformed, n= 585520 measurements).

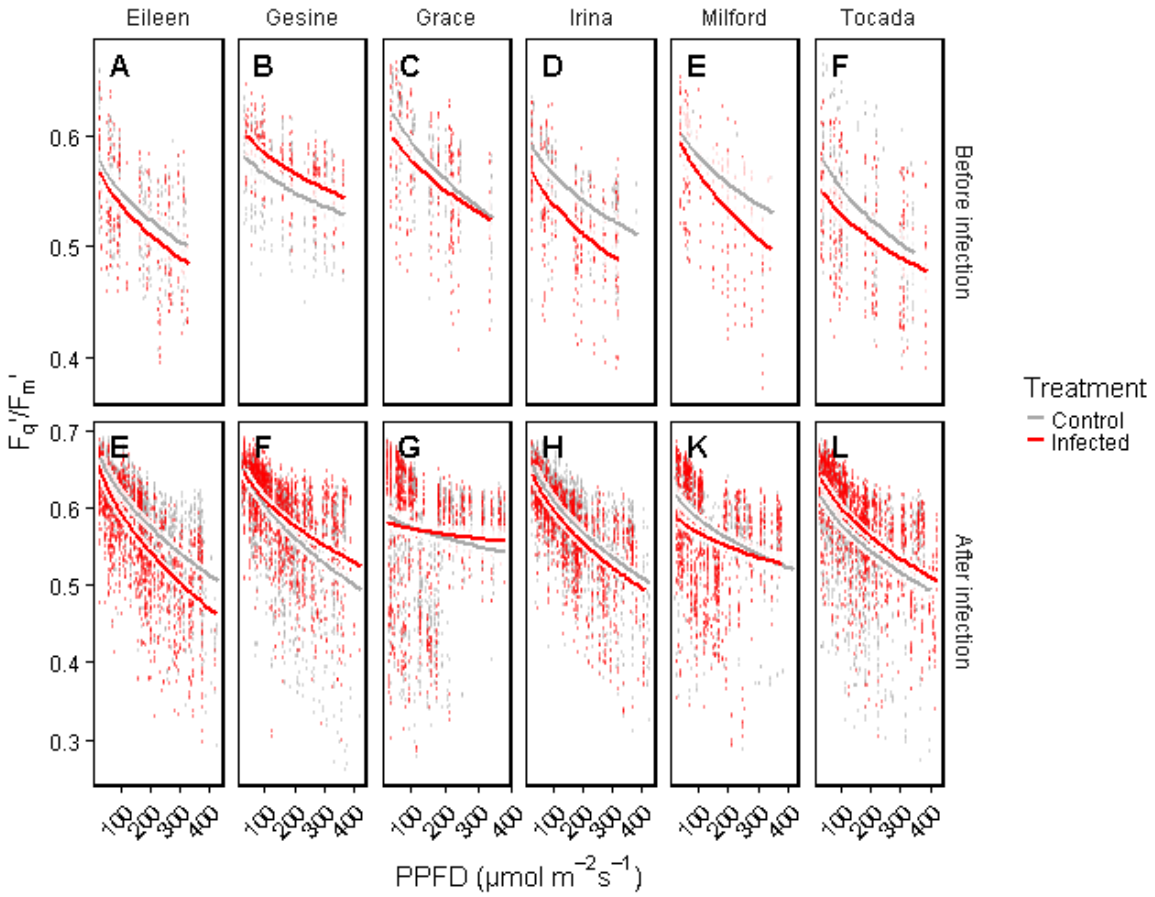


**Figure S 9** Photosystem II operating efficiency ($F_q'/F_m'$) values were split among different barley genotypes as well as measurements before (A to F) and after (G to L) powdery mildew infection. $F_q'/F_m'$ was fitted to a linear model depending on photon flux density (PPFD) and grouped after treatment. Light-induced fluorescence transient (LIFT) devices scanned canopy automatically acquiring fluorescence data every hour throughout a measuring day. PPFD was recorded every minute by three stations distributed in the unheated greenhouse and merged to the measurements done in the same minute. Measurements were derived from the first barley experiments November 2015 to February 2016. White intervals show 95% confidence intervals for the mean of (n= 37 to 2328, in total 25454 measurements, 6 genotypes in 12 containers).

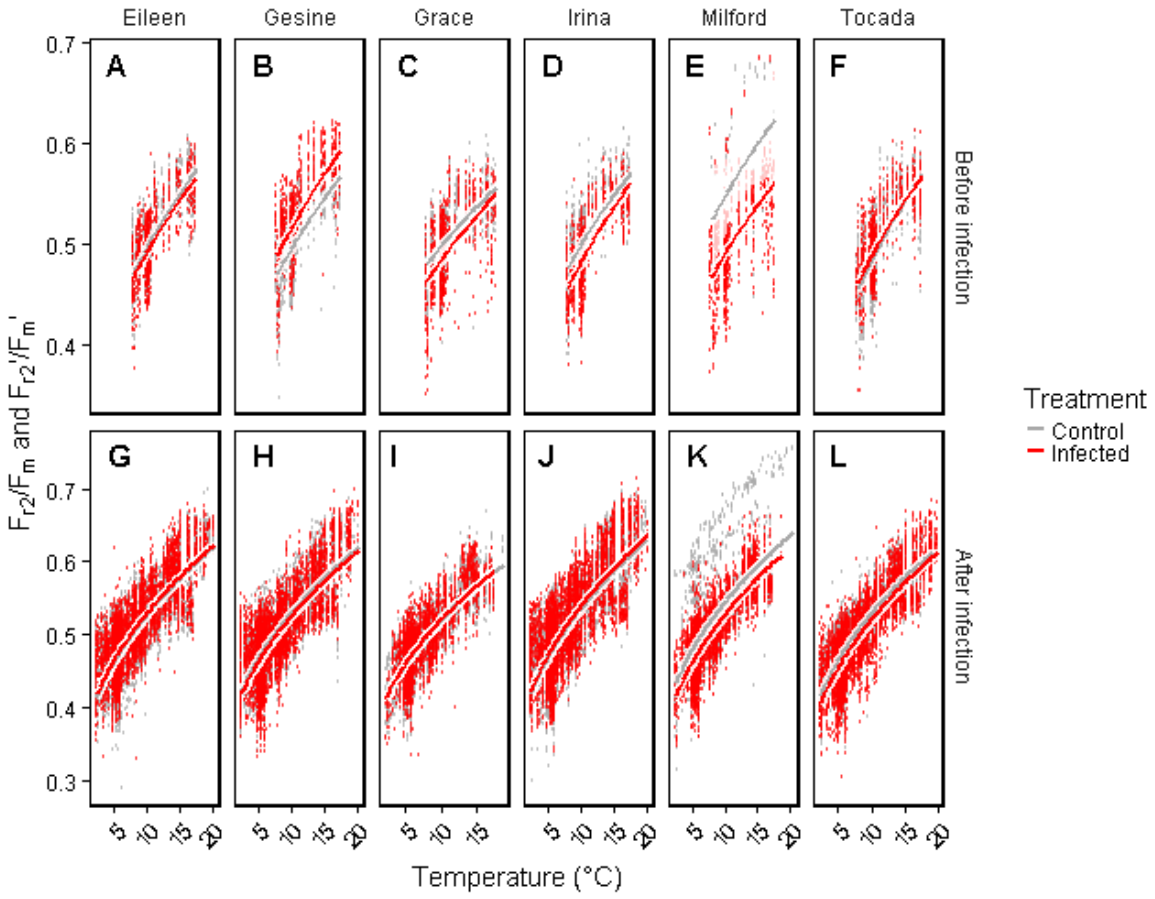


**Figure S 10** Reoxidation efficiency 5 ms after primary quinone ($Q_A$) reduction ($F_{r2}/F_m$ in the dark and $F_{r2}'/F_m'$ in the light) values were split among different barley genotypes as well as measurements before (A to F) and after (G to L) powdery mildew infection. $F_{r2}/F_m$ respective $F_{r2}'/F_m'$ was fitted to a linear model depending on temperature and grouped after treatment. Light-induced fluorescence transient (LIFT) devices scanned canopy automatically acquiring fluorescence data every hour throughout a measuring day. Temperature was recorded every minute by three stations distributed in the unheated greenhouse and merged to the measurements done in the same minute. Measurements were derived from the first barley experiments November 2015 to February 2016. White intervals show 95% confidence intervals for the mean of (n= 79 to 6302, in total 72325 measurements, 6 genotypes in 12 containers).

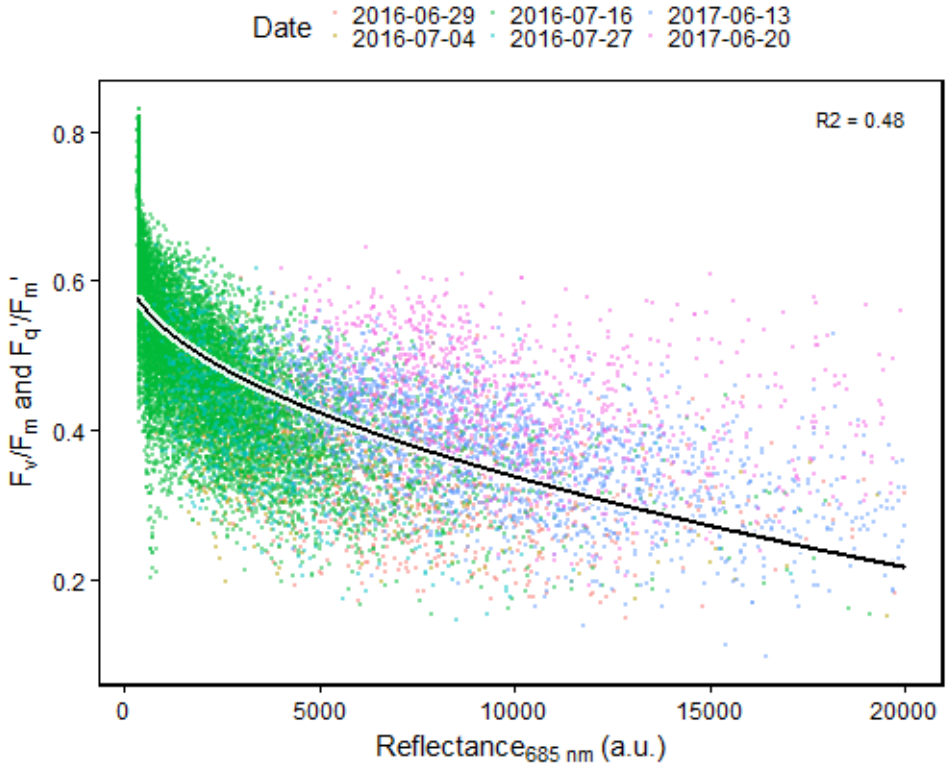


**Figure S 11** Quantum efficiency of the photosystem II ($F_v/F_m$ in the dark and $F_q'/F_m'$ in the light) measured in the maize field was mainly determined by the leaf sunlight reflectance of the measured leaf at 685 nm. Different measuring dates were identified as second important factor determining $F_q'/F_m'$ according to linear modelling. Fluorescence data was acquired by a light-induced fluorescence transient (LIFT) devices scanning crop canopy from an manually driven phenotyping bike. In total 13 different maize genotypes were measured in June and July 2016 and in June 2017. White intervals show 95% confidence intervals for the mean of the $F_v/F_m$ respective $F_q'/F_m'$ which was fitted to a linear model depending on reflectance at 685 nm (square root transformed, n=15406 measurements).

## 8.2 Supplemental tables

**Table S 1** Liner model of photosystem II operating efficiency ($F_q'/F_m'$) measured in soybean genotypes over two seasons an unheated greenhouse (n= 279470). Depending factors or covariates were photochemical reflectance index (PRI), photon flux density (PPFD), date of measurement, pseudo normalized difference vegetation index (NDVI), container (plot), genotype, daytime and humidity. Descriptors are degree of freedom (Df), sum of squares (Sum Sq), mean of squares (Mean Sq), ratio of Mean Sq and Mean Sq error (F value), the associated p value (Pr(>F)) and the explained Sum Sq per factor (ExpVar).

| | Df | Sum Sq | Mean Sq | F value | Pr(>F) | ExpVar |
|---|---|---|---|---|---|---|
| Residuals | 279401 | 1692.55 | 0.01 | NA | NA | 45 |
| PRI | 1 | 787.69 | 787.69 | 130029.6 | 0 | 20.9 |
| PPFD | 1 | 576.42 | 576.42 | 95153.4 | 0 | 15.3 |
| Date | 19 | 321.24 | 16.91 | 2791 | 0 | 8.5 |
| pNDVI | 1 | 115.95 | 115.95 | 19141.3 | 0 | 3.1 |
| Plot | 33 | 106.58 | 3.23 | 533.1 | 0 | 2.8 |
| $PPFD^{0.5}$ | 1 | 93.77 | 93.77 | 15479.8 | 0 | 2.5 |
| Genotype | 8 | 24.96 | 3.12 | 515.1 | 0 | 0.7 |
| Daytime | 3 | 23.53 | 7.84 | 1294.7 | 0 | 0.6 |
| Humidity | 1 | 17.75 | 17.75 | 2930.4 | 0 | 0.5 |

**Table S 2** Liner model of photosystem II operating efficiency ($F_q'/F_m'$) measured in different soybean and maize genotypes over two seasons in the field (n= 19235). Depending factors or covariates were leaf reflectance of sunlight at 685 nm (IRRAD), date of measurement, temperature, pseudo green normalized difference vegetation index (NDVI). Descriptors are degree of freedom (Df), sum of squares (Sum Sq), mean of squares (Mean Sq), ratio of Mean Sq and Mean Sq error (F value), the associated p value (Pr(>F)) and the explained Sum Sq per factor (ExpVar).

| | Df | Sum Sq | Mean Sq | F value | Pr(>F) | ExpVar |
|---|---|---|---|---|---|---|
| Residuals | 19212 | 98.49 | 0.01 | NA | NA | 50.5 |
| IRRAD | 1 | 50.61 | 50.61 | 9872.3 | 0 | 26 |
| Date | 10 | 23.53 | 2.35 | 459 | 0 | 12.1 |
| Temperature | 1 | 12.85 | 12.85 | 2506.9 | 0 | 6.6 |
| $IRRAD^{0.5}$ | 1 | 8.41 | 8.41 | 1641 | 0 | 4.3 |
| pGNDVI | 1 | 0.75 | 0.75 | 147.1 | 0 | 0.4 |

**Table S 3** Reoxidation efficiency 5 ms after primary quinone ($Q_A$) reduction ($F_{r2}/F_m$ in the dark and $F_{r2}'/F_m'$ in the light) measured in different soybean and maize genotypes over two seasons in the field (n=22414). Depending factors or covariates were temperature, crop species, time in seconds of the measurement, temperature, leaf reflectance of sunlight at 685 nm (IRRAD), and daytime. Descriptors are degree of freedom (Df), sum of squares (Sum Sq), mean of squares (Mean Sq), ratio of Mean Sq and Mean Sq error (F value), the associated p value (Pr(>F)) and the explained Sum Sq per factor (ExpVar).

| | Df | Sum Sq | Mean Sq | F value | Pr(>F) | ExpVar |
|---|---|---|---|---|---|---|
| Temperature | 1 | 84.69 | 84.69 | 33631.5 | 0 | 35.2 |
| Crop | 1 | 63.42 | 63.42 | 25183.1 | 0 | 26.4 |
| Residuals | 22404 | 56.42 | 0 | NA | NA | 23.5 |
| $Temperature^{0.5}$ | 1 | 16.29 | 16.29 | 6468.6 | 0 | 6.8 |
| TimeSec | 1 | 14.7 | 14.7 | 5837 | 0 | 6.1 |
| IRRAD | 1 | 3.08 | 3.08 | 1223.6 | 0 | 1.3 |
| Daytime | 4 | 1.68 | 0.42 | 166.6 | 0 | 0.7 |

**Table S 4** Analysis of variance (ANOVA) was carried out for signal to noise ratio (S/N ratio), maximum quantum efficiency of the photosystem II ($F_v/F_m$) and reoxidation efficiency 5 ms after primary quinone ($Q_A$) reduction ($F_{r2}/F_m$) with distance from 750 mm to 1200 mm and fixed or natural leaf angle as depending factors. ANOVA is described by degree of freedom (Df), sum of squares (Sum Sq), mean of squares (Mean Sq), ratio of Mean Sq and Mean Sq error (F value), the associated p value (Pr(>F)) and the explained Sum Sq per factor (ExpVar). Measurements were done during the night (n=123).

| | Variable | Df | Sum Sq | Mean Sq | F value | Pr(>F) | ExpVar |
|---|---|---|---|---|---|---|---|
| Distance | S/N ratio | 3 | 26464.13 | 8821.38 | 9.4 | 1.00E-05 | 14.9 |
| Leaf angle | | 1 | 39819.06 | 39819.06 | 42.3 | 0 | 22.4 |
| Residuals | | 118 | 111170.81 | 942.13 | NA | NA | 62.6 |
| | | | | | | | |
| Distance | $F_v/F_m$ | 3 | 0.01 | 0 | 0.7 | 0.53691 | 1.4 |
| Leaf angle | | 1 | 0.11 | 0.11 | 37.2 | 0 | 23.6 |
| Residuals | | 118 | 0.35 | 0 | NA | NA | 75 |
| | | | | | | | |
| Distance | $F_{r2}/F_m$ | 3 | 0.01 | 0 | 9.7 | 0.00001 | 19.3 |
| Leaf angle | | 1 | 0 | 0 | 3.4 | 0.06953 | 2.2 |
| Residuals | | 118 | 0.02 | 0 | NA | NA | 78.4 |